USATRECOM TECHNICAL REPORT 65-14

UH-2 HELICOPTER HIGH-SPEED FLIGHT RESEARCH PROGRAM UTILIZING JET THRUST AUGMENTATION

FINAL REPORT

By

A. A. Whitfield
W. E. Blackburn

March 1965

U. S. ARMY TRANSPORTATION RESEARCH COMMAND
FORT EUSTIS, VIRGINIA

CONTRACT DA 44-177-AMC-105(T)
KAMAN AIRCRAFT CORPORATION

Qualified requesters may obtain copies of this report from DDC.

* * *

This report has been furnished to the Department of Commerce for sale to the public.

* * *

The findings in this report are not to be construed as an official Department of the Army position, unless so designated by other authorized documents.

* * *

When Government drawings, specifications, or other data are used for any purpose other than in connection with a definitely related Government procurement operation, the United States Government thereby incurs no responsibility nor any obligation whatsoever; and the fact that the Government may have formulated, furnished, or in any way supplied the said drawings, specifications, or other data is not to be regarded by implication or otherwise as in any manner licensing the holder or any other person or corporation, or conveying any rights or permission, to manufacture, use, or sell any patented invention that may in any way be related thereto.

* * *

Destroy this report when it is no longer needed. Do not return it to the originator.

HEADQUARTERS
U S ARMY TRANSPORTATION RESEARCH COMMAND
FORT EUSTIS VIRGINIA 23604

This report has been reviewed by the U. S. Army Transportation Research Command and is considered to be technically sound. The report summarizes the results of a flight research program to determine the high-speed flight characteristics of a multibladed, fully articulated, servo-flap controlled rotor system utilizing auxiliary jet thrust augmentation. These results are published for the exchange of information and stimulation of ideas.

The Army is currently continuing to sponsor several high-speed programs of a similar nature to provide basic technology for use in the design of future high-performance rotary-wing aircraft.

Task 1D121401A152
Contract DA 44-177-AMC-105(T)
USATRECOM Technical Report 65-14

March 1965

UH-2 HELICOPTER HIGH-SPEED FLIGHT RESEARCH PROGRAM UTILIZING JET THRUST AUGMENTATION

Kaman Aircraft Corporation Report No. R-527B

by

A. A. Whitfield
Assistant Project Engineer

and

W. E. Blackburn
Flying Qualities Group Leader

Kaman Aircraft Corporation
Bloomfield, Connecticut

for

U. S. ARMY TRANSPORTATION RESEARCH COMMAND
FORT EUSTIS, VIRGINIA

ABSTRACT

The results of a flight research program conducted to determine the behavior of a fully articulated, servo-flap controlled rotor system at various power levels in high-speed flight are presented. The research aircraft, instrumentation, and test program are described. The test results are discussed and compared with those predicted by analytical study.

A standard Kaman UH-2 helicopter was modified by the addition of a General Electric YJ-85 jet engine, without afterburner, mounted on the right side of the fuselage for horizontal thrust augmentation. Research flights were conducted up to a level-flight true airspeed of 188 knots. Airspeeds limited by retreating blade stall or advancing blade compressibility were established. The effects of density altitude, rotor speed and power, tip speed ratio, thrust augmentation and aircraft gross weight on the limit airspeeds are discussed.

Aircraft and rotor structural loads and vibration characteristics remained within acceptable levels up to the limit airspeed. The handling characteristics of the helicopter during normal powered and autorotation flight and following simulated failure of the primary or auxiliary engines were found to be satisfactory. Static pitch stability is not affected strongly by either airspeed or jet thrust. Lateral-direction stability remained generally positive but showed a tendency to deteriorate with increasing jet thrust.

It is concluded that the speed envelope for rotary wing aircraft can be substantially expanded by unloading the main rotor through the application of horizontal thrust augmentation.

PREFACE

This report summarizes the results of a flight research program to determine the high-speed characteristics of a multiblade fully articulated rotor system utilizing a UH-2 helicopter modified to include external horizontal thrust augmentation from a YJ-85 turbojet engine. The program was conducted by Kaman Aircraft Corporation under USATRECOM Contract DA 44-177-AMC-105(T), Reference 1. Design of the jet engine installation was initiated in July 1963, and was followed by modification of the test aircraft in August 1963. Flight testing commenced on 26 November 1963 and was completed on 10 April 1964.

Subsequent flight testing of the helicopter in this configuration was conducted in September 1964 to evaluate the effects of jet augmentation on maneuverability flight and dynamic stability. The results of this testing are reported in Reference 25.

This program was conducted under the technical cognizance of the Applied Aeronautical Engineering Group of USATRECOM. Principle Kaman Aircraft Corporation personnel associated with the program were Messrs. W. Blackburn, A. Whitfield, A. Rita, D. Clymer, A. Ashley, F. Smith, E. Eckhart, and R. Jones.

TABLE OF CONTENTS

ILLUSTRATIONS

LIST OF SYMBOLS

DIMENSIONAL QUANTITIES

G.W.	Gross Weight - Pounds
H	Rotor Drag Force - Pounds
T	Rotor Thrust - Pounds
T_J	Net Jet Thrust of Auxiliary Propulsion Engine (Acting on Aircraft) - Pounds
R	Blade Radius - Feet
V_c	Speed of Sound - Feet/Second
V	True Airspeed - Knots
a_{1s}	Rotor Longitudinal Flapping Angle - Degrees
b_{1s}	Rotor Lateral Flapping Angle - Degrees
g	Gravitational Acceleration Unit - $Feet/Sec^2$
H_D	Density Altitude - Feet
r	Distance from Center of Rotation to a Point on the Rotor Blade - Feet
α	Rotor Angle of Attack - Degrees
ψ	Blade Azimuth Angle - Degrees
Ω	Rotor Angular Velocity - Rad/Sec

NONDIMENSIONAL QUANTITIES

C_P	Power Coefficient
C_{P_i}	Induced Power Ceofficient
C_{P_c}	Climb Power Ceofficient
C_{P_o}	Profile Power Coefficient
C_{P_p}	Parasite Power Ceofficient
C_{Q_i}	Induced Torque Coefficient

LIST OF SYMBOLS (Continued)

C_{Q_o}	Profile Torque Coefficient
C_T	Thrust Coefficient
M	Mach Number
M_{cr}	Critical Mach Number
M_o	Hover Blade Tip Mach Number
M_T	Advancing Blade Tip Mach Number
c_{d_o}	Blade Section Profile Drag Coefficient
x	Rotor Nondimensional Radius Station, r/R
μ	Tip-Speed Ratio, $\frac{V \cos \alpha}{\Omega R}$
σ	Density Ratio or Rotor Solidity
λ	Rotor Inflow Ratio, $\frac{V \sin \alpha - v}{\Omega R}$
θ	Blade Pitch Angle (Measured at 75% Radius)

UH-2 HIGH-SPEED RESEARCH HELICOPTER
WITH JET THRUST AUGMENTATION

SUMMARY

This report presents the results of a research program conducted to determine the behavior of a multibladed, fully articulated servo-flap controlled rotor system up to the 180- to 200-knot airspeed region. The test vehicle was a standard Kaman UH-2 helicopter modified by the addition of a YJ-85 engine, without afterburner, mounted on the right side of the fuselage for horizontal thrust augmentation.

Included in this report are the pertinent results of ground and preliminary flight testing up to 140 knots, funded by the contractor, conducted to substantiate the design and operation of the auxiliary propulsion system and to determine its effect on the helicopter characteristics. The results of this phase of the program, which involved 28 flights covering 20 flight hours, were previously reported by References 4 and 5.

This report also presents the results obtained in the high airspeed (above 140 knots) phase of the program, as authorized under U.S. Army Transportation Research Command Contract DA 44-177-AMC-105(T). Preliminary results of the latter phase, which involved 47 flights and 32 flight hours, were included in Reference 6.

The maximum level-flight speed examined in this program was 188 knots TAS (192 knots CAS) at an aircraft gross weight of 9200 pounds and a density altitude of -1200 feet (OAT = 25°F.). A speed of 190 knots TAS (194 knots CAS) was recorded in a shallow dive of 390 feet per minute.

A discussion of main and tail rotor blade loads and pertinent airframe loads, vibration, stability and control, and performance characteristics throughout the speed range to the maximum airspeed examined utilizing varying amounts of augmenting thrust up to 2500 pounds is presented. The limiting airspeed envelope as determined by stall or compressibility is established.

Correlation of flight test results and those predicted by analytical study is presented in the areas of performance, trim and controllability, blade bending moments and high-speed flight limitations due either to stall or to compressibility. In general, the analytical methods for predicting these characteristics are shown to be satisfactory.

It is concluded that horizontal thrust augmentation can provide a substantial expansion of the speed envelope for rotary-wing aircraft.

CONCLUSIONS

Based upon the results of this program, it is concluded that:

The utilization of horizontal thrust augmentation to extend the retreating blade stall boundary of rotary-wing aircraft is shown to be a valid concept. Although some gains in airspeed were achieved at low levels of thrust, the effect of thrust augmentation is more significant at high levels. On an average, a change in the limit speed, as established by stall, in the order of 12 knots per 1000 pounds of thrust augmentation was demonstrated up to the maximum thrust capability of the YJ-85 engine.

Compressibility is shown to be a factor which presently limits the airspeed that may be achieved with rotary-wing aircraft. The application of horizontal thrust augmentation with the resulting reduction in rotor horsepower expands the compressibility speed boundary by increasing the limit rotor Mach number. The compressibility boundary is also expanded by a decrease in rotor thrust or a decrease in rotor tip speed.

The effect of thrust augmentation is also beneficial from a total horsepower standpoint. This is particularly significant at speeds above 150 knots where the total power versus thrust augmentation gradient increases markedly. At each airspeed there appears to be a level of thrust augmentation which permits flight at minimum total power.

Longitudinal static stability is not affected strongly by either airspeed or jet thrust. Lateral-directional static stability remained generally positive for all conditions tested but showed a tendency to deteriorate with increasing jet thrust. A yaw rate damper, utilizing components of the standard UH-2 automatic stabilization equipment, was evaluated and shown to significantly enhance the lateral-directional stability characteristics of the aircraft at high jet thrust.

The use of auxiliary thrust has the effect of reducing cyclic and collective requirements at high speed such that no modifications to the standard UH-2 control system were necessary to remain within acceptable control limits as defined by MIL-H-8501A.

The handling characteristics of the helicopter in the event of failure of either the T-58 or the YJ-85 were found to be acceptable up to maximum speed at which these failures were simulated: 150 knots for T-58 failure and 163 knots for YJ-85 failure.

The basic vibration characteristics of the UH-2 helicopter were maintained up to the airspeeds limited by stall or compressibility. Maximum levels of vibration recorded at the pilot's seat during flights not limited by stall or compressibility remained within the limits defined by MIL-H-8501A.

Structural loads were found to be acceptable on all components during normal flights to high speed. At limit points, which represented penetration into the compressibility or stall boundary, loads in the rotating system, particularly main rotor blade out-of-plane bending at station 190, were found to exceed the endurance limits. The endurance limit of the horizontal stabilizer in edgewise bending was exceeded at limit points.

The present analytical methods for the fully articulated servo-flap controlled rotor, in general, are satisfactory for predicting performance, trim and controllability, vibratory blade bending moments and flight limitation speeds.

In the areas of performance, trim, and controllability, the correlation is generally good. The largest discrepancy is in the area of main rotor flapping. This is attributed to the one-per-rev inflow variation assumed in the analyses as compared to the nonuniform inflow that actually occurs in flight.

The correlation of the calculated flatwise bending moments over the outboard region of the blade (which is the most critical) is excellent for the nonlimit speed flight conditions. The calculated bending moments over the inboard blade region are low compared to flight test results. This discrepancy is probably due to the one-per-rev assumption in the inflow distribution. For the flight condition in which stall and/or compressibility was encountered, the calculated flatwise bending moments were unconservative.

From the correlation of the analytically predicted flight limitations and the limitations as encountered in flight, it is found that the stall limits for the UH-2 rotor are established when stall occurs at the retreating blade three-quarter radius station. The compressibility limit is reached at approximately that combination of rotor speed and flight speed where the tangential Mach number at the advancing blade 90 percent radius station exceeds the maximum section critical value (in this case .77) by approximately .025 or about 3 percent. This is equivalent to a limiting advancing blade tip Mach number of .852.

While the speed limitation conditions are generally predictable by current theoretical methods and the speeds at which limit conditions occurred are predicted quite accurately, the distribution of the local blade section angle of attack is not. The theory predicts essentially tip or outboard stall, whereas a more inboard distribution of stall actually occurs in flight.

Comparison of analytical and flight test limit airspeeds shows that at low rotor r.p.m. stall effects predominate, while at high r.p.m. compressibility is of primary importance. Test results tend to confirm that maximum airspeed for any combination of gross weight and altitude is achieved when both stall and compressibility limits coincide.

RECOMMENDATIONS

Based upon the results of this research program, it is recommended that:

- Additional flight testing of the jet-augmented research helicopter be conducted to investigate the areas of maneuverability and dynamic stability which were not originally included as part of this program. This recommendation was implemented by USATRECOM Contract DA 44-177-AMC-151(T), Modification No. 1, dated 21 August 1964; the results of which are presented in Reference 25.

- A wing be added to the research vehicle in order to evaluate the effects of lift augmentation on the UH-2 helicopter and rotor system. This recommendation is currently being implemented under USATRECOM Contract DA 44-177-AMC-151(T), dated 16 March 1964.

- Action be initiated to provide for the addition of greater thrust augmentation to the research vehicle after completion of the lift augmentation program. This should make possible the acquisition of research data in the 220- to 240-knot region.

- An analytical and test program be conducted to evaluate the potential configuration changes to blade tip sections in achieving flight envelope expansion through relief of compressibility limitations in a fully articulated rotor system.

- An analytical program be conducted to examine the effects of individual or simultaneous failure of the main and auxiliary power plants. Such a study would supplement the analysis and test results obtained in this program by examining the effects of engine failure at the higher operating speeds of future rotary-wing aircraft. This study should include a determination of the characteristics of automatic devices which might be required to achieve satisfactory recovery from such failure.

- An analytical study be conducted in the area of control and power management for future rotary-wing aircraft, incorporating both horizontal and lift augmentation. The objective of such a study would be to establish criteria for designing the system for integrating the pilot's power management and flight control activities. The study must take into account the flight requirements for future rotary-wing vehicles, as established by current research programs, and human factor considerations.

INTRODUCTION

Each successive generation of helicopters has exhibited a marked increase in speed. These speed increases, from early flight items on, have been based upon state-of-the-art advance resulting from industry and government sponsored research programs.

Continued high-speed flight research in all commonly used basic types of rotor systems provides the answers for increased operational speeds of future generation helicopters.

Kaman Aircraft Corporation, as part of its continuing independent research, conducted analytical studies indicating that with the addition of thrust augmentation, research flights of 180- to 200-knots could be made safely with acceptable flying qualities with the UH-2 helicopter.

A proposal for a flight research program, in the 180- to 200-knot region, was submitted to USATRECOM in Reference 2. On 27 June 1963, a contract was awarded to Kaman Aircraft Corporation for the design, modification, and flight testing of a helicopter utilizing thrust augmentation. The objectives of this program were:

(a) to explore the operating limits of the present UH-2 rotor system as defined by retreating blade stall, compressibility, blade bending moments and vibration;

(b) to obtain data on rotor behavior and helicopter flying qualities at combinations of rotor power and jet thrust throughout the defined speed range;

(c) to correlate the results with those predicted by analytical study; and

(d) to determine the adequacy of present methods for calculating general helicopter characteristics at high speed.

The information obtained from this program provides advance data for use in the design of future high-speed rotary-wing aircraft.

I. DESCRIPTION OF TEST VEHICLE

The test vehicle made available for the program was a standard UH-2 helicopter (BuNo. 147978). The aircraft was first flown in February 1961 and had accumulated 951 hours of flight time in development and qualification programs for the U.S. Navy. The UH-2 helicopter utilizes a fully articulated, servo-flap controlled main rotor system described as follows:

Number of Blades	4
Airfoil Designation	NACA 23012 (Mod)
Chord	20 inches
Diameter	44 feet
Blade Twist	-16 degrees (effective total); 2 step
Blade Area (Total)	146 square feet
Disc Area	1520.5 square feet
Solidity	.0965 (theoretical)
Rotor Speed (100%)	276.7 r.p.m.
Tip Speed	638 feet/second
Disc Loading	5.68 pounds per square foot

Other pertinent data on the standard UH-2 helicopter includes:

Power Plant	(1) T58-8B
Normal Gross Weight	8637 pounds
Fuselage Length	39.6 feet
Fuselage Width	5.3 feet
Fuselage Height	13.5 feet
Operational V_{cruise}	130 knots
Operational V_{max}	140 knots

Modification of the test aircraft for a thrust augmentation system as originally proposed in Reference 2 is described below.

JET ENGINE INSTALLATION

A YJ-85-5 engine, without afterburner, is mounted midway along the right side of the helicopter as shown in Figure 6. The engine is suspended from a pylon which in turn is cantilevered from two increased depth frames. The forward flange of the jet engine mounts a straight engine air inlet of approximately one engine diameter. The jet engine power setting is controlled through a mechanical system which is pilot operated from a conventional throttle quadrant located on the console between the pilot and copilot. Pertinent parameters for monitoring jet operation are displayed on a centrally located panel adjacent to the standard aircraft instrument panel as shown in Figure 7.

EXTERNAL CONFIGURATION

In addition to the jet engine installation, the test vehicle differs externally in that the incidence of the horizontal stabi-

lizer chord line is indexed 3 degrees leading edge down as compared to a standard UH-2. Retrimming of the horizontal stabilizer from the standard UH-2 incidence in this manner was required to stay within the endurance limit for the main rotor hub with increased flapping at the higher airspeeds. During the initial phase, flight testing was conducted without the landing gear fairings and the upper portion of the tail rotor pylon cowl. Omission of the tail rotor pylon cowl was necessitated by installation of the tail rotor instrumentation slip ring as depicted in Figure 8.

INTERNAL CONFIGURATION

To offset the additional weight of the YJ-85 engine installation, radio and navigational equipment considered unnecessary for the program was removed, resulting in a flight test gross weight approximating the operational UH-2. The only control system deviation required was a 7 percent change in lateral cyclic stick rigging to offset the shift in lateral center of gravity associated with the jet engine installation. The aircraft fuel system configuration was somewhat modified by installation of higher capacity fuel pumps for the jet engine and the additional internal plumbing required.

II. TEST INSTRUMENTATION

Test instrumentation was installed to record flight test data in the areas of performance, controllability, stability, rotor and airframe loads and aircraft vibrations.

Aircraft instrumentation consisted of a 9-channel telemetry system, a 36-channel recording oscillograph, and a 13-channel 35mm photo panel together with the appropriate sensors for measuring the various parameters.

Locations of the various sensors on the aircraft are depicted in Figures 4 and 5.

Dual instrumentation was required in some cases (e.g., control positions, main rotor flapping, and vibratory loads) to provide simultaneous telemetry monitoring, visual pilot indications, and/or oscillograph recording during the flight.

Continuous telemetry monitoring provided an instantaneous and comprehensive assessment of pertinent aircraft loads and vibrations throughout each flight to assure that the levels did not exceed the limits for safe operation.

During flights made to define the stall boundary and limiting airspeeds, main rotor blade tuft behavior was recorded on a hub mounted motion picture camera.

As part of the original design of the jet engine installation, an attempt was made to provide a means of determining engine thrust by the direct measurement of strain in the links providing fore and aft restraint. As testing proceeded, however, it was found that the influence of engine compartment temperature resulted in a shifting of the strain gage null data. An alternative method of thrust determination, based upon engine performance data relating compressor discharge pressure (CDP) to thrust, was used. An indicator was installed on the pilot's YJ-85 instrument panel, as shown in Figure 7, to provide a direct indication of thrust from compressor discharge pressure.

Accelerometers were used primarily to measure the accelerations of the aircraft and YJ-85 jet engine. Additional velocity pickups were incorporated on the YJ-85 engine to determine its displacement and resultant mode shape to supplement the vibration data recorded in this area.

General views of the instrumentation installation are shown in Figures 10, 11, and 12. Figure 13 shows the Kaman Telemetry Ground Station.

CALIBRATION

All instrumented items were calibrated in the laboratory prior to installation on the aircraft. Preflight and postflight calibrations were made for all oscillograph and telemetry recorded items with periodic calibrations of all visual and photo panel aircraft instruments. All data presented herein are corrected for instrument and installation errors.

III. GROUND TESTS

Prior to the tie-down ground testing of the aircraft, proof loading and vibration tests were conducted to establish the adequacy, structural integrity, and dynamics of the design.

STRUCTURAL PROOF LOAD TEST

The YJ-85 engine mounts and associated structure were tested to 100 percent of the design limit loading. An illustration showing the test setup for proof load tests is presented in Figure 9. Proof loading to the design limit revealed no excessive deflections or indications of incipient failure.

Proof loading of the YJ-85 engine air inlet cowling in anticipation of expected air loading was conducted. Loading to an overhang moment of 4500 inch-pounds was conducted, revealing no signs of failure or yielding after removal of the loads.

CONTROLS

Proof loading of the YJ-85 engine control system was accomplished prior to tie-down of the helicopter for functional checks. The operational engine was installed and the control was rigged to the flight configuration. The control system was tested to a simulated jam load condition since operating loads are so low as to be trivial.

VIBRATION TESTS

The vibration tests conducted subsequent to the static proof load indicated that the jet pod supporting structure had adequate stiffness. This testing was conducted with and without vertical support struts. The stiffness change had some effect on resonant peaks above 30 cycles per second but was not noticeable below this frequency. Frequency sweeps indicated freedom from resonance in the vertical and pitching modes at the exciting frequencies normally encountered in flight.

Lateral excitation of the engine produced a significant resonant peak near four per rev of the main rotor as a yaw motion of the engine about a point on the centerline between the thrust links. Subsequent flight experience showed that vibration in this mode was higher than desirable. This was traced to excessive friction in the inboard horizontal link bearing. Reducing this friction substantially reduced the vibratory loads recorded.

Fore and aft excitation of the jet engine showed no resonant peaks at any of the exciting frequencies that may be encountered in flight at the upper end of the main rotor speed range. It appeared that tail rotor excitation at low r.p.m. could cause significant amplification; however, further tests have indicated that this is not a problem.

It is worth noting that the frequency sweeps were extended beyond the frequency ranges investigated to the region which includes compressor speed frequency and that no significant resonant peaks were detected.

TIE-DOWN TESTS

A tie-down test program was conducted and measurements were made of engine vibratory motion in the vertical, fore and aft, and lateral directions at various thrust levels. The results showed acceptably low amplitudes in the measured directions during testing.

Operation in the high temperature environment in close proximity to the YJ-85 engine diffuser case resulted in cadmium diffusion of the bolts securing the engine to the aft mounting blocks. This caused embrittlement of the bolts as evidenced by the presence of hairline cracks in the radius between the bolt shank and head. Satisfactory resolution of the problem was made by removal of all plating from the subject bolts. These bolts were inspected periodically and found to be satisfactory.

During ground testing with high jet thrust, high-frequency vibrations were measured in skin panels and frames on the right-hand side of the aft fuselage in an area aft of the YJ-85 exhaust. These measured vibrations were the result of sonic frequencies generated by the exhaust. Structural inspections were made periodically to promptly indicate any structural problems. Several minor cracks confined primarily to areas having localized panel resonance were found and repaired during the subsequent flight test program. No major structural load path areas were affected.

Based upon the results of the ground and tie-down test programs, reported in Reference 5, it was concluded that:

- The jet pod installation is completely adequate from a static strength standpoint.
- The YJ-85 throttle control system showed no evidence of failure or yielding under static proof loads.
- The cantilevered jet pod support structure is adequate to carry the engine without the added vertical stiffness of the struts.
- Resonant frequencies of the jet pod do not coincide with the major exciting frequencies produced by the helicopter.
- The fuel, lubrication, electrical, and mechanical control systems for the YJ-85 installation are functionally satisfactory for flight.
- Engine compartment temperatures are satisfactory throughout the operating regime.

- Airframe temperatures in the jet wake area were acceptably low in the critical static thrust regime where no cooling air due to forward speed is supplied.

- No discernible effects on the T-58 inlet total pressure as a function of varying YJ-85 thrust were noted.

IV. FLIGHT TESTS

The helicopter, reconfigured with thrust augmentation, was first flown on 26 November 1963. The flight test portion of the program was completed in two phases. Preliminary results of testing were presented following completion of the individual phases as reported in References 4 and 6.

PHASE I

Following the familiarization and shakedown flights, the aircraft was flown to obtain quantitative data on controllability, vibration and aircraft loads through the level flight speed range at zero and idle jet thrust. Required deviations in the lateral cyclic rigging and incidence of the horizontal stabilizer were made at this time. Comprehensive evaluation flights were conducted at selected airspeeds through a full range of jet thrusts within the established UH-2 level-flight speed envelope.

Development of satisfactory engine failure recovery techniques and static stability of the aircraft were investigated in detail during this phase. A total of 28 flights, involving 20 hours of aircraft time, were conducted.

PHASE II

This phase of the flight program explored the operating limits of the present UH-2 rotor system, utilizing horizontal thrust augmentation, as defined by retreating blade stall, compressibility, blade bending moments and vibration. Comprehensive evaluation flights were conducted to investigate rotor behavior and helicopter flying qualities in these areas at various combinations of airspeed, altitude, rotor r.p.m. and power, and jet thrust. During the course of this evaluation, a high-speed flight was made to 188 knots true airspeed (192 knots calibrated airspeed) at a gross weight of 9200 pounds. Consistent with the aims of the program, simulated power failures and recovery techniques were investigated during the envelope expansion.

Flight testing was completed on 10 April 1964, after 47 flights involving 32 hours of aircraft time during this phase. At the conclusion of the flight test evaluation, qualitative flight evaluation of the test vehicle was made by USATRECOM pilots at the Kaman Aircraft Corporation Flight Test Facility in Bloomfield, Connecticut.

The data taken on Phase I and Phase II flights are presented in graphical form in Appendix I.

V. FLIGHT TEST RESULTS

PILOT QUALITATIVE EVALUATION

The jet-augmented UH-2 helicopter handles nicely at high speed with a feeling of solidity throughout.

The YJ-85 engine was started on the ground, in hover, and at various airspeeds with negligible attitude changes noted as a result of jet thrust developed at idle.

A slight but noticeable shuffle or yaw kick can be felt as the helicopter becomes more nose-up while under jet thrust with reduced main rotor power. This characteristic is similar to a standard UH-2 in a partial power descent. The airflow and general aircraft attitude are quite similar in these conditions. At 100 knots with 2200 pounds jet thrust and the T-58 at idle, a 9-degree nose-up attitude was recorded. Although the helicopter is slightly more sensitive to control in pitch and roll in this condition, it presented no handling problems.

Overall vibration levels are acceptable and relatively low up to within 5 knots of limiting test points flown.

The auxiliary jet alone sustained the helicopter in level flight near 110-115 knots with a resulting needles split rotor r.p.m. near 92 percent. Both airspeed and rotor r.p.m. can vary somewhat as a function of gross weight and ambient conditions.

The maximum level-flight speed attained during the flight program was 188 knots true airspeed. Rates of climb in the order of 5000 feet per minute at a 9300-pound gross weight were seen using full jet thrust and maximum continuous rotor power.

Controllability of the jet-augmented helicopter is good and compares closely to the standard UH-2. Adequate control margins as specified in MIL-H-8501A remain through all phases of flight. Without thrust augmentation, the aircraft appears no different except for a slight tendency to hang "right wing low" in a hover and to land right wheel first. As jet thrust is added, at a fixed airspeed, the right pedal required also increases to where at full thrust at 100 knots, 89 percent of total pedal is used to maintain zero yaw. As airspeed is increased at full jet thrust, the amount of right pedal decreases, until at 140 knots only 81 percent of right pedal is required to hold zero yaw.

Simulated T-58 failures, at low jet thrust, are much like those of a standard UH-2. Rotor speed decay following throttle chops at 130 and 140 knots (1 second delay on collective depression) is comparable to a standard helicopter. Due to the horizontal stabilizer angle of attack change, the nose attitude on the test helicopter is easier to maintain during autorotation entry. This aids

in establishing the flare and regaining normal rotor speed lost during the autorotation entry. As thrust is increased on the YJ-85 (and power reduced correspondingly to the main rotor), the rate of rotor r.p.m. decay is much less following a T-58 throttle cut, requiring very little control position change. Satisfactory simulated T-58 power failures were demonstrated up to an airspeed of 150 knots.

Simulated power failures of the YJ-85 throughout this program presented no handling problems. The highest point investigated was 163 knots under full jet thrust (430 shaft horsepower on the T-58). Under these conditions, the aircraft rolled to the right approximately 10 degrees, accompanied by a slight nose-down attitude. Adequate time is available for the pilot to return the helicopter to straight and level flight, as no rapid changes of pitch or roll occur. Some yaw was noted, but the rate was relatively slow, requiring no immediate response by the pilot.

Static lateral directional stability was evaluated from trim points of 95 to 160 knots. At 95 knots and lower YJ-85 power settings, plus or minus 15 degrees of yaw was obtained. With maximum YJ-85 thrust at 160 knots, 10 degrees of yaw was attained in each direction. Static lateral directional stability is generally positive; however, there appears to be some small angle neutral stability in yaw which shows up at the higher thrust levels. A yaw rate damper was installed in the final phases of the program to improve the directional stability characteristic. This proved to be 100 percent effective and eliminated the only undesirable handling characteristic noted during the test program.

Static longitudinal stability was recorded from trim points of 95 to 166 knots under several YJ-85 thrust conditions. Records were taken in 5-knot increments to 15 knots each side of trim except at the highest airspeed as limited by the stall envelope. The data indicates a fairly flat gradient, as in the standard UH-2, which appears relatively unaffected by varying jet thrust.

STRUCTURAL LOADS AND VIBRATION

Summary graphs illustrating the effect of thrust augmentation on rotor and airframe loads of particular interest and vibration are presented in Figures 15 through 22. The terms flatwise and edgewise used throughout this report are synonomous with flapwise and chordwise, respectively.

Main Rotor Loads

Up to 140 knots, Figure 15 shows that main rotor loads are in good agreement with those measured on a standard UH-2. Increasing airspeed above 140 knots appears to increase the magnitude of the loads, but significant reduction in the rate of increase can be achieved by adding thrust augmentation particularly as limit airspeeds are approached. The effect of thrust augmentation on vibratory hub torque and servo-flap bending is shown in Figures 16 and 17.

Main rotor flatwise bending moments proved to be the most significantly affected, and endurance limits were exceeded as limit airspeeds were approached. However, cumulative fatigue was not excessive, resulting in only a small reduction in blade life as calculated by methods reported in References 7 and 8.

Main rotor hub bending moment, which is directly proportional to blade flapping angle relative to the rotor shaft, depends upon the trim attitude of the helicopter. Figure 18 illustrates the effect of thrust augmentation on the flapping angle, and, since they are directly proportional, it also shows that hub bending moment remains within the endurance limit for all conditions investigated.

Control system loads showed no significant changes resulting from increasing airspeed or thrust augmentation.

Tail Rotor Loads

As shown in Figure 19, the tail rotor flatwise and edgewise bending moments are generally reduced by thrust augmentation as compared to the standard UH-2.

Airframe Loads

Generally, all airframe loads measured were within acceptable limits. Increased jet thrust augmentation resulted in lower levels in most areas measured at the higher airspeeds as represented by data obtained at selected locations on the aircraft.

The horizontal stabilizer edgewise bending levels, shown in Figure 20, exceeded the endurance limit as a limit airspeed was approached at low values of thrust augmentation.

Flatwise bending moments on the horizontal stabilizer remained well below the endurance limit throughout the program.

Vibration

Vibration levels at the pilot seat and the helicopter center-of-gravity (C.G.) are summarized in Figure 21 and 22, respectively. The vibratory levels monitored at the pilot seat were generally between $\pm$0.1g and $\pm$0.2g, which is below the limits specified in MIL-H-8501A, throughout the speed range examined. Pilot seat vibration shows only small increase with airspeed and remains generally unaffected by thrust augmentation. In contrast, the vibration levels at the C.G. tend to increase appreciably with airspeed and are considerably reduced by thrust augmentation at higher speed. Vibration levels presented are the sum of all harmonics.

STABILITY AND CONTROL

Data showing the static directional stability of the test aircraft is presented in Figure 23. Increasing airspeed appears to have negligible effect, while increasing thrust augmentation deteriorates the stability at small angles. At large angles (greater than 5 degrees), stability characteristics improve as the aft section of the fuselage emerges from the blanketing effect created by the nose-up attitude associated with higher thrust augmentation.

Static longitudinal stability appears to be deteriorated slightly with jet thrust; the longitudinal cyclic stick position gradient is nearly flat for small airspeed excursions from trim for all conditions examined as seen in Figure I-29 in Appendix I.

All data points were flown without use of the automatic stabilization equipment (ASE). With ASE engaged, the stability characteristics of the aircraft were positive, with the yaw rate damping of the ASE system completely effective in eliminating the previously noted lateral-directional small-angle neutral stability. Adequate control margins as defined by MIL-H-8501A, remained through all phases of flight as is shown in Figure I-30 of the Appendix.

SIMULATED POWER FAILURE

Sudden power loss of either the T-58 engine or the YJ-85 was satisfactorily demonstrated at various combinations of T-58 power and YJ-85 thrust. These power failure maneuvers were performed in order to familiarize the pilot with the consequences of loss of either YJ-85 or T-58 power and to establish techniques for handling the helicopter in this situation. The speeds and power levels at which power failures were simulated were consistent with the objectives noted above while not requiring the extensive flight program which would otherwise be necessary for build-up to higher speeds.

YJ-85 failure simulations at full thrust were conducted up to 163 knots (TAS) without difficulty. Results are shown in Figure 24.

The nose drops slightly and moves to the right as expected from loss of a forward acting force below and to the right of the helicopter center-of-gravity. The condition is docile, requiring only minor addition of left pedal to correct for yaw, and aft and left cyclic to maintain aircraft pitch and roll attitude. From the results of this testing, it is concluded that no major problems would be expected with a YJ-85 failure at even higher speeds than demonstrated.

Simulated T-58 power failures were examined at several values of thrust augmentation and airspeed. Higher rotor power levels prior to T-58 failure produce more rapid rotor speed decay. As airspeed increases, the allowable decay in rotor speed is reduced, since the blade stall margin is smaller. The condition of maximum T-58 power to the rotor and low jet thrust levels presents no problem, since it is similar to the standard aircraft. At 2320 pounds of thrust and 368 horsepower delivered to the main rotor, no difficulty was experienced at 150 knots, 99 percent rotor speed. A rotor speed decay to 92 percent was recorded. The time history of this T-58 simulated power failure is shown in Figure 25.

PERFORMANCE

Level flight performance is presented in Figure 26 as a function of thrust augmentation and airspeed. The results presented have been reduced to sea level standard conditions in order to utilize as much of the test data as possible taken over a wide range of gross weight, temperature and altitude conditions.

Preliminary flight testing showed higher than normal hover horsepower, which was attributed primarily to increased rotor profile drag due to extensive blade instrumentation and tufting required for most phases of the test program. The level flight performance of the standard UH-2 helicopter, as computed from Reference 11 and shown in Figure 26, includes the effect of the added rotor profile drag. Comparison of these power requirements with those obtained on the test helicopter with no jet thrust indicates that the installation of the jet increases the equivalent flat-plate area of the helicopter by about 6 square feet. Combined with the 16 square feet which has been determined for the standard machine, the total equivalent flat-plate area of the research aircraft is 22 square feet, assuming just sufficient jet engine power to overcome the windmilling drag.

The data shown in Figure 26 have been cross-plotted on Figure 27 to illustrate the effect of net propulsive force on main rotor horsepower. Net propulsive force is defined as the net jet thrust minus the fuselage drag. The point at which the net propulsive force is equal to zero shows the main rotor horsepower required to overcome the main rotor profile drag, to provide the main rotor thrust, and to pull the rotor against the rotor in-plane drag force.

Figure 28 includes thrust horsepower of the jet engine and, consequently, shows the total power required to maintain level flight as a function of thrust augmentation with the exception of losses due to gearboxes, accessory drives, and the tail rotor. This figure illustrates the substantial gains that may be expected using auxiliary propulsion, particularly as speeds are increased.

The information from Figures 27 and 28 is combined in Figure 29 where it appears that auxiliary propulsion sufficient to overcome the resistance of the airframe components is not the optimum operating point. Further power gains may be achieved by supplying somewhat more auxiliary thrust, presumably of a magnitude that minimizes the effect of the rotor in-plane drag force.

The effect of main rotor r.p.m. on main rotor horsepower was found to be negligible. The decrease in main rotor power which would be expected from a decrease in rotor speed is apparently offset by the higher rotor profile drag associated with the increased blade angle of attack at the lower rotor speed.

DEFINITION OF LIMIT AIRSPEED ENVELOPE

One of the principal objectives of this research effort was to establish, by flight test, the limiting airspeed that could be achieved with this aircraft as a function of thrust augmentation at varying density altitude. Theory predicts that significant stall relief may be obtained, for example, by reducing the parasite drag area (or increasing jet thrust). This program was aimed at confirming the theoretical conclusions and obtaining quantitative experimental information on the amount of relief that may be expected.

Figure 30 shows the stall-limited airspeed of the test aircraft as a function of density altitude and thrust augmentation at a gross weight of 8900 pounds and 100 percent rotor speed. The figure is derived from 19 stall-limited airspeed points tabulated in Table I and shown in Figure I-33 of Appendix I corrected to 8900 pounds gross weight and 100 percent rotor speed. The corrections applied on the stall-limit airspeeds, presented in Figure I-34 of Appendix I, are derived from data previously obtained for the UH-2 and appear to be good approximations of the effect of gross weight and rotor speed for the research vehicle.

The results presented in Figure 30 indicate that substantial stall relief may be obtained using thrust augmentation for propulsion. Stall relief appears to be a nonlinear function of thrust augmentation up to the levels tested, becoming more significant as thrust increases. On an average basis, relief in the order of 12 knots per thousand pounds of thrust augmentation was achieved at sea level reducing to about 8 knots per thousand pounds at 7500 feet density altitude.

Included in Figure 30 is the dashed line showing the stall-limit airspeed for the standard UH-2 as a function of density altitude. The change in limit airspeed with density altitude is seen to be

in good agreement with that established for the research helicopter, but there exists a substantial difference in the stall-limited airspeed at a given altitude between the research aircraft with the jet engine off (T_J = 0) and the standard UH-2. Analysis indicates that this difference can be attributed to the additional 6 square feet of equivalent flat-plate area of the research helicopter and to the roughness of the main rotor blades due to instrumentation and tufting. Calculations indicate that the effect of the additional equivalent flat-plate area on limit airspeed is approximately 4 knots at sea level, reducing to about 1 knot at 7500 feet density altitude, and blade roughness is responsible for a reduction of 8 knots. Consequently, it appears that 1200 to 1600 pounds of thrust augmentation is required to compensate for the additional flat plate and the reduced blade stall angle of the roughened blades on the research aircraft.

The limit airspeed points where compressibility was the limiting factor are plotted in Figure 31 to determine the effect of gross weight and jet thrust. Although there is some scatter in the data, the trend indicates that increasing the gross weight will decrease the limit tip Mach number and will result in a limit airspeed reduction in the order of 6 knots per 1000 pounds. This data also suggests that thrust augmentation may be responsible for some compressibility relief. Further, more detailed analyses of these effects are presented later in this report.

The effect of varying main rotor speed on the limit airspeed was examined by conducting a series of flights at a constant level of thrust augmentation (2500 pounds) and approximately 8900 pounds gross weight. Figure 32 summarizes the results of these flights.

Examination of the motion picture records of the tufts on the rotor blade at typical limit points, Figures 33 and 34 reveals large areas of disturbed flow in Cases 1 and 2 on the retreating blade, indicating stall as the limiting factor. In comparison, Figure 35 shows a relatively small region of disturbance for Case 4, eliminating stall as the limiting factor. For Cases 1 and 2, the advancing tip Mach numbers at the limit airspeed were 0.801 and 0.822 respectively; while for Case 4, the advancing tip Mach number was 0.859. It is concluded that Case 4 is limited by compressibility.

The limit airspeed envelope line on Figure 32 can therefore be divided into a stall-limited region for lower rotor speed; compressibility-limited region for the higher rotor speed; and a combination area where both conditions exist at the mid-speed range (96-97 percent r.p.m.) and at which the highest airspeed was achieved.

Figure 36 summarizes the airspeed limits as determined by stall or compressibility at various temperatures. The limits shown apply for a gross weight/σ of 8900 pounds and a limit tip Mach number of 0.86 with 2500 pounds of thrust augmentation.

VI. CORRELATION OF ANALYTICAL AND FLIGHT TEST RESULTS

Calculations for correlation with the flight test results were done with existing digital computer programs, for the fully articulated servo-flap controlled rotor, utilized at Kaman. The correlation between analytical and flight test results is presented in the following discussion.

PERFORMANCE, TRIM AND CONTROLLABILITY

Although these three items represent distinct areas of interest, they are closely related theoretically and it is most convenient to consider them as a group in a discussion of this nature.

The calculated main rotor horsepower at various levels of thrust augmentation for the research vehicle showed good correlation with the test data as shown in Figure I-32 of Appendix I.

Trim correlation, which is specifically represented in terms of main rotor longitudinal flapping and fuselage attitude, is summarized in Figures 37 and 38. The failure to obtain better correlation of trim parameters is attributed to the uniform rotor inflow assumption used in the analysis, which is probably not representative of actual inflow conditions.

It is pointed out that although trim correlation is not as exact as correlation in other areas, the errors represent minor variations in terms of control, horizontal stabilizer trim loads, and c.g. positions, and are therefore relatively unimportant, in affecting the overall design of a vehicle operating in these flight regimes.

Figures 39 through 41 show the controllability correlation in terms of collective, and longitudinal and lateral cyclic. In general, correlation is good. In all flight conditions investigated, adequate control margins are maintained.

BENDING MOMENT CORRELATION

Flatwise bending moments were calculated, using the airloads and bending moment analyses for the jet-augmented flights in the speed range of 145 knots to 170 knots in increments of 5 knots. Typical comparisons between calculated and flight tests results are presented in Figures 42 and 43.

It is seen from these figures that while the overall levels of calculated bending moments show good agreement with test data, calculated levels over the inboard region of the blade are considerably lower than the flight test results. This discrepancy over the inboard region can be mainly attributed to the difference between assumed and actual inflow.

Figure 43 is included to illustrate the effects of operation at a limit airspeed on blade bending moment levels and distribution. It compares the measured bending moments at a limit flight point with the bending moments calculated for the same flight conditions under the assumption that the limit point had not been reached.

FLIGHT SPEED LIMITS

Main Rotor Stall Limits

The UH-2 main rotor employs a NACA 23012 airfoil section for which the stall angle is taken to be 13 degrees. While 13 degrees may be used in defining the theoretical stall boundary, it is suspected that a lower blade section stall angle actually existed due to the additional surface roughness of the blade instrumentation and tufting. In the flight test section of this report, it is shown that the test vehicle stall boundary may be as much as 8 knots below the standard UH-2 boundary. This airspeed increment can be shown to be equivalent to a reduction in blade section stall angle from 13 degrees to 12 degrees.

Main Rotor Compressibility Limits

Two dimensional airfoil data provides important information regarding the operation of airfoils at high Mach numbers. It is noted that force divergence is first manifested in lift, then drag, and finally pitching moment. However, results of full-scale hover rotor whirl tests by NACA (References 13, 14 and 15) indicate that compressibility limits are manifested first by an increase in drag with no noticeable loss in lift.

Flight experience with the jet-augmented UH-2 indicates that the compressibility limit is evidenced by a simultaneous increase in vibration level and main rotor power which would result from drag divergence. It would therefore seem that the limiting factor is drag divergence, although lift divergence effects may also contribute to the increased vibration level.

The high Mach number data of Reference 17 for a 23015 airfoil will be used in this study since it provides a 3 percent increase in thickness ratio deemed appropriate to account for the rough condition of the instrumented blades of the test vehicle.

For this analysis, the drag divergence Mach number is defined as the point where the drag coefficient increases .01 over the subcritical value. This drag divergent relationship to section angle of attack is shown in Figure 1.

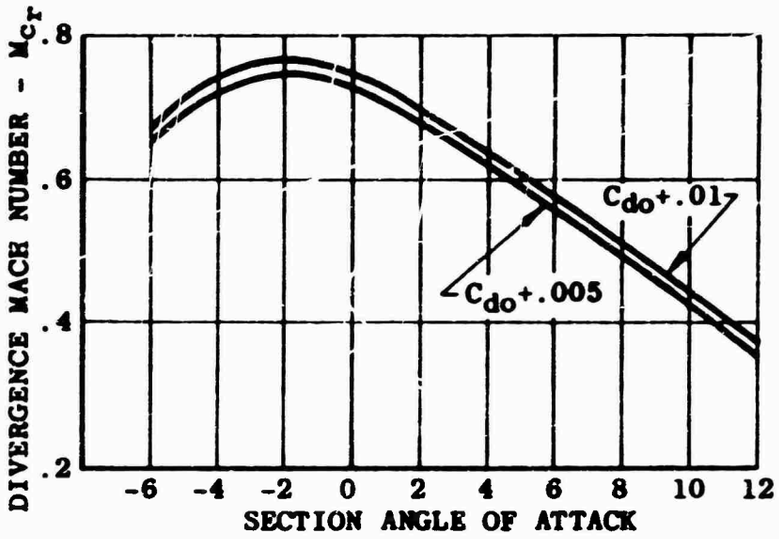

Figure 1. DRAG DIVERGENCE MACH NUMBER FOR NACA 23015 AIRFOIL.

For the UH-2 main rotor blade, the normal Mach number at the 90 percent radius station of the advancing blade is used to define the flight limit conditions where compressibility is the governing factor. This radius station is established by an approximate average of the 87 and 94 percent radius values discussed in References 13 and 19, respectively.

Correlation of Flight Speed Limits

In this study, theoretical stall and compressibility contour plots were constructed for cases where speed limits had been established experimentally. These plots were used to determine the nature of the limit.

Six representative experimental flight limit cases, as shown in Table I, were selected for detailed analysis. Each of these six cases was analysed on the rotor airloads program and angle of attack contours were constructed. Using Figure 1, a drag divergence Mach number was assigned to each section angle of attack contour line. The compressibility boundary is that point on the blade where the local tangential Mach number just equals the local section critical Mach number.

Figures 44 through 49 were constructed to show the blade angle of attack contours and compressibility boundaries for these six case studies. The experimentally observed stall regions discussed earlier in this report are also shown for the appropriate cases.

A. Stall Limited Flight Speeds

Figures 44 and 45 show large areas of the rotor disc where the section angle of attack exceeds 12 degrees but only small areas where compressibility effects would be predicted. Consequently, it is concluded that the limit airspeed is established predominantly by retreating blade stall for Cases 1 and 2. In contrast, Figures 47, 48 and 49 show the angle of attack as less than 12 degrees, but the areas where compressibility effects would be felt appear significantly more extensive. This suggests that the airspeed limit is now determined by compressibility effects rather than by retreating blade stall. These conclusions are in agreement with those reached based on experimental observation and tend to confirm the relationship shown on Figure 32.

Although theory predicts tip stall at high negative inflow ratios, classic tip stall has not been observed in any of the numerous tuft studies conducted on the UH-2. As shown in Figures 33 and 34, the stall which occurs in Cases 1 and 2 does not extend to the tip. In both cases, the stall appears to start at the inboard blade stations and progress outboard to the 85 to 95 percent radius.

It is believed that the above noted discrepancy between theory and test is due largely to the nature of the uniform inflow assumption that is currently used. At present the tip effect is accounted for by terminating lift integrations at the 97 percent radius station, but allowance is not made for this when calculating section angles near the blade tip. It is expected that the recently developed theories which make possible the treatment of wake induced inflow effects (such as Reference 12) will make it possible to produce more exact blade stall predictions. It should be pointed out, however, that although the present inflow assumptions do not lead to the exact prediction of the experimentally observed airload distributions on the retreating blade, they do permit reasonable prediction of rotor stall speed limits.

It is suggested that the high induced velocities in the vicinity of the blade tip (Reference 13), resulting from the close proximity to the strong tip vortex, preclude the occurrence of tip stall. Thus, correlation between theory and test is expected to be reasonable for those conditions where inflow ratio is such as to produce inboard stall but will be less clearly defined for those cases where tip stall is indicated. In the cases where classic tip stall is indicated, it must be assumed that a stall condition is present but that the critical area is shifted inboard since a redistribution of the loading is implied by the nonuniformity of the inflow.

B. Compressibility Limited Flight Speeds

A survey of the compressibility limit points presented in Table I indicates that the critical advancing tip Mach number ranges between .840 and .867 with an average of .852. A certain portion of this spread is expected due to normal experimental scatter, and the remaining portion is due to variations in trim parameters such as gross weight, altitude, rotor r.p.m., and jet thrust.

Referring to standard rotor theory, it can be determined that blade section angles of attack are completely defined by the rotor parameters μ, λ and θ. Since section critical Mach number is defined by section angle of attack, limit rotor Mach number, $M_{.90,90}$ (defined here as normal Mach number at 90 percent radius station and 90 degree azimuth position), would be expected to correlate with μ, λ, and θ, or equally with μ, C_p and C_T.

Following this approach, the compressibility limit points of Table I were expressed nondimensionally as $M_{.90,90}$, μ, $GW/\sigma N^2$, and $MRHP/\sigma N^3$ where N is percent main rotor r.p.m. expressed as a decimal and σ is the density ratio. The latter two "referred" values are proportional to C_T and C_p respectively.

Because of the experimental scatter in the data and the complex variation between limit rotor Mach number and the three independent variables (tip speed ratio, referred thrust, and power coefficients), it was necessary to "normalize" the data statistically in order to evaluate the trends. This was done by establishing the effects of two of the variables on the third and, through an iterative process, correcting all test points to a constant set of conditions. Figure 50 shows the effects of these nondimensionalized parameters on limit rotor Mach number.

An increase in limit rotor Mach number with a reduction in main rotor horsepower is indicated by the test data as depicted in Figure 50. The effect of increasing horizontal thrust augmentation, which reduces main rotor power requirements, is to reduce the area where compressibility effects prevail. This is shown in Figure 51 where the compressibility boundary for the lower thrust level defines a limit airspeed. The reduction in area at the higher thrust level is attributed to the decrease in section angle of attack in the high Mach number regions of the blade. This decrease results in a higher critical Mach number and a shift of the compressibility boundary outboard. Since this shift results in a reduction in compressibility effects, it follows that a higher limit airspeed can be achieved. Thus it is shown analytically that the reduction in main rotor horsepower results in increased limit rotor Mach number, showing good qualitative correlation with the test data.

The trend of increasing limit rotor Mach number with decreasing main rotor thrust shown in Figure 50 is readily understandable upon examination of the blade angle of attack contour plots on Figures 44 through 49. As forward speed is increased, the loading

on the rotor shifts to the fore and aft portions of the disc. It can be seen that the critical area of compressibility at the 40 degree azimuth position is primarily a result of the high section angles that occur in this region. Since these angles are directly influenced by main rotor thrust coefficient, reduction in main rotor thrust level would be expected, within limits, to result in increased limit rotor Mach numbers.

The trend of increasing limit rotor Mach number with increasing tip speed ratio presented in Figure 50 can also be shown to correlate well with analytical study. In examining this trend it is obvious that at a constant rotor r.p.m. this tip speed ratio effect on limit rotor Mach number cannot be realized when the limit airspeed is reached, since, by the definition of tip speed ratio, an airspeed beyond the limit would be required. However, reducing the rotor speed, which also increases the tip speed ratio, permits a higher limiting airspeed than would be obtained from a simple trade-off of rotor speed for airspeed. This can be demonstrated by considering the effect of tip speed ratio on the Mach number loci as typified in Figure 51. It can be shown that the curvature of these lines is reduced by increasing the tip speed ratio. The implications of this can be understood by referring to Figure 2. If it is assumed for simplicity that the lines drawn for low and high tip speed ratio represent compressibility boundaries, neglecting the effect of angle of attack variation, it is apparent that the area of compressibility is greater at the lower tip speed ratio. In the actual case, when blade section angles of attack are considered and the predominant area of compressibility occurs at the 40 degree azimuth angle, the above described effect of tip speed ratio on the compressibility area is applicable.

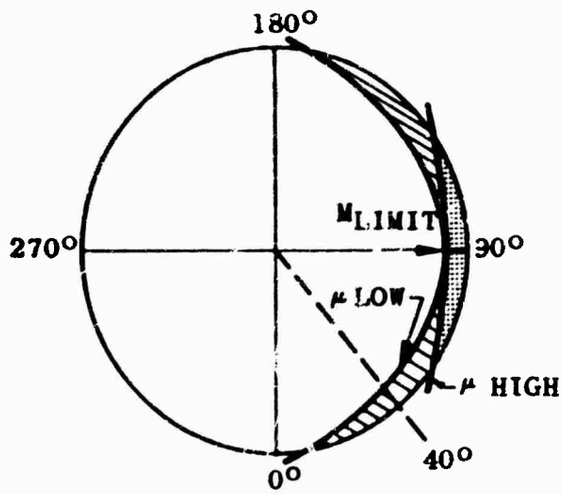

Figure 2. SIMPLIFIED REPRESENTATION OF μ -EFFECT ON COMPRESSIBILITY BOUNDARIES.

Mathematically, the effect of tip speed ratio can be determined by considering the ratio of normal Mach numbers at 40 degrees and 90 degrees azimuth and 90 percent radius.

From

$$M_{X,\Psi} = \frac{\Omega R}{V_c}\left[X + \mu \sin \Psi\right]$$

the following relationship can be derived:

$$\frac{M_{.90,40}}{M_{.90,90}} = \frac{0.9 + \mu \text{ Sin } 40^{o}}{0.9 + \mu} .$$

This ratio can be thought of as a weighting factor that relates the relative magnitude of the compressibility area at the 40 degree azimuth station to that at the 90-degree azimuth. Since the compressibility area at 40 degree azimuth area establishes the limit airspeed, the reciprocal factor (M 9090/M 9040) is a measure of the limit rotor Mach number (previously defined as normal Mach number at 90-degree azimuth, .90 radius) that can be attained at any tip speed ratio. This effect is shown in Figure 3, which indicates approximately a 2 percent rise in limit rotor Mach number in going from a tip speed ratio of .40 to .50. This slope correlates very well with the test data as shown in Figure 50.

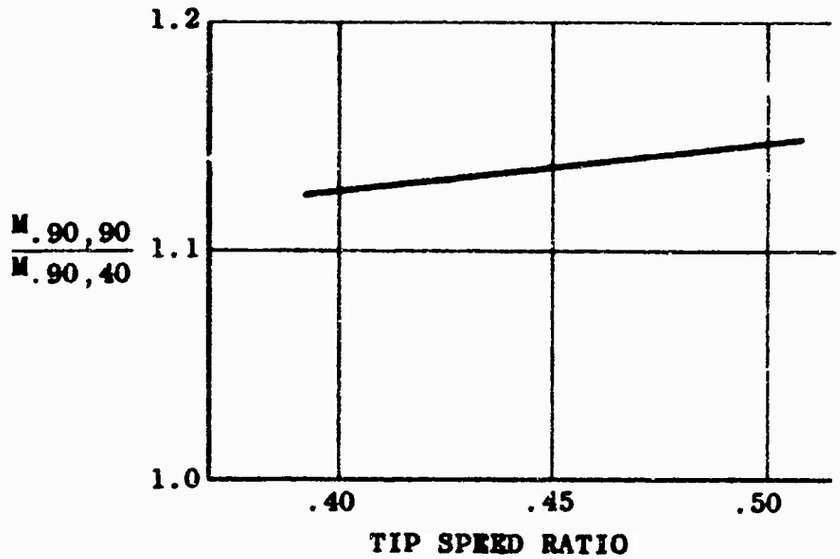

Figure 3. THEORETICAL EFFECT OF TIP SPEED RATIO ON LIMIT ROTOR MACH NUMBER.

In summary, it is concluded that, within the range of variables investigated, there is a trend for increased limit rotor Mach number with reduced rotor power, reduced rotor thrust, and increased rotor tip speed ratio.

From a compressibility standpoint, the optimum trim point for a thrust-augmented helicopter would appear to be at maximum jet thrust and maximum tip speed ratio commensurate with the maintenance of adequate rotor stall margins.

From the above discussion, it becomes apparent that by adding a wing to the research vehicle, it will be possible to obtain higher limit rotor Mach numbers due to the trends in this direction with increased advance ratio and reduced main rotor thrust. The advantages in terms of improved rotor stall margins, which are to a certain extent implied in the above points, are also quite apparent.

BIBLIOGRAPHY

1. Contract DA-44-177-AMC-105(T), June 1963

2. Steinback, J. E., Proposal - Flight Research of a Multi Bladed Fully Articulated Rotor System in the 180-200 Knot Region, Kaman Aircraft Corporation Report R-448, March 1963

3. Thrust Augmented Helicopter - Phase II, Flight Test Agenda, Kaman Aircraft Corporation, December 1963

4. Rita, A. D., and Blackburn, W. E., Summary Report of Phase I Flight Testing of the UH-2 Helicopter Utilizing Thrust Augmentation from a YJ-85 Turbo-Jet Engine, Kaman Aircraft Corporation Report T-395, January 1964

5. Rita, A. D., and Blackburn, W. E., Summary Report of Phase I Ground and Tie-Down Testing of the UH-2 Helicopter Utilizing Thrust Augmentation from a YJ-85 Turbo Jet Engine, Kaman Aircraft Corporation Report T-395-I and II, January 1964

6. Rita, A. D., and Blackburn, W. E., Summary Report of Phase II Flight Testing of the UH-2 Helicopter Utilizing Thrust Augmentation from a YJ-85 Turbo Jet Engine, Kaman Aircraft Corporation Report T-400, April 1964

7. Porterfield, J. D., and Bovenzi, J. F., Vibratory Flight Loads and Frequency of Occurrence - UH-2A/B Rotor Components, Kaman Aircraft Corporation Report S-163, October 1963

8. Porterfield, J. D., and Bovenzi, J. F., Fatigue Life of UH-2A/B Rotor Components, Kaman Aircraft Corporation Report S-164, October 1963

9. Smith, F. L., and Ellis, C. W., Development of a Vibration Absorber for the Kaman Model UH-2A Helicopter, Kaman Aircraft Corporation Report T-367, November 1962

10. Ellis, C. W., and Jones, R., "Application of an Absorber to Reduce Helicopter Vibration Levels", Journal of the American Helicopter Society, July 1963

11. Blackburn, W. E., Results of the Contractor's Performance Demonstration of the UH-2A (Formerly HU2K-1) Helicopter at Patuxent River, Maryland, Kaman Aircraft Corporation Report T-265-1, October 1962

12. Piziali, R., Daughaday, H., and DuWaldt, F., Rotor Airloads, CAL/TRECOM Symposium, Proceedings Vol. 1, June 26-28, 1963

13. Shivers, James P., and Carpenter, Paul J., Effects of Compressibility on Rotor Hovering Performance and Synthesized Blade Section Characteristics Derived from Measured Rotor Performance of Blades Having NACA 0015 Airfoil Tip Sections, NACA TN 4356, September 1958

14. Carpenter, Paul J., Lift and Profile Drag Characteristics of an NACA 0012 Airfoil Section as Derived from Measured Helicopter Rotor Hovering Performance, NACA TN 4357, September 1958

15. Carpenter, Paul J., Effects of Compressibility on the Performance of Two Full Scale Helicopter Rotors, NACA TR 1078, 1952

16. Hoerner, Sighard F., Fluid Dynamic Drag, published by the Author, 1958

17. Graham, Donald J., Nitzberg, Gerald E., and Olson, Robert N., A Systematic Investigation of Pressure Distributions at High Speeds Over Five Representative NACA Low-Drag and Conventional Airfoil Sections, NACA Report 832, 1945

18. Stack, John, and Lindsey, W. F., Characteristics of Low Aspect Ratio Wings at Super Critical Mach Numbers, NACA TR 922, 1949

19. Gustafson, F. B., The Application of Airfoil Studies to Helicopter Rotor Design, NACA TN 1812, February 1949

20. Berman, Alex, A Parametric Analysis Method for Rotor Blade Design, Proceedings of the Thirteenth Annual Forum, American Helicopter Society, May 1957

21. Berman, Alex, "Response Matrix Method of Rotor Blade Analysis", Journal of the Aeronautical Sciences, Vol. 23, No. 2, February 1956

22. Schuett, E., Bellow, B., and Berman, Alex, HU2K-1 Load Analysis of Main and Directional Control Rotors, Kaman Aircraft Corporation Report No. S-113, dated 26 February 1959

23. Gessow, A., and Tapscott, R., Charts for Estimating the Performance of High Performance Helicopters, NACA TR 1266, 1956

24. Crim, A., and Gessow, A., An Extension of Lifting Rotor Theory to Cover Operation at Large Angles of Attack and High Inflow Conditions, NACA TN 2665, April 1952

25. Kaman Aircraft Corporation Report R-553, UH-2 Jet Augmented High-Speed Research Helicopter Maneuverability and Dynamic Stability Evaluation, December 1964

TABLE I
SUMMARY OF FLIGHT TEST LIMIT POINTS

Flt./Rec. No./ No.	Study Case #	Type of Limit (Note 1)	CAS (kt)	H_D (ft)	TAS (kt)	T_J (lb)	MRHP	RPM %	M_T	μ	GW (lb)
50/3		S	83.0	7850	93.5	72	817	93.1	.693	.266	9271
50/4		S	83.0	7900	93.5	75	802	93.7	.697	.264	9261
50/8		S	80.0	7900	90.1	400	566	93.5	.693	.255	9141
50/13		S	89.0	7650	99.9	911	450	92.8	.701	.285	9021
51/4		S	114.0	7500	127.7	72	847	101.2	.796	.334	9030
51/7		S	120.5	7400	134.8	614	773	101.4	.807	.352	8950
51/11		S	121.0	7250	135.0	1239	658	99.4	.792	.360	8770
56/3		S	150.0	4850	161.3	1995	403	101.0	.842	.423	8980
58/2		S	143.0	4750	153.4	1156	831	99.9	.815	.407	9190
58/4		S	149.0	4150	158.3	2048	585	100.2	.829	.419	9050
59/3	(6)	C	145.0	2000	149.2	900	994	101.7	.841	.388	9040
59/7		C	169.5	- 600	168.0	2295	630	100.5	.861	.443	8420
61/1		C	163.0	-2200	158.0	2041	860	100.9	.843	.415	9240
61/2		C	166.0	-2100	161.0	2400	630	101.6	.854	.420	9210
62/3	(5)	C	158.5	250	159.0	1081	1134	101.3	.843	.415	9100
62/8		S	169.5	175	169.9	1832	958	97.2	.832	.463	8660
62/9		C	163.0	550	163.8	1629	1141	99.8	.840	.435	8530
62/10		C	164.0	550	164.8	1648	1146	99.9	.842	.437	8500
62/11		C	182.0	-1400	178.3	2404	806	99.0	.863	.477	8430
63/5		C	150.5	2400	156.8	1872	780	100.7	.841	.413	3790
63/7		C	158.5	2450	164.2	1971	751	101.1	.855	.430	8590
65/4		S	162.5	2950	169.7	2400	498	99.5	.835	.452	8850
68/3		S	142.0	2900	148.1	1286	850	100.9	.836	.389	8944
68/6		C	150.0	2800	156.4	1700	881	101.0	.849	.410	8664
68/9		C	161.5	2350	167.2	2409	412	100.5	.863	.441	8384
69/5	(4)	C	172.0	900	174.1	2479	692	100.3	.859	.458	8801
70/5		S	169.5	650	170.9	2494	609	96.6	.831	.469	8921
71/4		S	165.0	450	166.0	1915	1100	96.8	.779	.454	9151
71/11	(3)	S	178.0	300	178.7	2538	797	96.5	.841	.490	8641
73/7	(2)	S	177.5	650	178.9	2532	686	94.3	.822	.501	8600
74/4		S	165.0	600	166.5	2540	492	92.8	.792	.475	9071
74/5	(1)	S	168.0	600	169.5	2530	447	93.4	.801	.480	9031

TABLE I (Continued)
SUMMARY OF FLIGHT TEST LIMIT POINTS

Flt./Rec. No./ No.	Study Case #	Type of Limit (Note 1)	CAS (kt)	H_D (ft)	TAS (kt)	T_J (lb)	MRHP	RPM %	M_T	μ	GW (lb)
74/8		S	161.0	650	162.3	1590	966	93.0	.790	.462	8881
81/4		C	161.0	650	162.2	1707	1035	100.1	.849	.429	9081
81/7		C	166.0	800	167.8	2280	720	100.7	.860	.442	8931
82/2		C	171.5	900	173.7	2488	535	98.0	.853	.470	9481
82/3		C	169.0	1000	171.4	2483	540	98.7	.853	.460	9301
82/4		C	169.0	1250	172.0	2473	618	98.8	.856	.461	8901
83/5		C	184.0	-1400	180.0	2583	789	97.7	.859	.488	9211
83/6		C	192.0	-1350	188.2	2574	946	97.5	.869	.511	9201
85/2		C	171.5	50	171.7	2527	676	97.9	.850	.465	9551
85/4		C	164.0	2750	169.8	2340	519	98.0	.859	.459	9200
85/5		C	179.0	270	179.5	2502	686	97.8	.861	.486	8500
85/6		C	182.0	300	182.7	2492	725	98.0	.867	.494	8470

Notes:

1. The Type of Limit point listed above is defined as: S = Stall; C = Compressibility.

2. Flights up to 82 were made with main rotor blade S/N 203, 204, 205, 212; succeeding flights were made with blade S/N 135, 154, 155, 156. The latter blades had less blade tufting and consequently were aerodynamically cleaner blades.

3. Flights 61-1 and 61-2 were approaching limit airspeed.

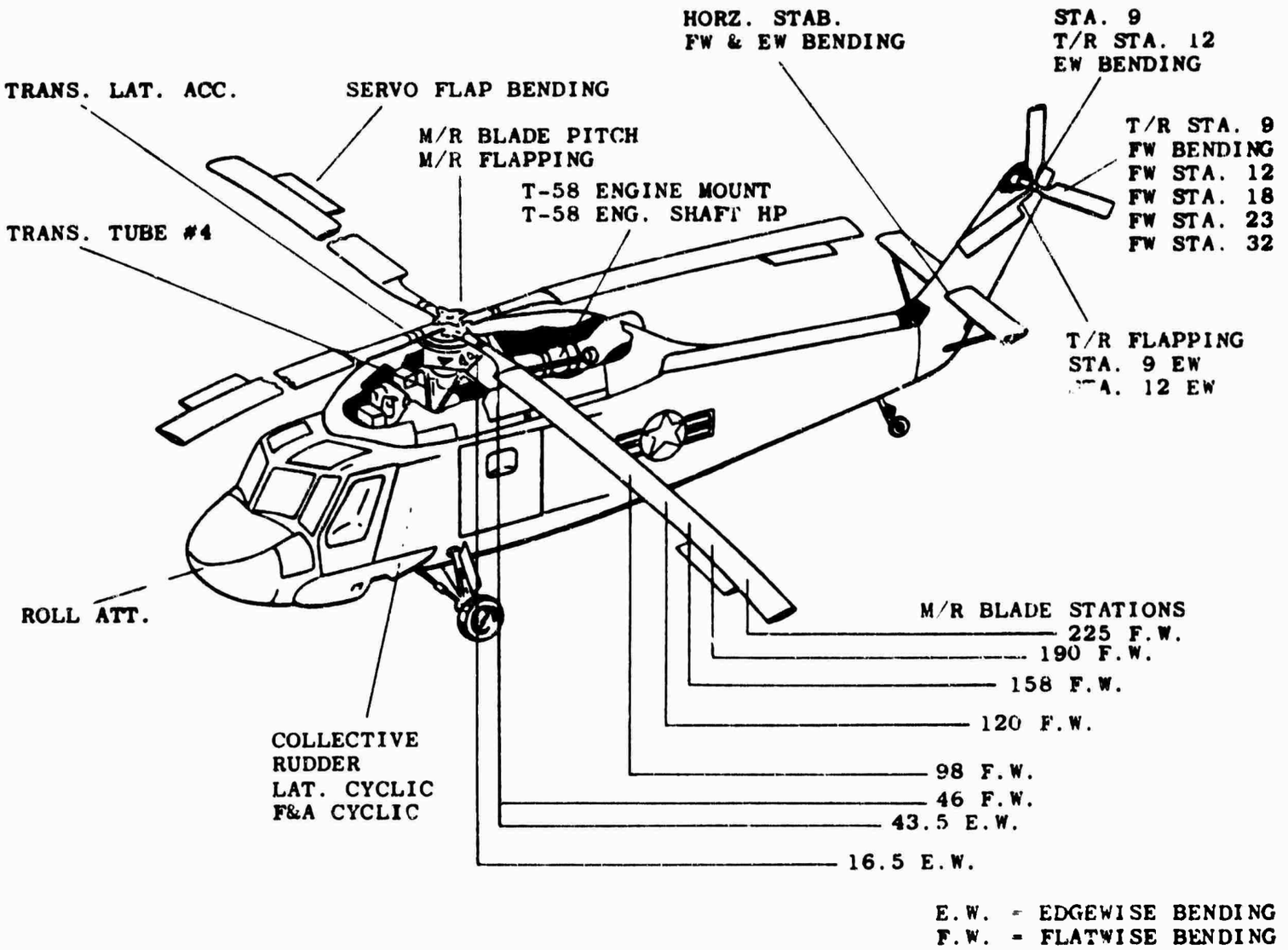

Figure 4. INSTRUMENTATION LOCATIONS

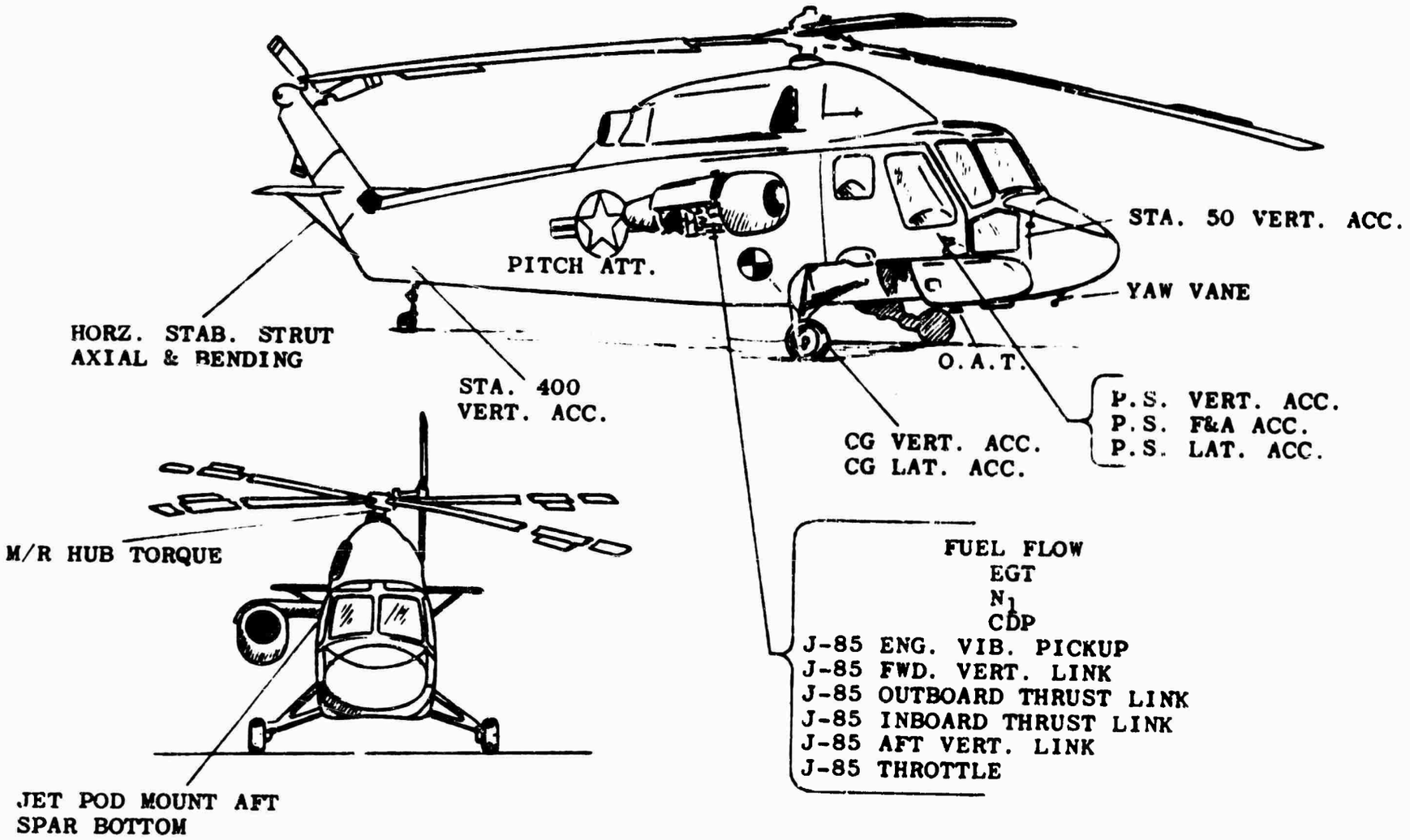

Figure 5. INSTRUMENTATION LOCATIONS

Figure 6. THRUST AUGMENTED UH-2 HELICOPTER

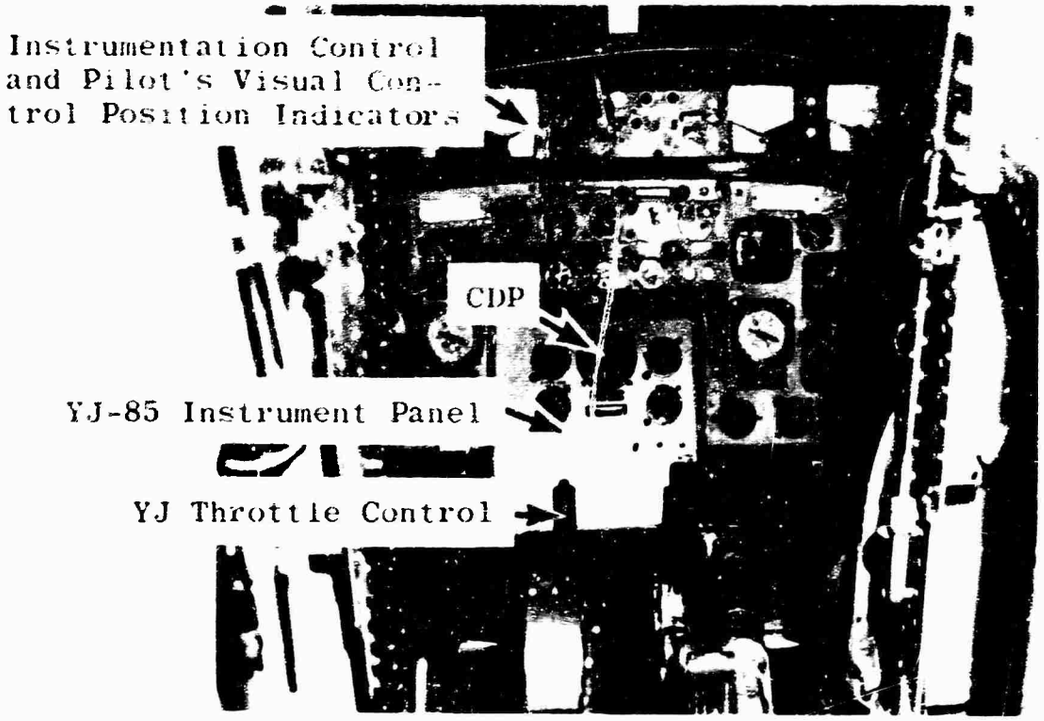

Figure 7. THRUST AUGMENTED UH-2 HELICOPTER COCKPIT INSTRUMENT PANEL AND YJ-85 THRUST CONTROL

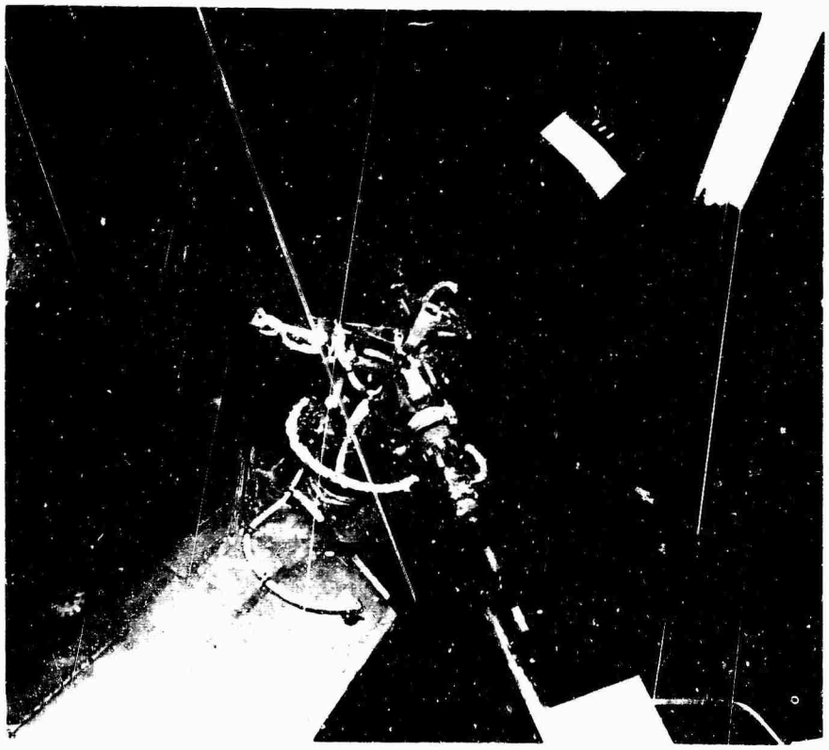

Figure 8. TAIL ROTOR AND ASSOCIATE INSTRUMENTATION

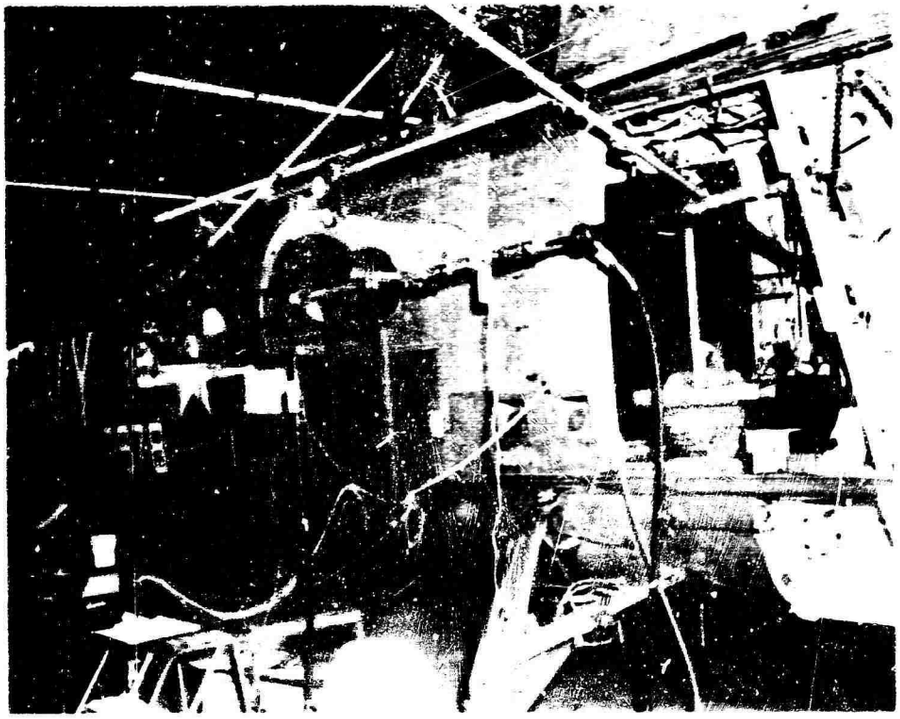

Figure 9. STATIC PROOF LOAD TESTS ON THE ENGINE POD STRUCTURE - 3/4 FRONT VIEW

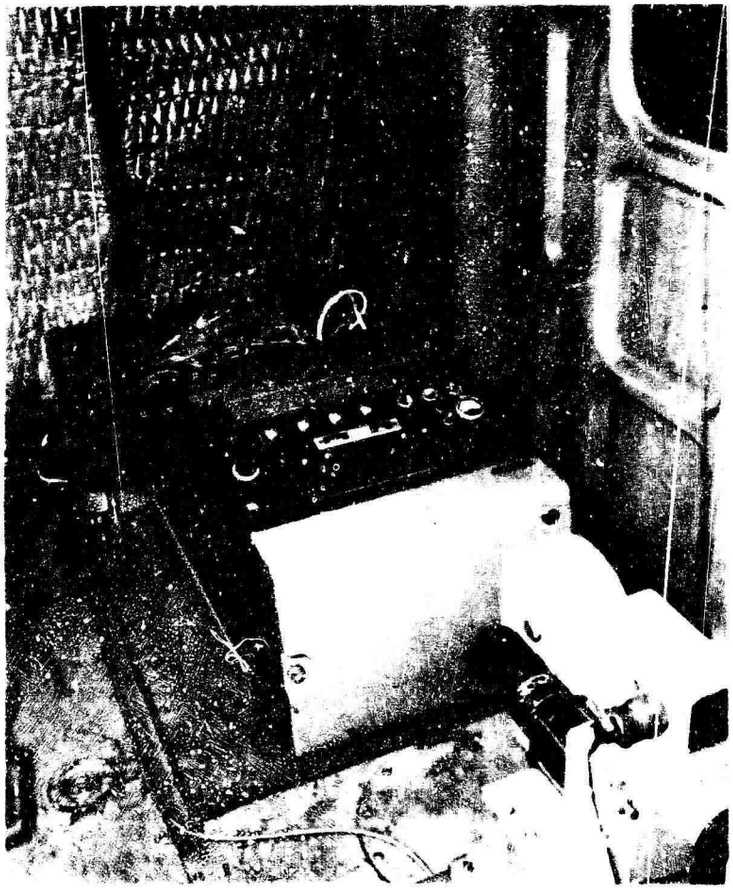

Figure 10. RECORDING OSCILLOGRAPH

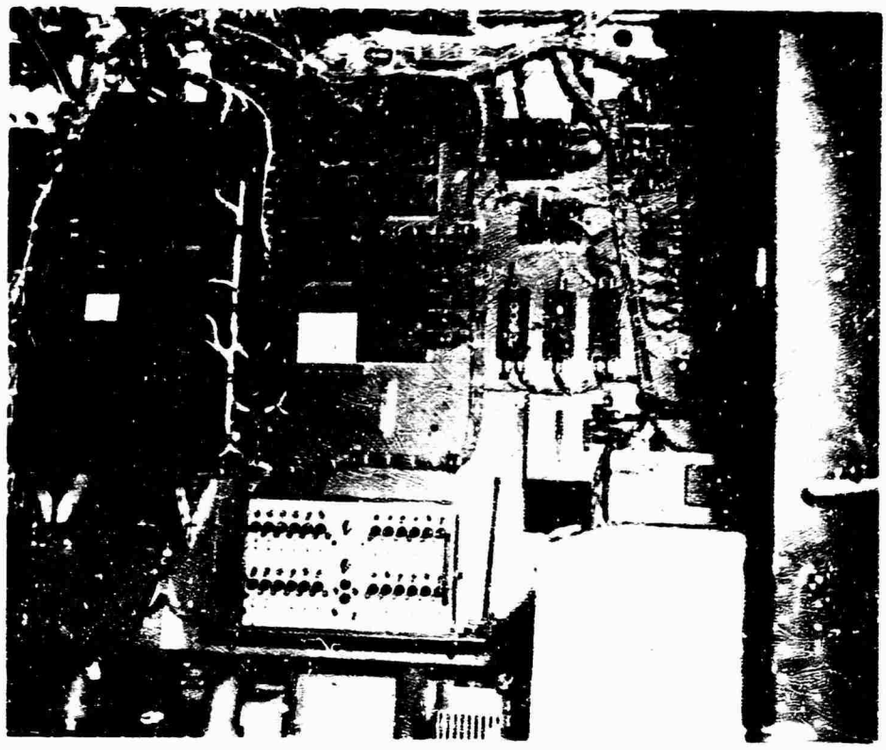

Figure 11. FLIGHT TEST INSTRUMENTATION BOARD IN AIRCRAFT

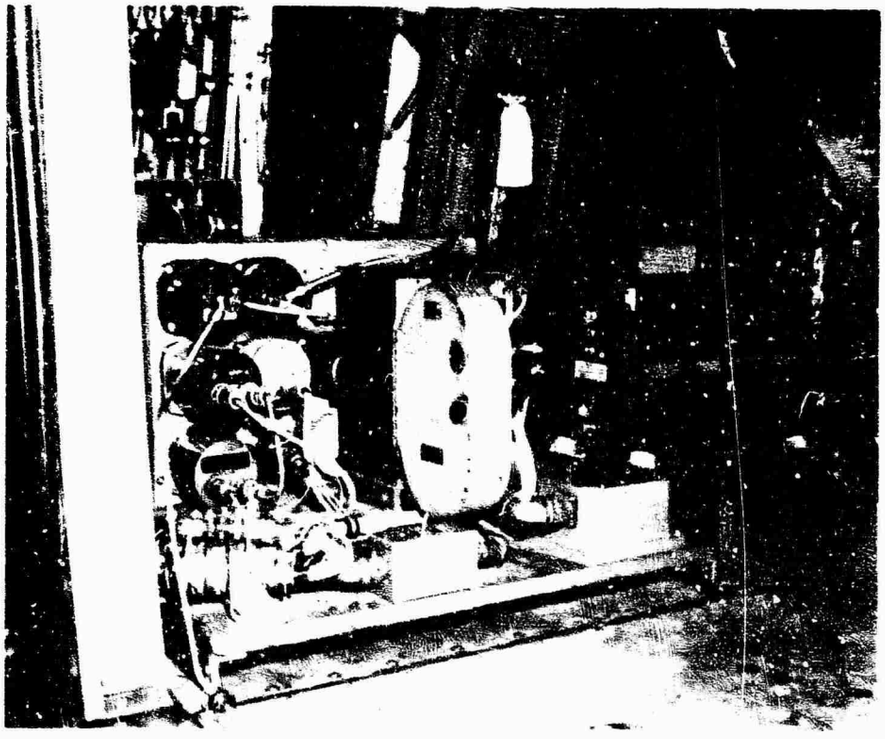

Figure 12. PHOTO INSTRUMENT PANEL

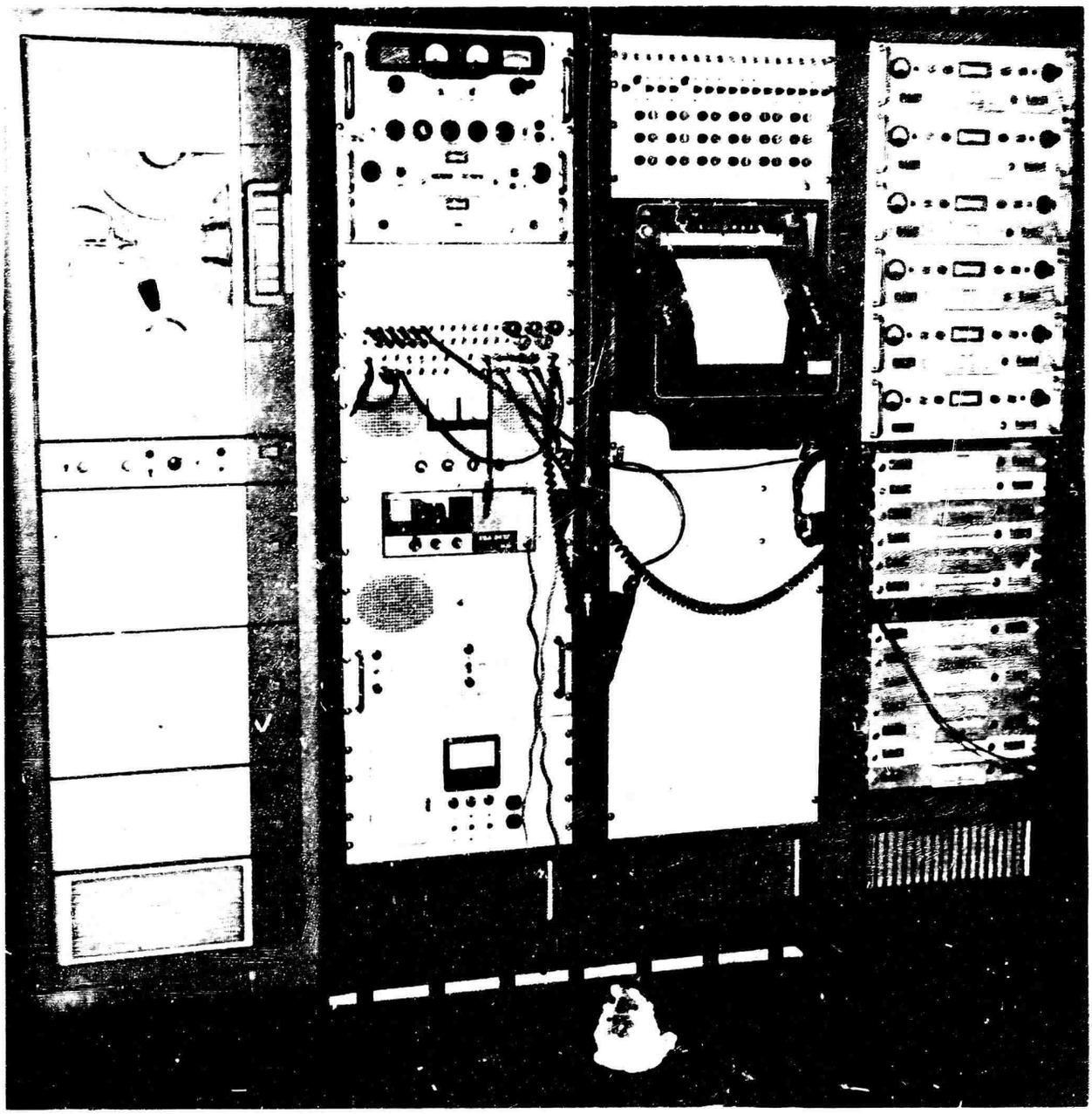

Figure 13. TELEMETRY GROUND CONTROL STATION

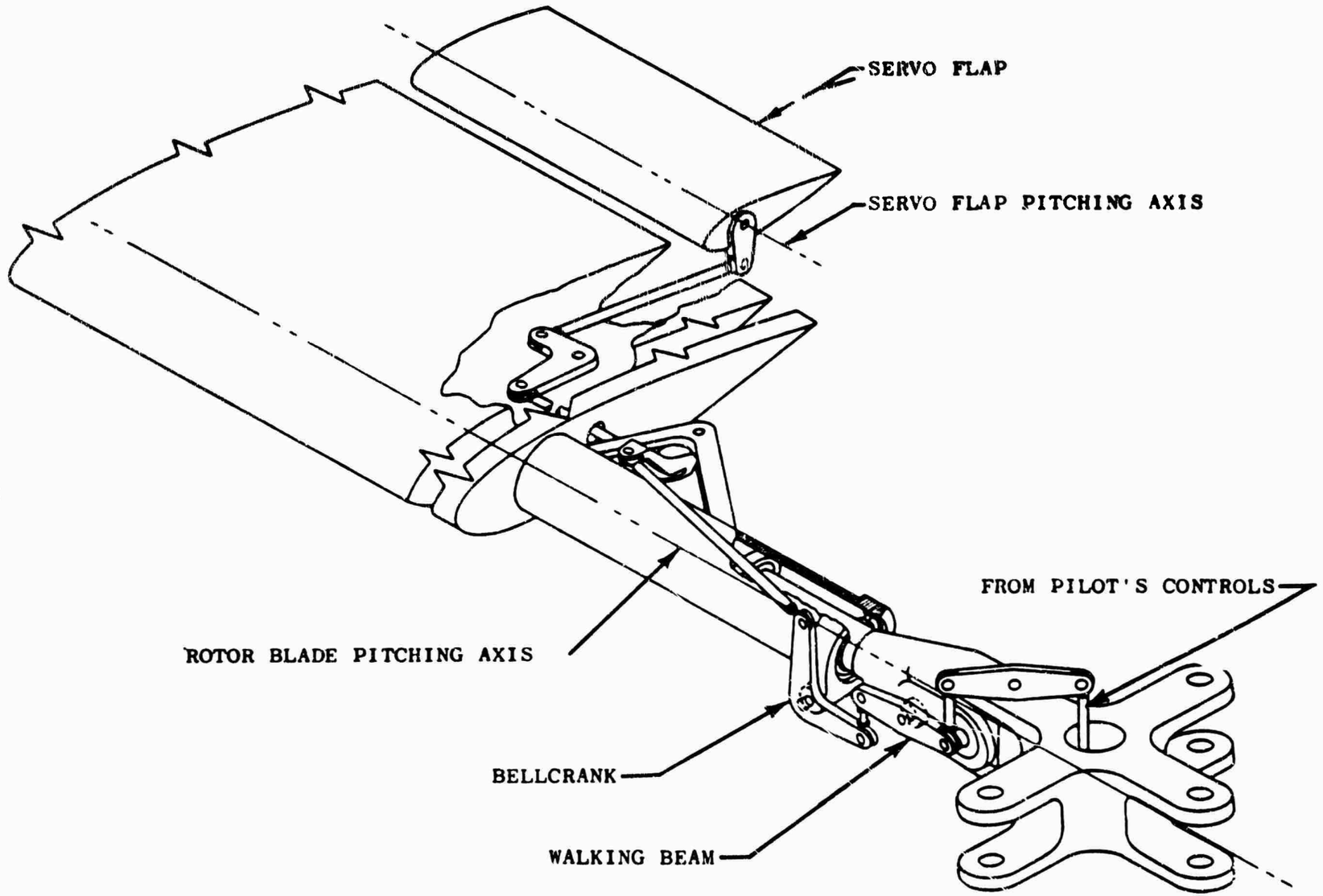

Figure 14. KAMAN SERVO-FLAP ROTOR CONTROL SYSTEM, SCHEMATIC

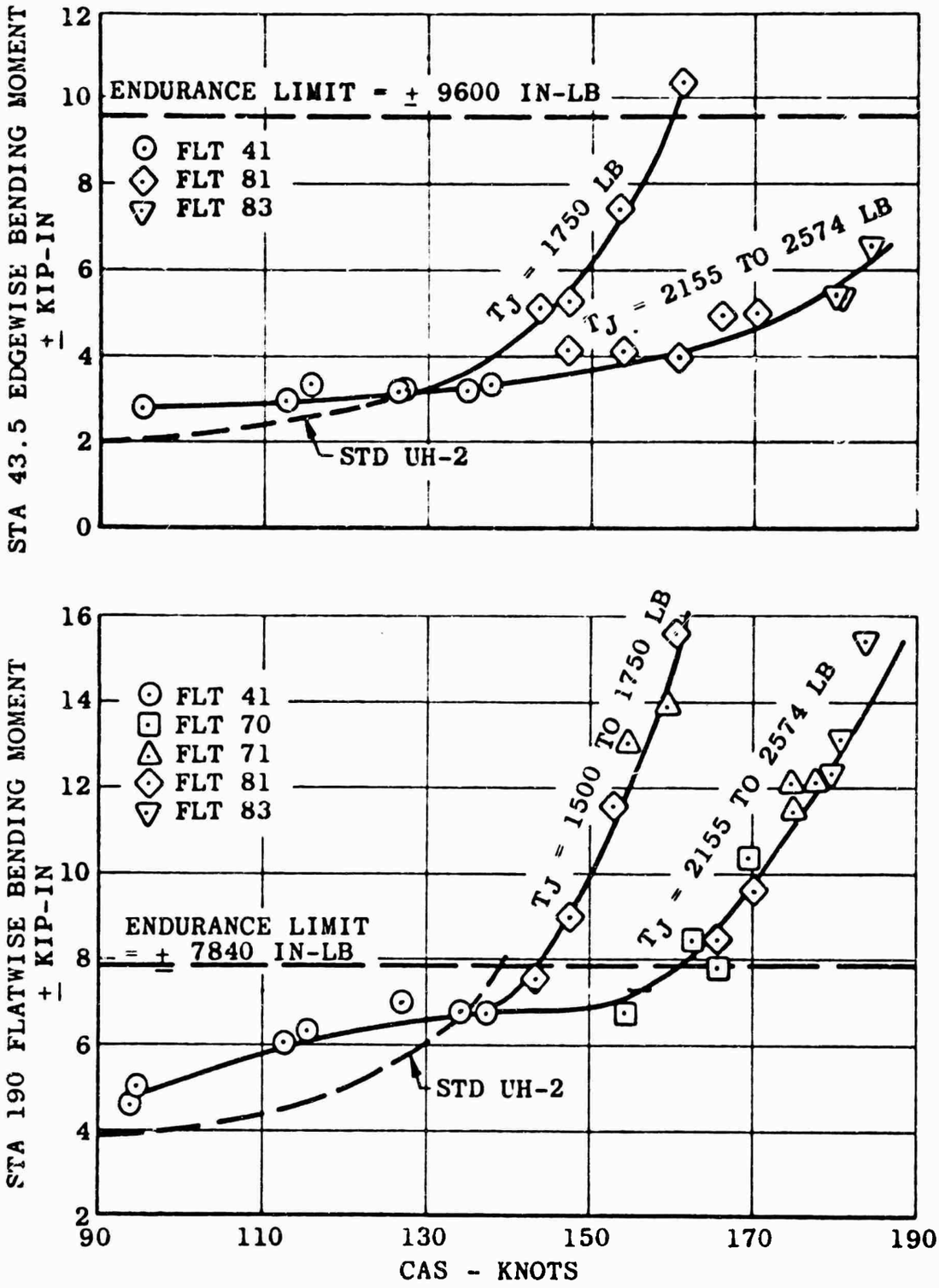

Figure 15. EFFECT OF THRUST AUGMENTATION ON MAIN ROTOR BLADE BENDING

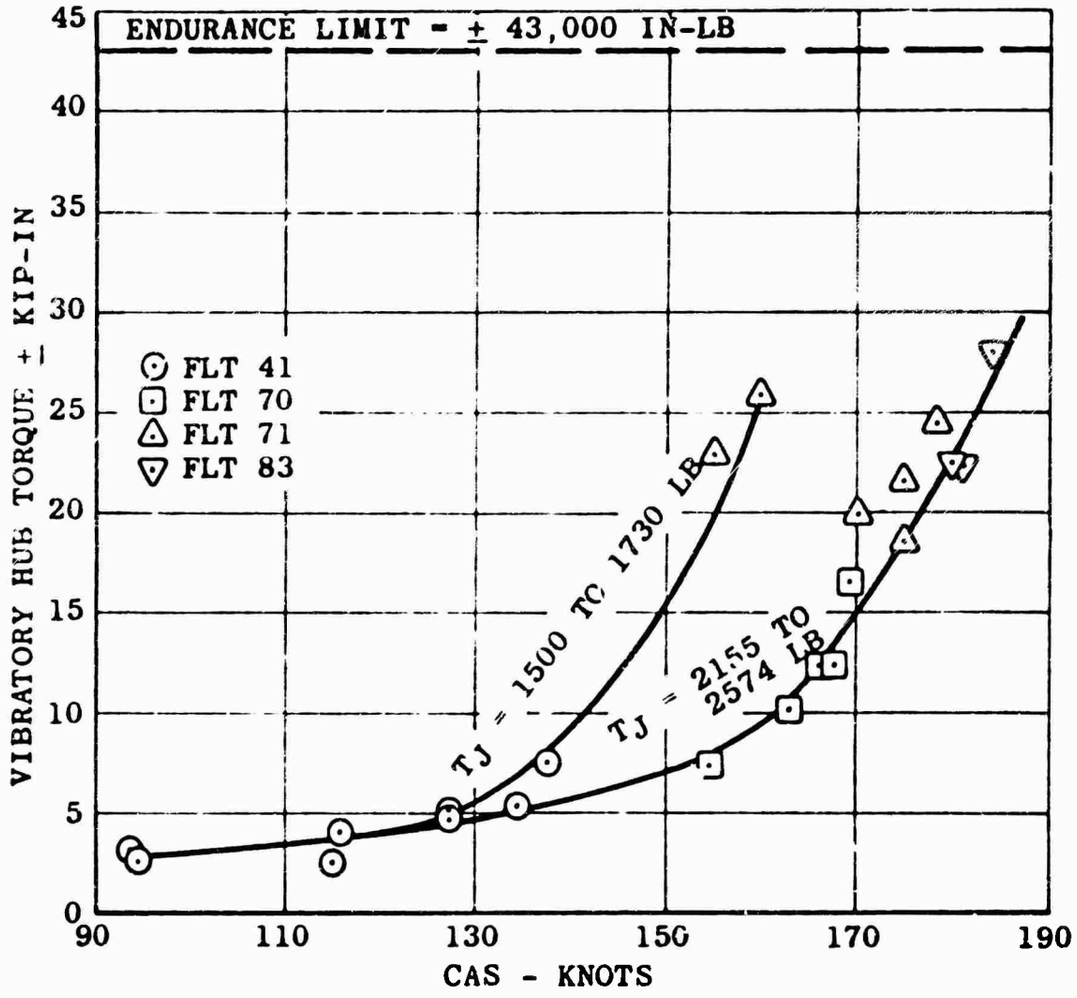

Figure 16. EFFECT OF THRUST AUGMENTATION ON MAIN ROTOR SHAFT VIBRATORY TORQUE

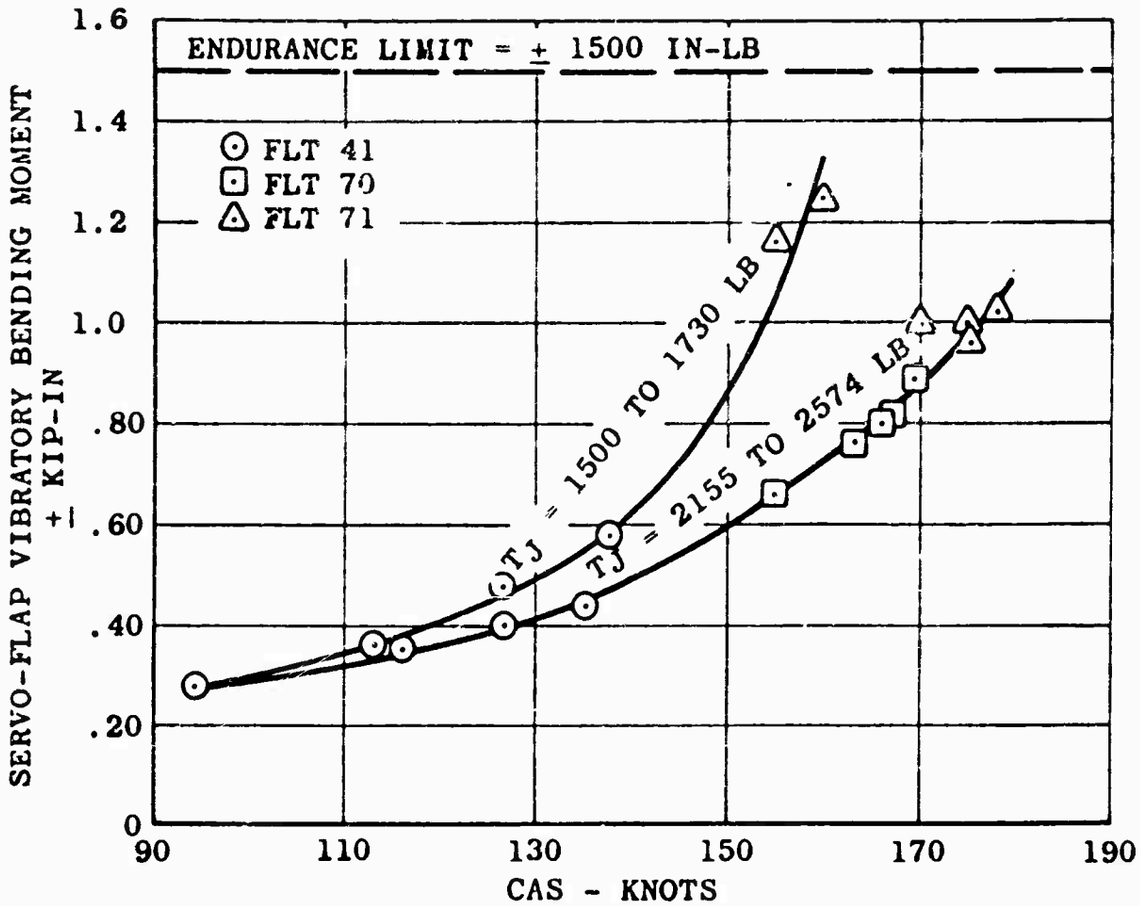

Figure 17. EFFECT OF THRUST AUGMENTATION ON SERVO-FLAP BENDING

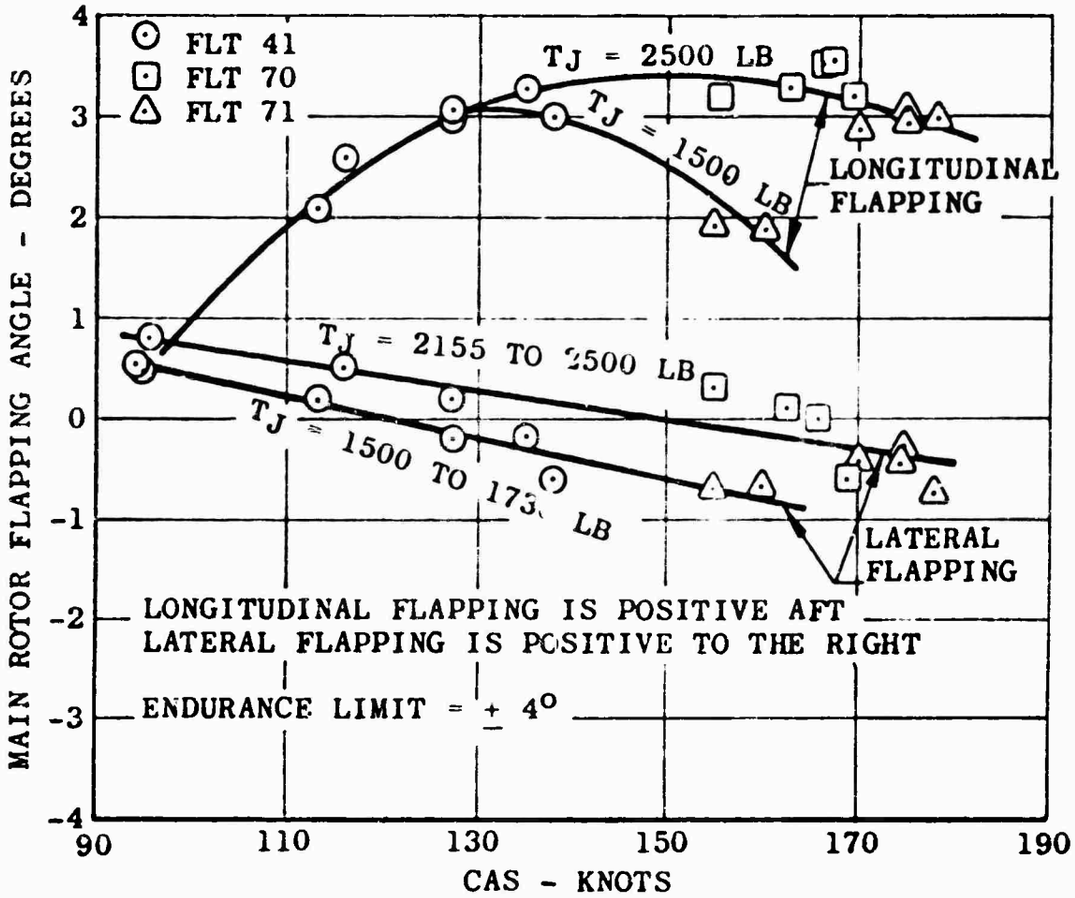

Figure 18. MAIN ROTOR FLAPPING ANGLE RELATIVE TO THE SHAFT AS AFFECTED BY THRUST AUGMENTATION

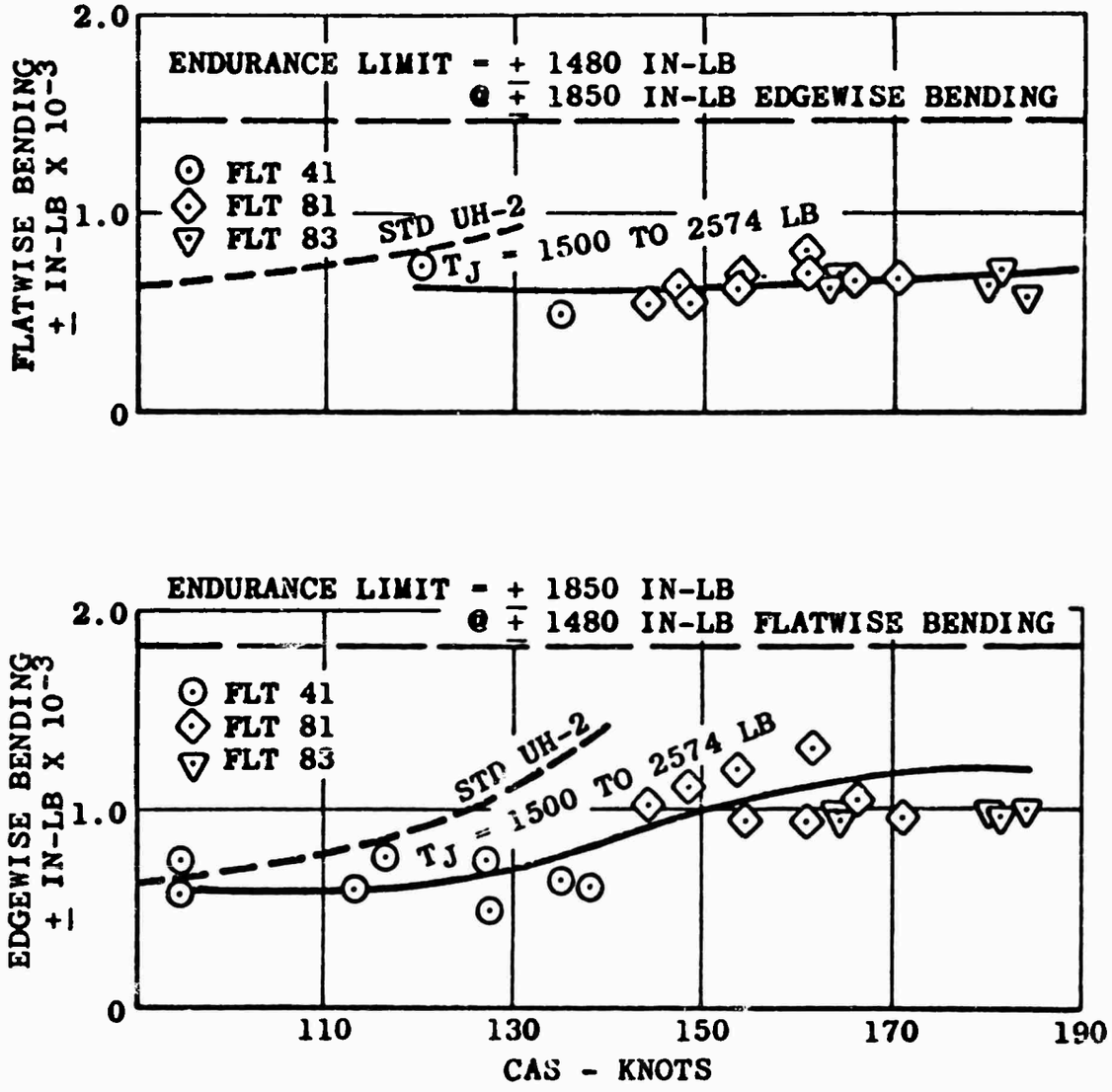

Figure 19. EFFECT OF THRUST AUGMENTATION ON TAIL ROTOR BENDING MOMENT

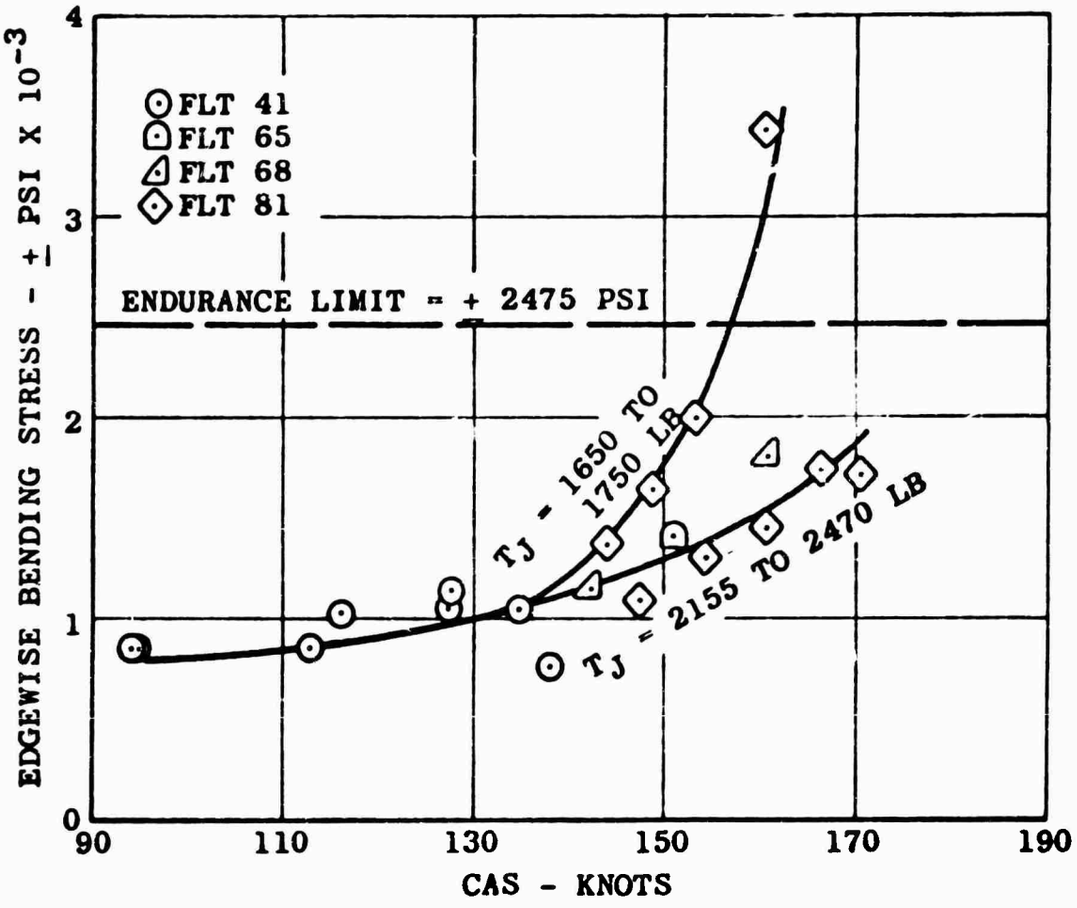

Figure 20. EFFECT OF THRUST AUGMENTATION ON HORIZONTAL STABILIZER EDGEWISE BENDING

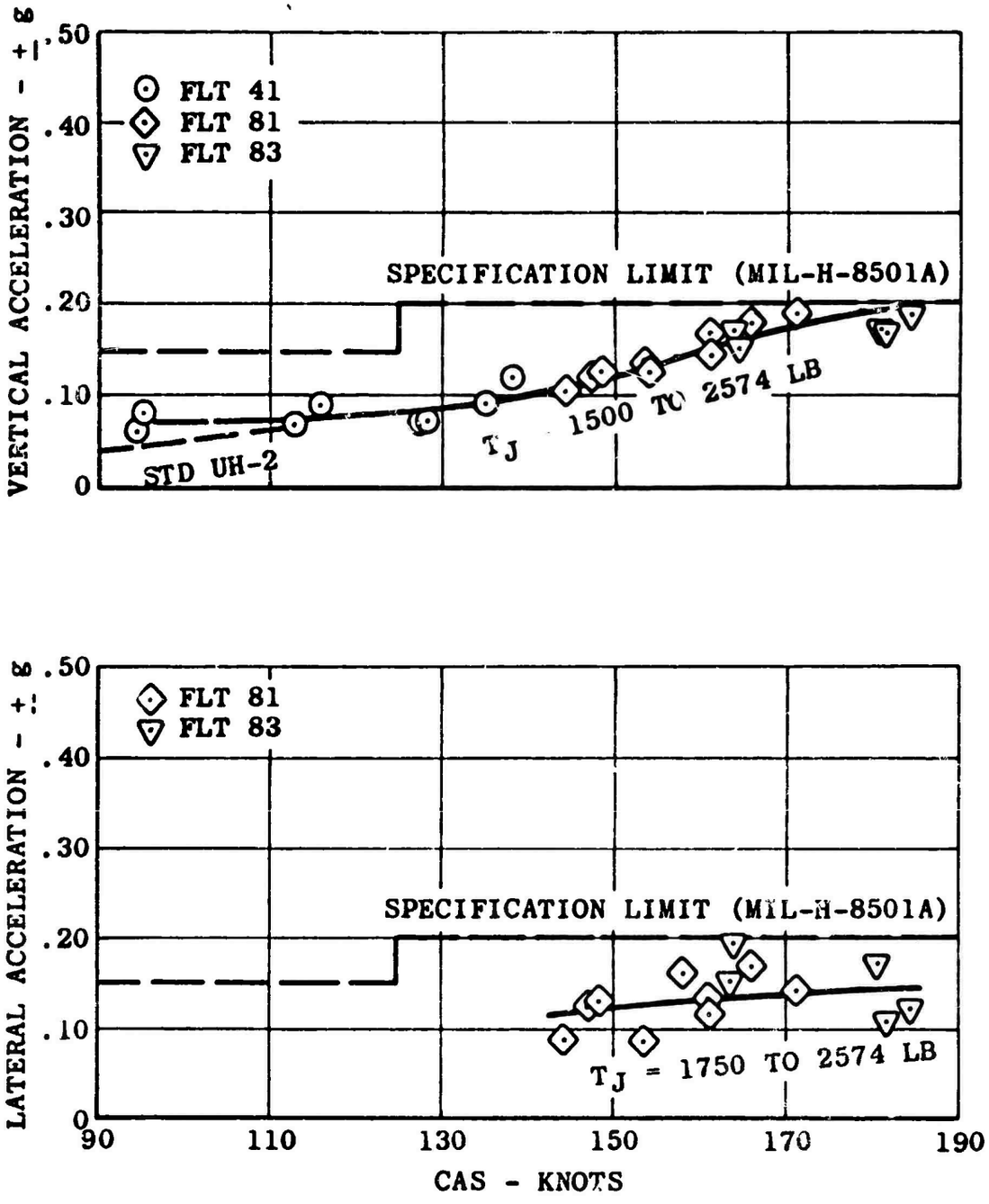

Figure 21. VIBRATORY ACCELERATIONS AT THE PILOT SEAT

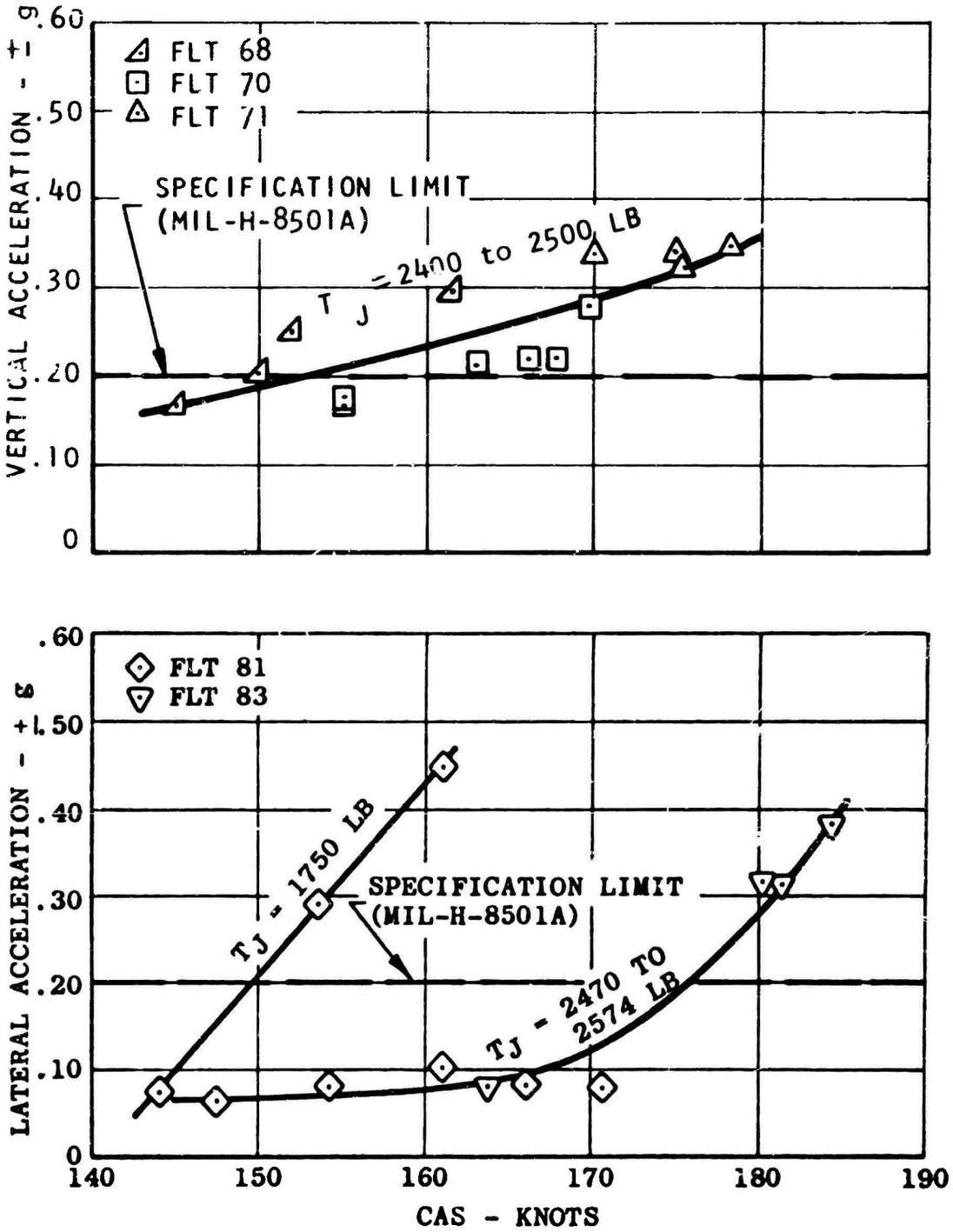

Figure 22. VIBRATORY ACCELERATION AT THE AIRCRAFT CENTER OF GRAVITY

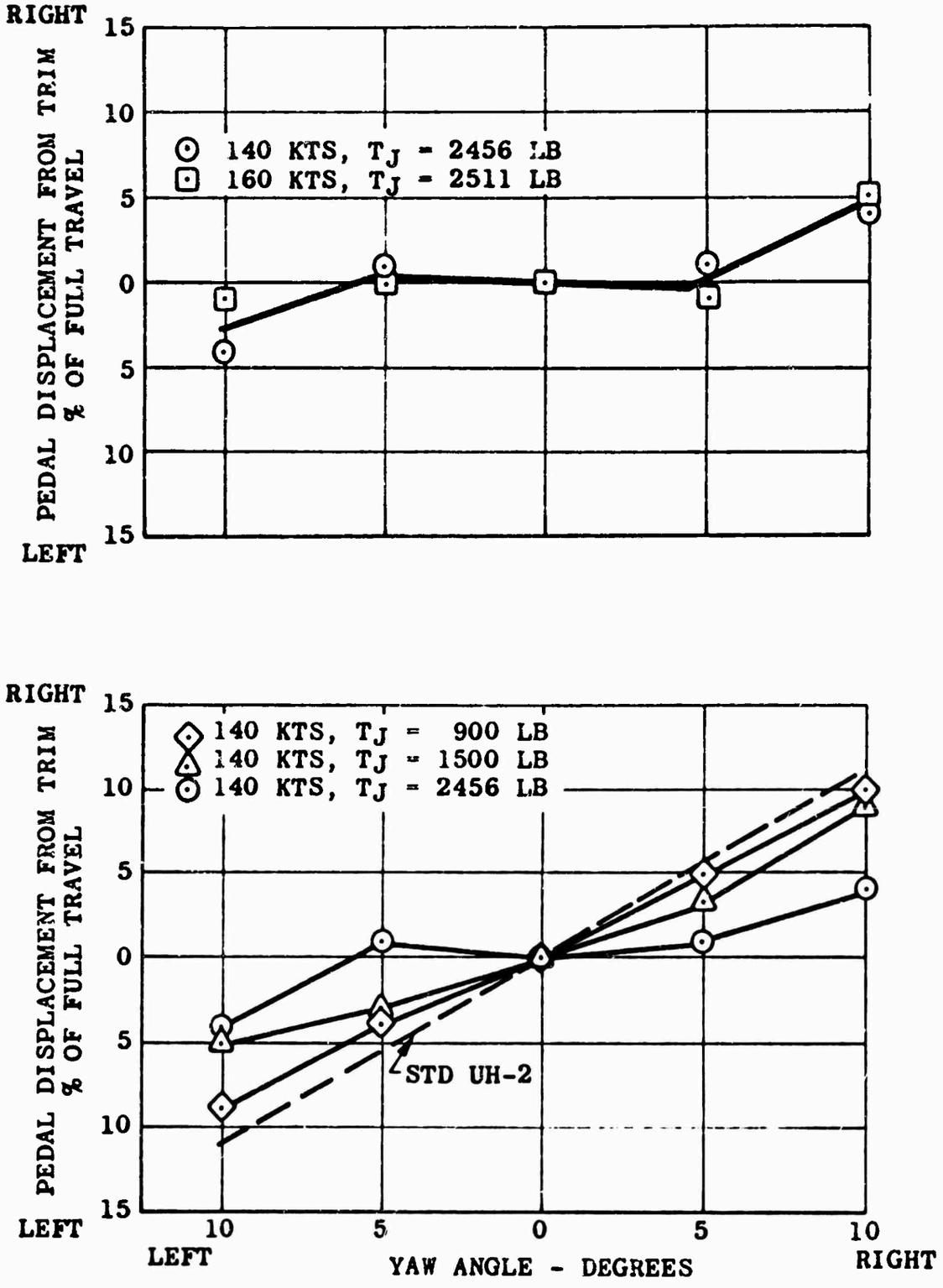

Figure 23. STATIC DIRECTIONAL STABILITY AS AFFECTED BY AIRSPEED AND THRUST AUGMENTATION

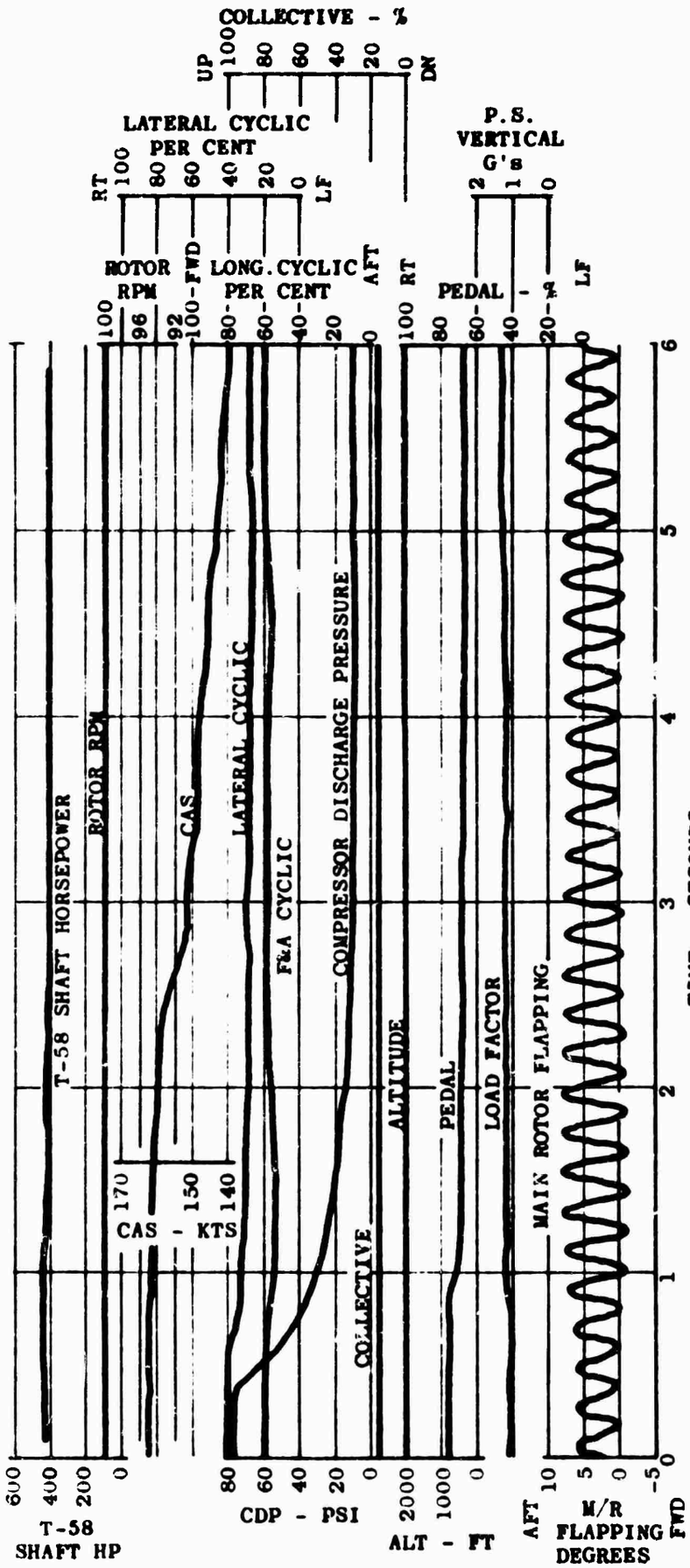

Figure 24. YJ-85 THROTTLE CHOP FROM HIGH JET THRUST (2500 POUNDS) AND 164 KNOTS TAS

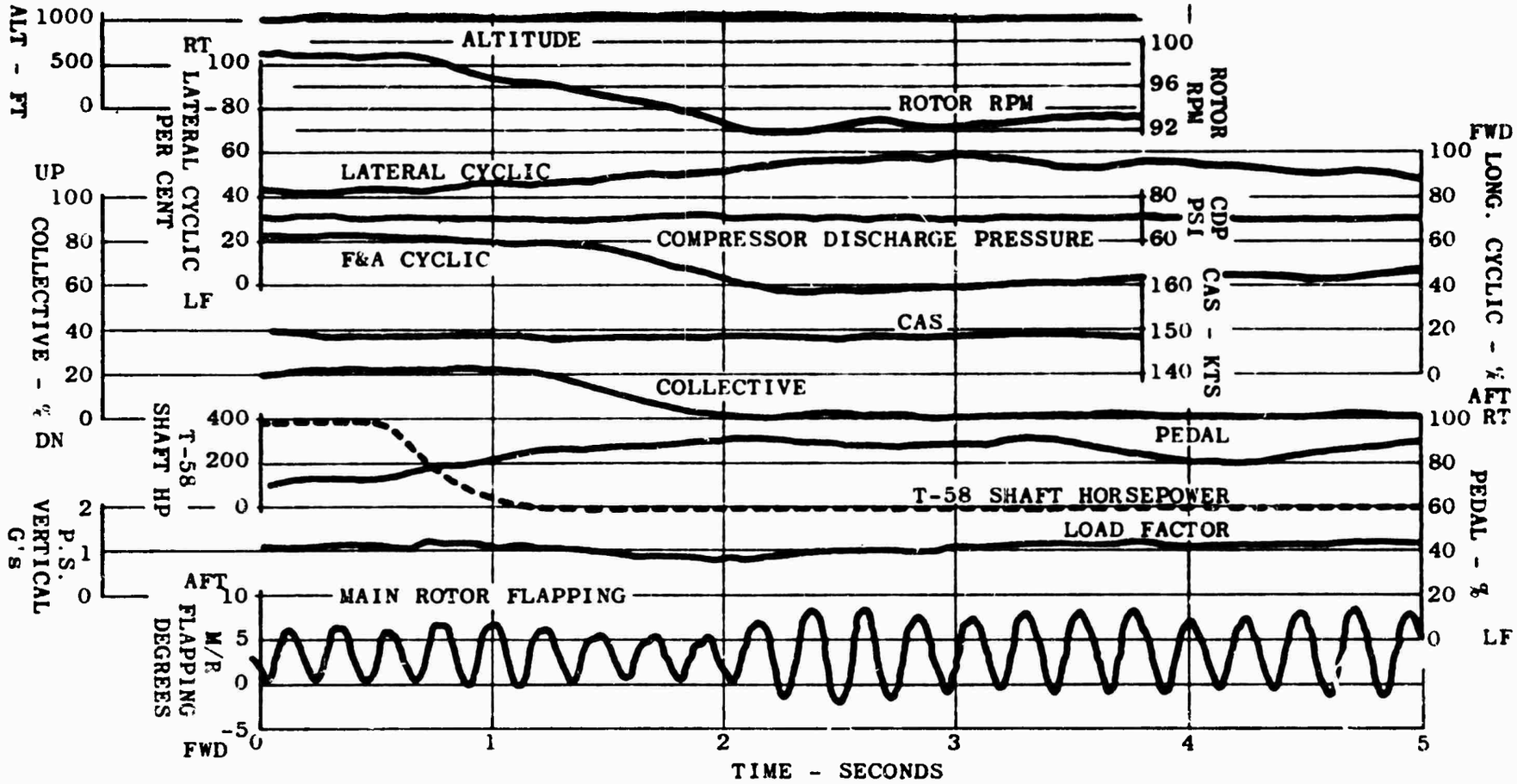

Figure 25. T-58 THROTTLE CHOP FROM 368 MAIN ROTOR HORSEPOWER WITH 2320 POUNDS OF JET THRUST AT 150 KNOTS TAS

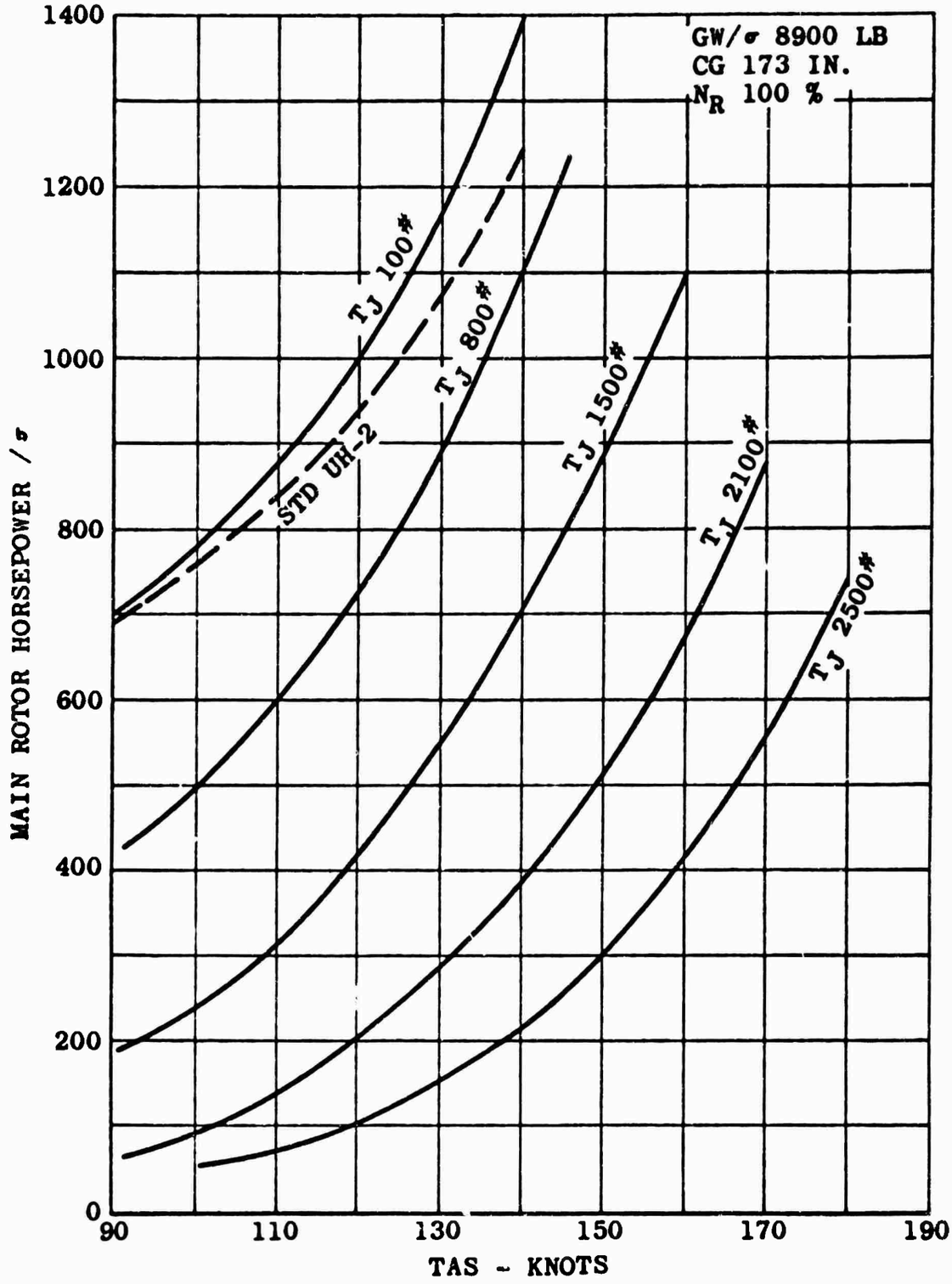

Figure 26. HELICOPTER LEVEL-FLIGHT PERFORMANCE VARIATION WITH THRUST AUGMENTATION

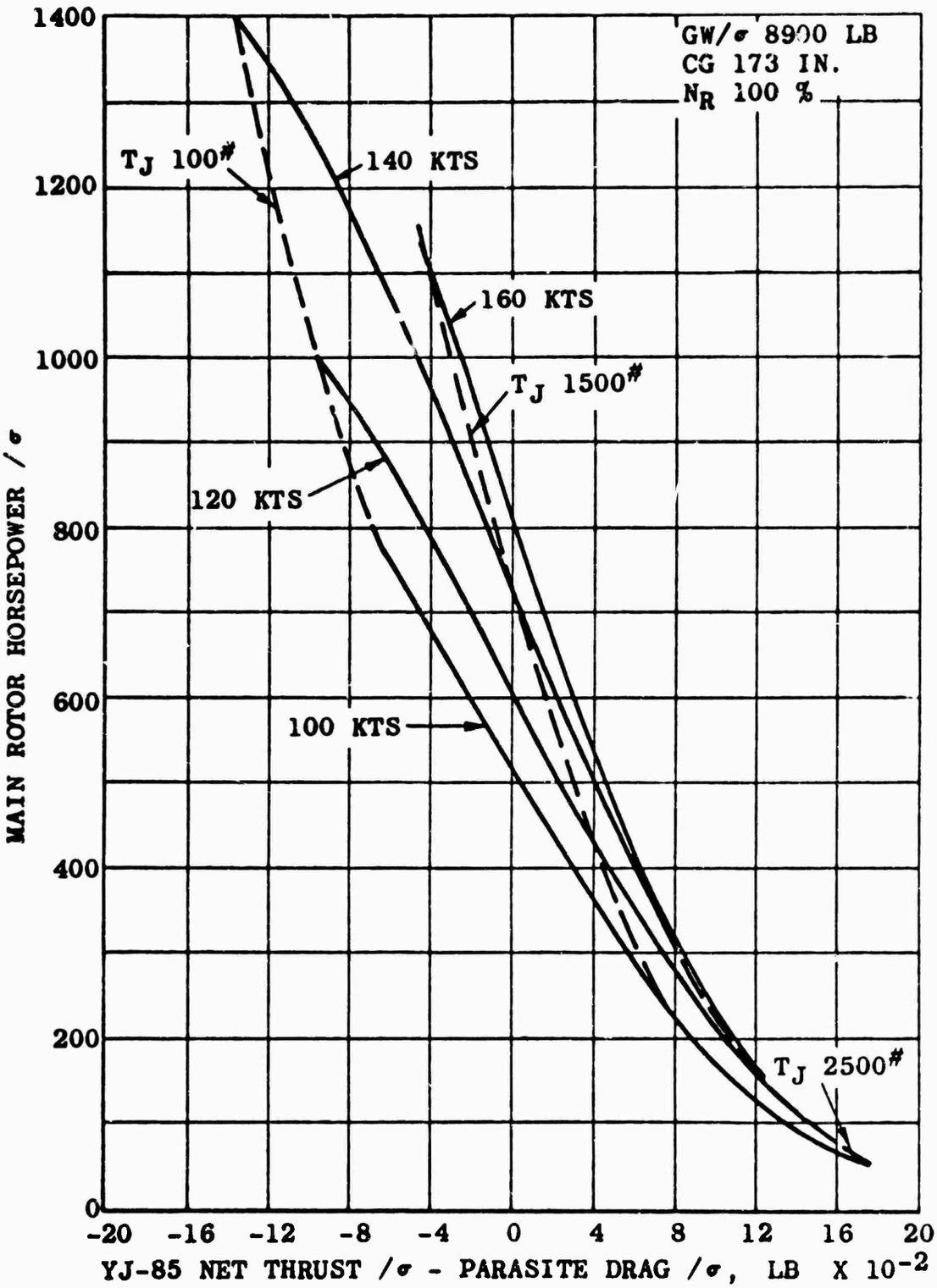

Figure 27. EFFECT OF NET PROPULSIVE FORCE ON MAIN ROTOR HORSEPOWER REQUIRED

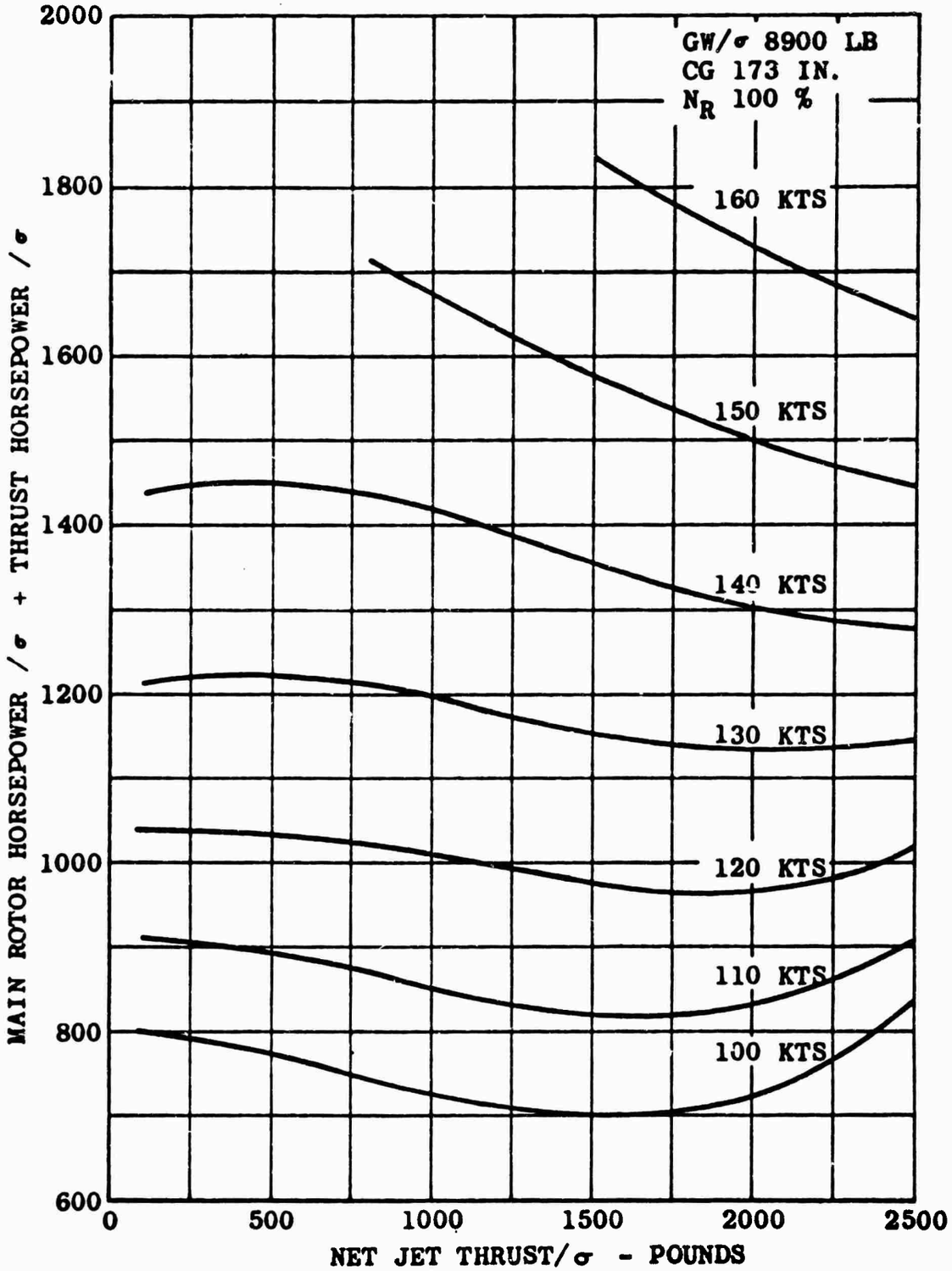

Figure 28. HORSEPOWER REQUIRED FOR LEVEL FLIGHT AS AFFECTED BY JET THRUST

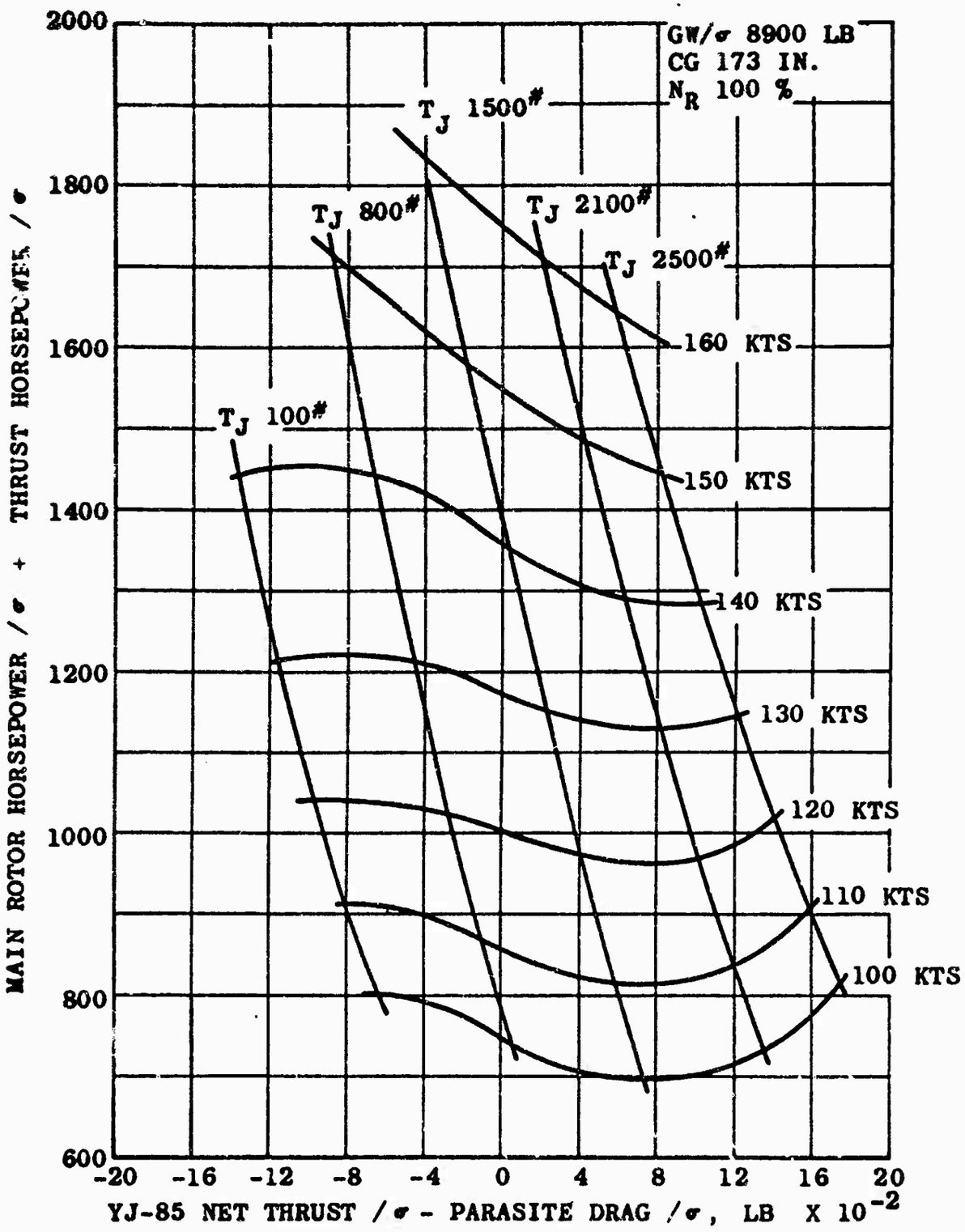

Figure 29. EFFECT OF NET PROPULSIVE FORCE ON TOTAL HORSEPOWER REQUIRED

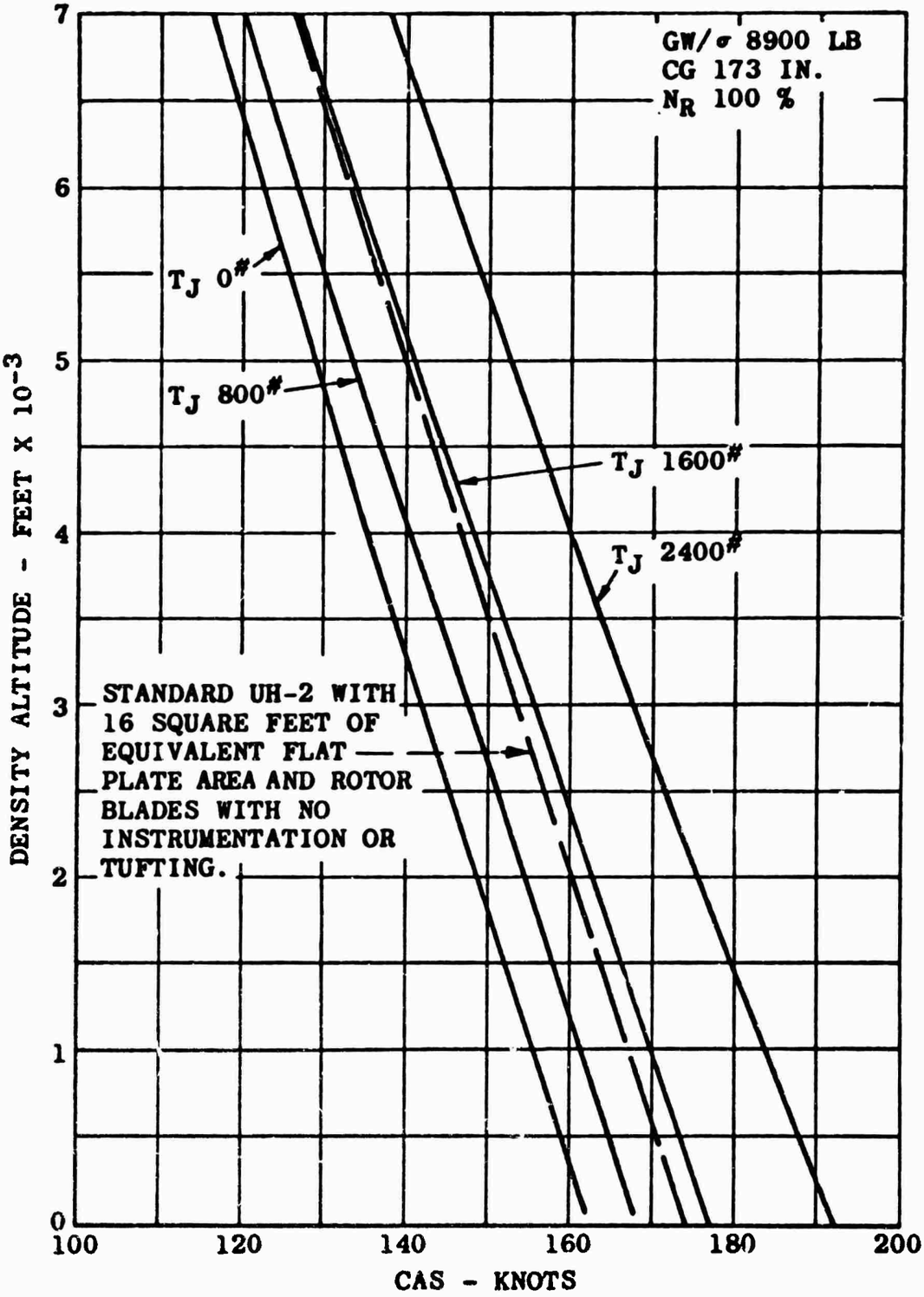

Figure 30. STALL LIMIT AS AFFECTED BY DENSITY ALTITUDE

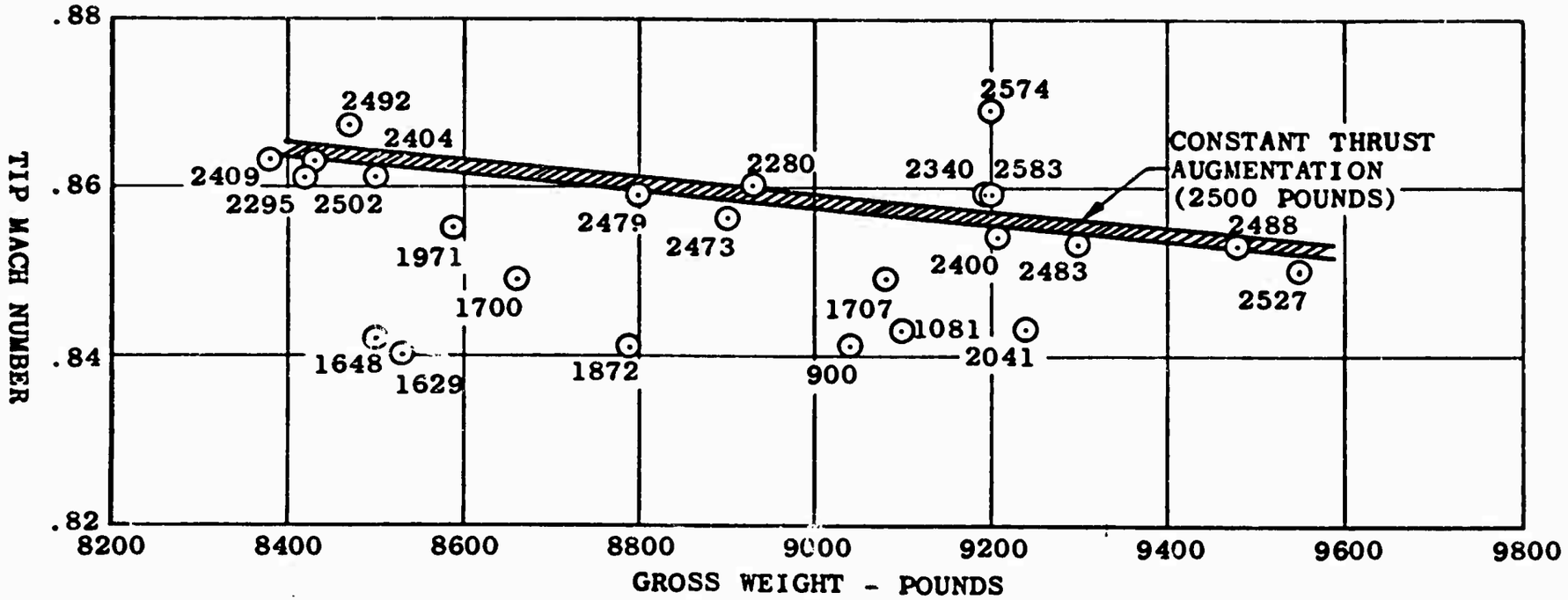

Figure 31. EFFECT OF GROSS WEIGHT ON TIP MACH NUMBER AT COMPRESSIBILITY LIMITED AIRSPEEDS

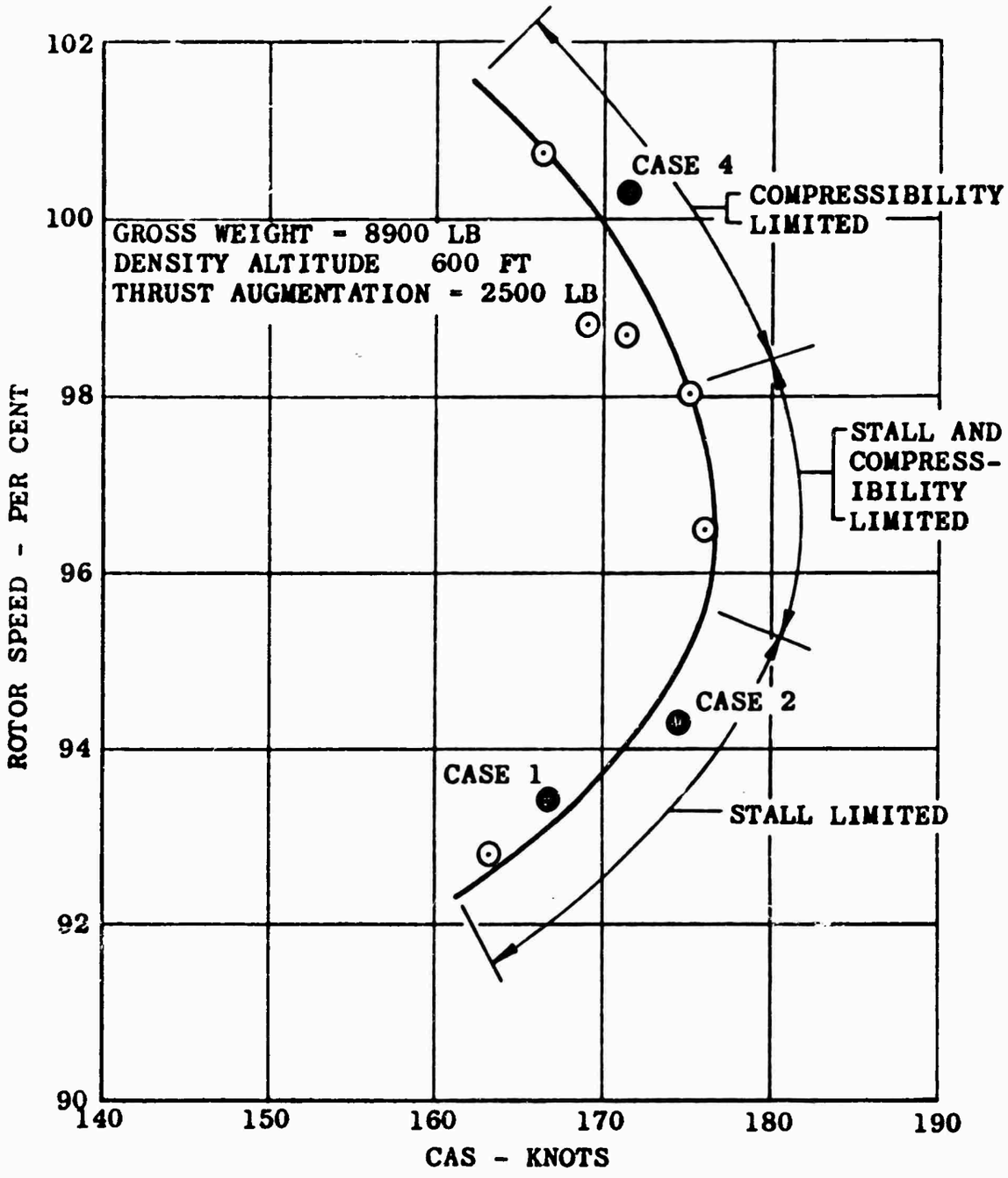

Figure 32. EFFECT OF MAIN ROTOR SPEED ON LIMIT AIRSPEED AT CONSTANT THRUST AUGMENTATION

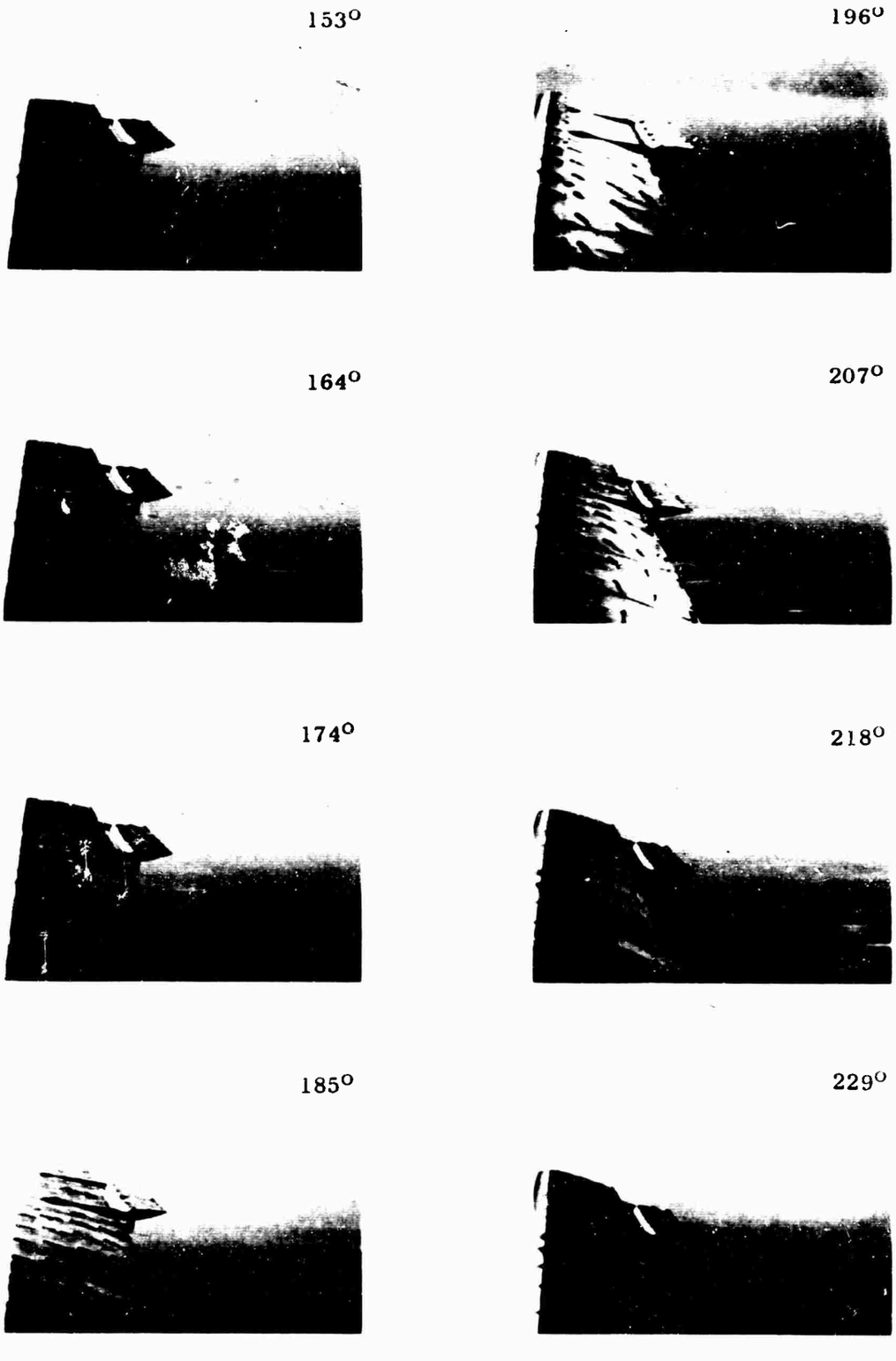

Figure 33. MAIN ROTOR BLADE TUFT BEHAVIOR - CASE 1; 93.4% RPM; 168 KTS CAS; 9031 LB GW; 600 FT h_D; = .480; M_T = .801

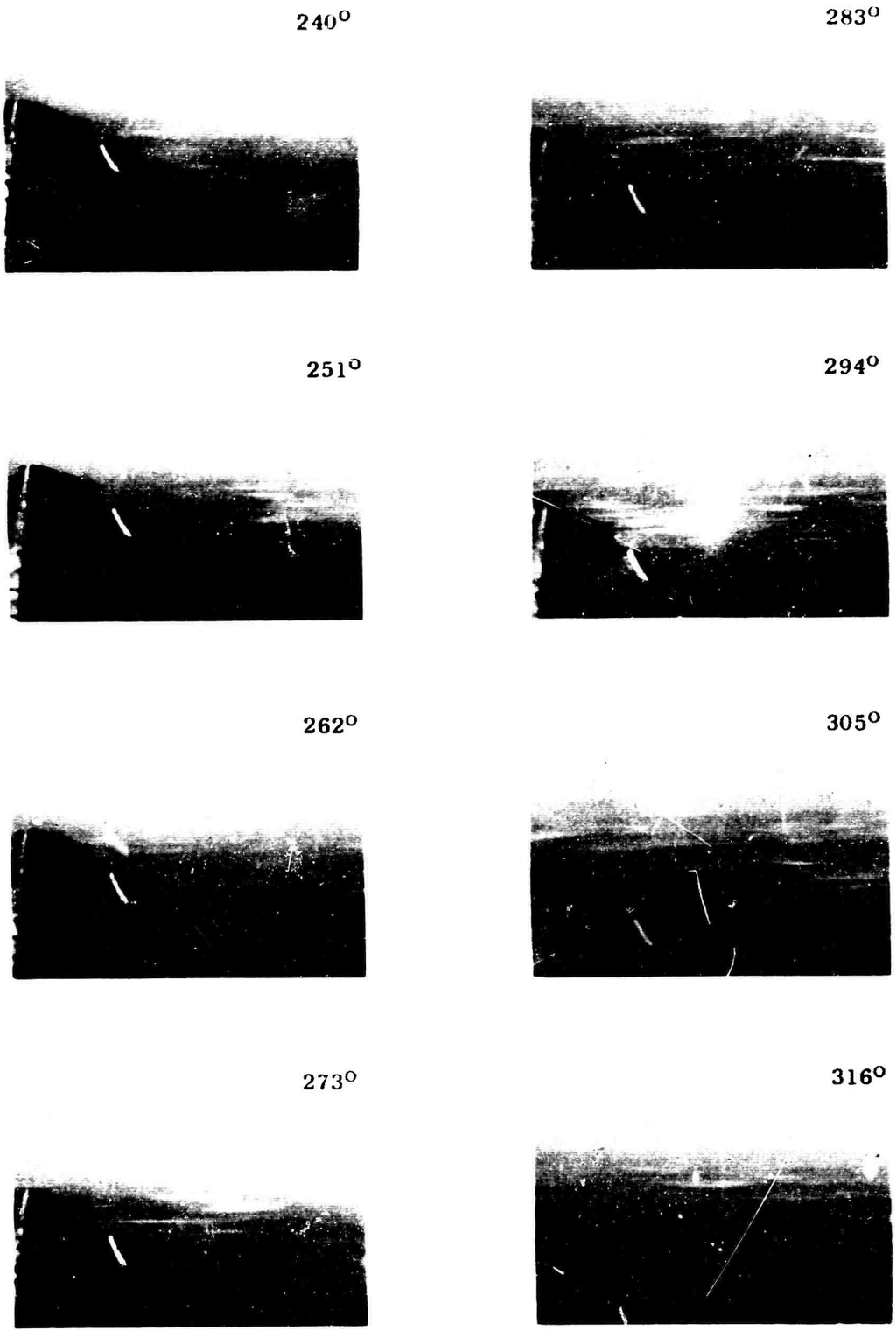

Figure 33. MAIN ROTOR BLADE TUFT BEHAVIOR - CASE 1 (Contd.)

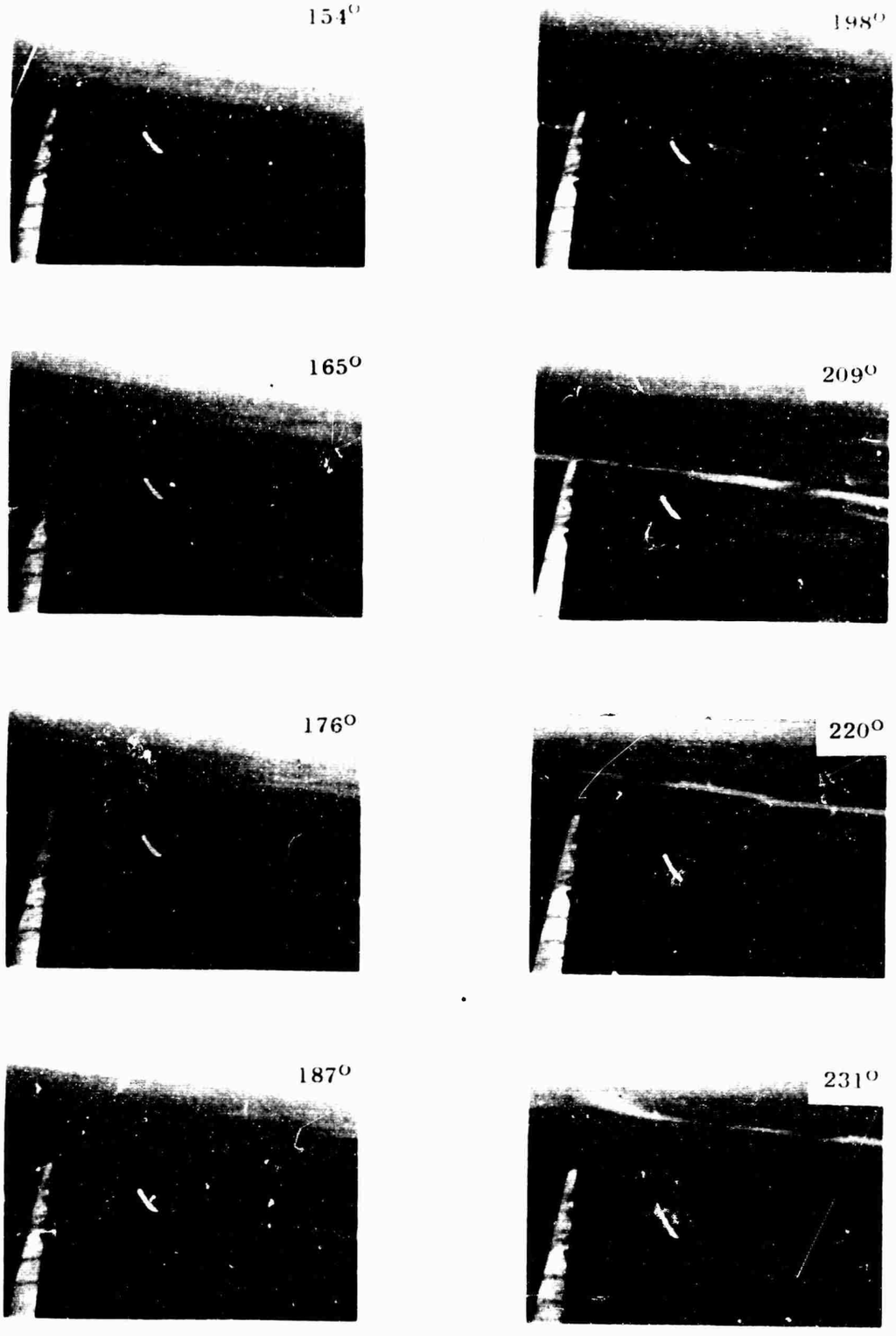

Figure 34. MAIN ROTOR BLADE TUFT BEHAVIOR - CASE 2; 94.3% RPM; 177.5 KTS CAS; 8600 LB GW; 650 FT h_D; = .501; M_T = .822

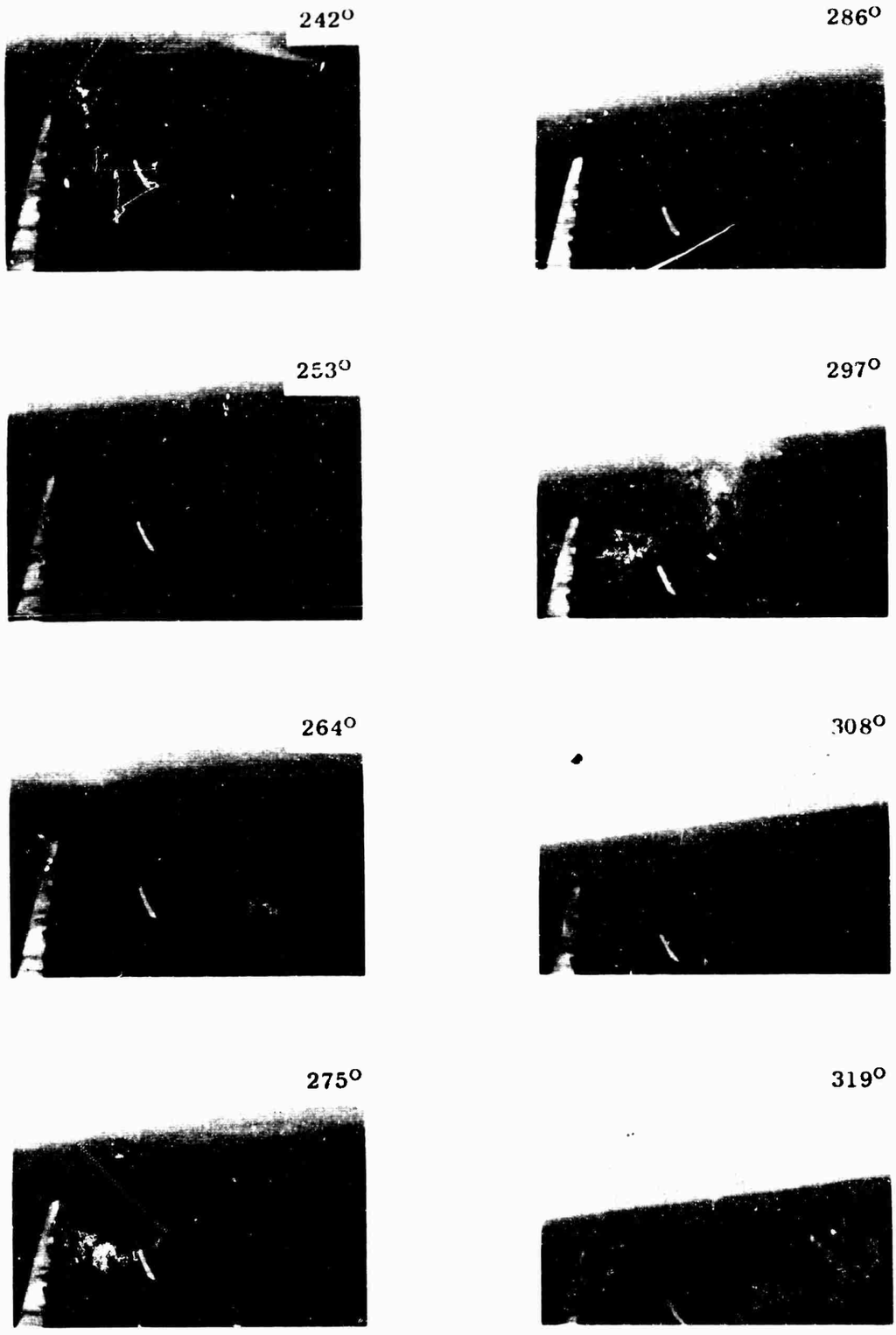

Figure 34. MAIN ROTOR BLADE TUFT BEHAVIOR - CASE 2 (Contd.)

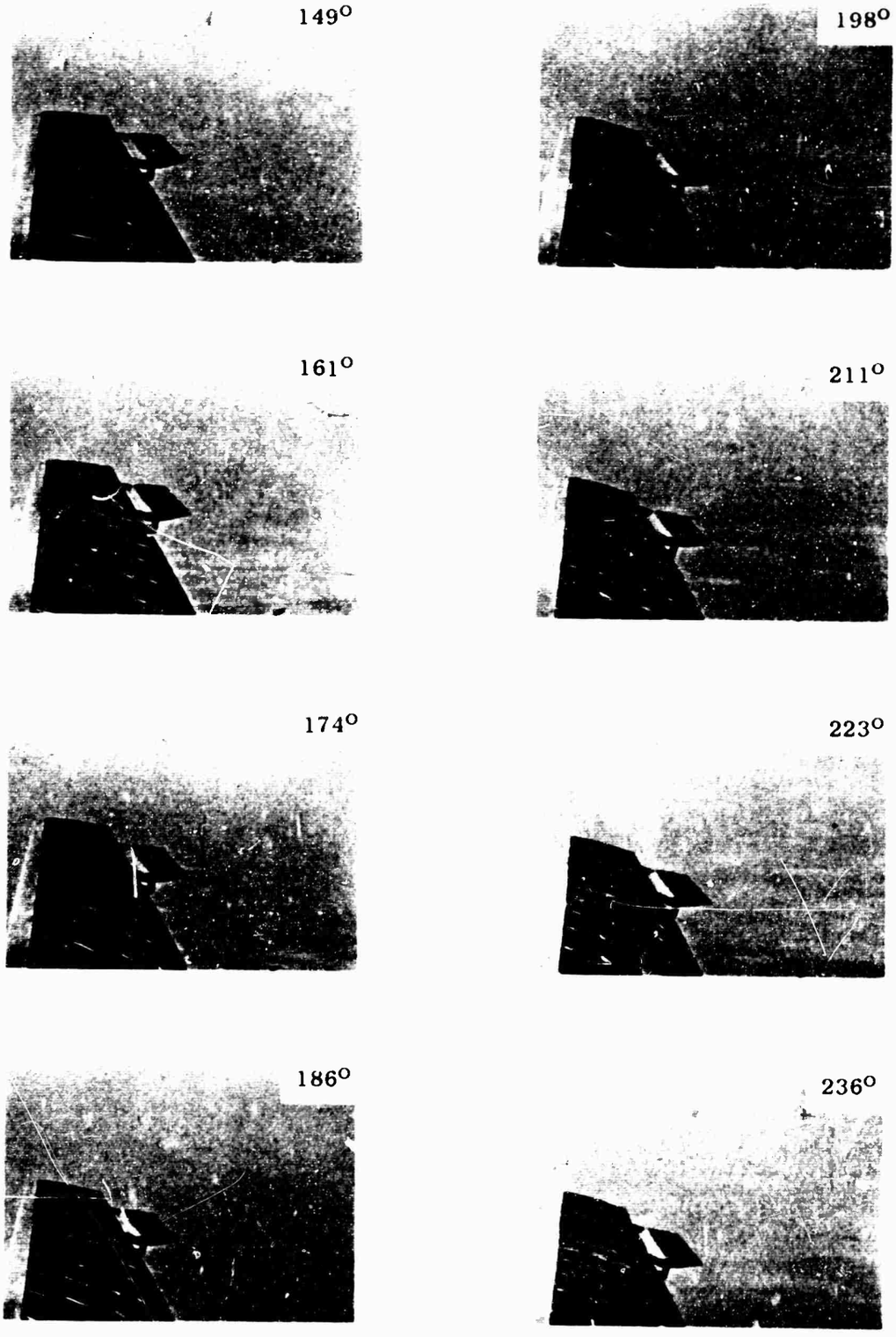

Figure 35. MAIN ROTOR BLADE TUFT BEHAVIOR - CASE 4; 100.3% RPM; 172 KTS CAS; 8801 LB GW; 900 FT h_D; = .458; M_T = .859

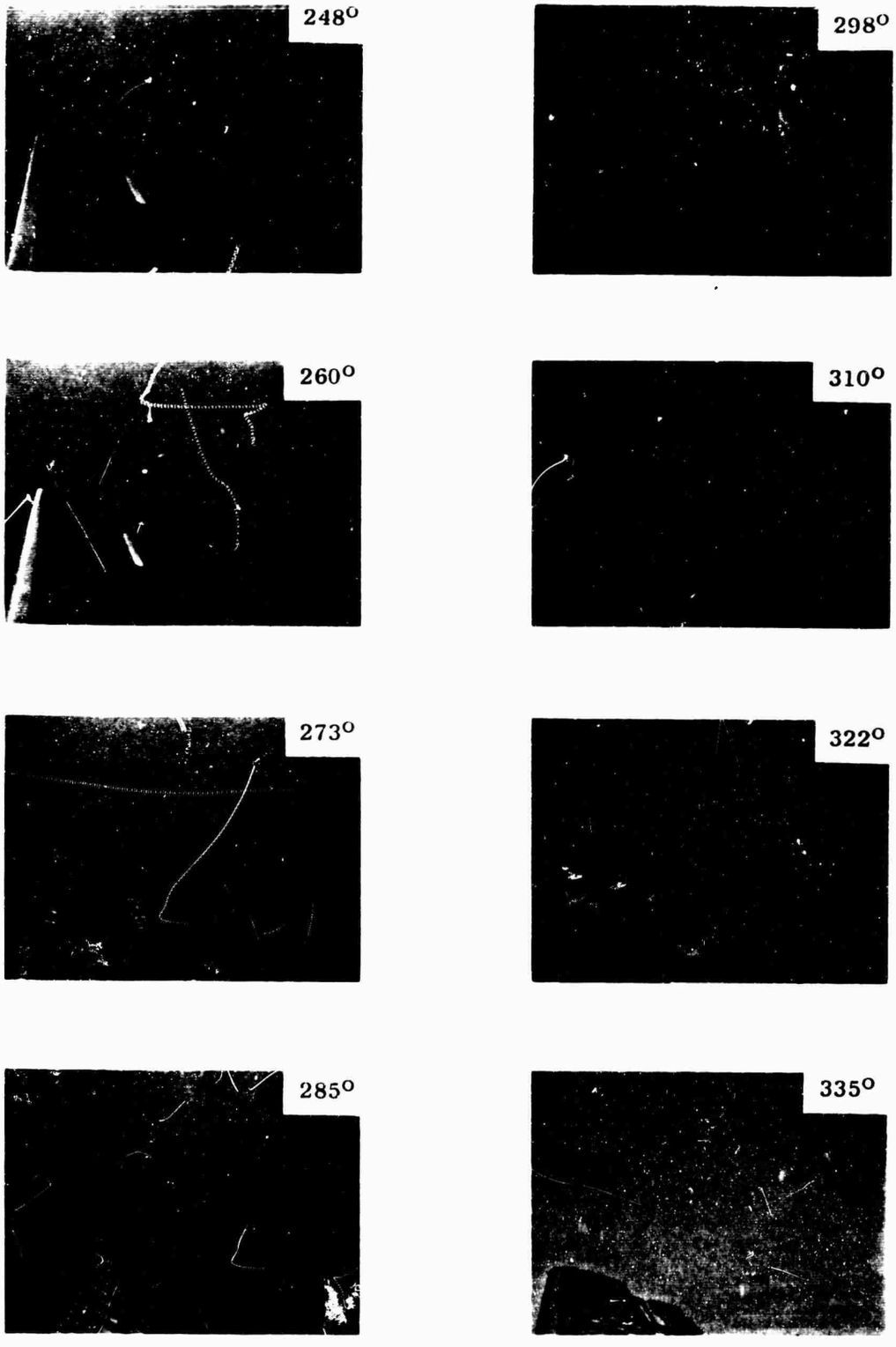

Figure 35. MAIN ROTOR BLADE TUFT BEHAVIOR - CASE 4 (Contd.)

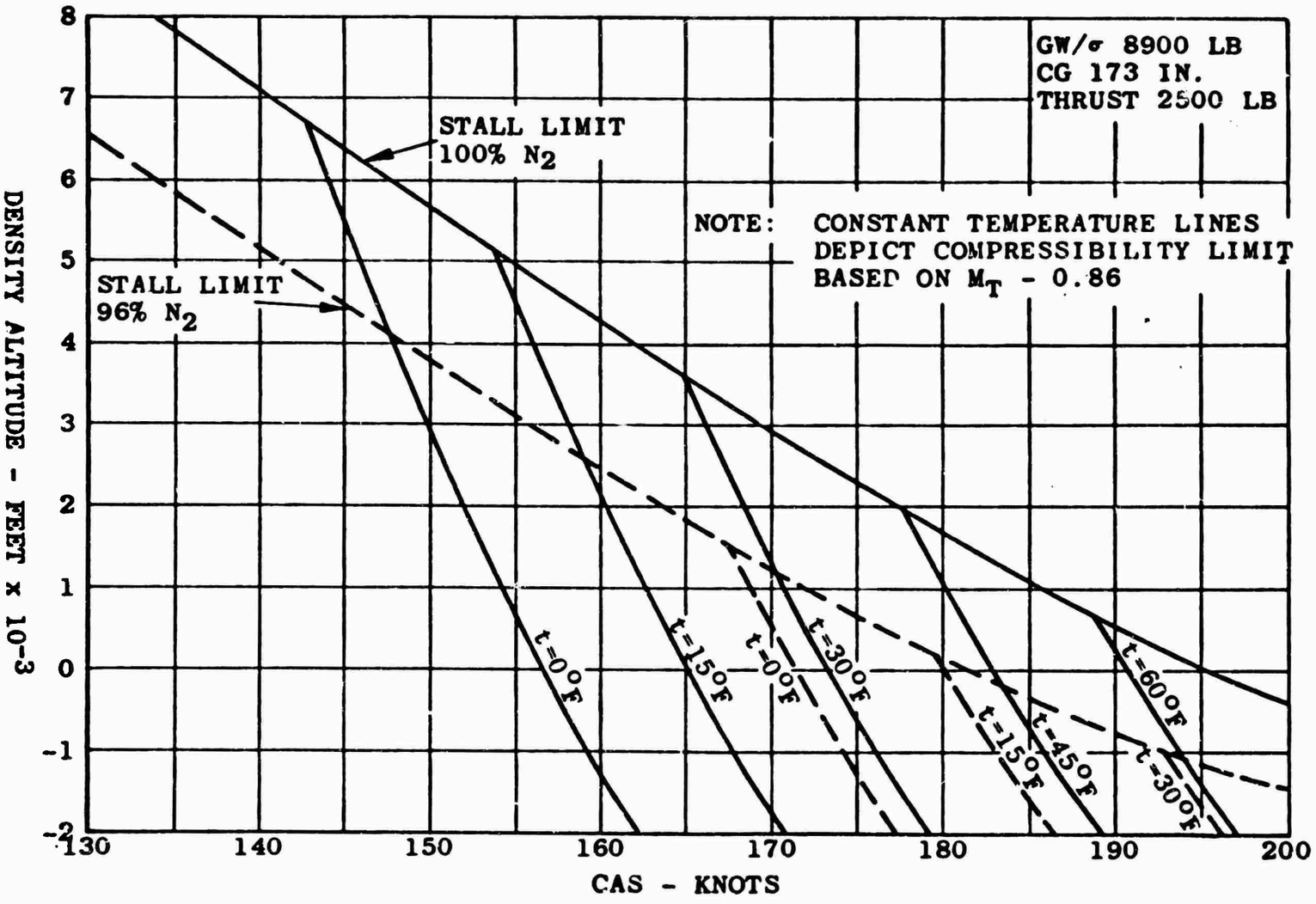

Figure 36. CALCULATED LIMIT AIRSPEED ENVELOPE

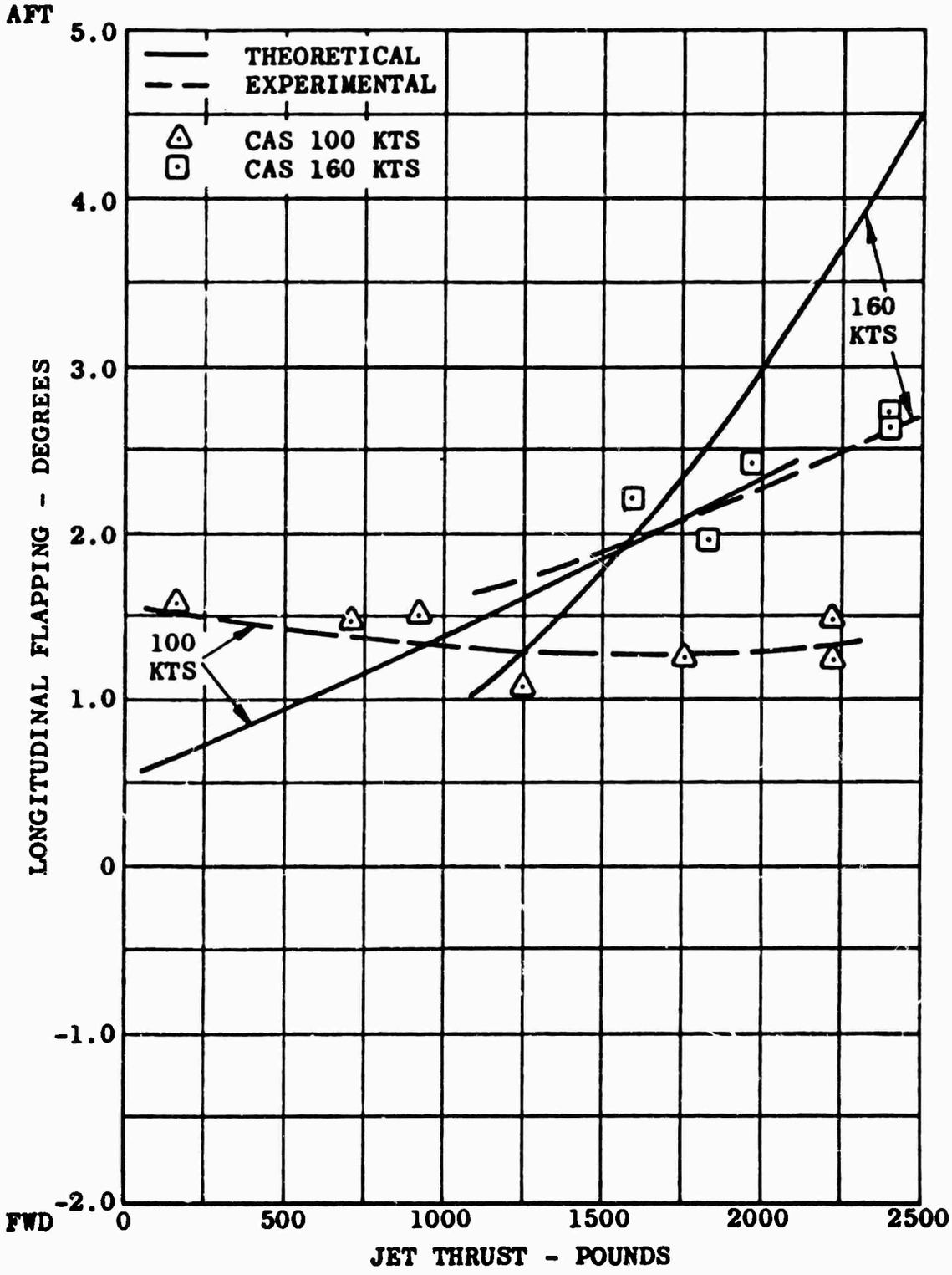

Figure 37. THEORETICAL AND EXPERIMENTAL CORRELATION OF LONGITUDINAL FLAPPING

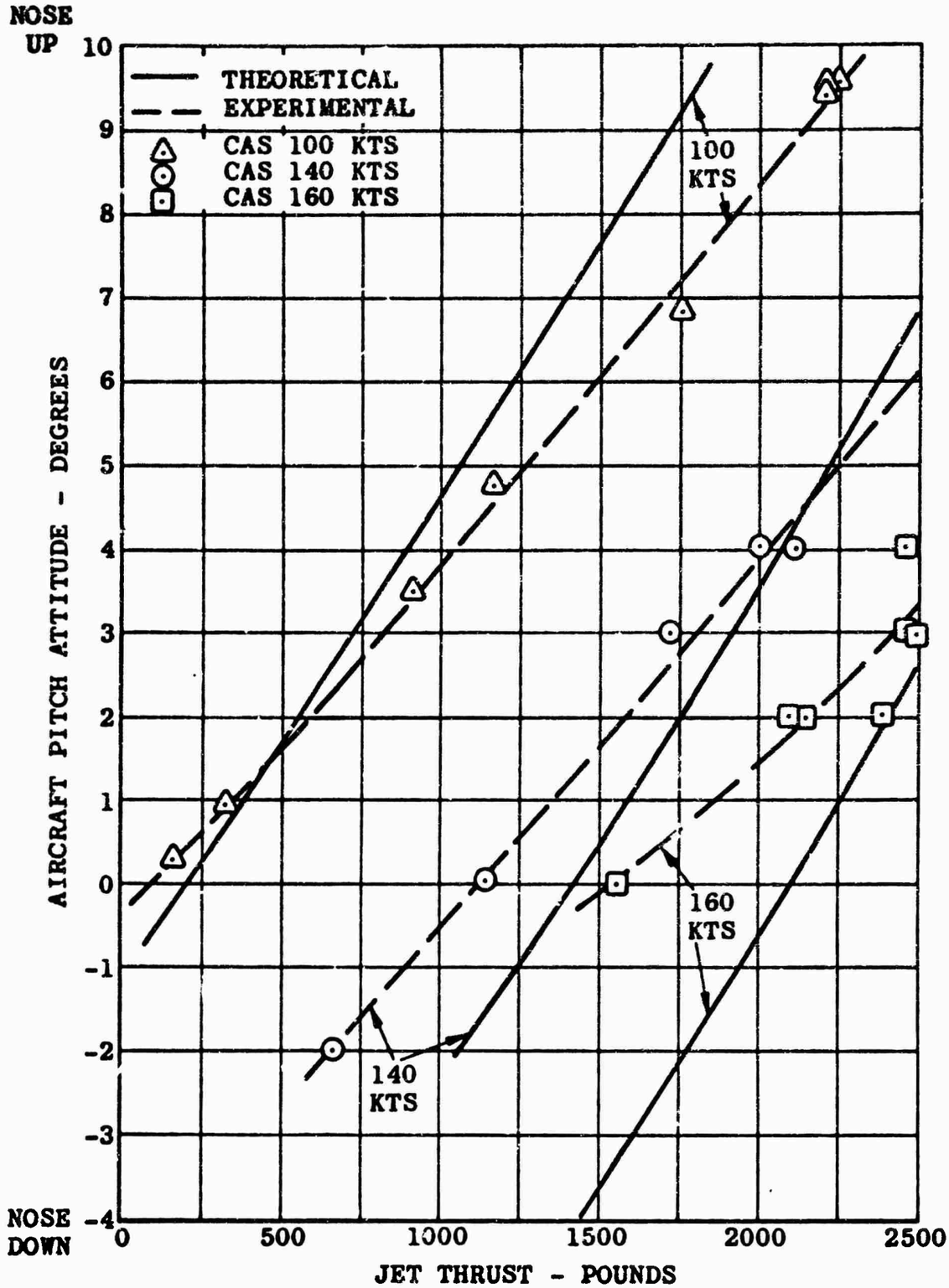

Figure 38. THEORETICAL AND EXPERIMENTAL CORRELATION OF PITCH ATTITUDE

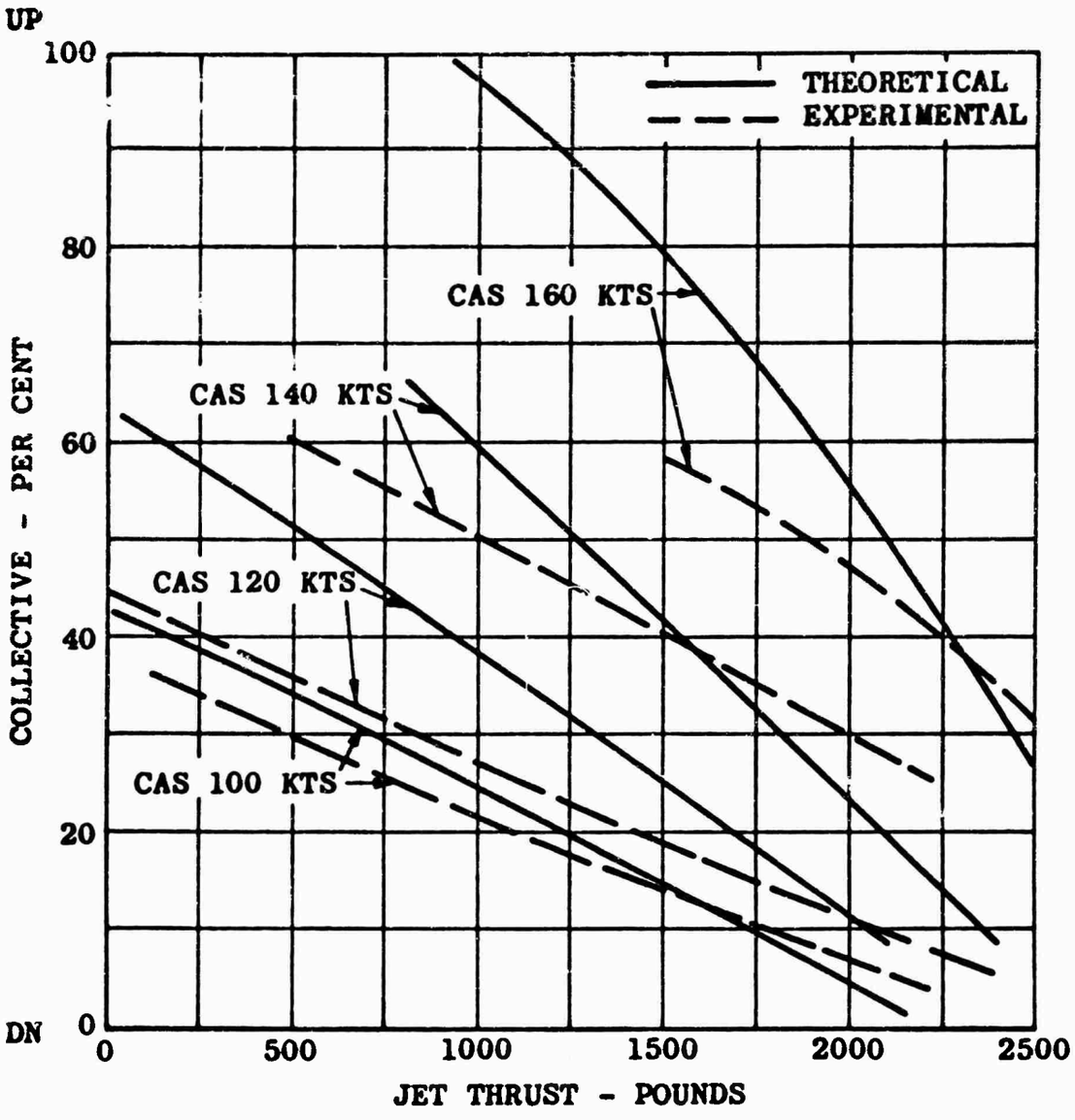

Figure 39. THEORETICAL AND EXPERIMENTAL CORRELATION OF COLLECTIVE

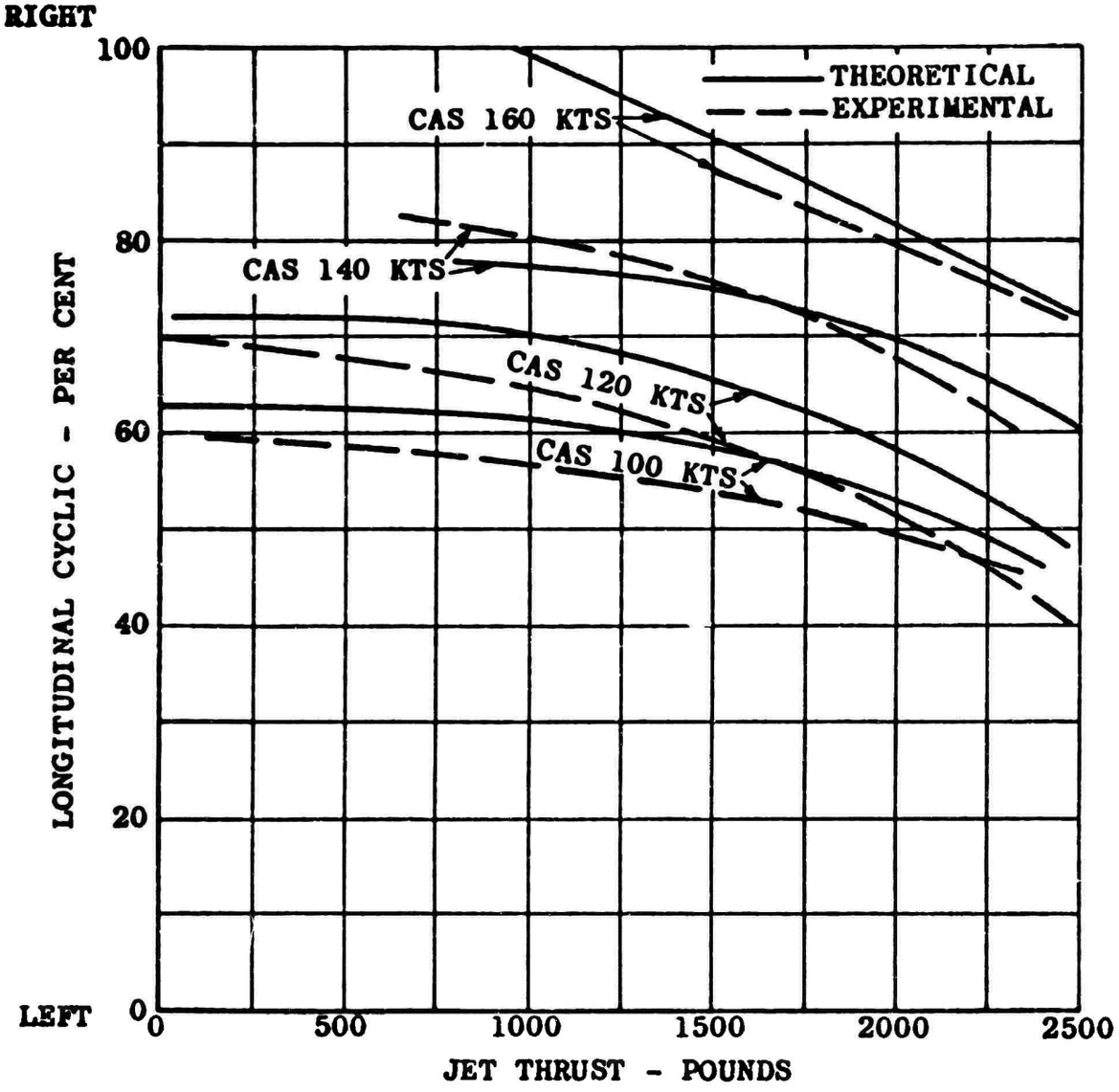

Figure 40. THEORETICAL AND EXPERIMENTAL CORRELATION OF LONGITUDINAL CYCLIC

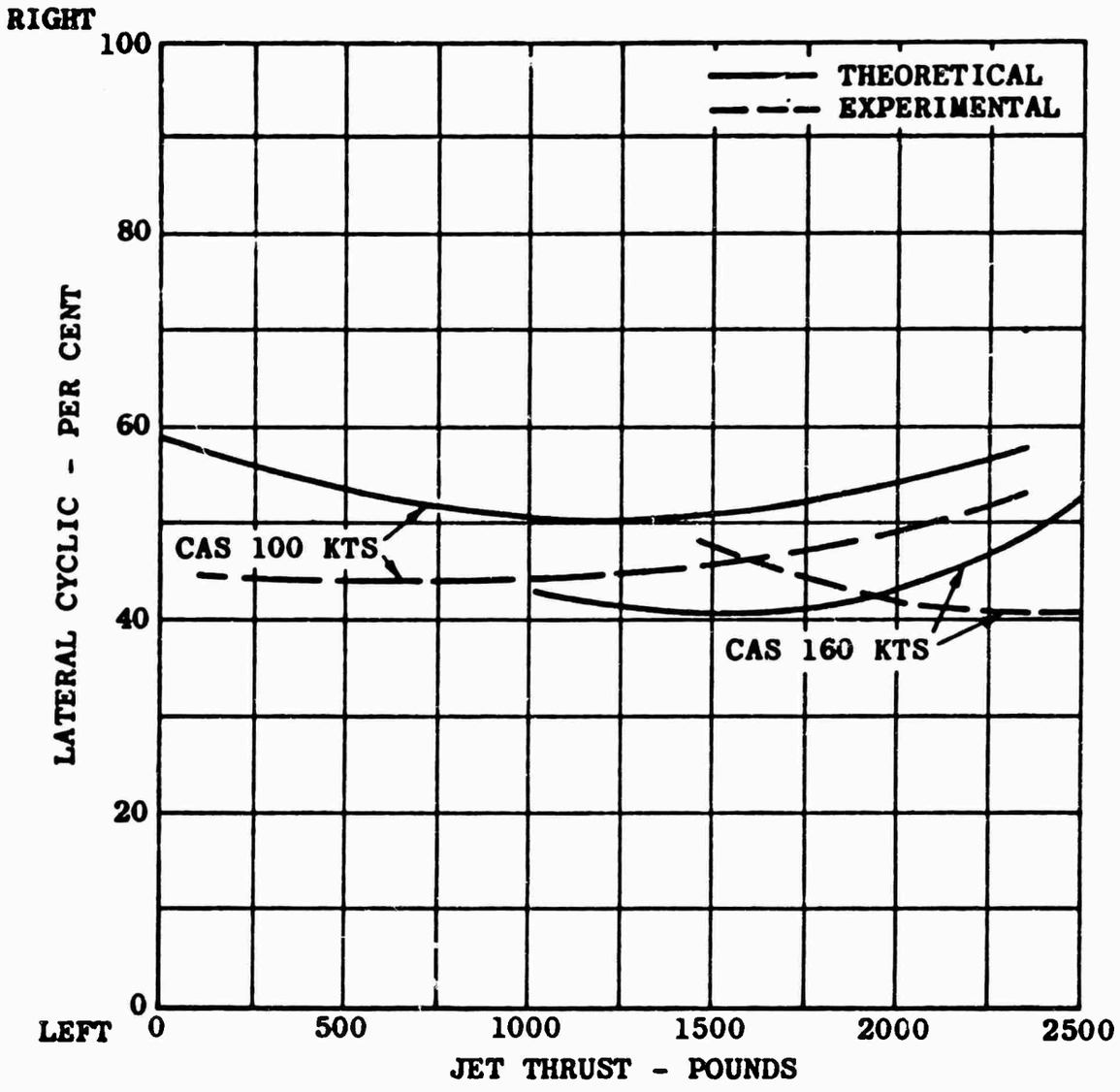

Figure 41. THEORETICAL AND EXPERIMENTAL CORRELATION OF LATERAL CYCLIC

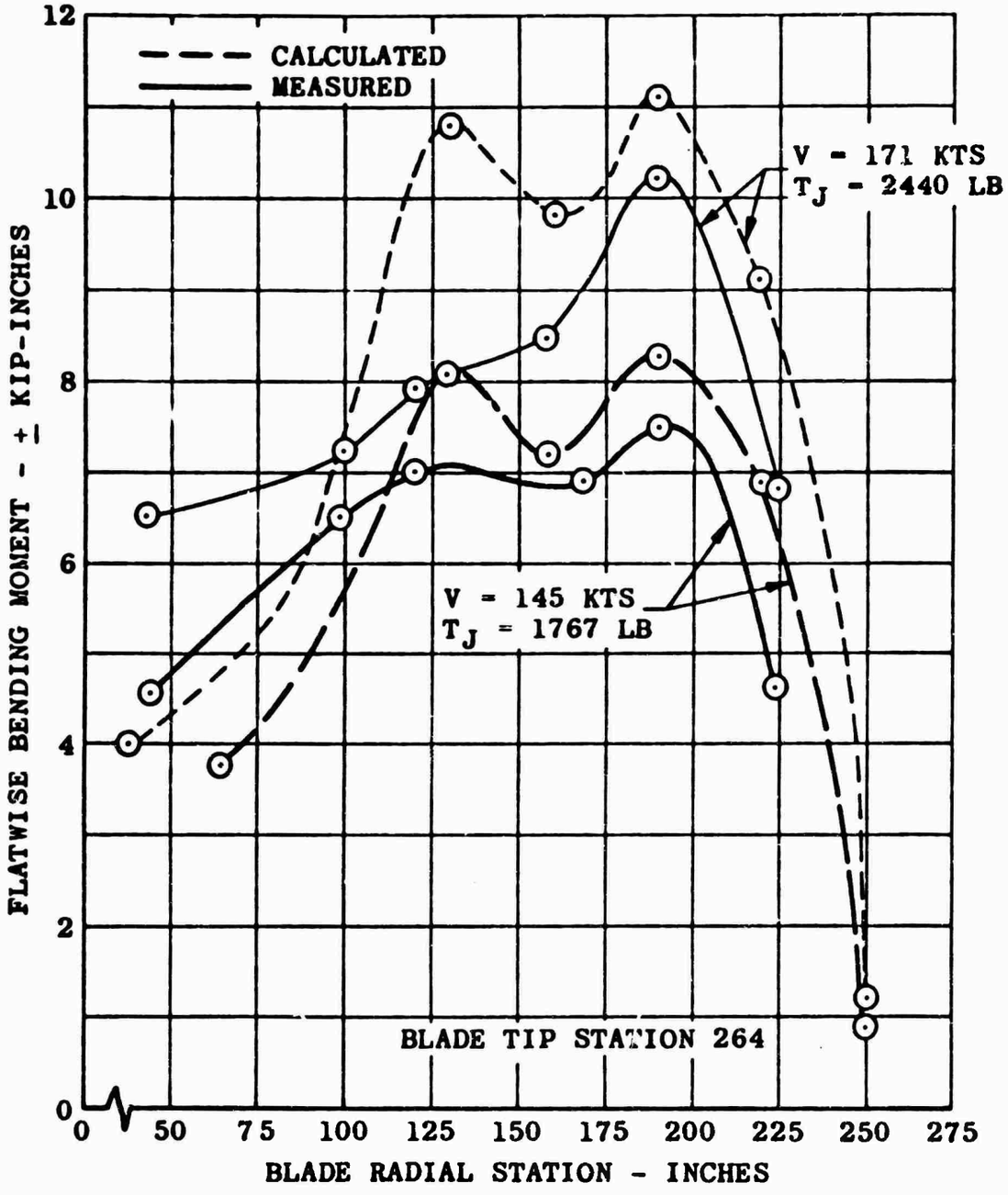

Figure 42. CALCULATED AND MEASURED FLATWISE BENDING MOMENT DISTRIBUTION BELOW LIMIT AIRSPEED

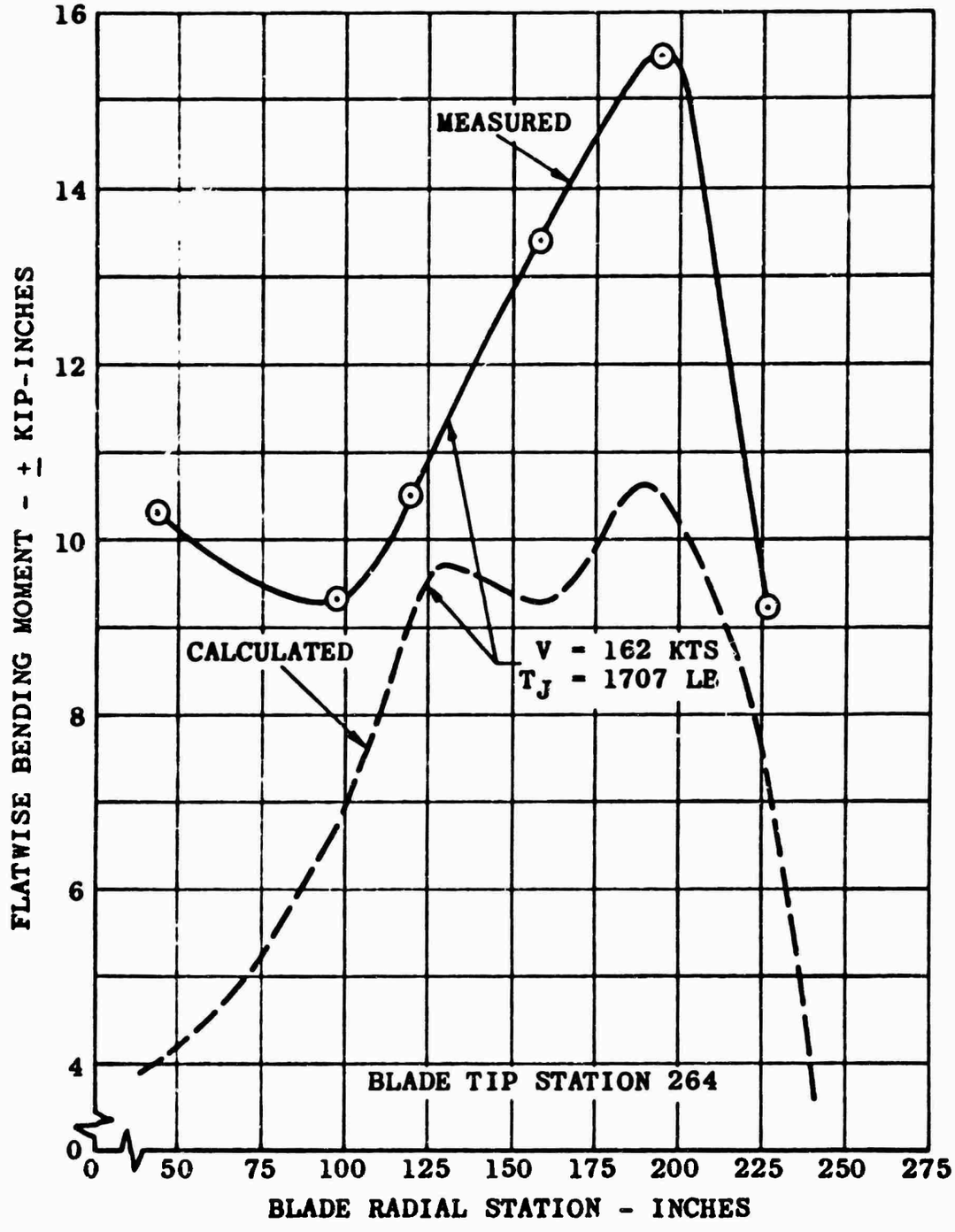

Figure 43. CALCULATED AND MEASURED FLATWISE BENDING MOMENT DISTRIBUTION AT LIMIT AIRSPEED

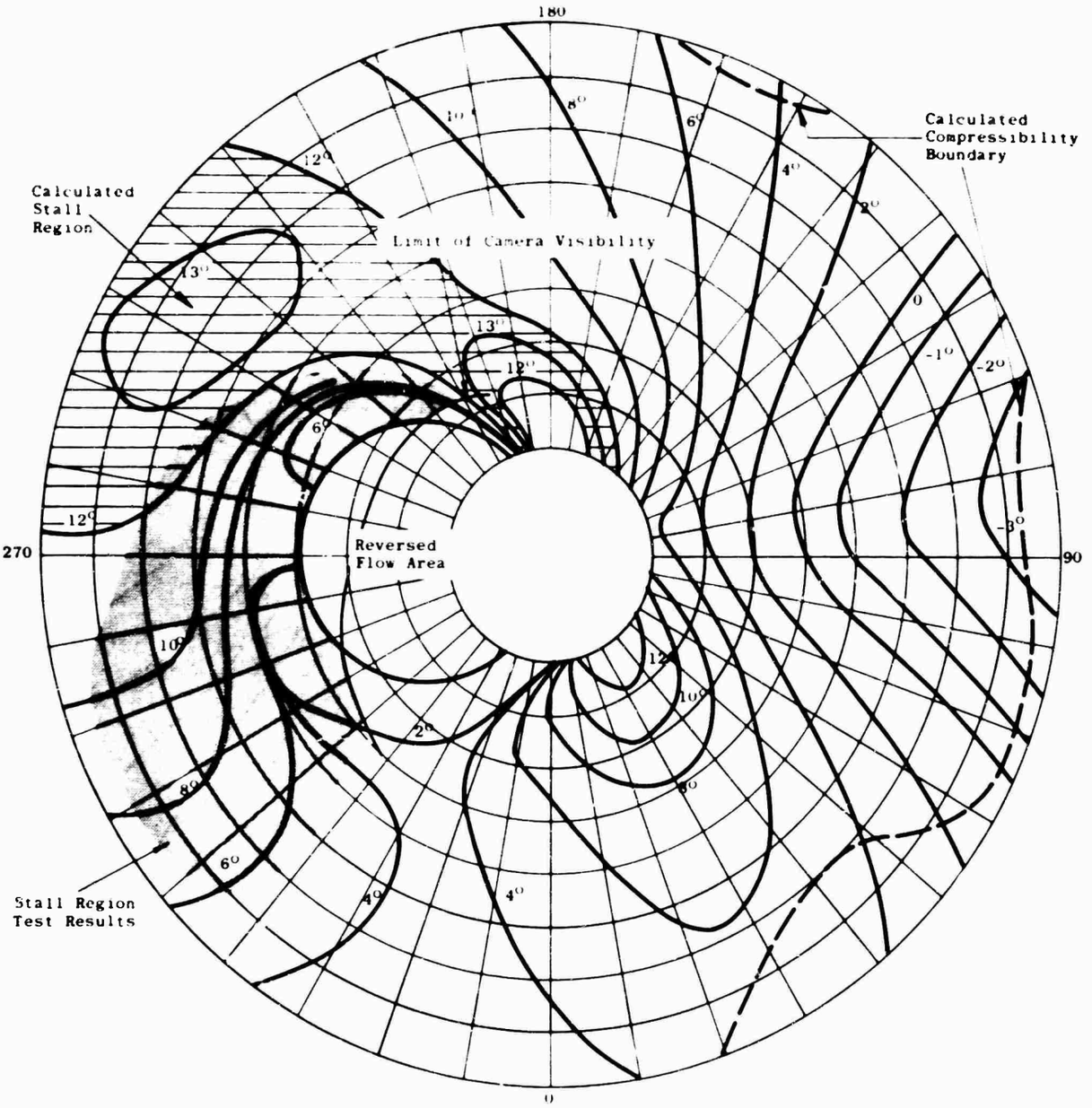

Figure 44. ROTOR OPERATING LIMITS SHOWING BLADE SECTION ANGLE OF ATTACK CONTOURS. CASE 1; 93.4% RPM; 168 KTS CAS; μ = .480; M_T = .801

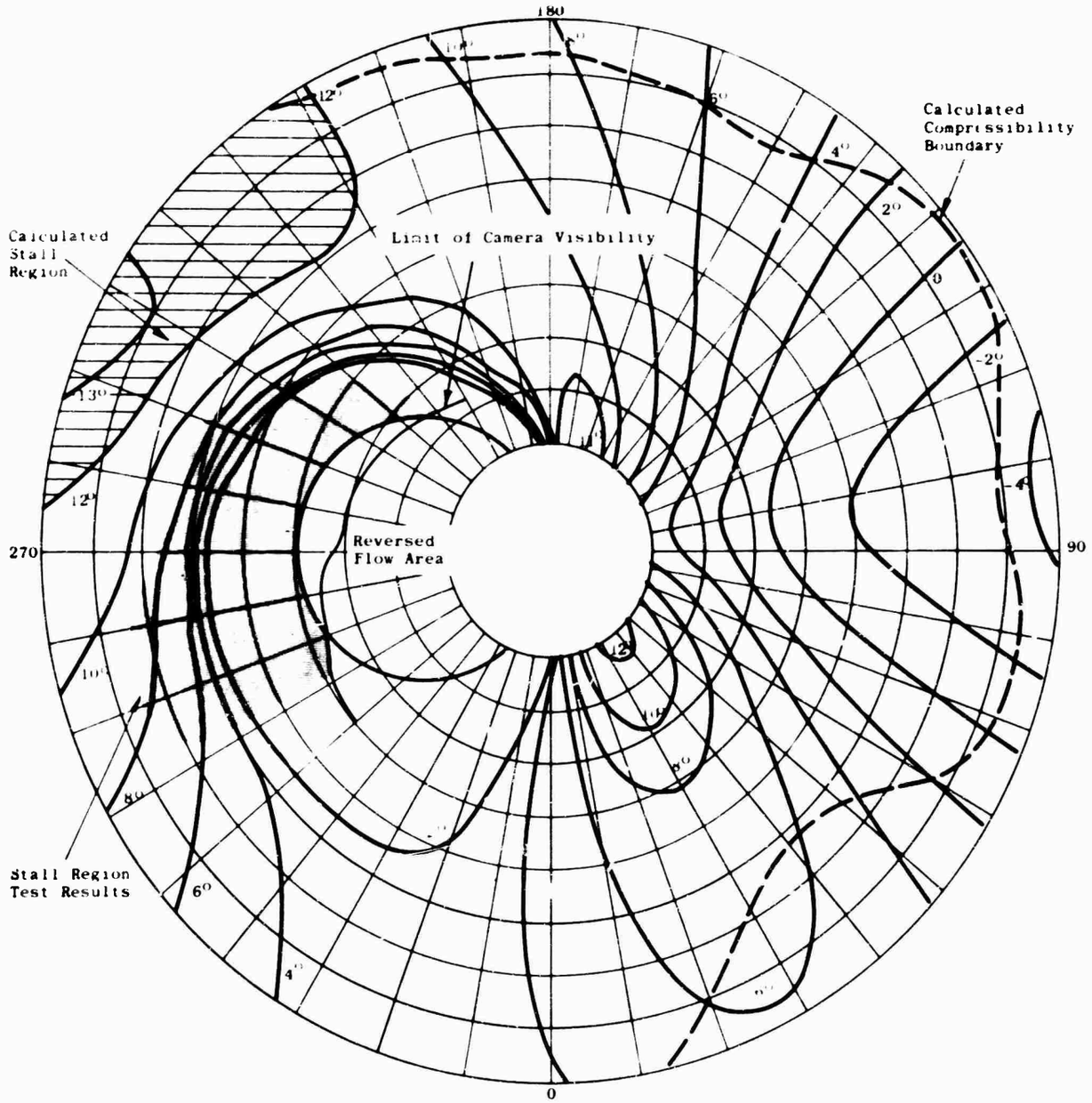

Figure 45. ROTOR OPERATING LIMITS SHOWING BLADE SECTION ANGLE OF ATTACK CONTOURS. CASE 2; 94.3% RPM; 177.5 KTS CAS; μ = .501; M_T = .822

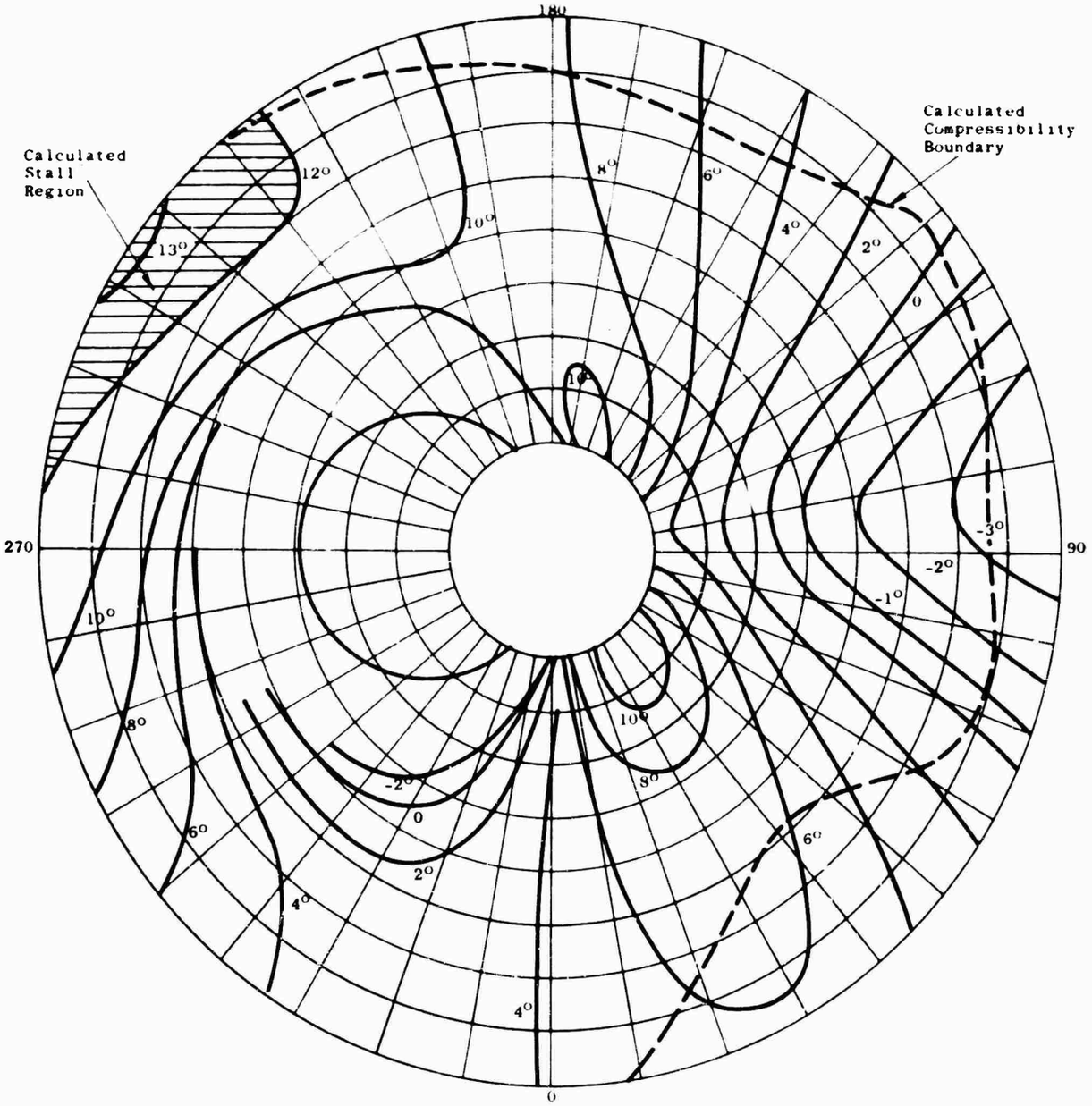

Figure 46. ROTOR OPERATING LIMITS SHOWING BLADE SECTION ANGLE OF ATTACK CONTOURS. CASE 3; 96.5% RPM; 178 KTS CAS; μ = .490; M_T = .841

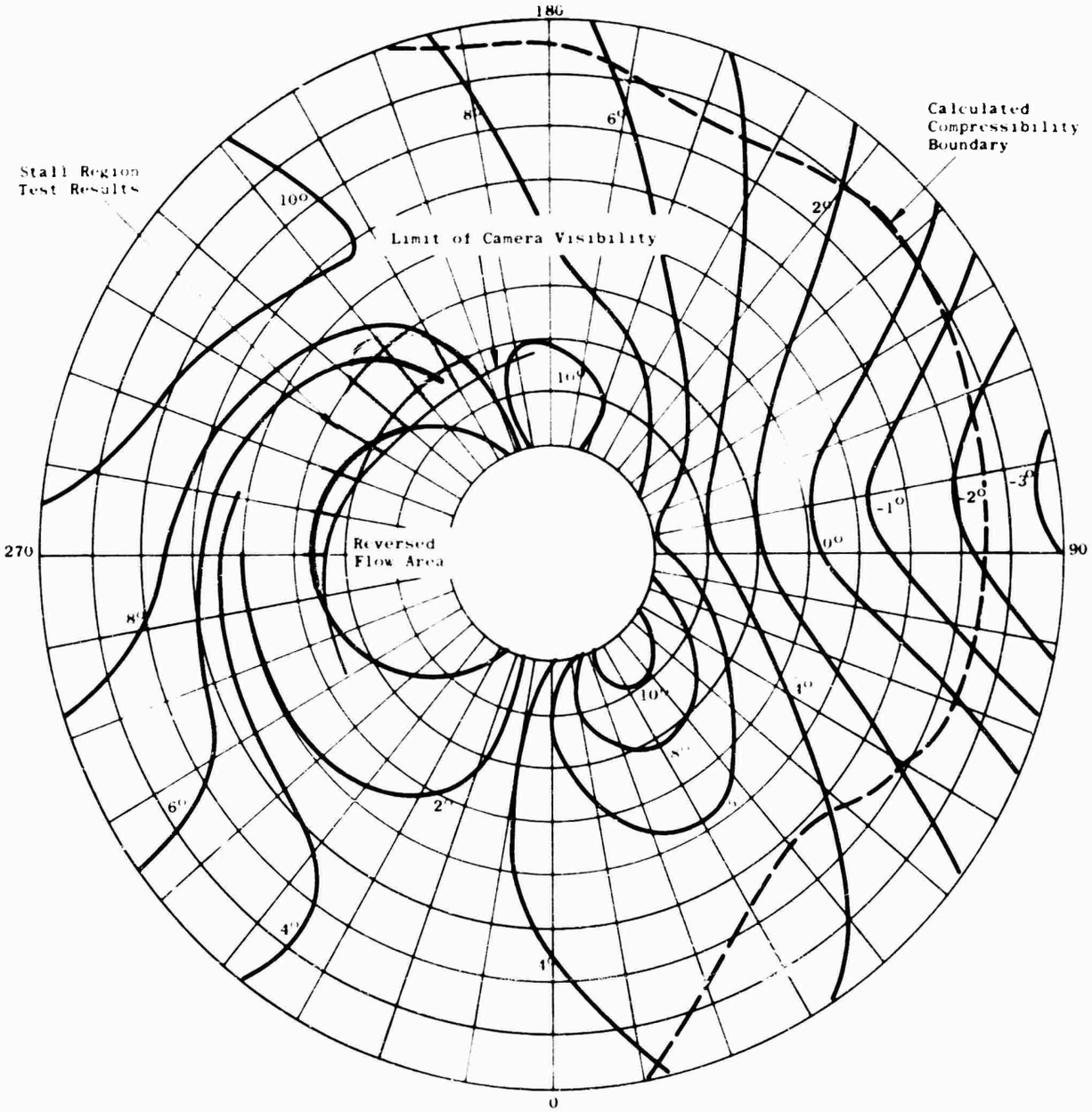

Figure 47. ROTOR OPERATING LIMITS SHOWING BLADE SECTION ANGLE OF ATTACK CONTOURS. CASE 4; 100.3% RPM; 172 KTS CAS; μ = .458; M_T = .859

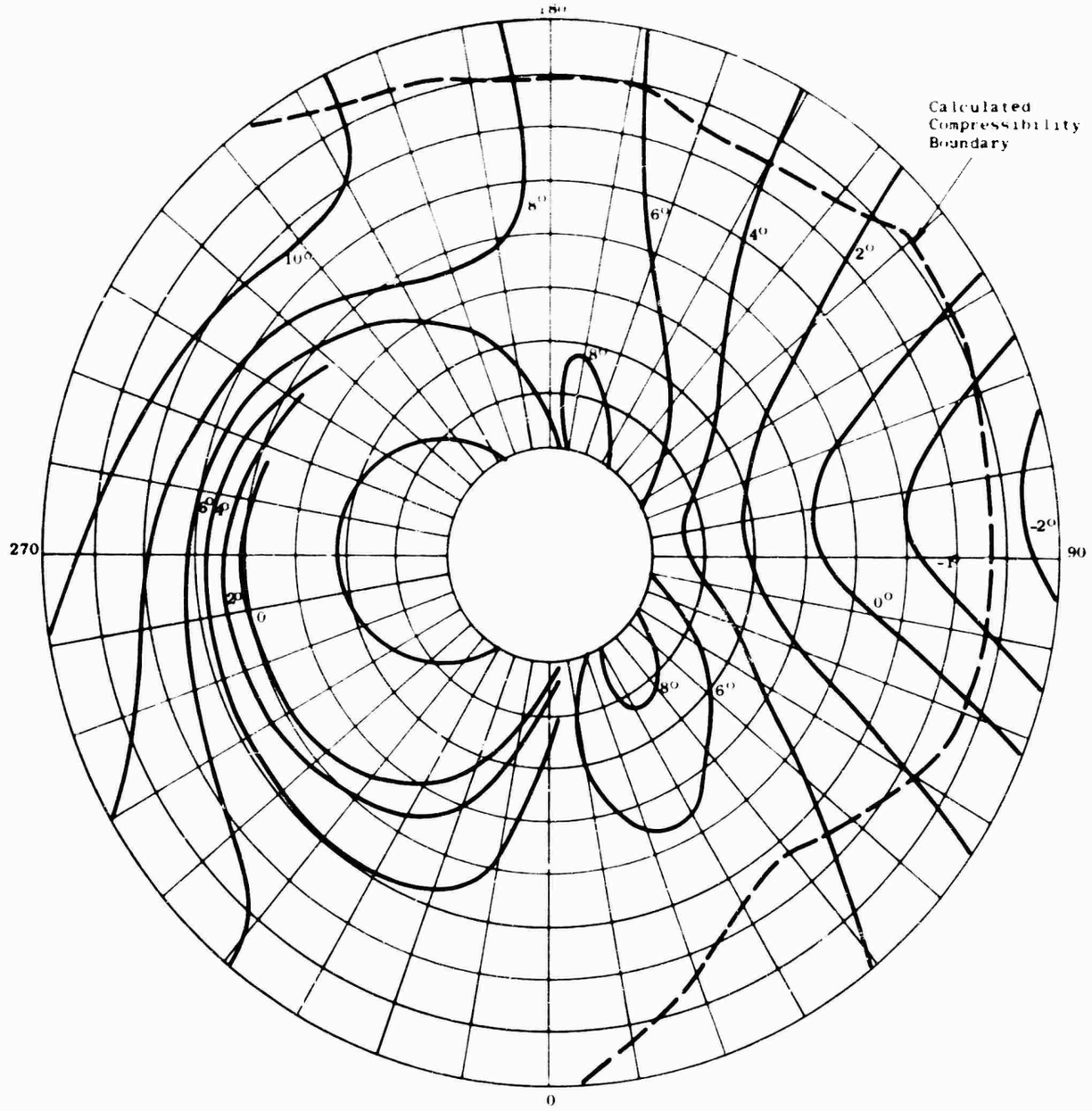

Figure 48. ROTOR OPERATING LIMITS SHOWING BLADE SECTION ANGLE OF ATTACK CONTOURS. CASE 5; 101.3% RPM; 158.5 KTS CAS; μ = .415; M_T = .843

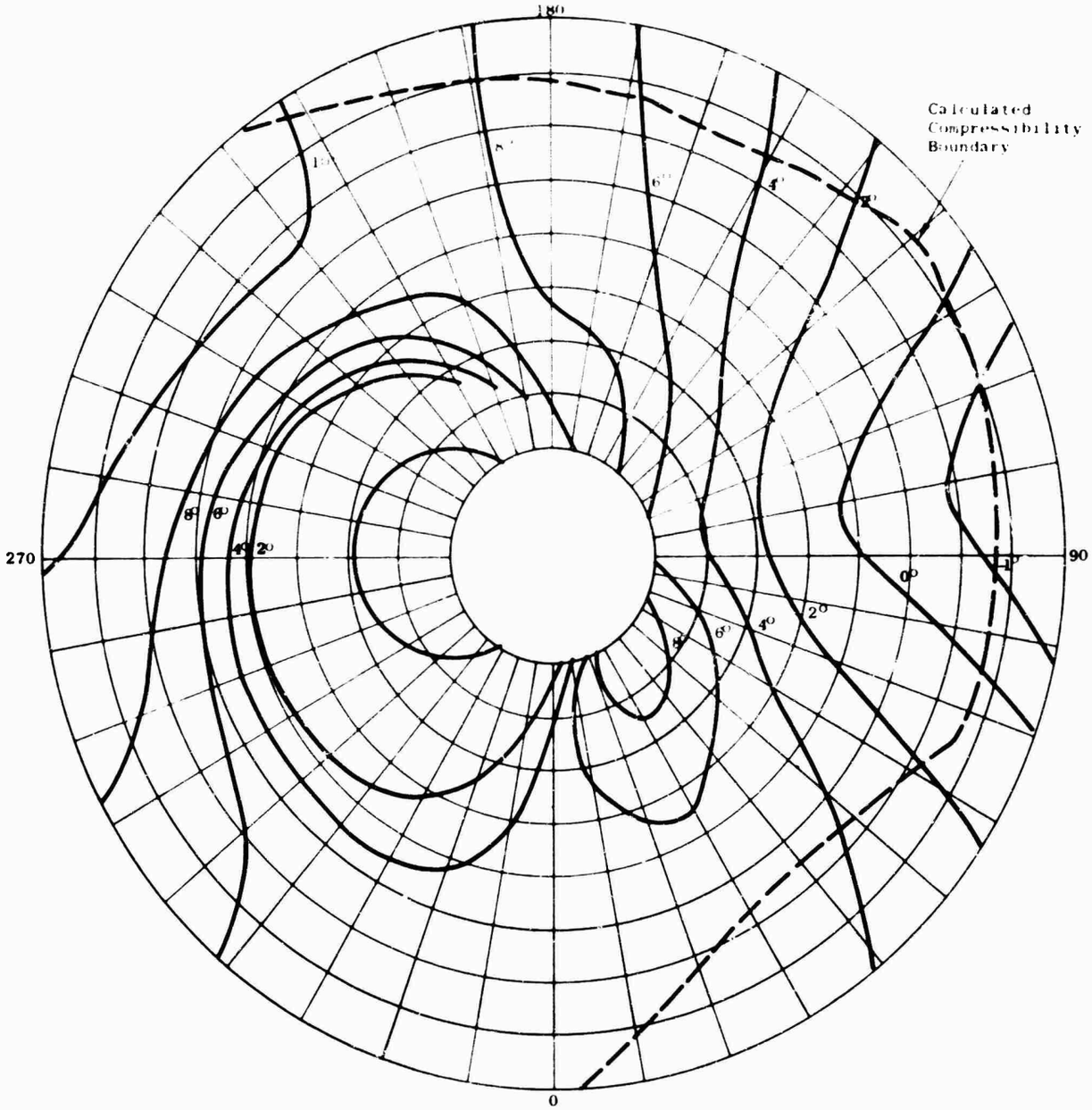

Figure 49. ROTOR OPERATING LIMITS SHOWING BLADE SECTION ANGLE OF ATTACK CONTOURS. CASE 6; 101.7% RPM; 145 KTS CAS; μ = .388; M_T = .841

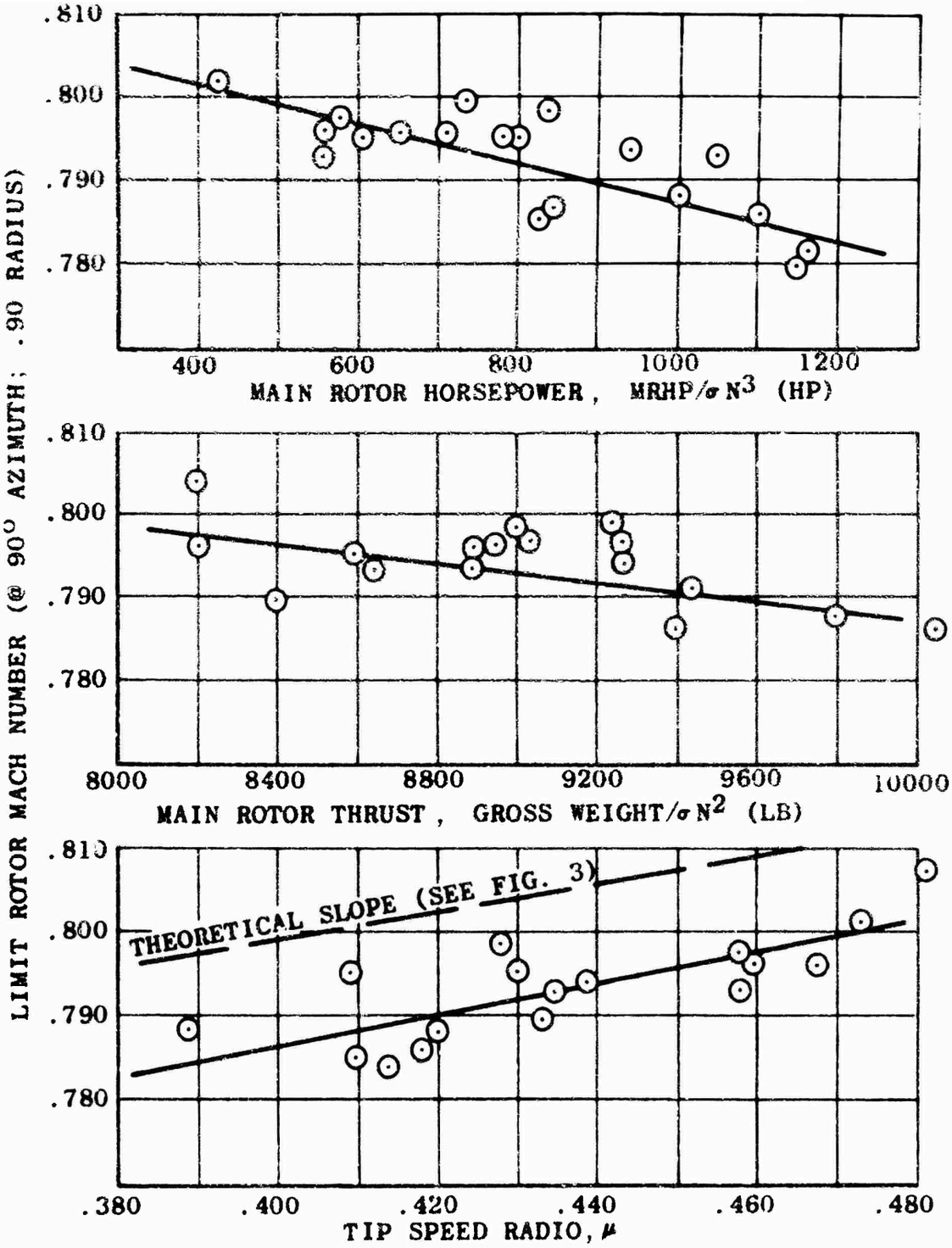

Figure 50. EFFECTS OF MAIN ROTOR HORSEPOWER, MAIN ROTOR THRUST AND TIP SPEED RATIO ON LIMIT ROTOR MACH NUMBER (TEST POINTS NORMALIZED TO μ = .430; $MRHP/\sigma N^3$ = 800; $GW/\sigma N^2$ = 9000).

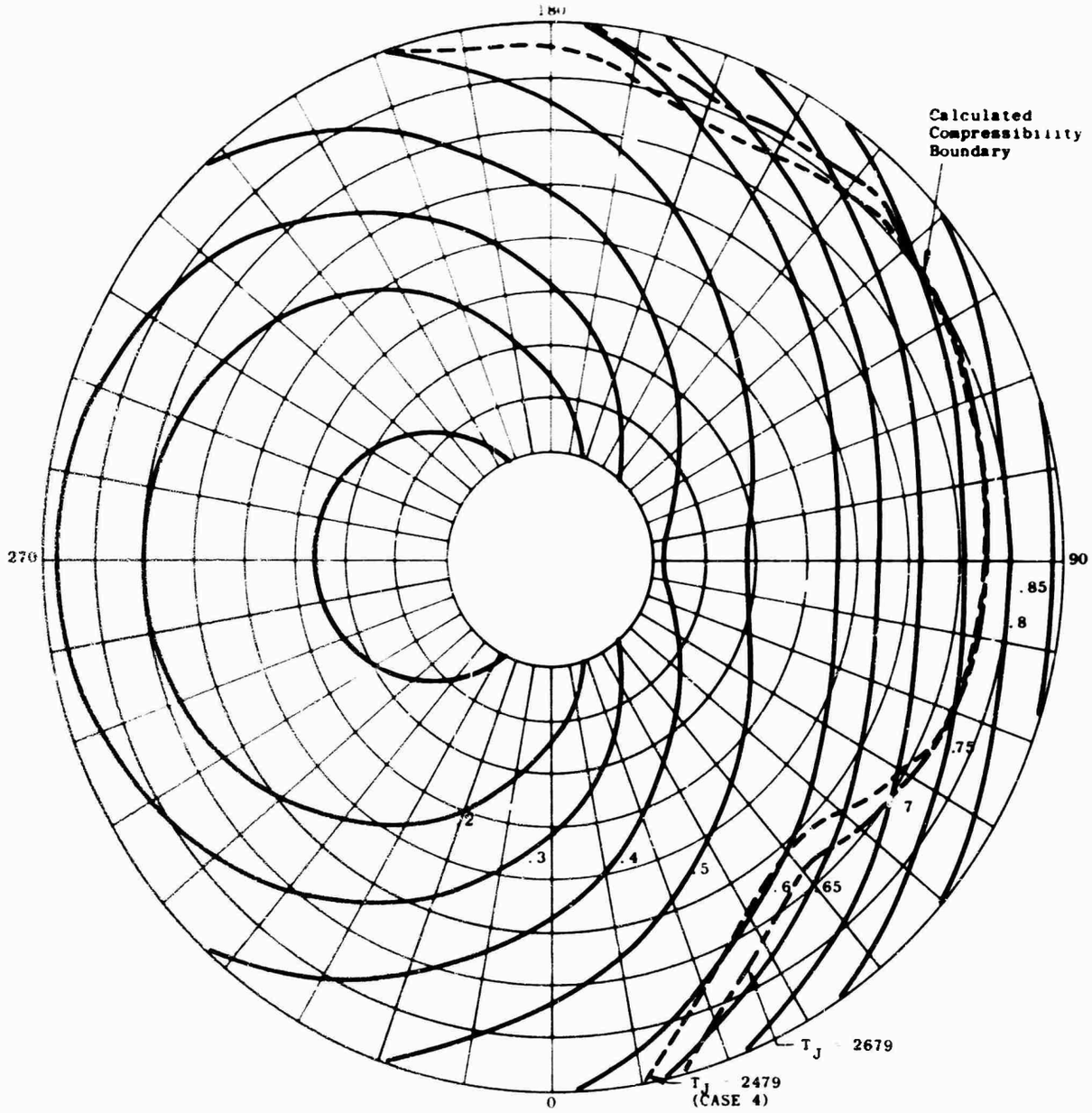

Figure 51. EFFECTS OF THRUST ON COMPRESSIBILITY BOUNDARY. (CONSTANT MACH NUMBER CONTOURS SHOWN)

Task 1D121401A152
Contract DA 44-177-AMC-105(T)
USATRECOM Technical Report 65-14

APPENDIX I

UH-2 HELICOPTER HIGH-SPEED FLIGHT RESEARCH PROGRAM UTILIZING JET THRUST AUGMENTATION

KAC Report R-527B

Prepared by

Kaman Aircraft Corporation
Bloomfield, Connecticut

for

U. S. ARMY TRANSPORTATION RESEARCH COMMAND
FORT EUSTIS, VIRGINIA

This Appendix presents, in graphical form, the pertinent test data obtained during the UH-2 helicopter jet augmented flight research program. Much of this data is summarized in the basic report and is included in this Appendix for detail reference.

APPENDIX I

ILLUSTRATIONS

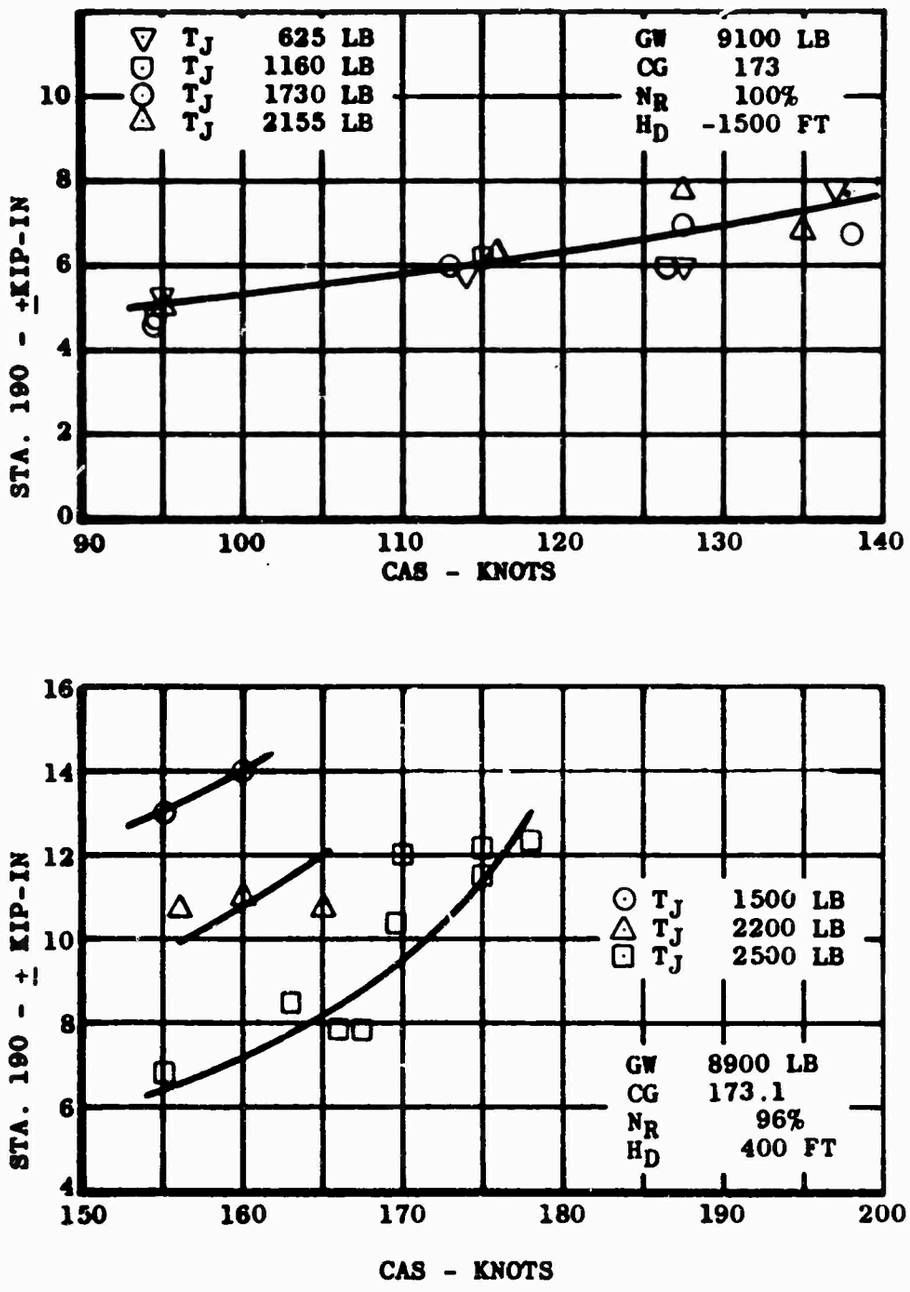

Figure I-1. MAIN ROTOR FLATWISE VIBRATORY BENDING.

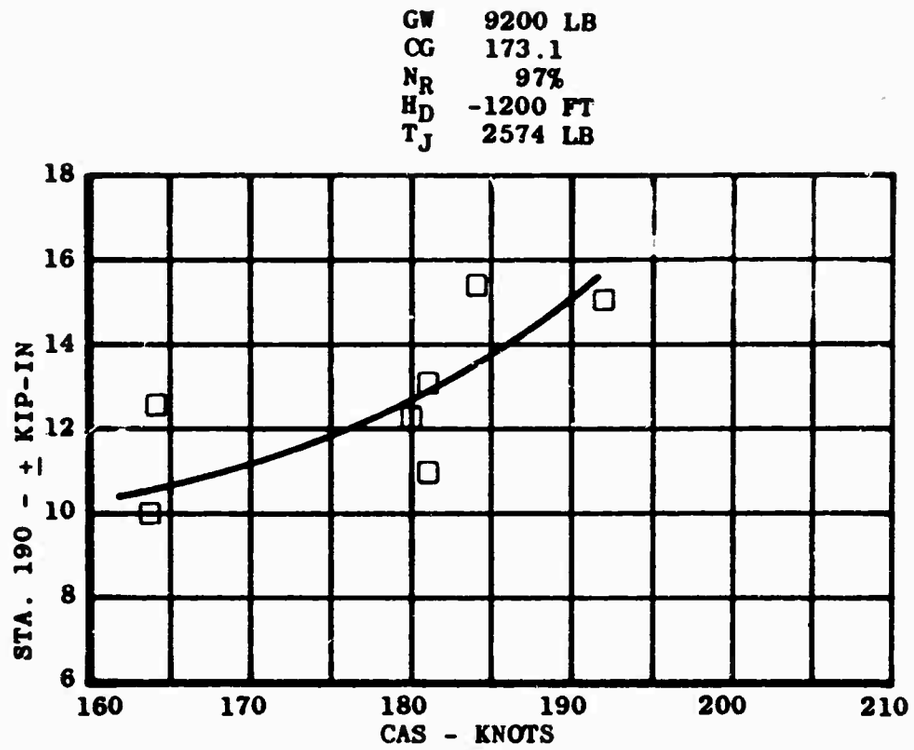

Figure I-1 (Continued)

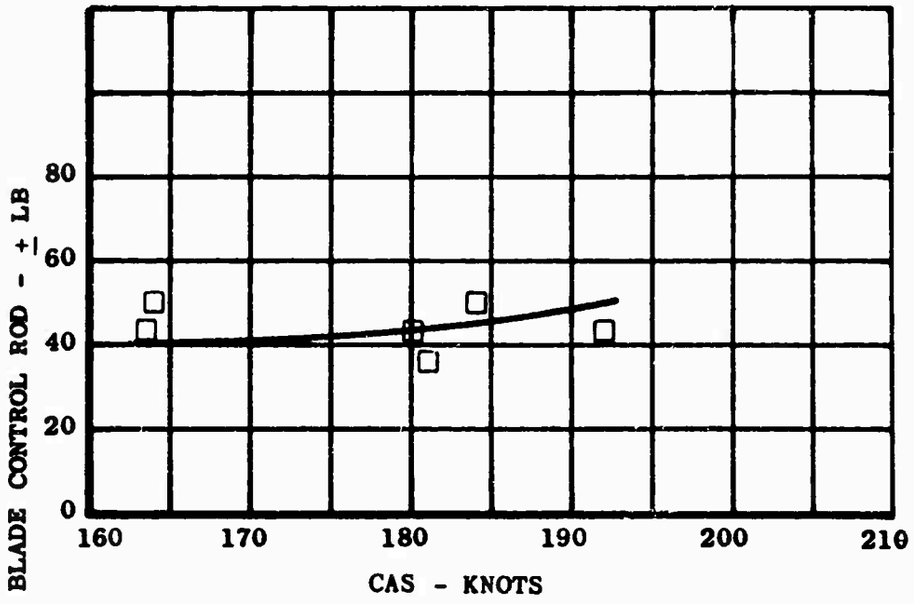

Figure I-2. CONTROL ROD VIBRATORY LOAD.

⊙ T_J 1750 LB
△ T_J 2250 LB
⊡ T_J 2470 LB

GW 8900 LB
CG 173.1
N_R 100%
H_D 400 FT

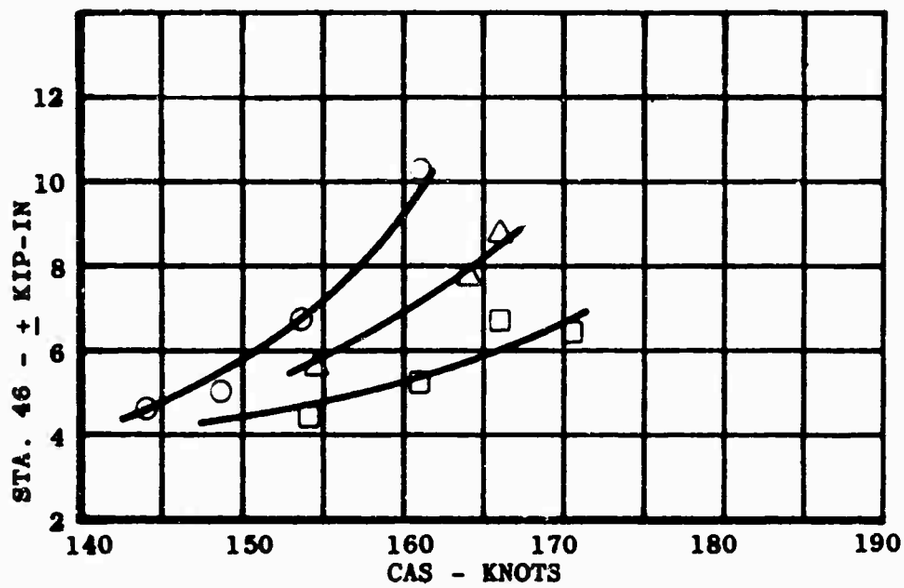

Figure I-3. MAIN ROTOR BLADE FLATWISE VIBRATORY BENDING DISTRIBUTION.

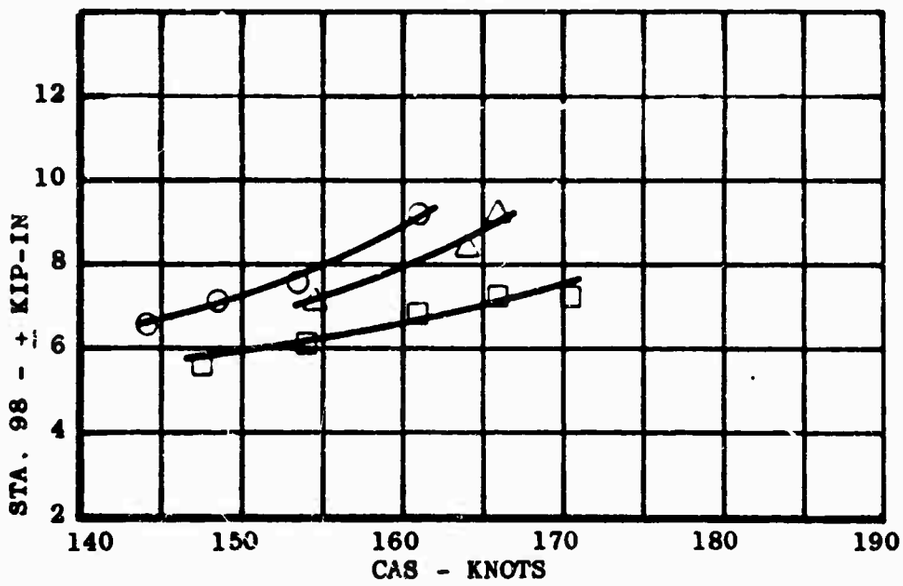

Figure I-3. (Continued)

⊙ T_J	1750 LB	GW	8900 LB
△ T_J	2250 LB	CG	173.1
⊡ T_J	2470 LB	N_R	100%
		H_D	400 FT

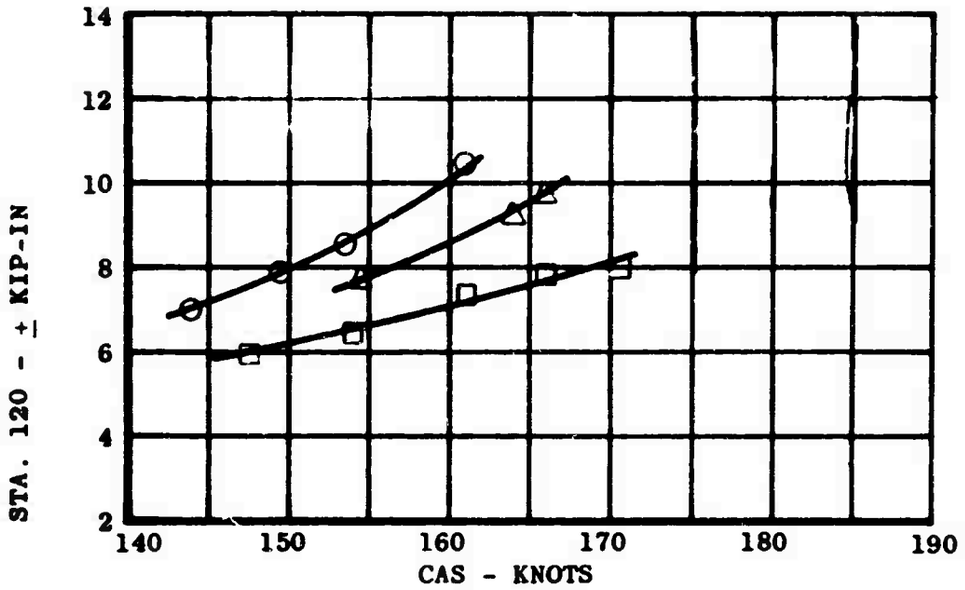

Figure I-3. (Continued)

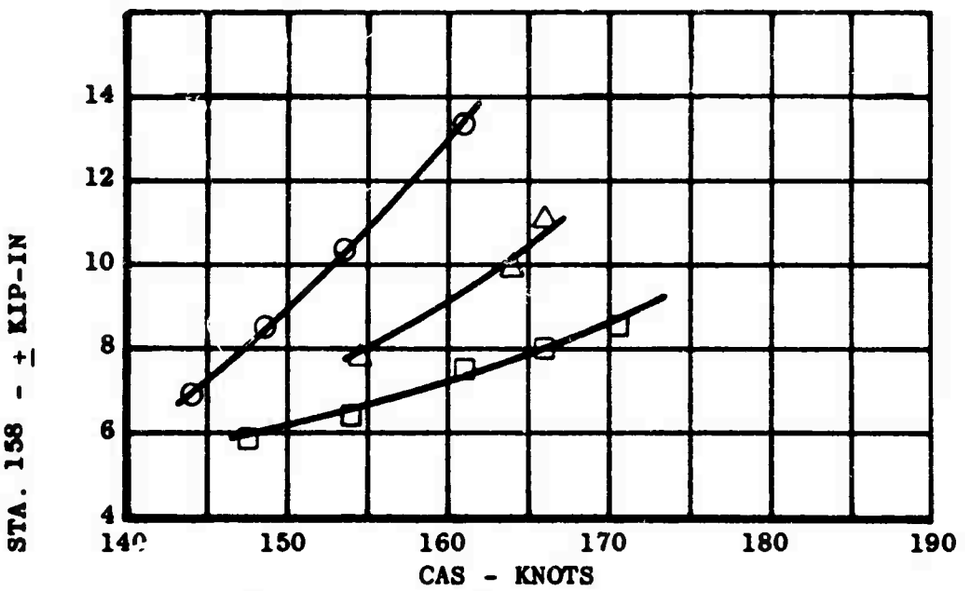

Figure I-3. (Continued)

⊙ T_J	1750 LB	GW	8900 LB
△ T_J	2250 LB	CG	173.1
⊡ T_J	2470 LB	N_R	100%
		H_D	400 FT

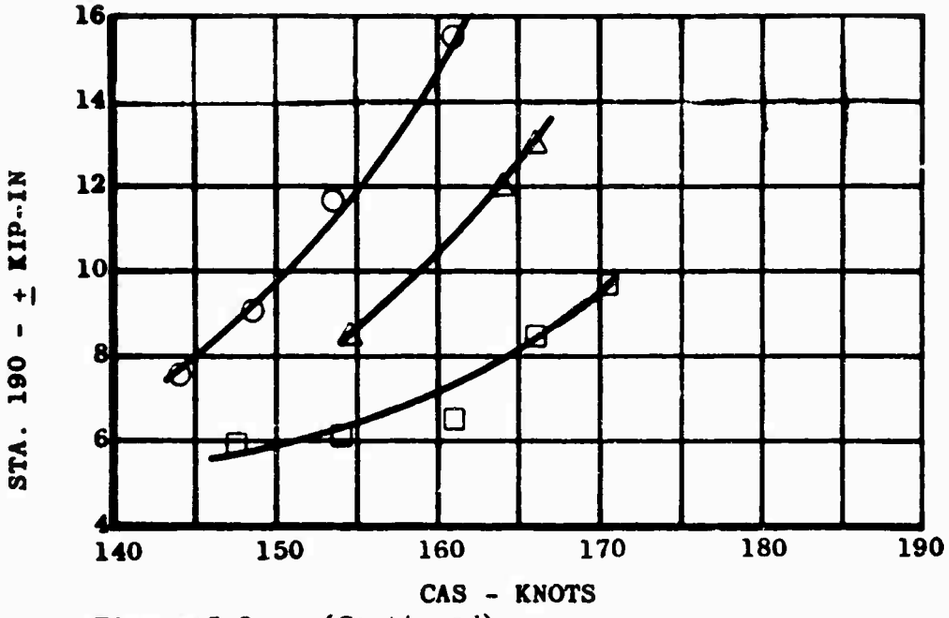

Figure I-3. (Continued)

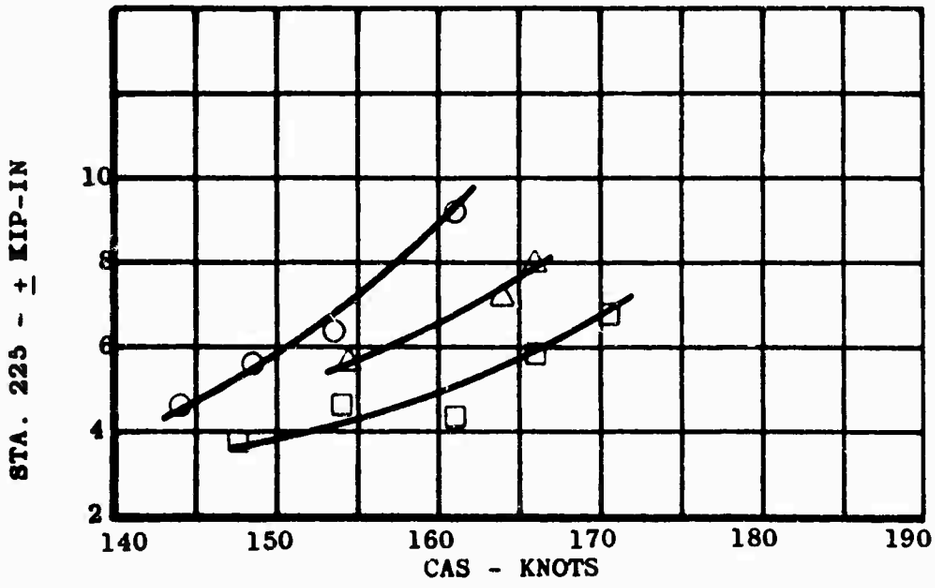

Figure I-3. (Continued)

⊙ T_J	1750 LB	GW	8900 LB
△ T_J	2250 LB	CG	173.1
⊡ T_J	2470 LB	N_R	100%
		H_D	400 FT

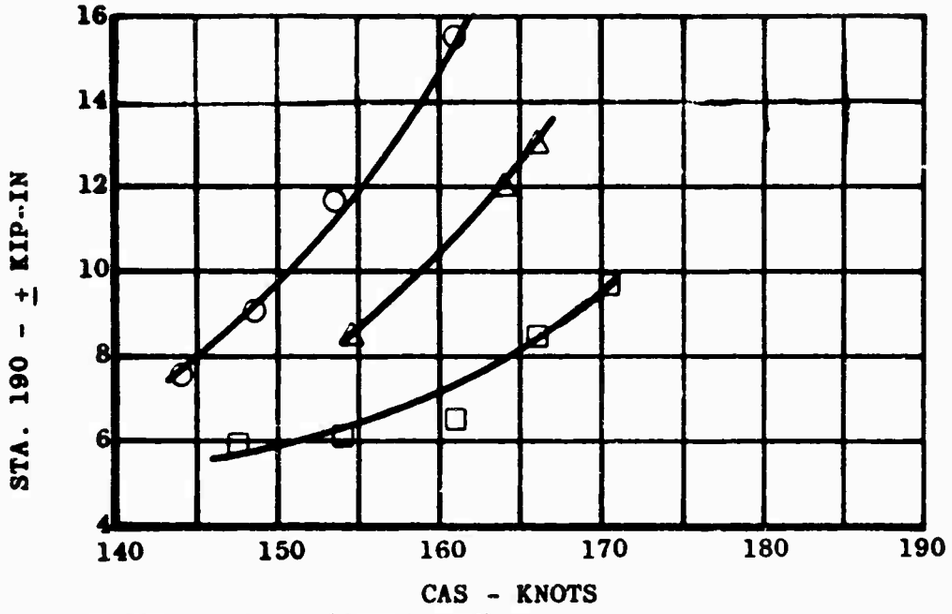

Figure I-3. (Continued)

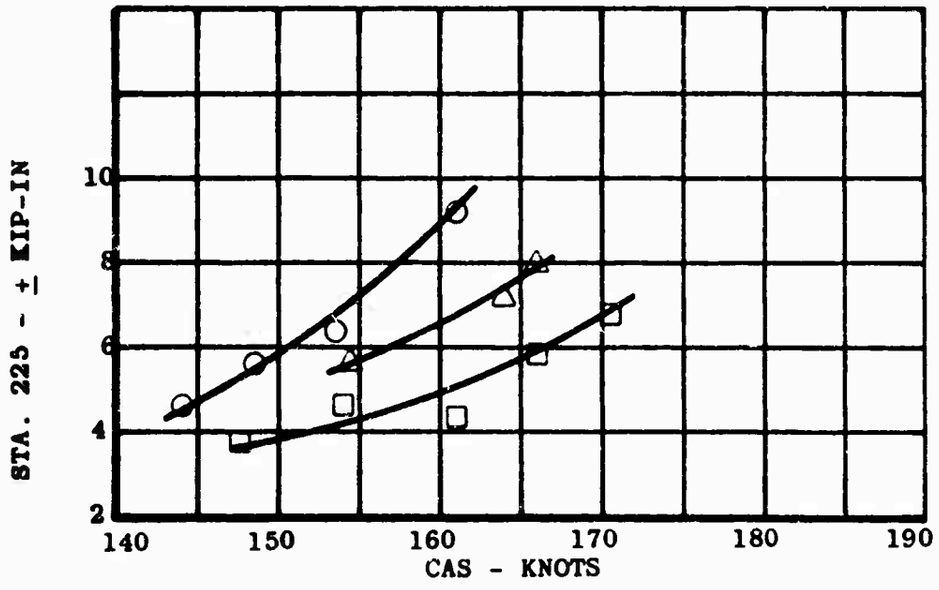

Figure I-3. (Continued)

⊙ T_J	1500 LB	GW	8900 LB
△ T_J	2000 LB	CG	173.1
□ T_J	2400 LB	N_R	100%
		H_D	2500 FT

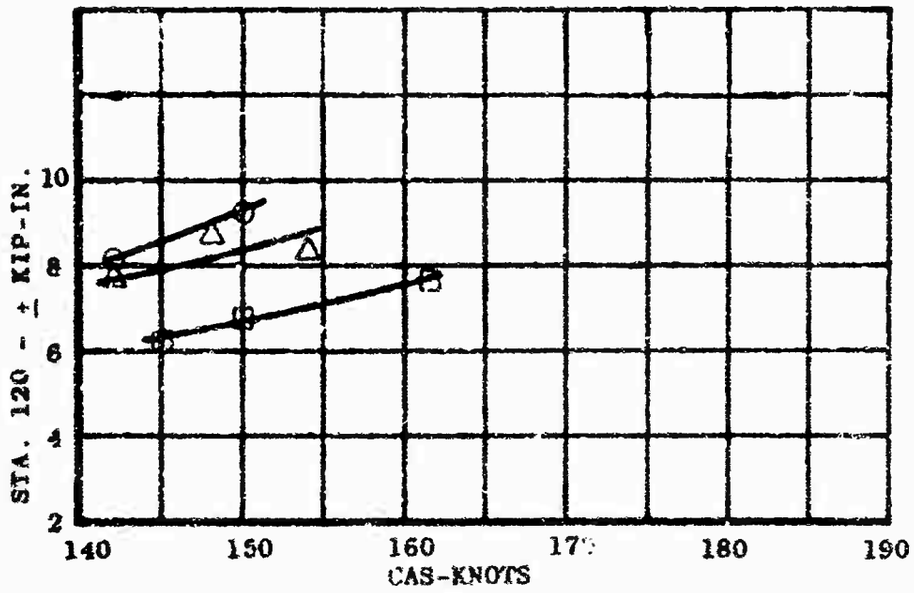

Figure I-3. (Continued)

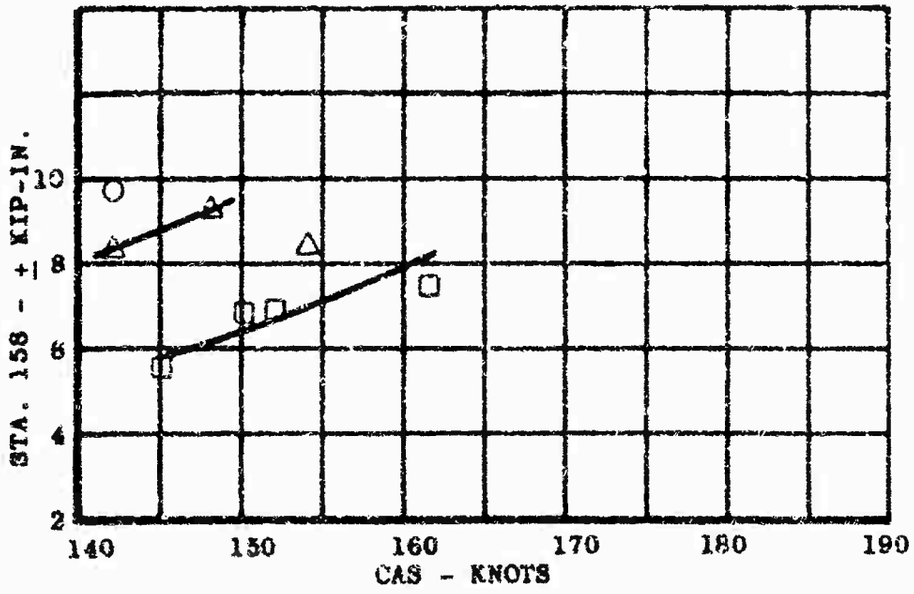

Figure I-3. (Continued)

○ T_J	1500 LB	GW	8900 LB
△ T_J	2000 LB	CG	173.1
□ T_J	2400 LB	N_R	100%
		H_D	2500 FT

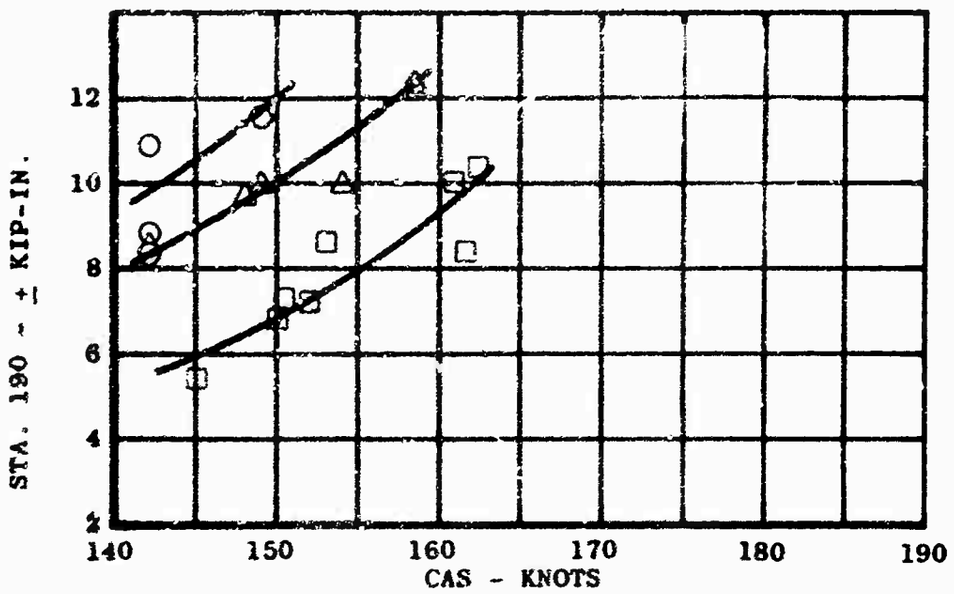

Figure I-3. (Continued)

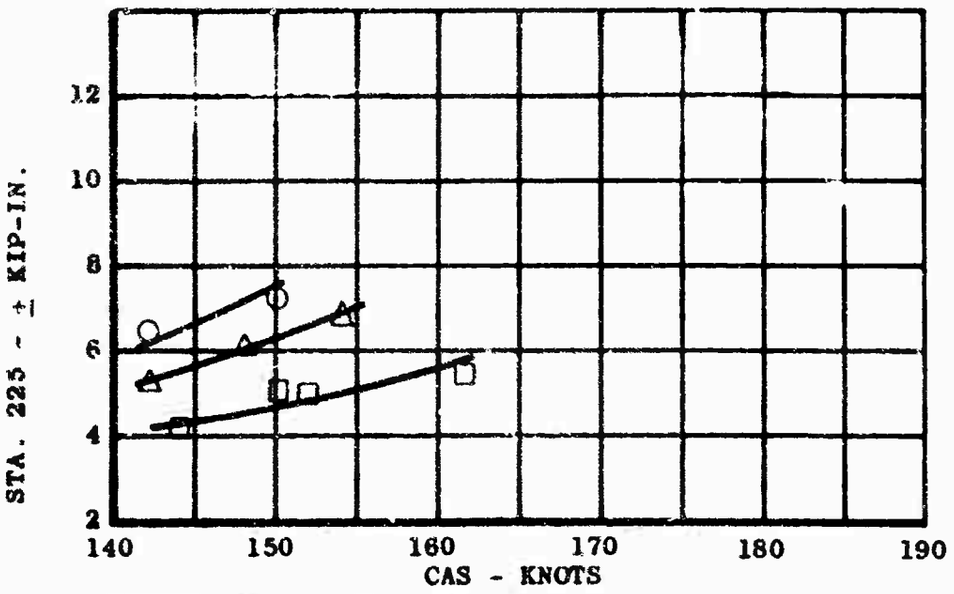

Figure I-3. (Continued)

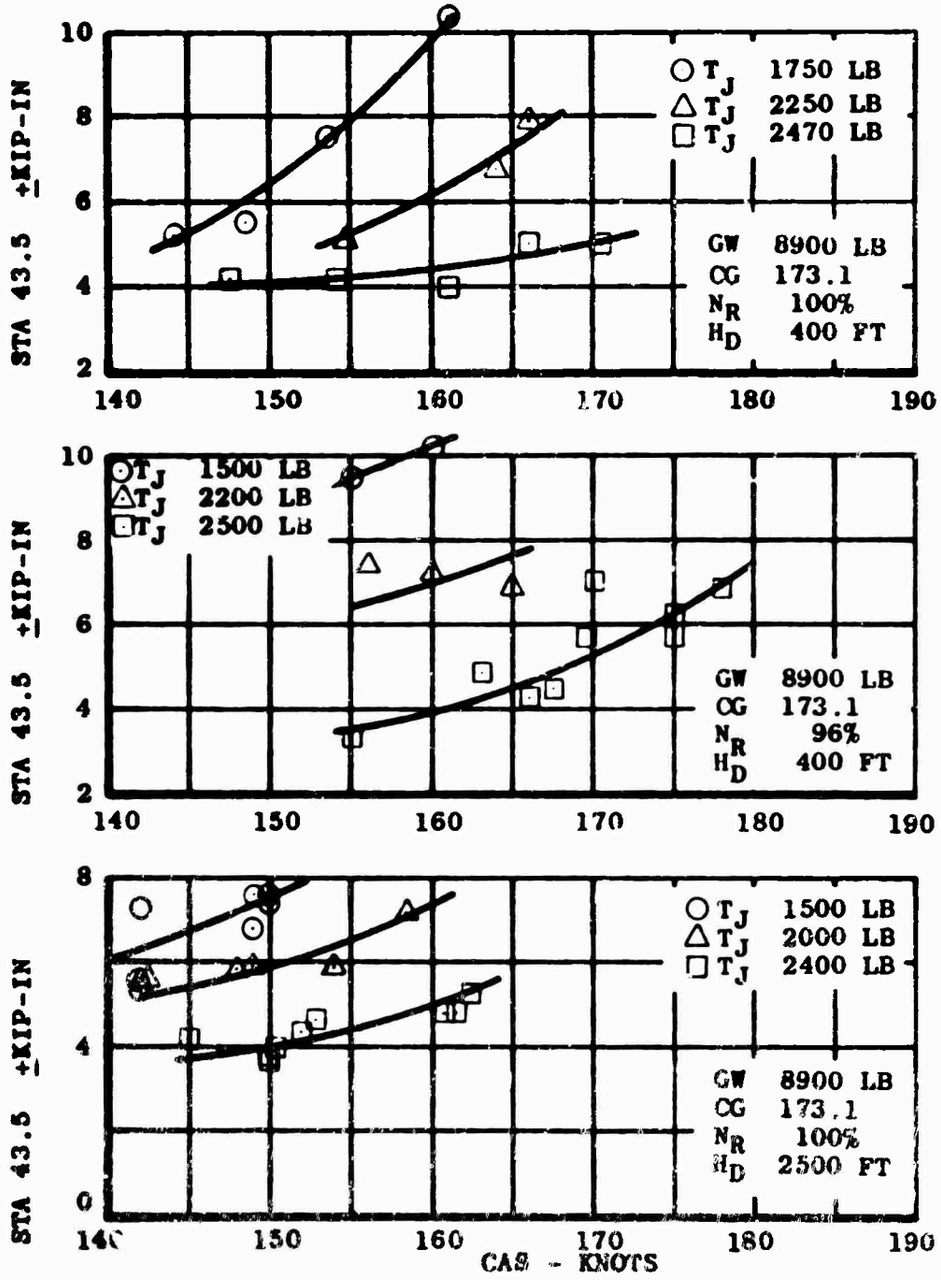

Figure I-4. MAIN ROTOR BLADE EDGEWISE VIBRATORY BENDING.

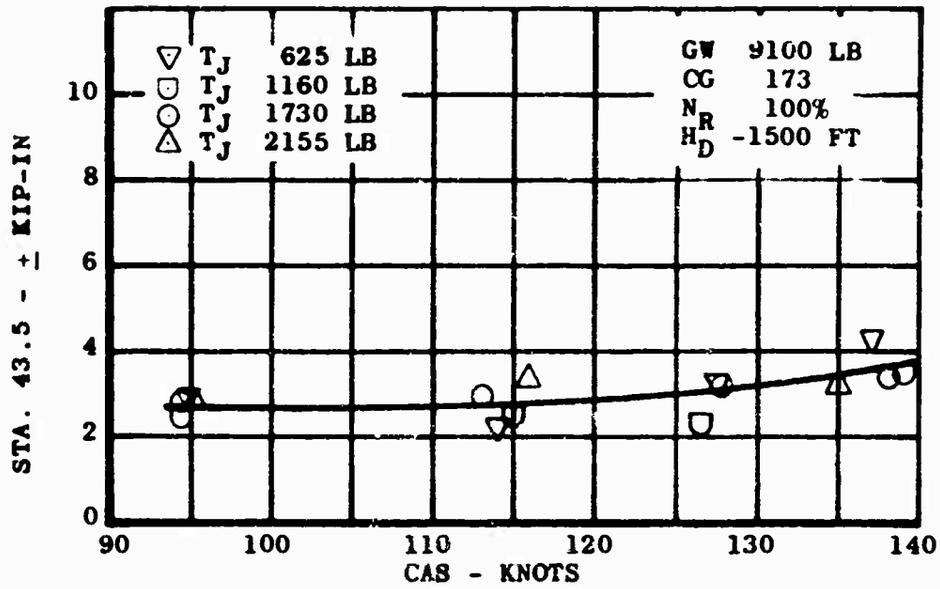

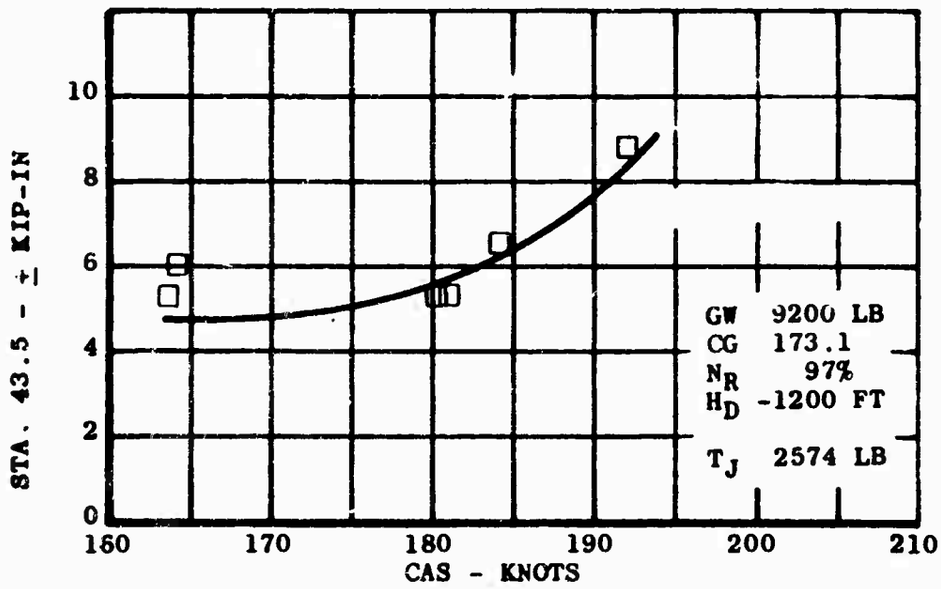

Figure I-4. (Continued).

▽ T_J 625 LB
▢ T_J 1160 LB
○ T_J 1730 LB
△ T_J 2155 LB

GW 9100 LB
CG 173
N_R 100%
H_D -1500 FT

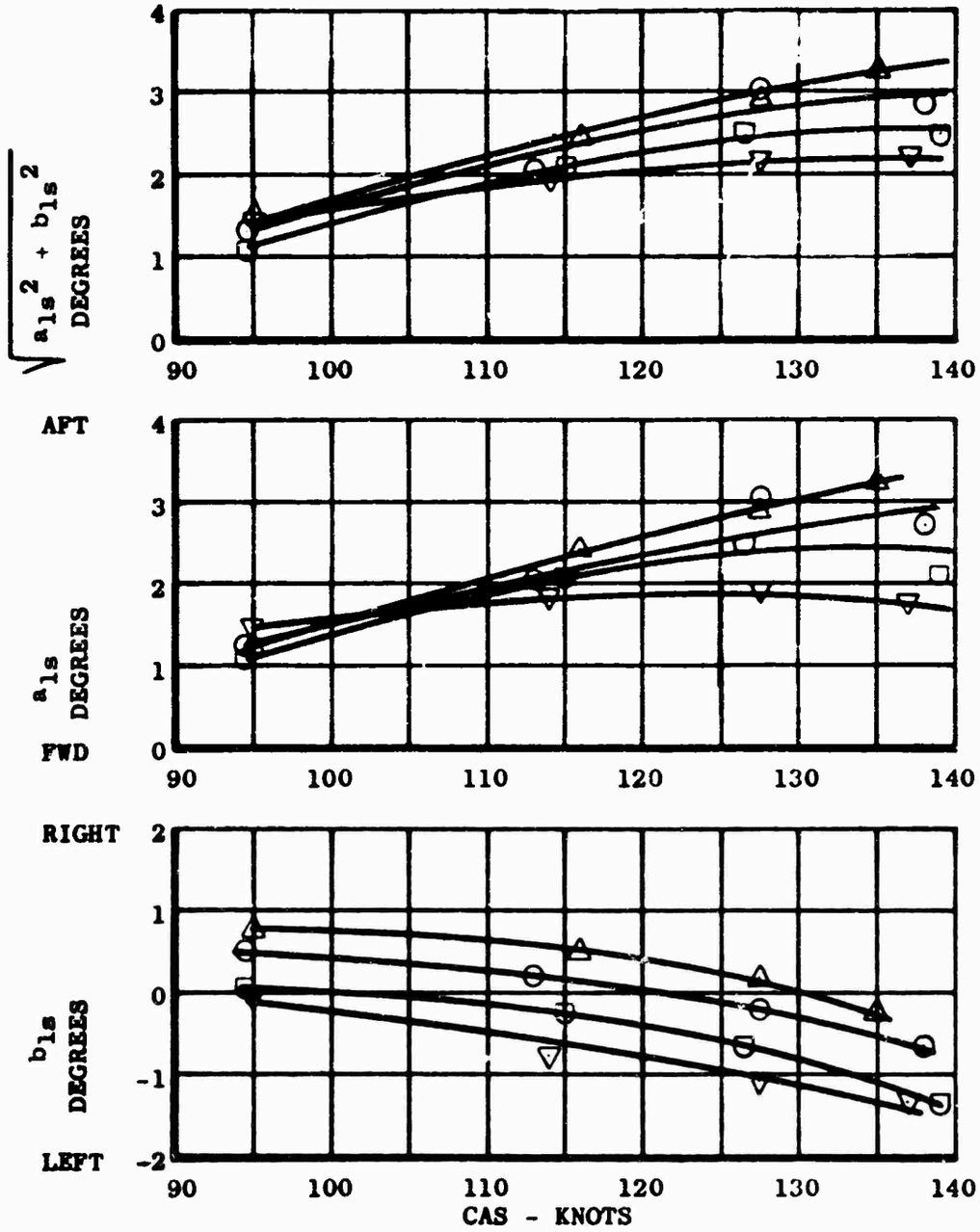

Figure I-5. MAIN ROTOR FLAPPING

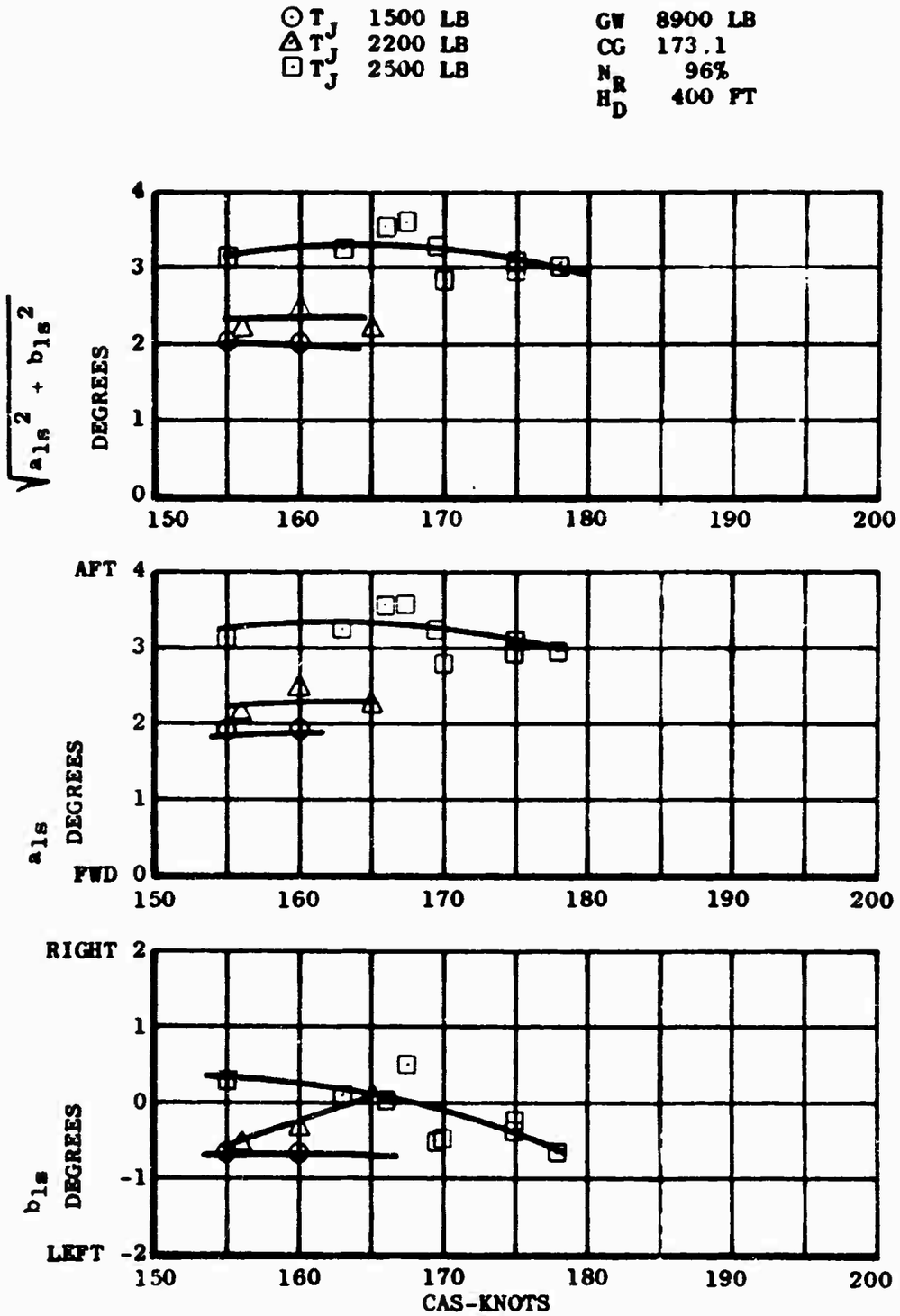

Figure I-5. (Continued)

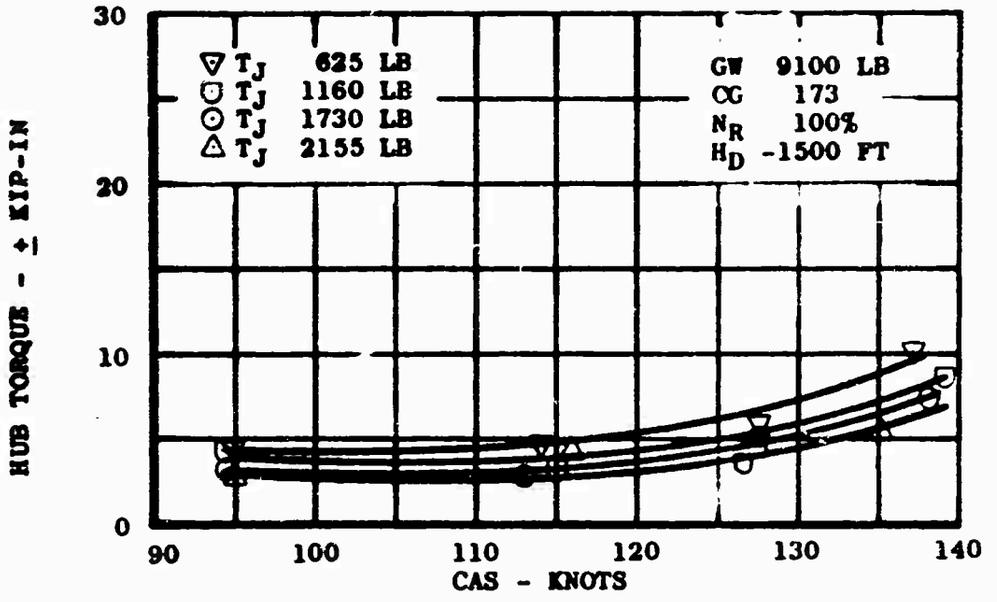

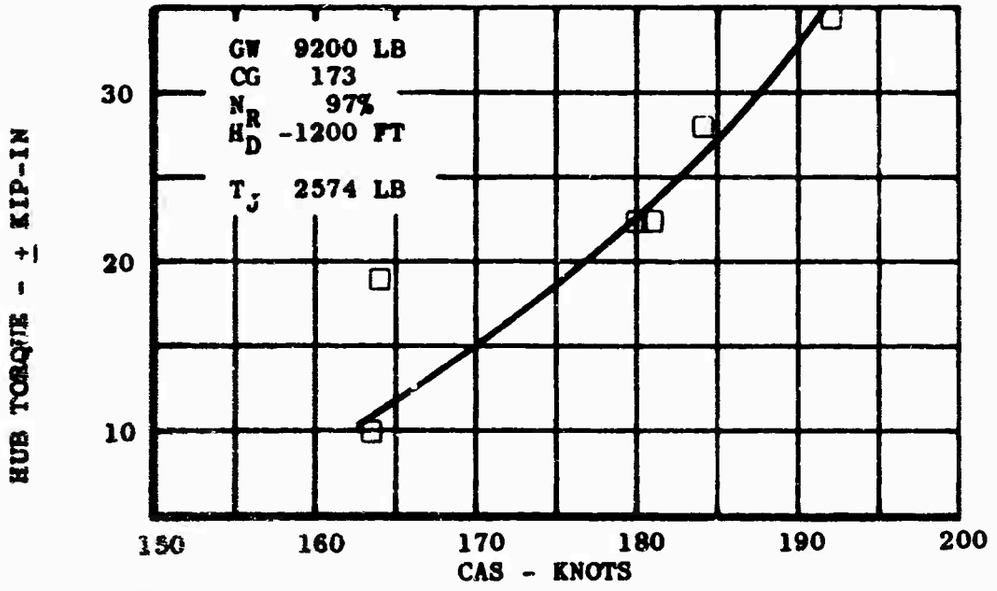

Figure I-6. MAIN ROTOR HUB VIBRATORY TORQUE

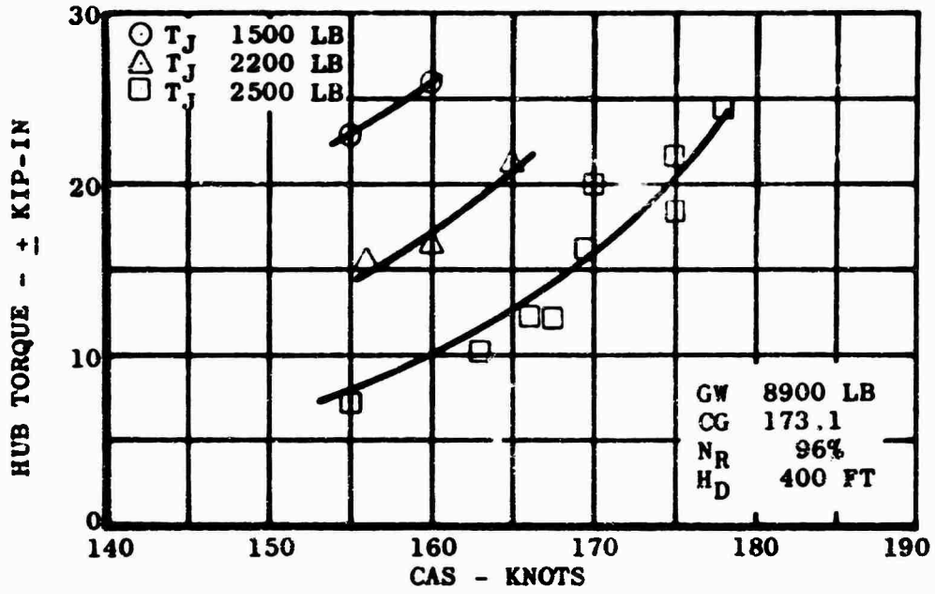

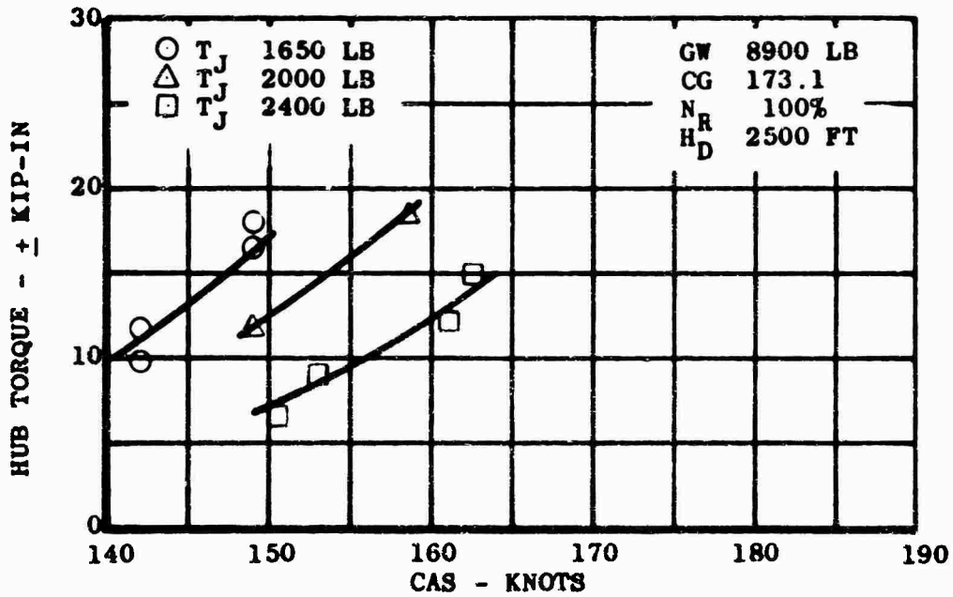

Figure I-8. (Continued)

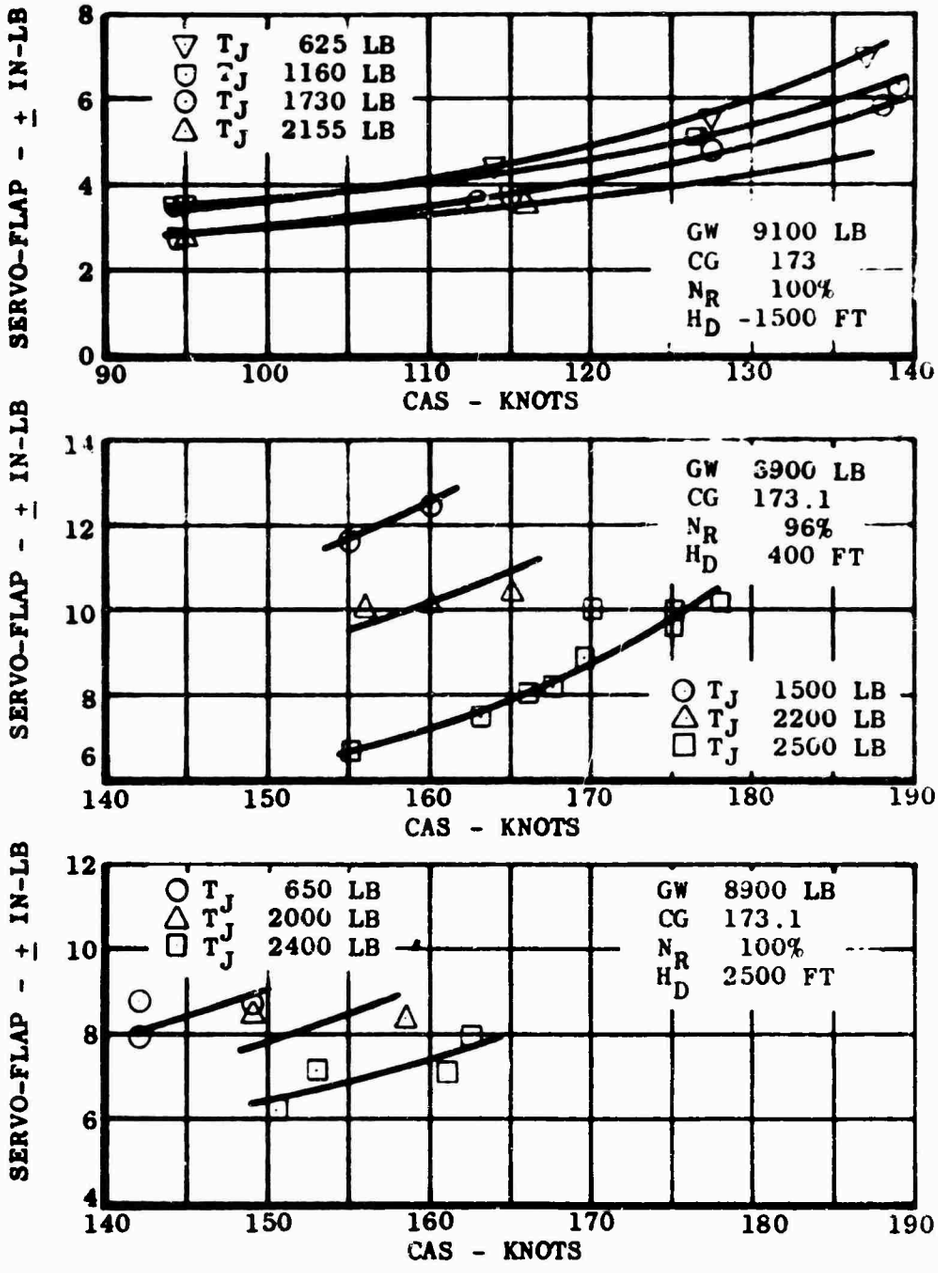

Figure I-7. SERVO-FLAP FLATWISE VIBRATORY BENDING

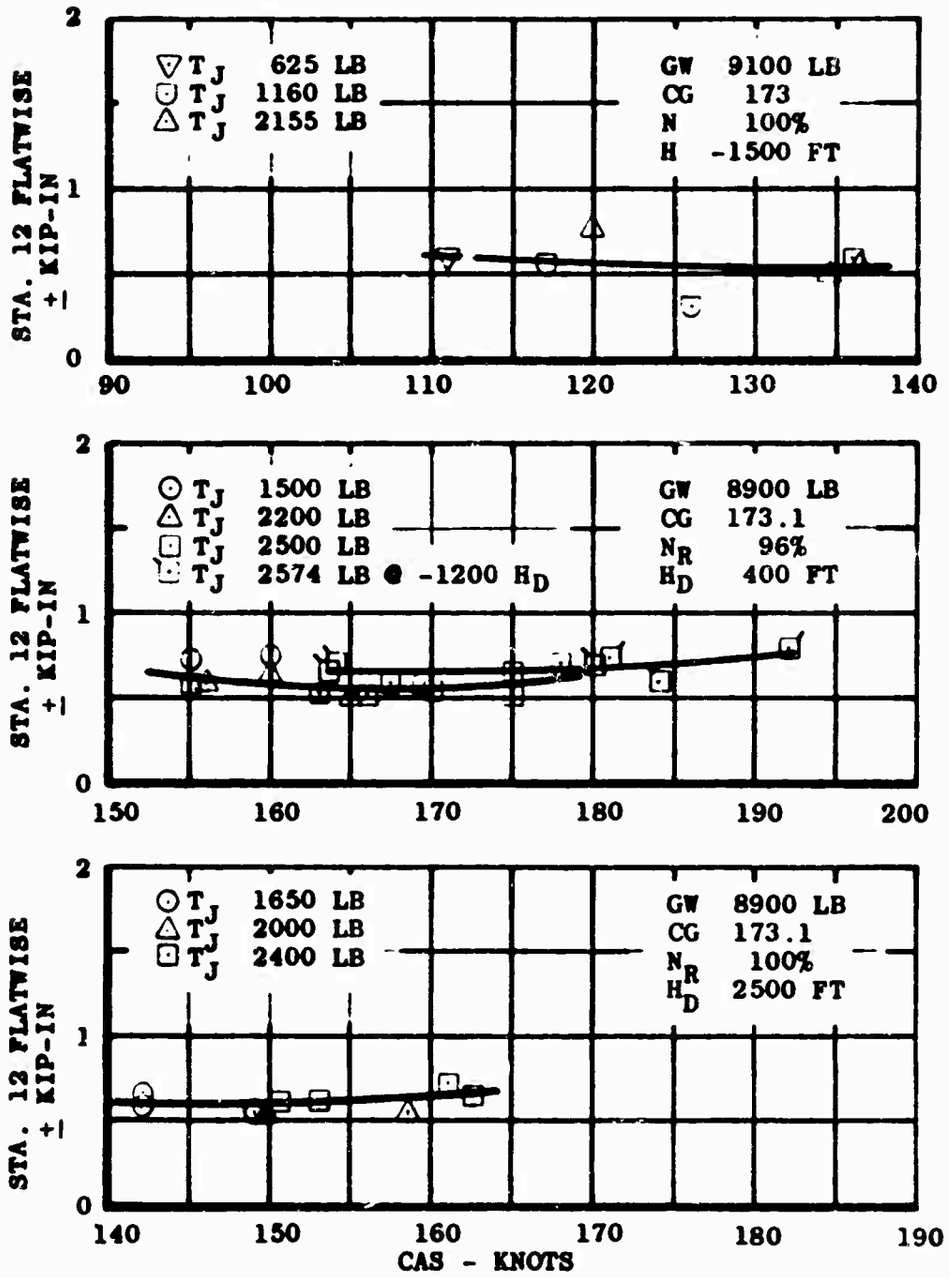

Figure I-8. TAIL ROTOR BLADE FLATWISE VIBRATORY BENDING.

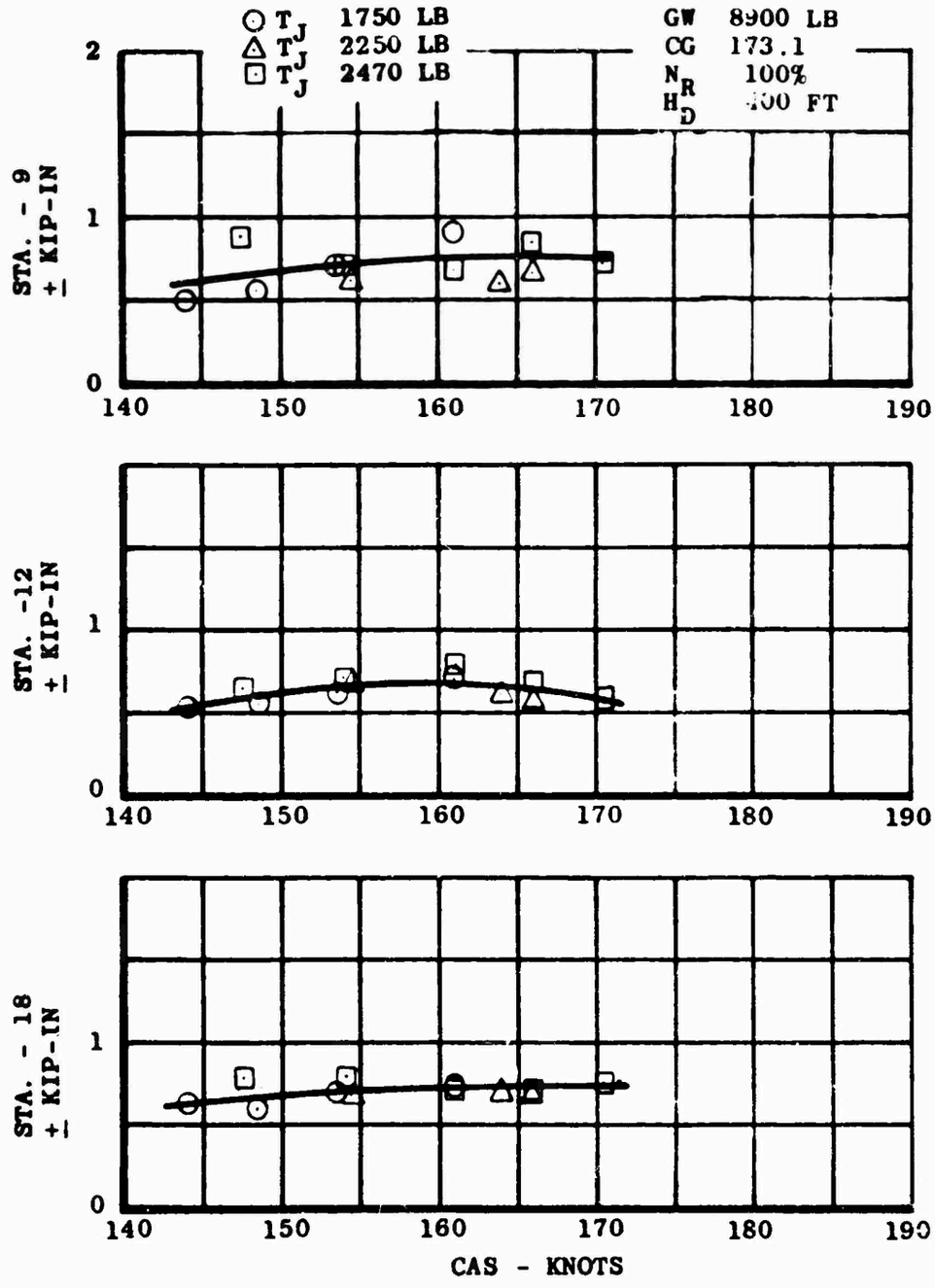

Figure I-9. TAIL ROTOR BLADE FLATWISE VIBRATORY BENDING MOMENT DISTRIBUTION.

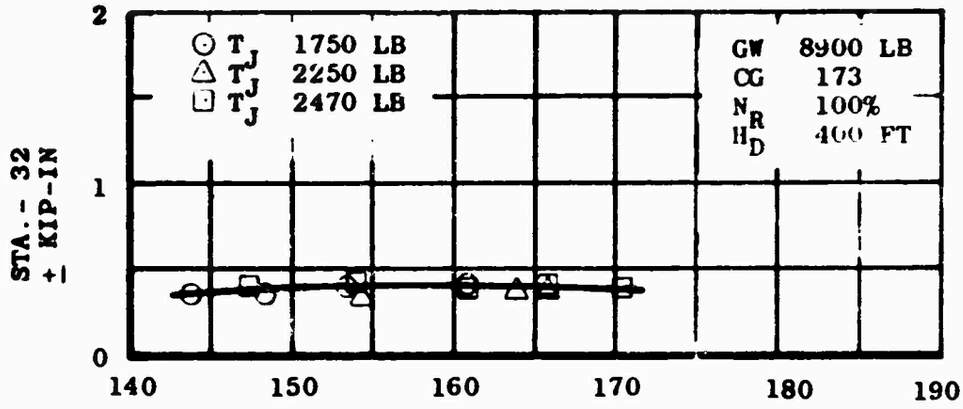

Figure I-9. (Continued)

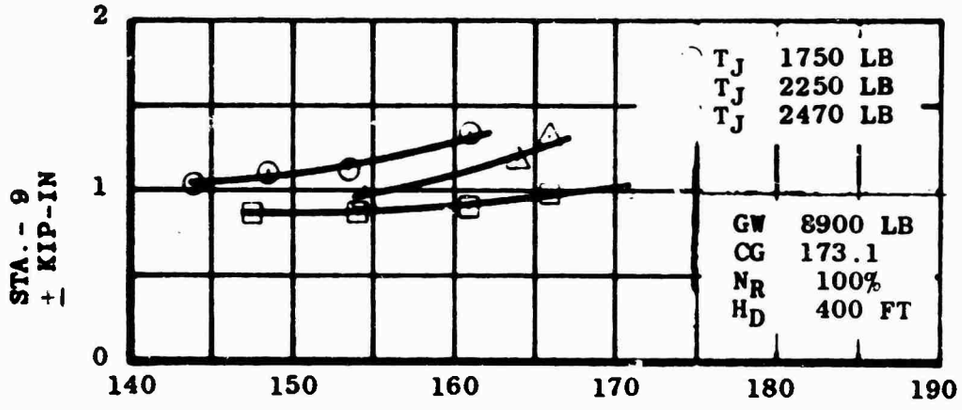

Figure I-10. TAIL ROTOR BLADE EDGEWISE VIBRATORY BENDING DISTRIBUTION.

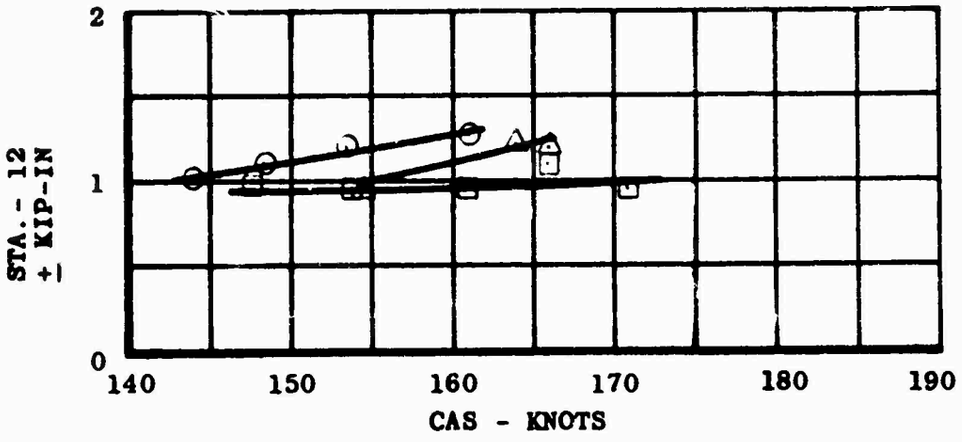

Figure I-10. (Continued)

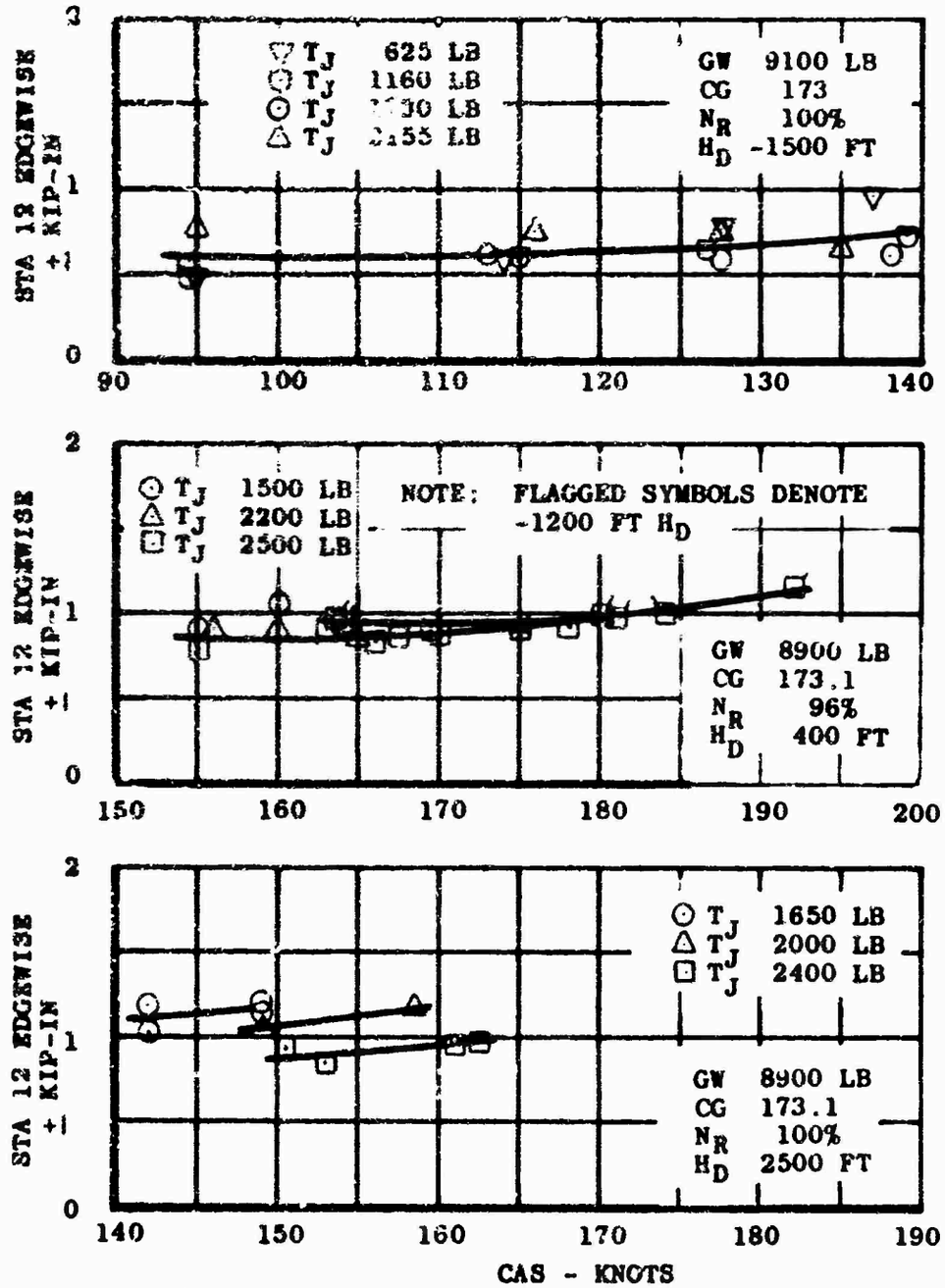

Figure I-11. TAIL ROTOR BLADE EDGEWISE VIBRATORY BENDING.

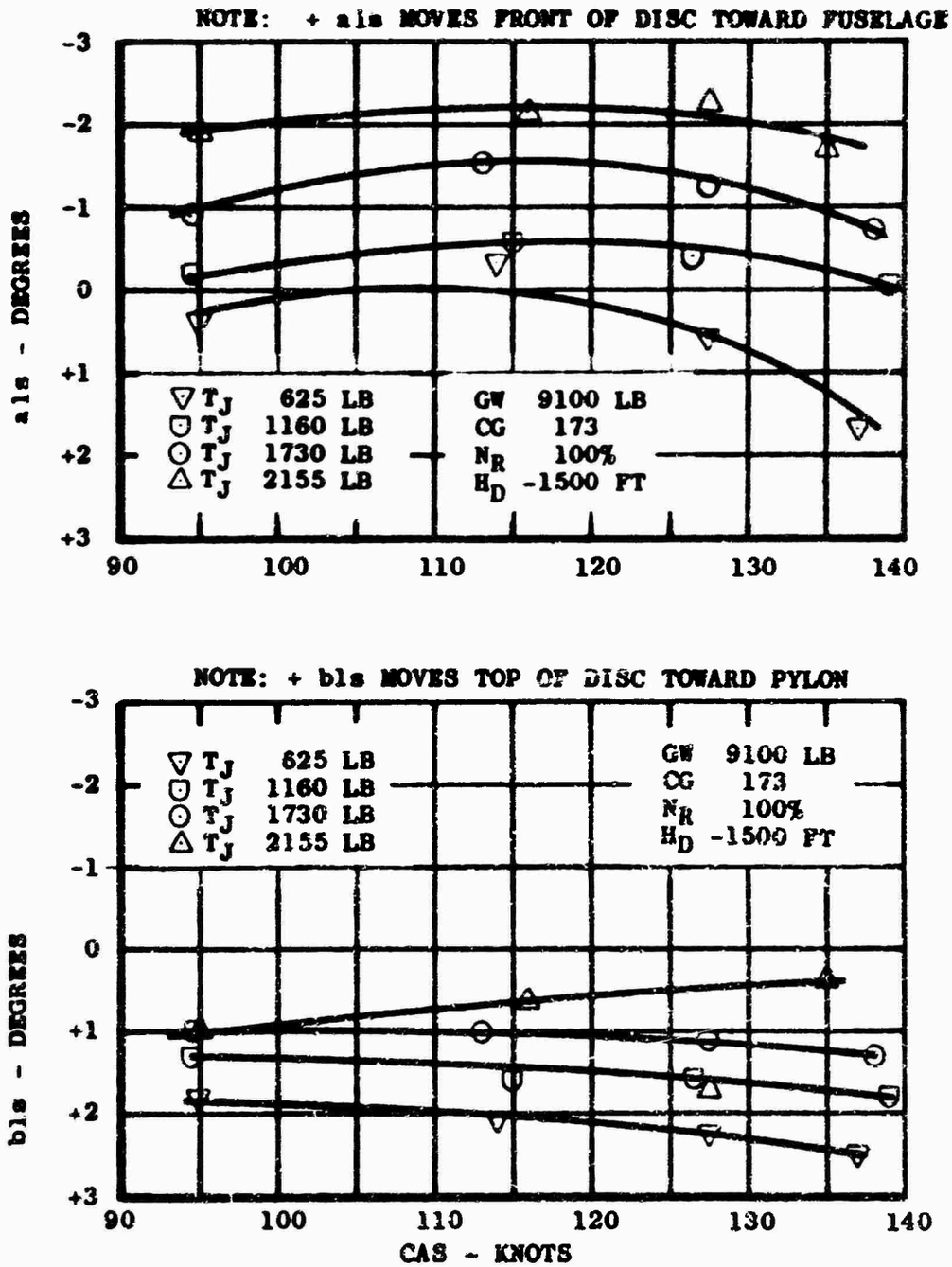

Figure I-12. TAIL ROTOR FLAPPING ANGLES

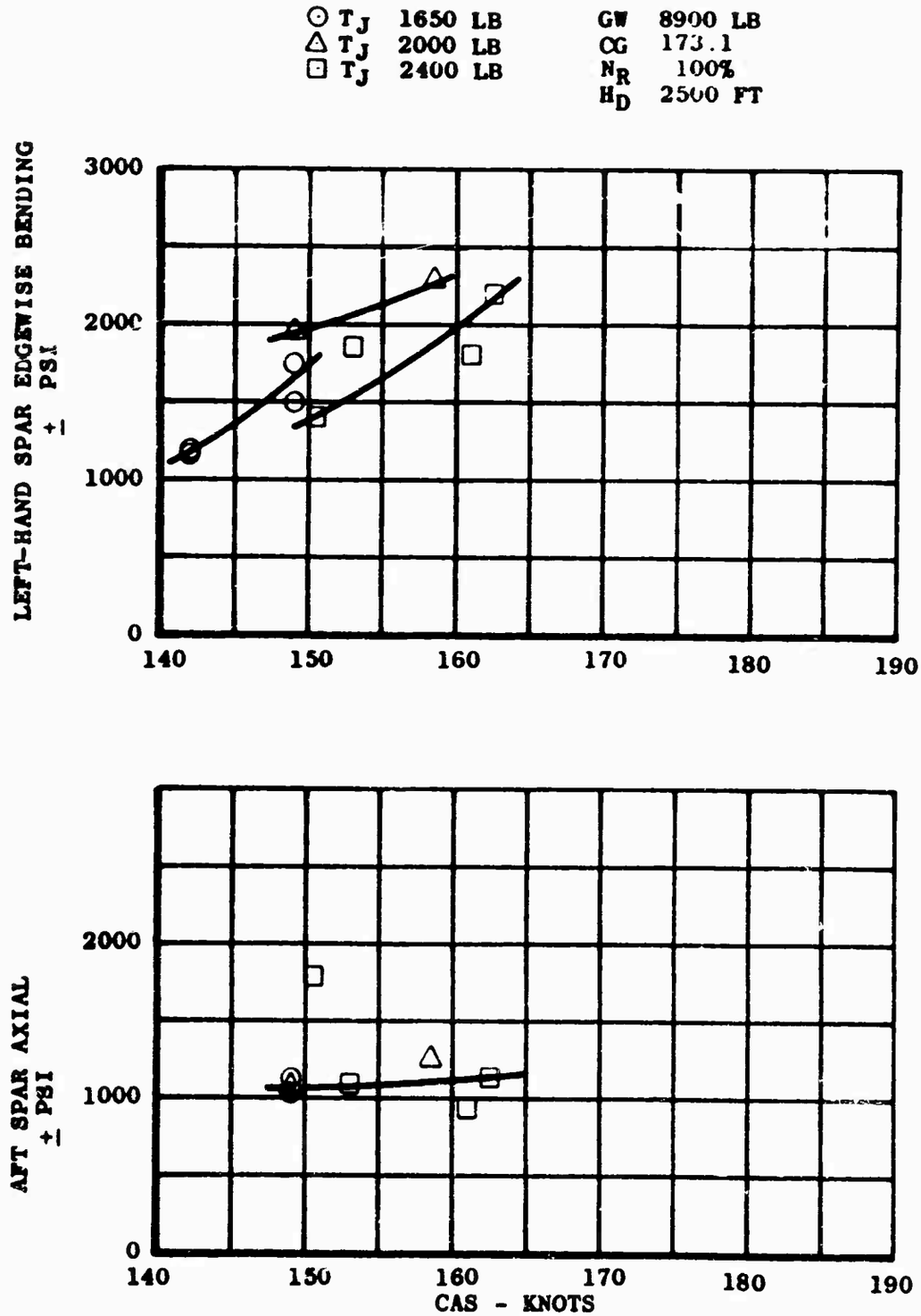

Figure I-13. HORIZONTAL STABILIZER VIBRATORY STRESSES

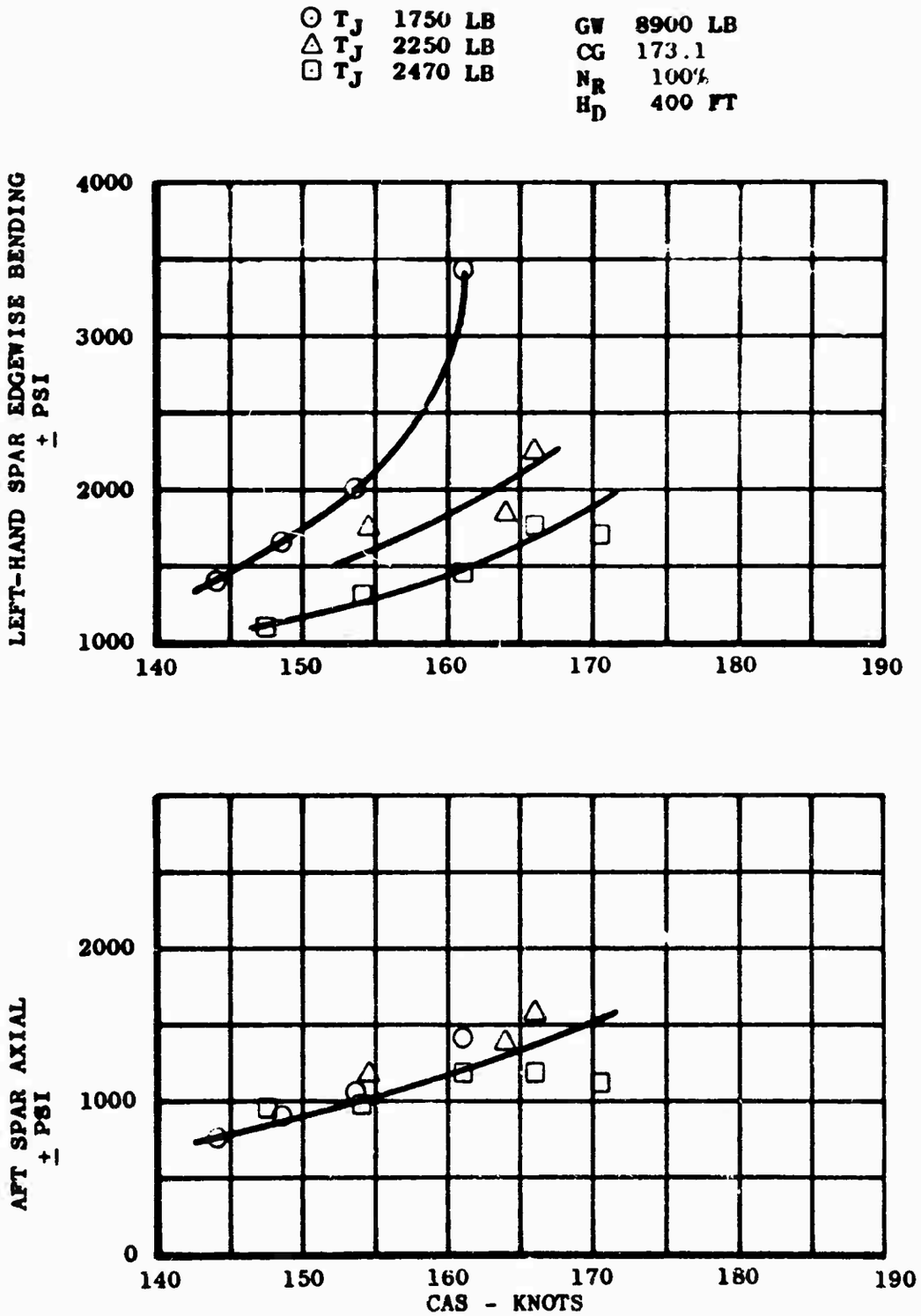

Figure I-13. (Continued)

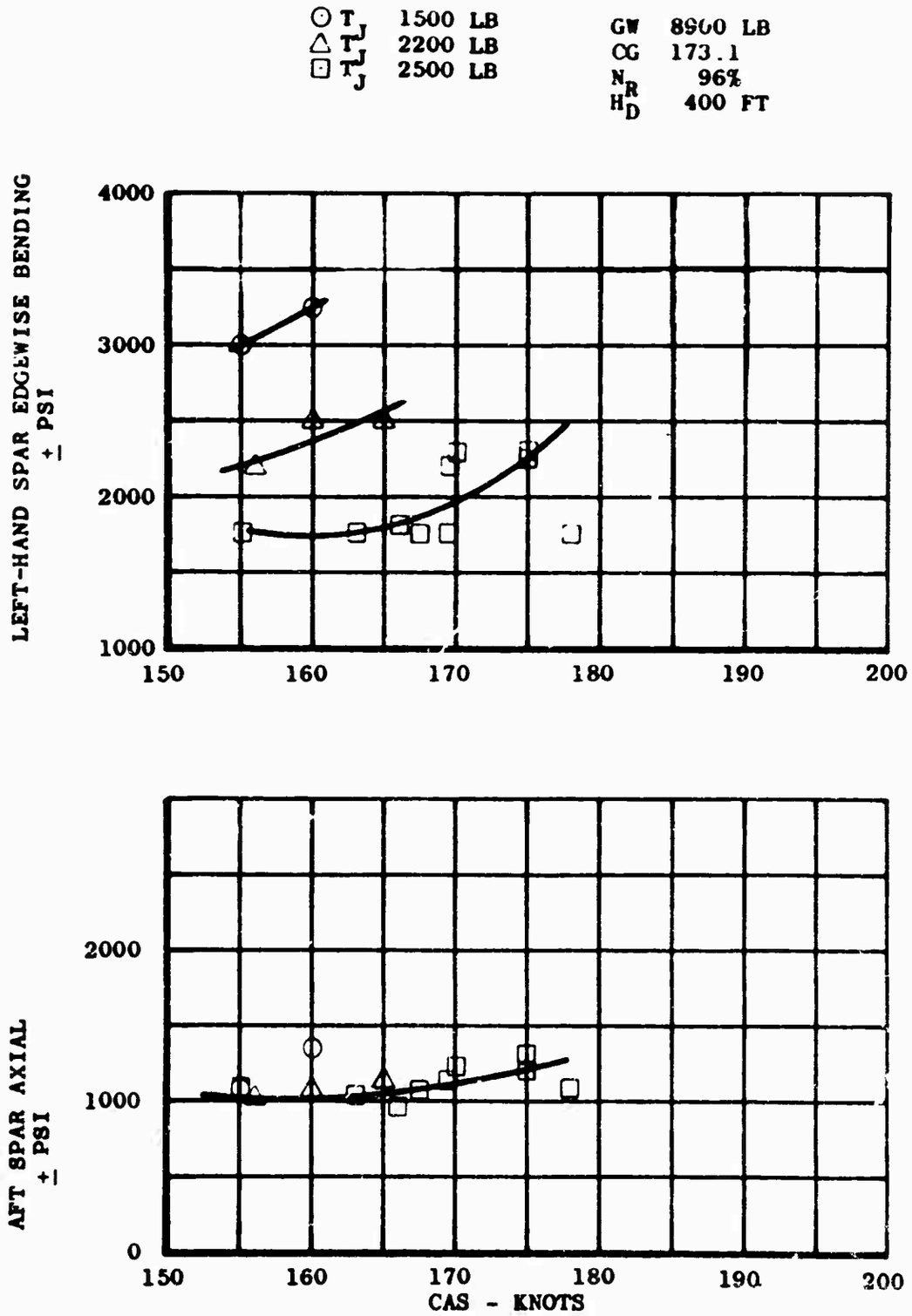

Figure I-13. (Continued)

T_J 2574 LB

GW 9200 LB
CG 173.1
N_R 97%
H_D -1200 FT

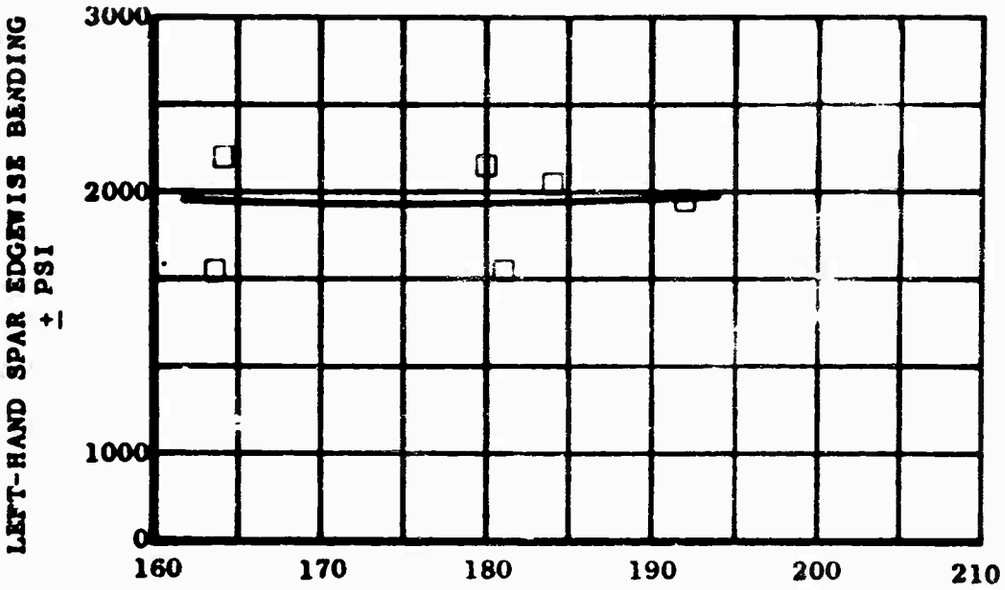

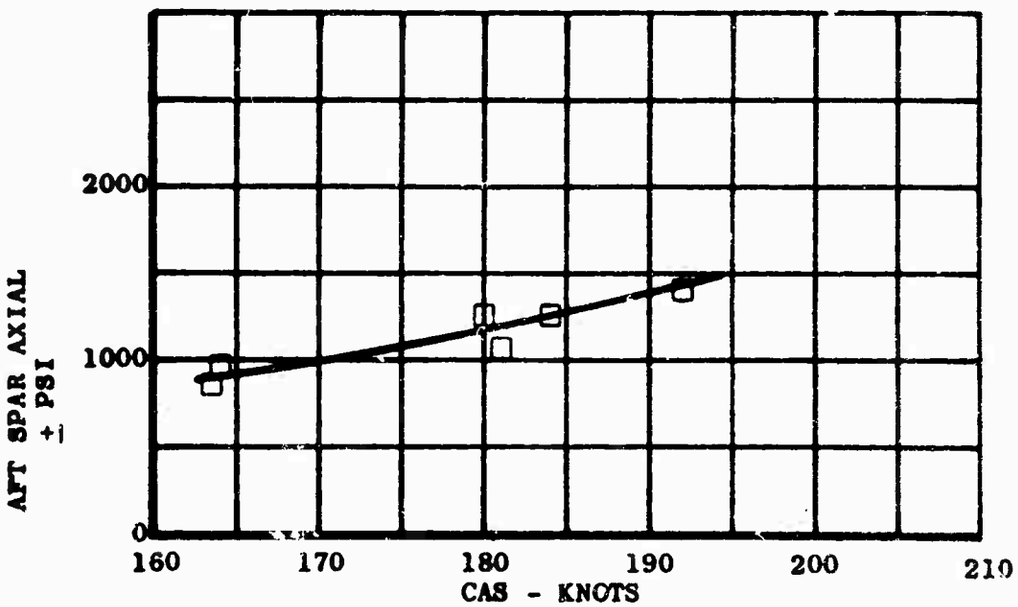

Figure I-13. (Continued)

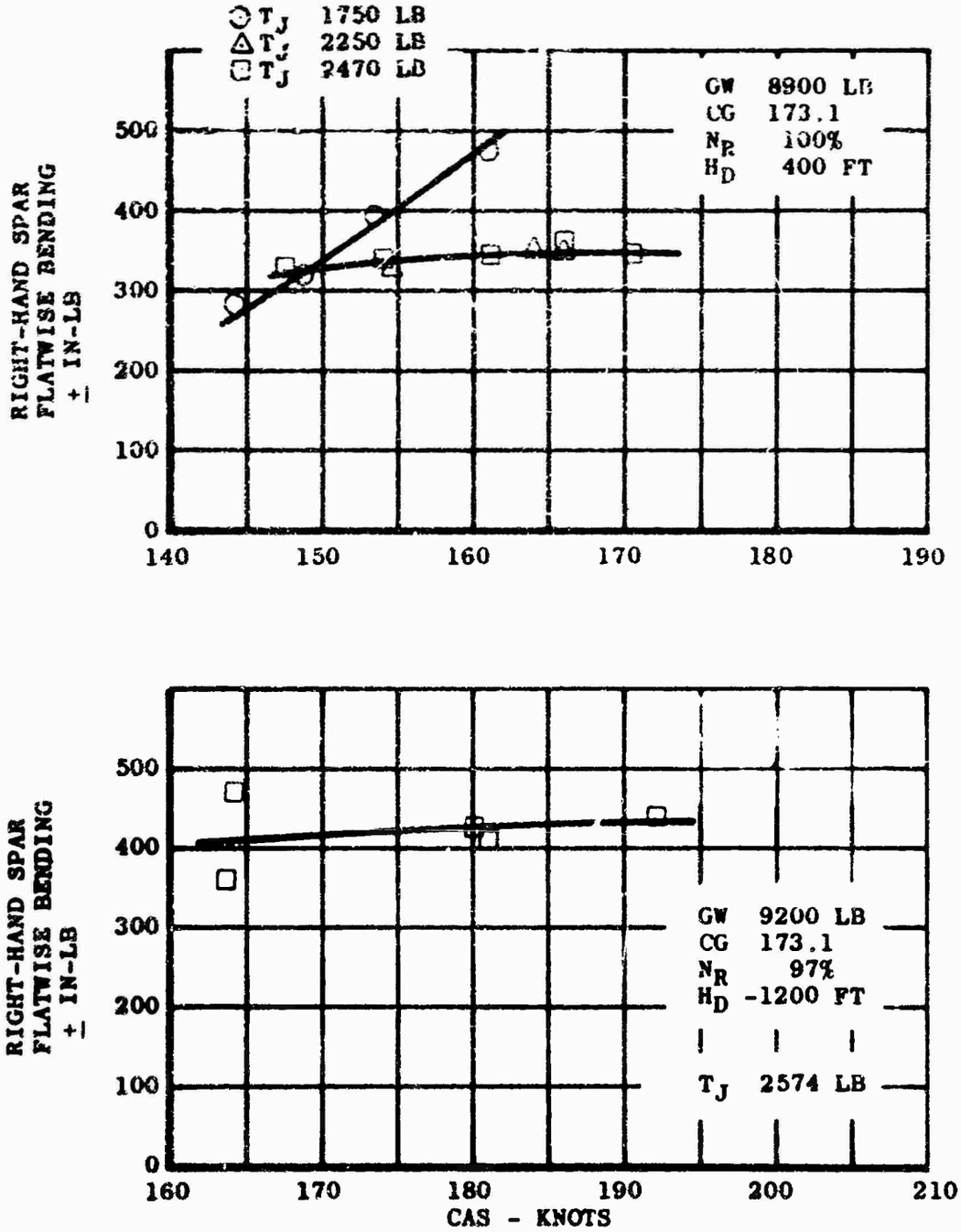

Figure I-13. (Continued)

▽ T_J	625 LB	GW	9100 LB
⊡ T_J	1160 LB	CG	173
⊙ T_J	1730 LB	N_R	100%
△ T_J	2155 LB	H_D	-1500 FT

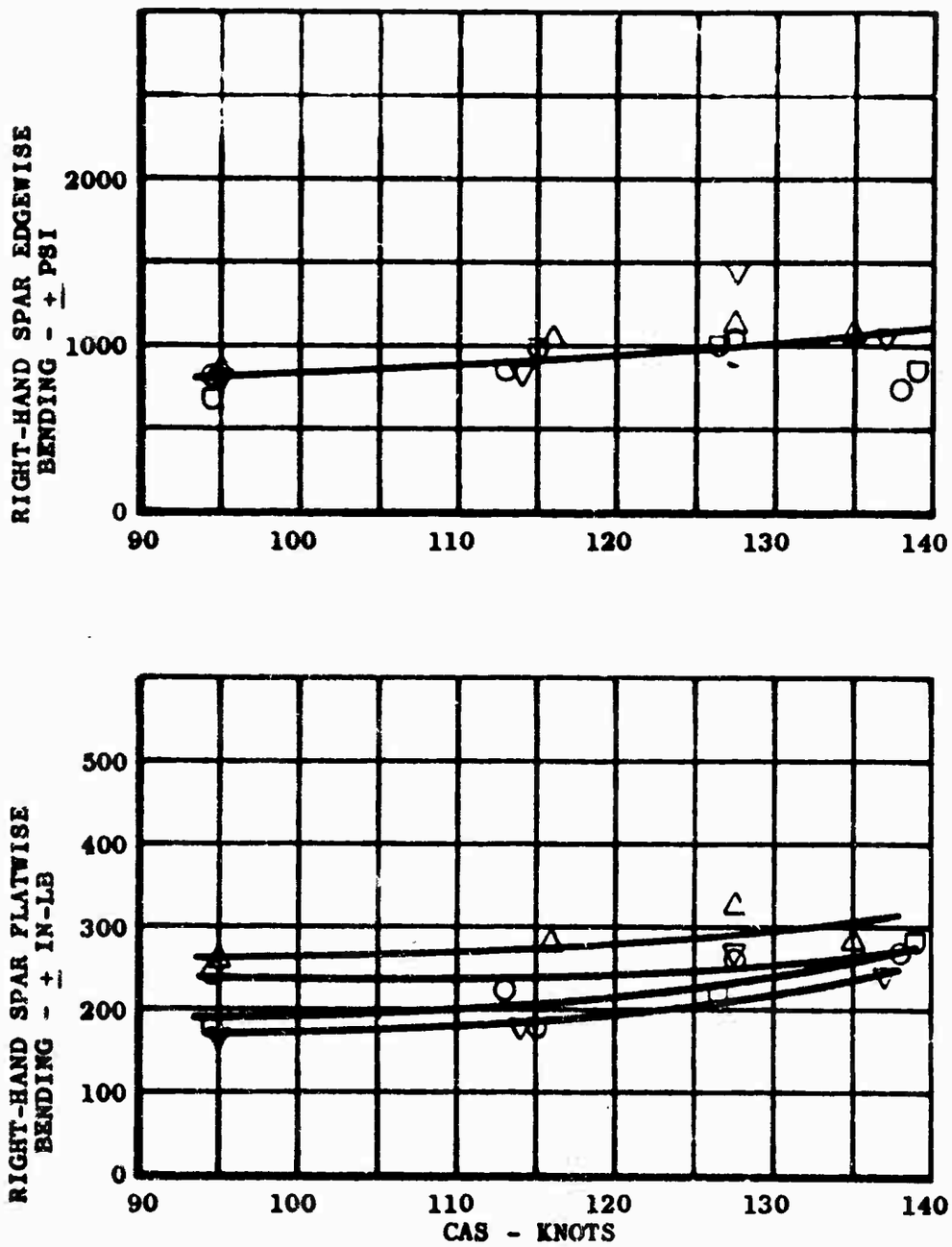

Figure I-13. (Continued)

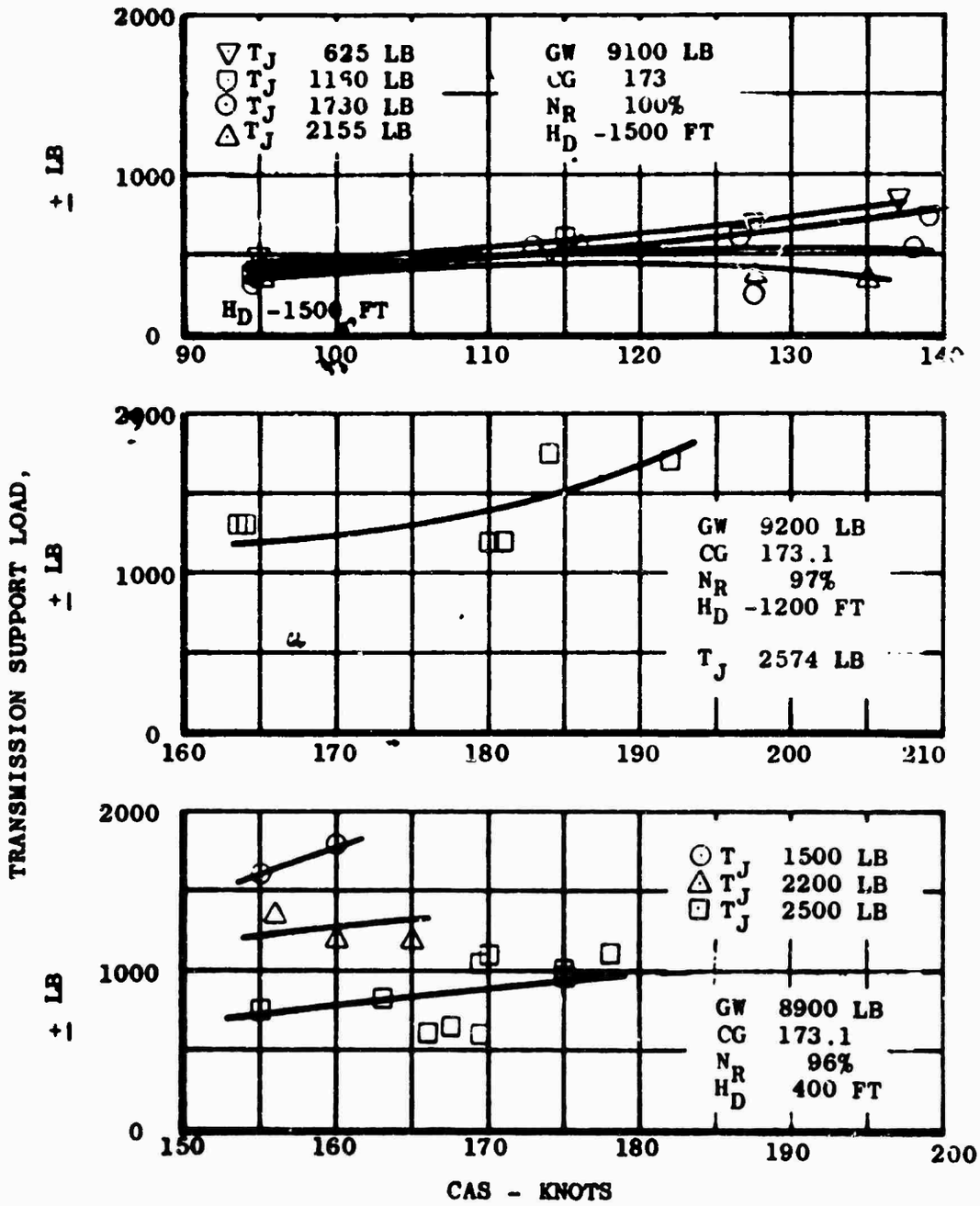

Figure I-14. TRANSMISSION SUPPORT TUBE VIBRATORY LOADS

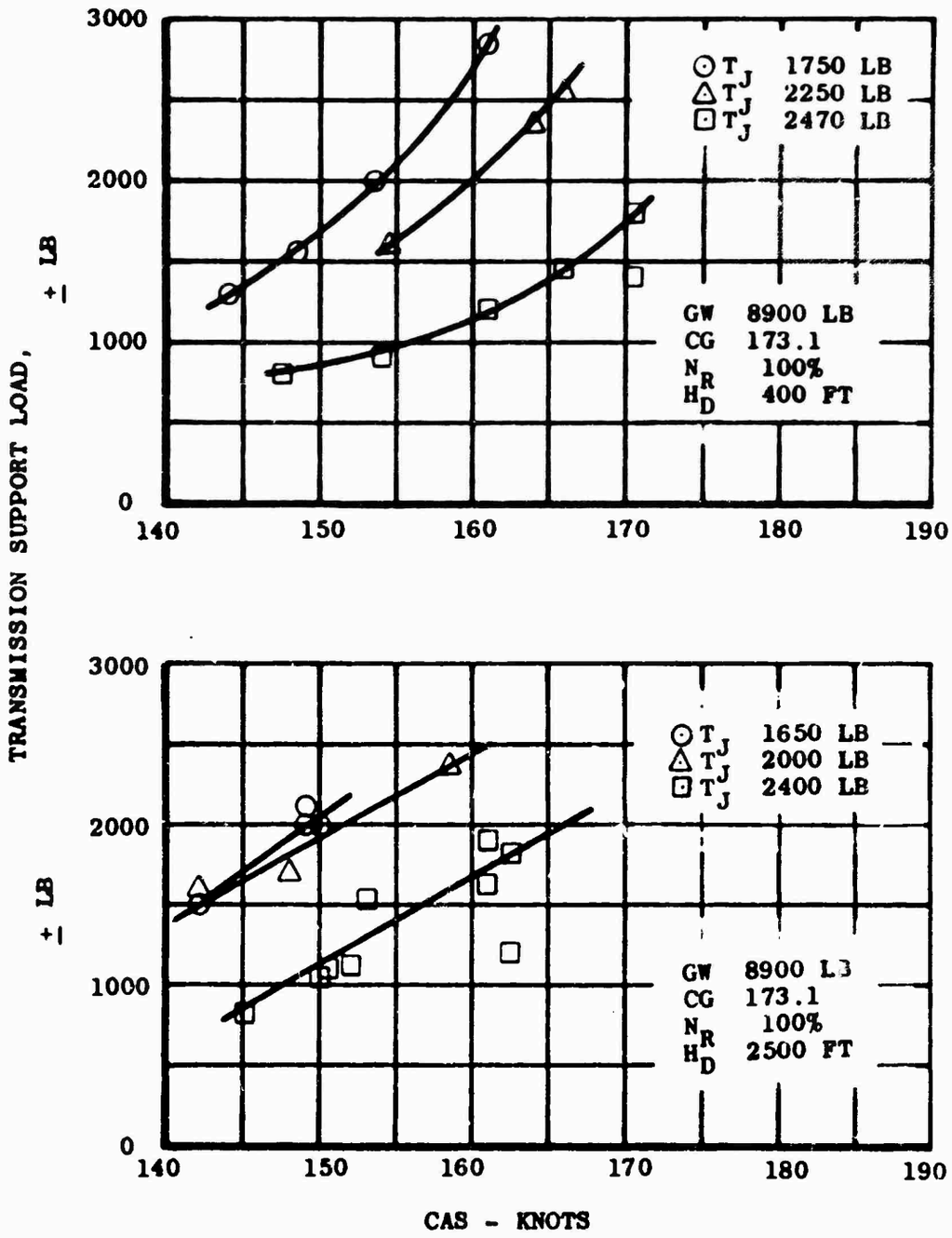

Figure I-14. (Continued)

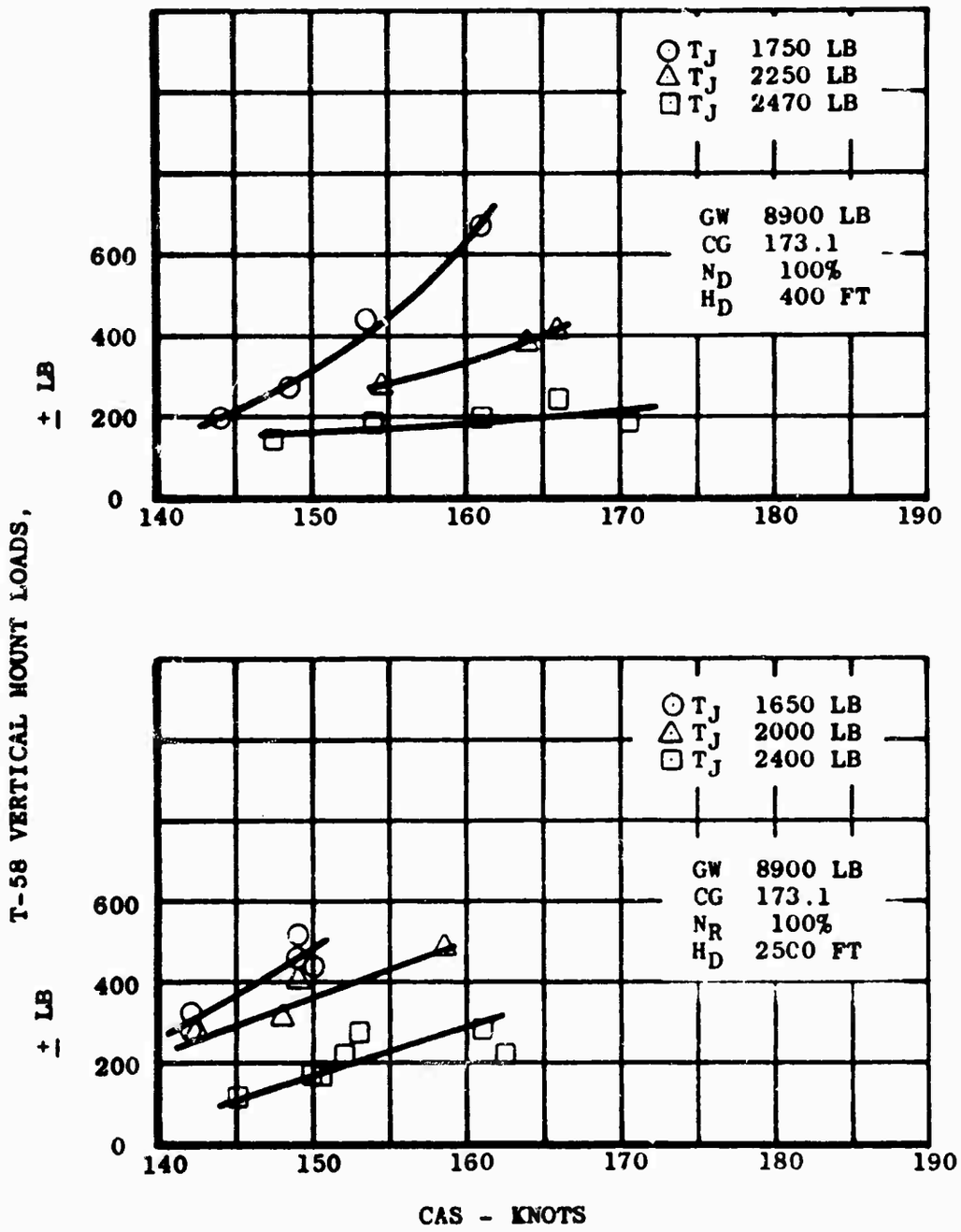

Figure I-15. T-58 VERTICAL MOUNT VIBRATORY LOADS

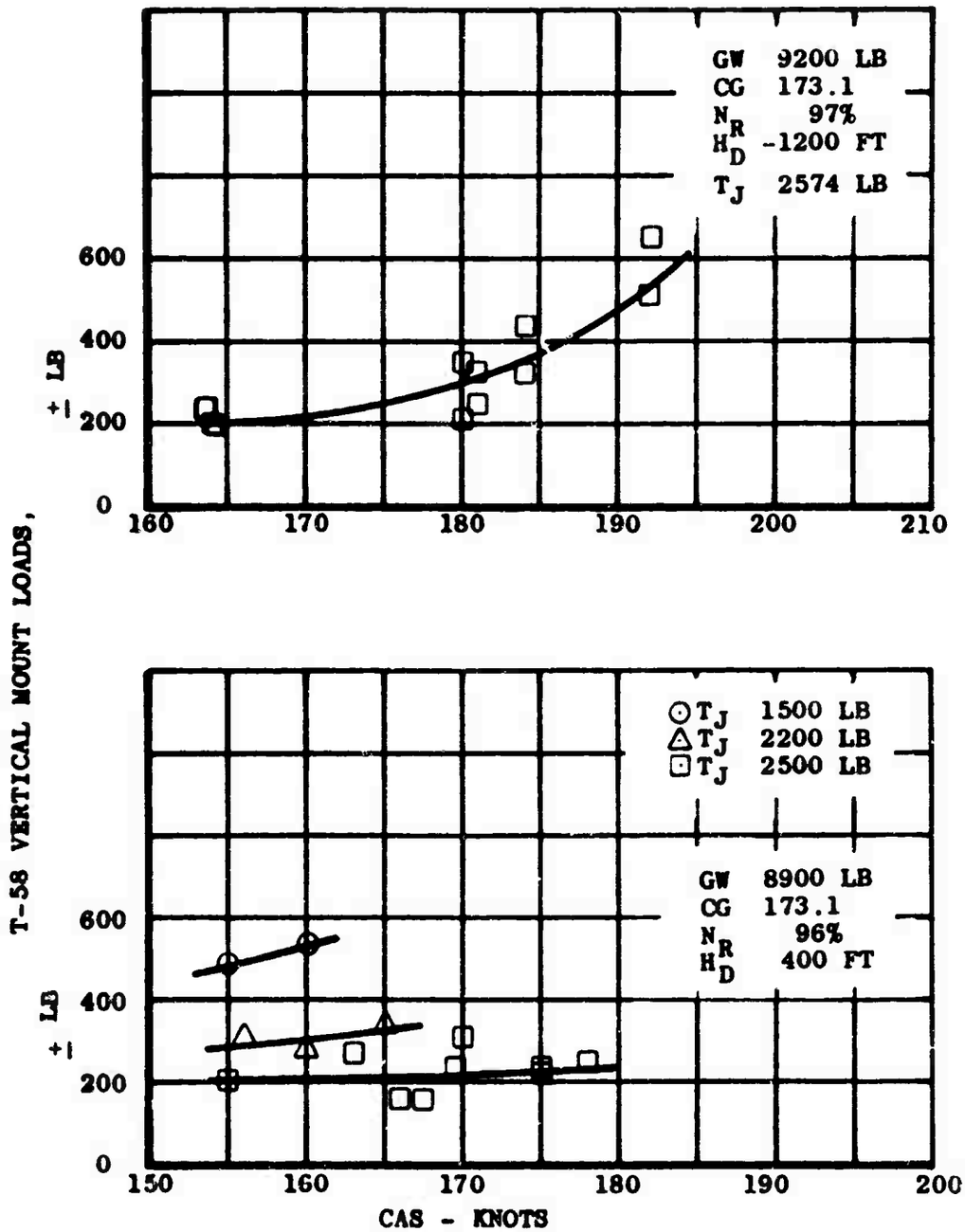

Figure I-15. (Continued)

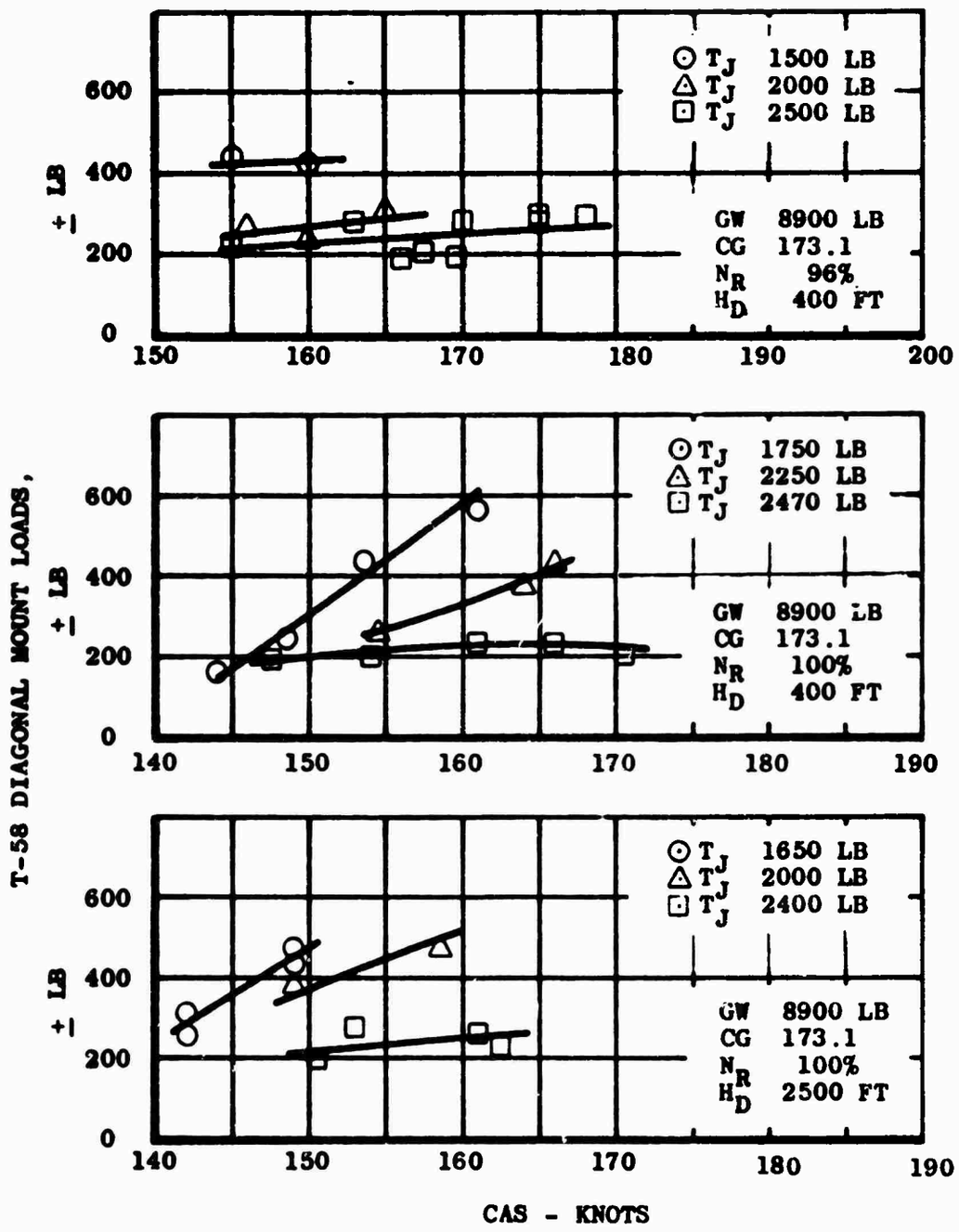

Figure I-16. T-58 DIAGONAL MOUNT VIBRATORY LOADS

▽ T_J	625 LB	GW	9100 LB
⊡ T_J	1160 LB	CG	173
⊙ T_J	1730 LB	N_R	100%
△ T_J	2155 LB	H_D	-1500 FT

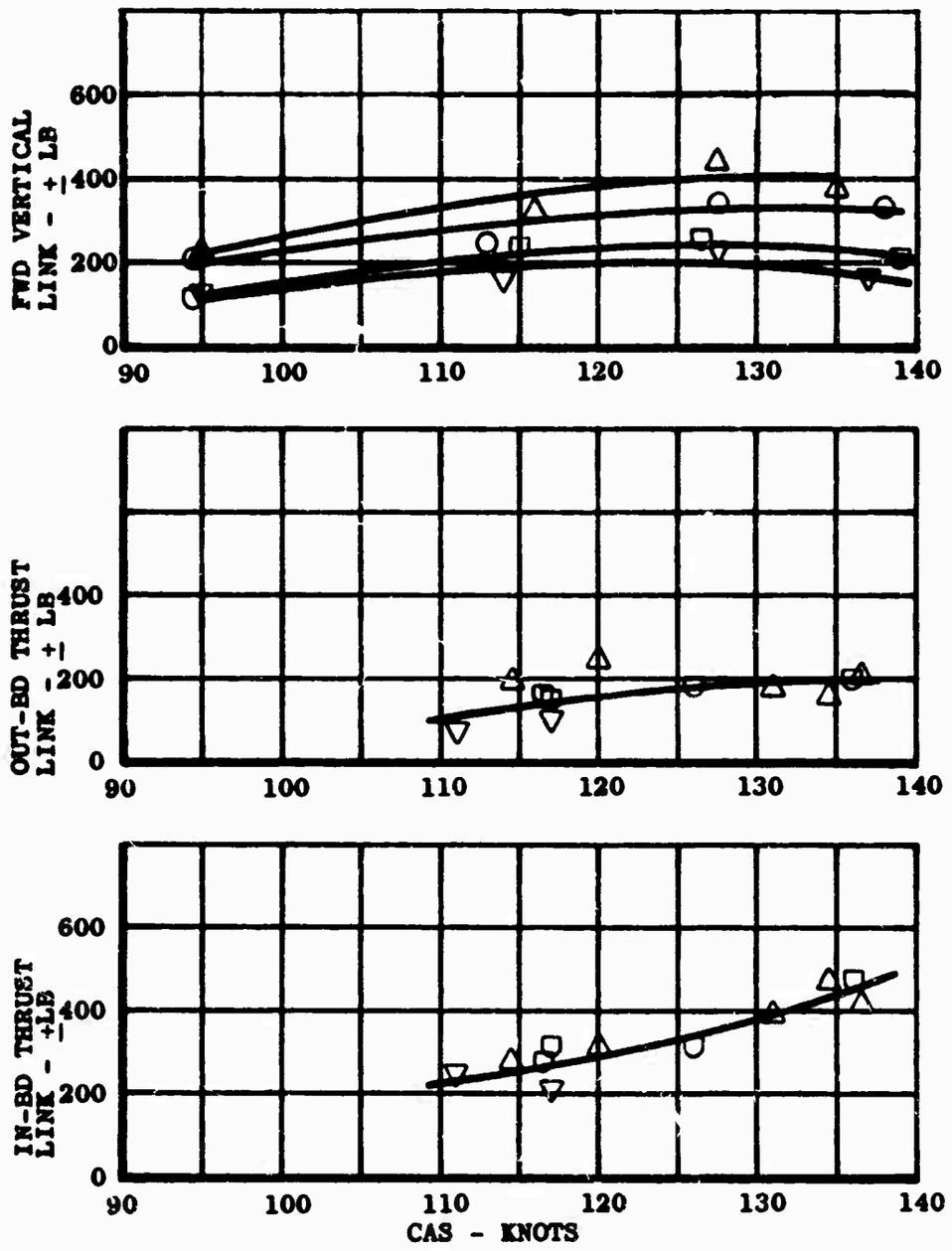

Figure I-17. YJ-85 MOUNT LINK VIBRATORY LOADS.

T_J 2574 LB

GW 9200 LB
CG 173.1
N_{R_D} 97%
H_D -1200 FT

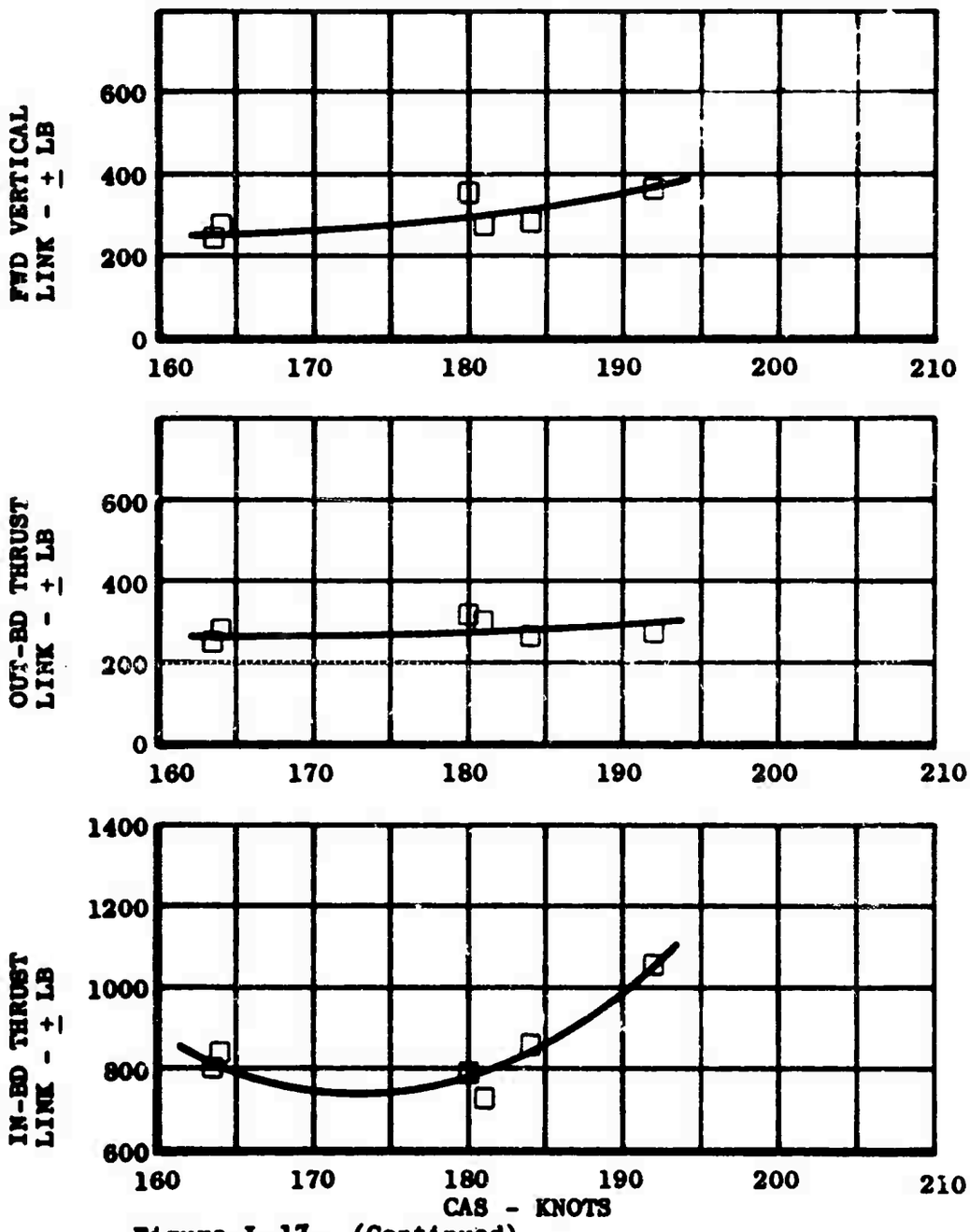

Figure I-17. (Continued)

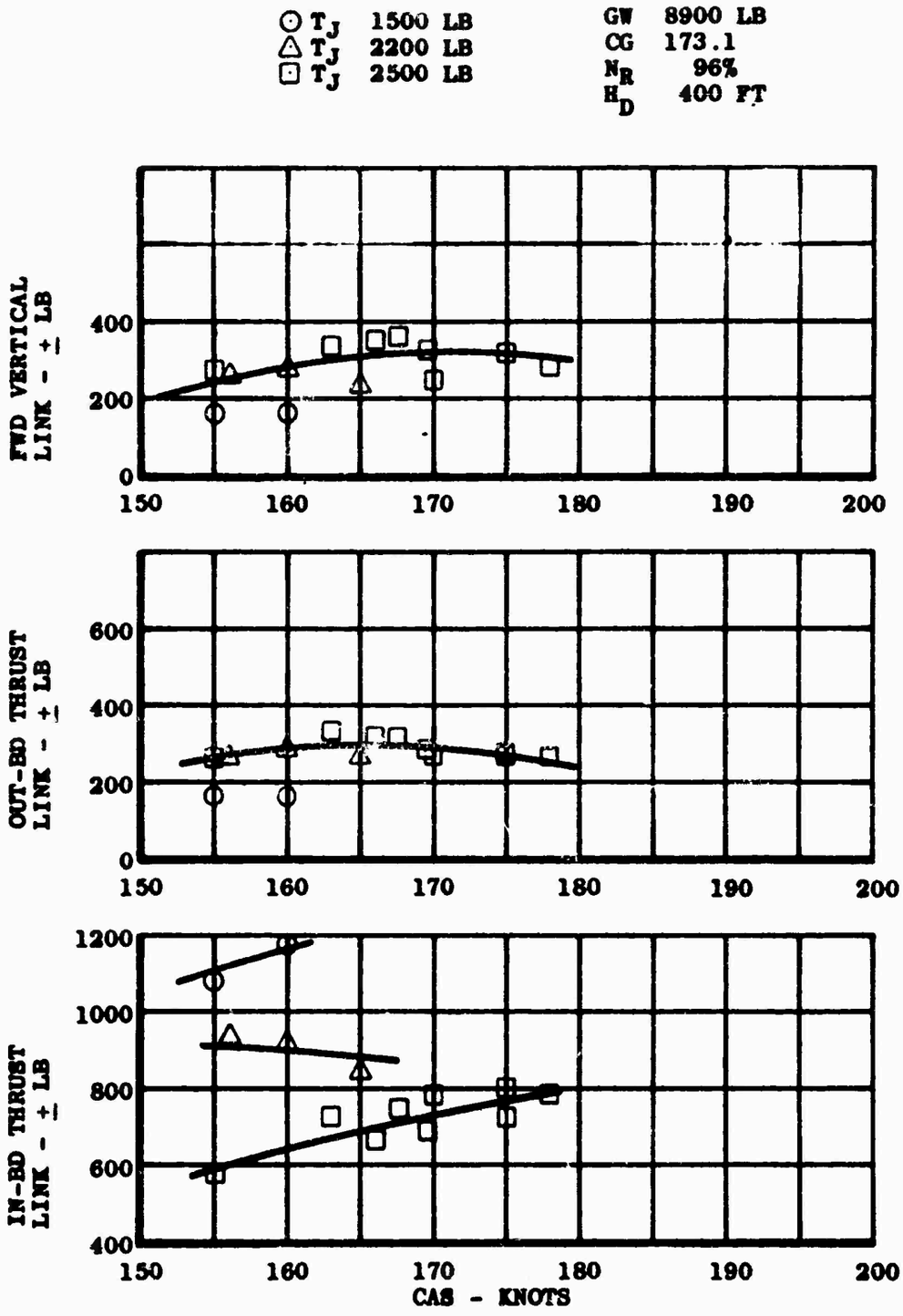

Figure I-17. (Continued)

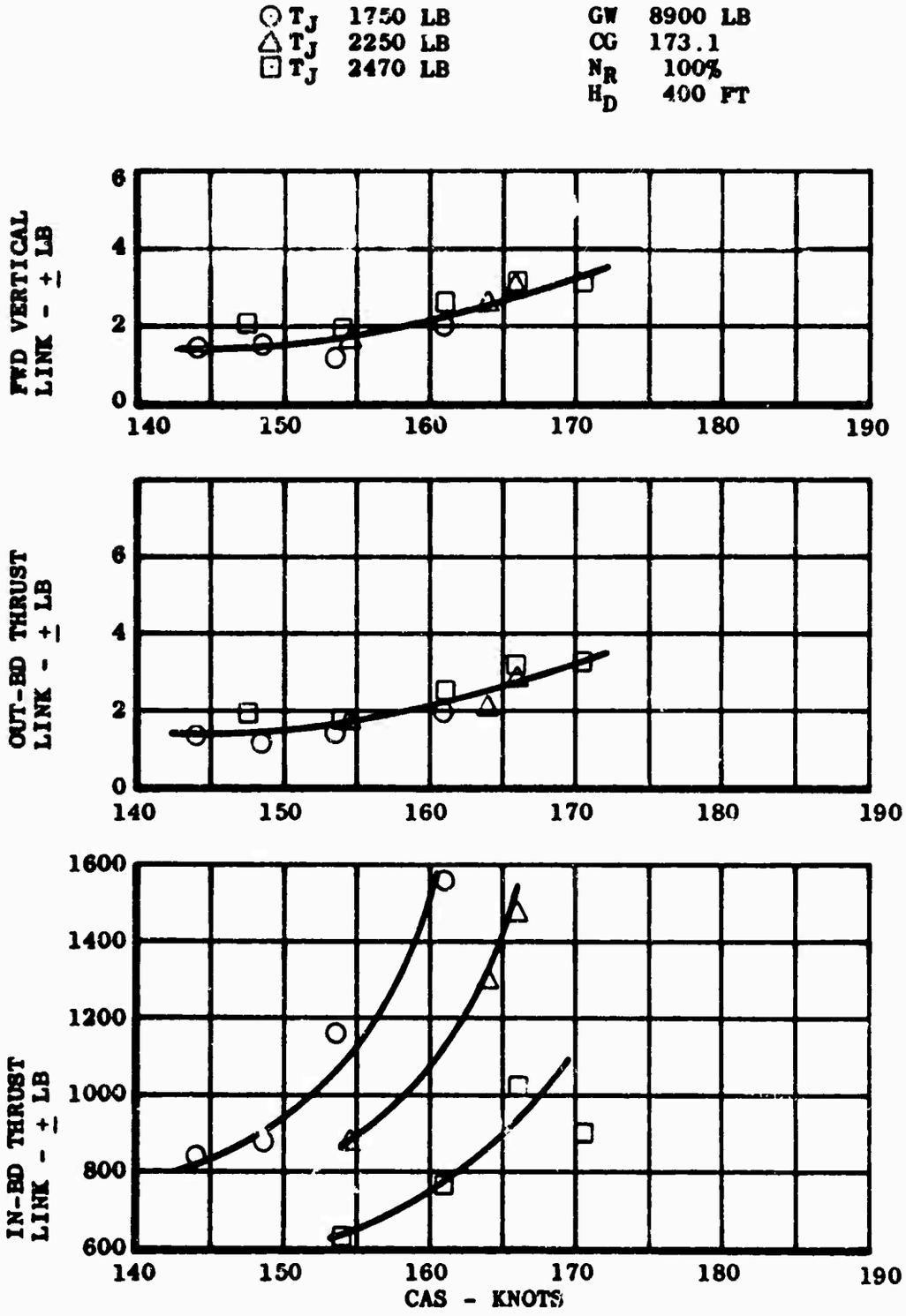

Figure I-17. (Continued)

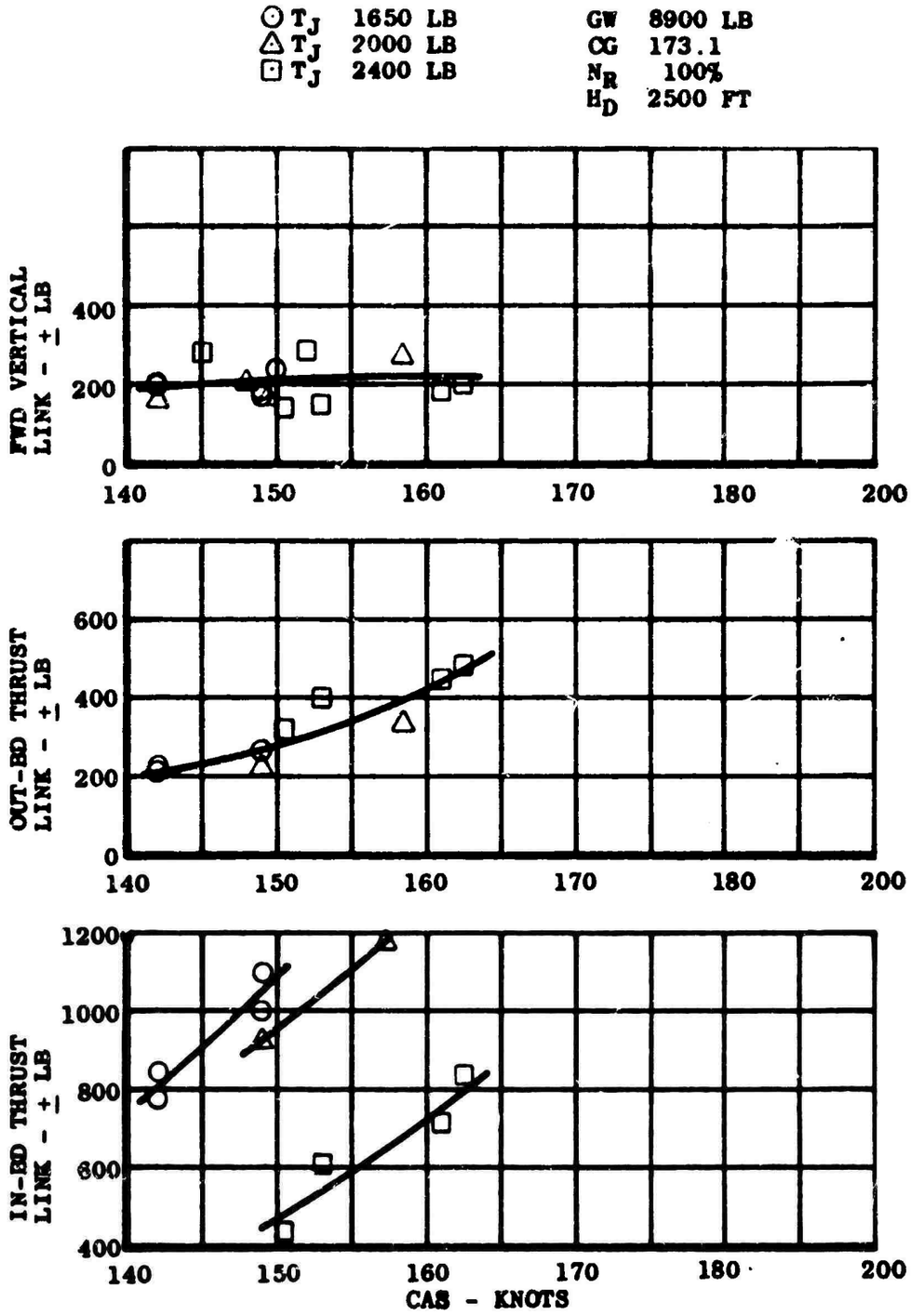

Figure I-17. (Continued)

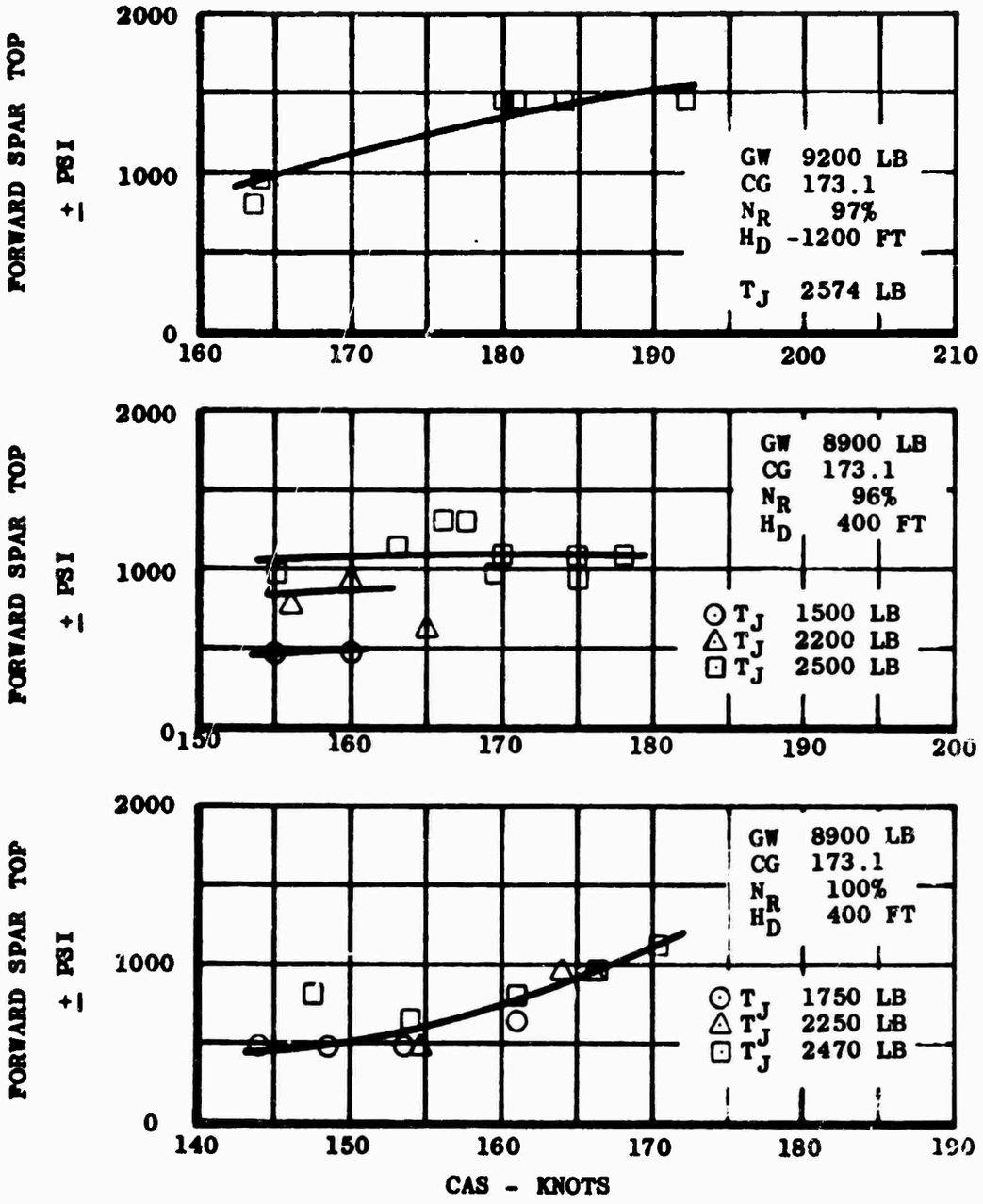

Figure I-18. YJ-85 SUPPORT PYLON VIBRATORY STRESS

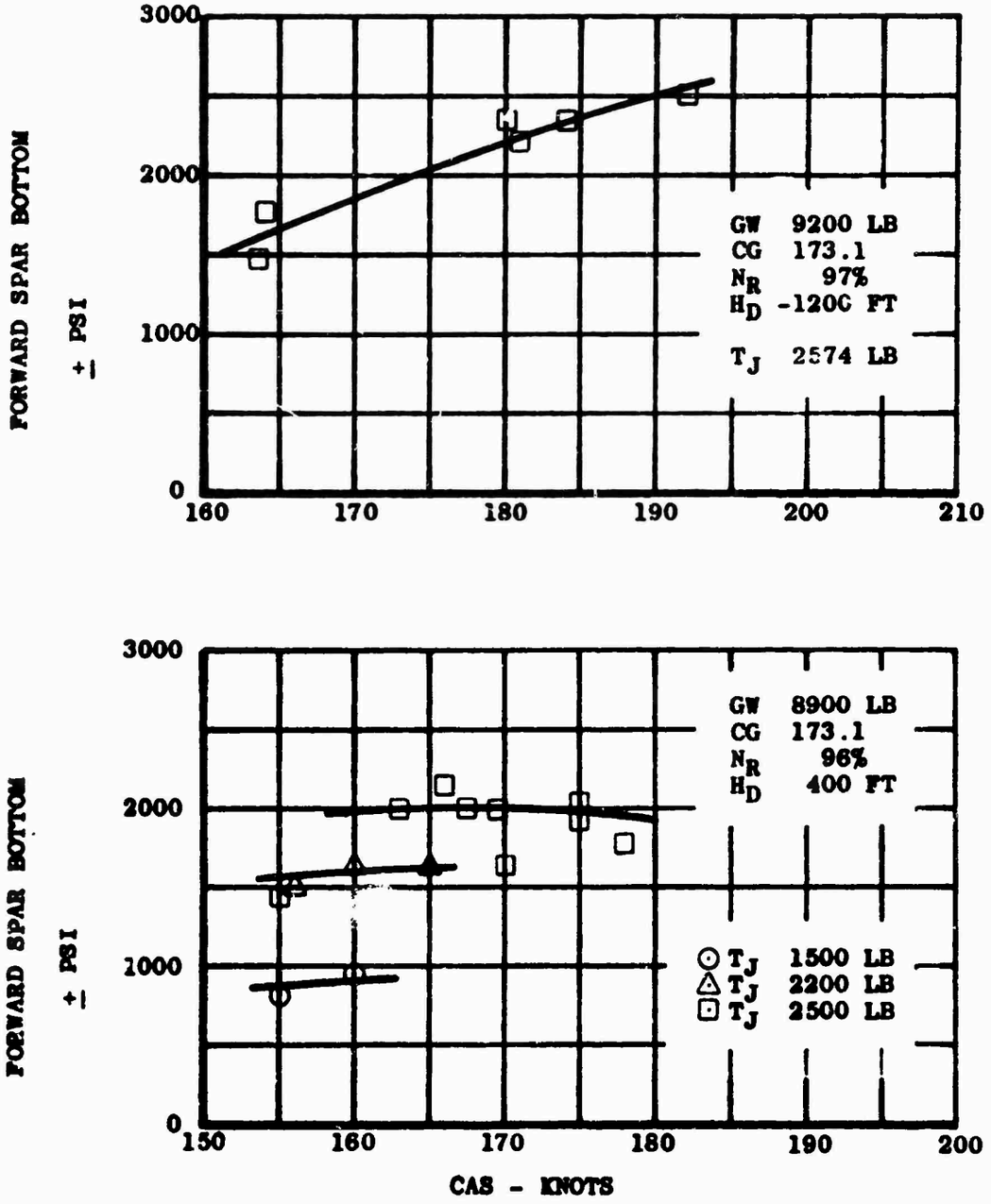

Figure I-18. (Continued)

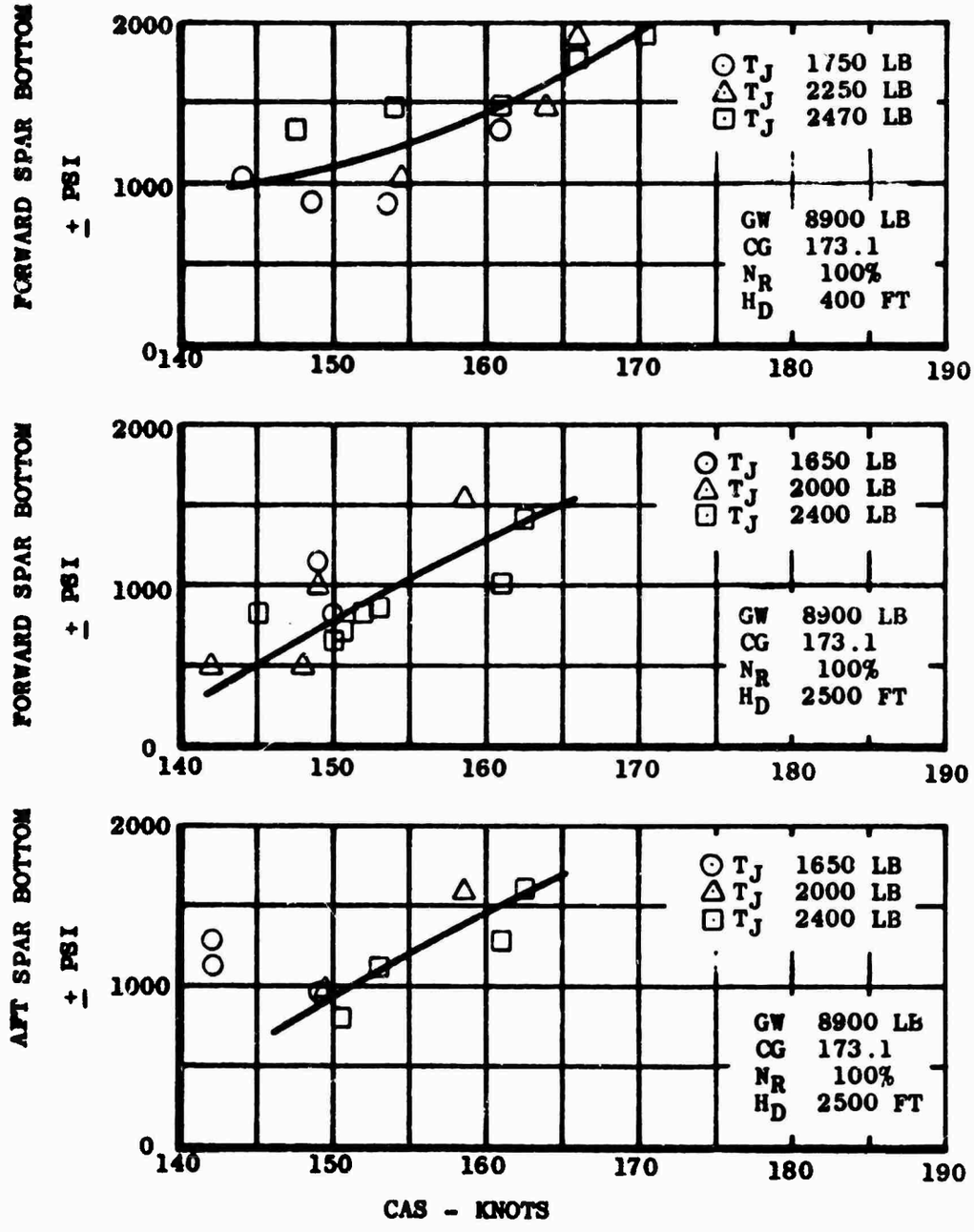

Figure I-18. (Continued)

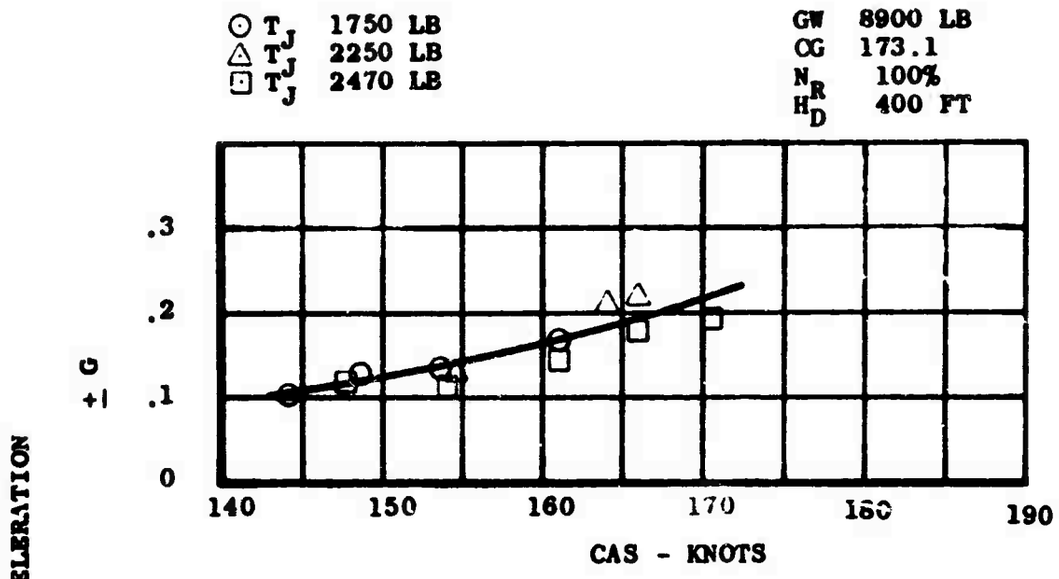

Figure I-19. PILOT SEAT VERTICAL VIBRATORY ACCELERATION

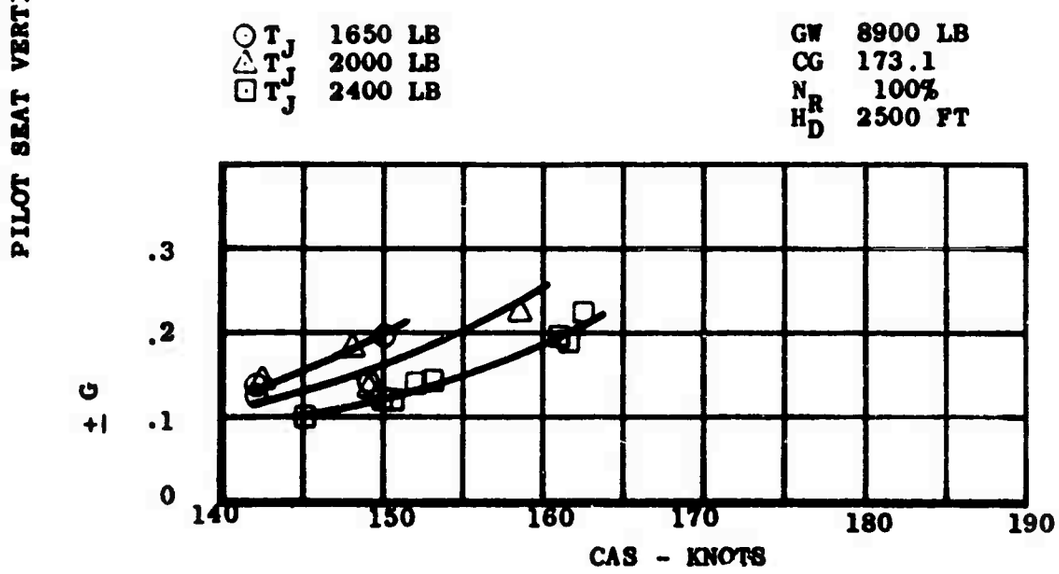

Figure I-19. (Continued)

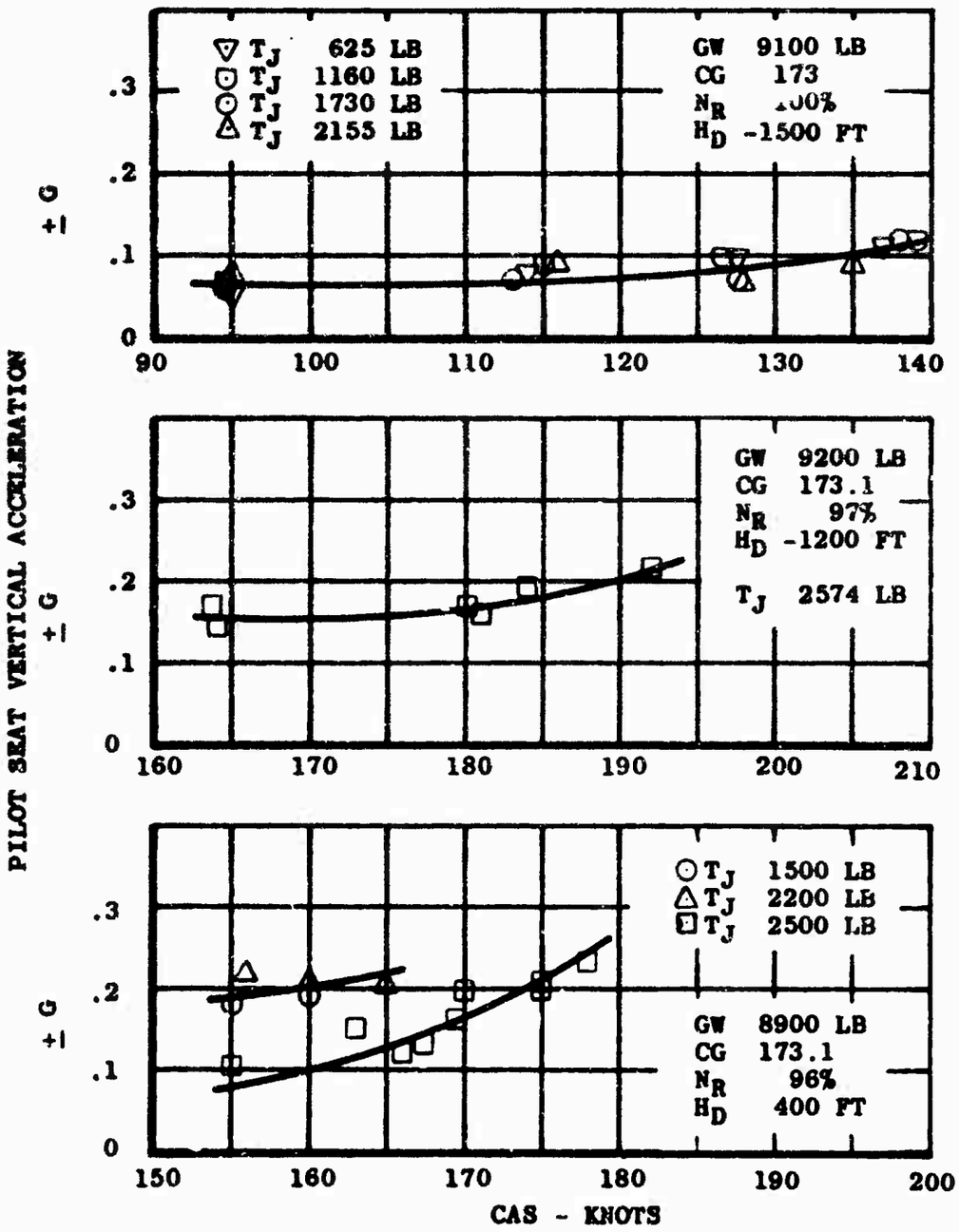

Figure I-19. (Continued)

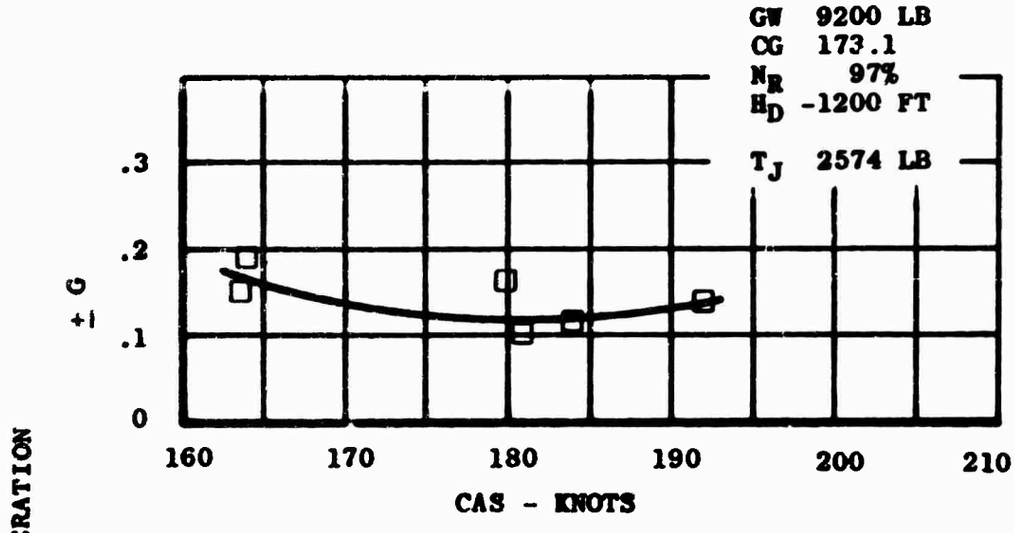

Figure I-20. PILOT SEAT LATERAL VIBRATORY ACCELERATION

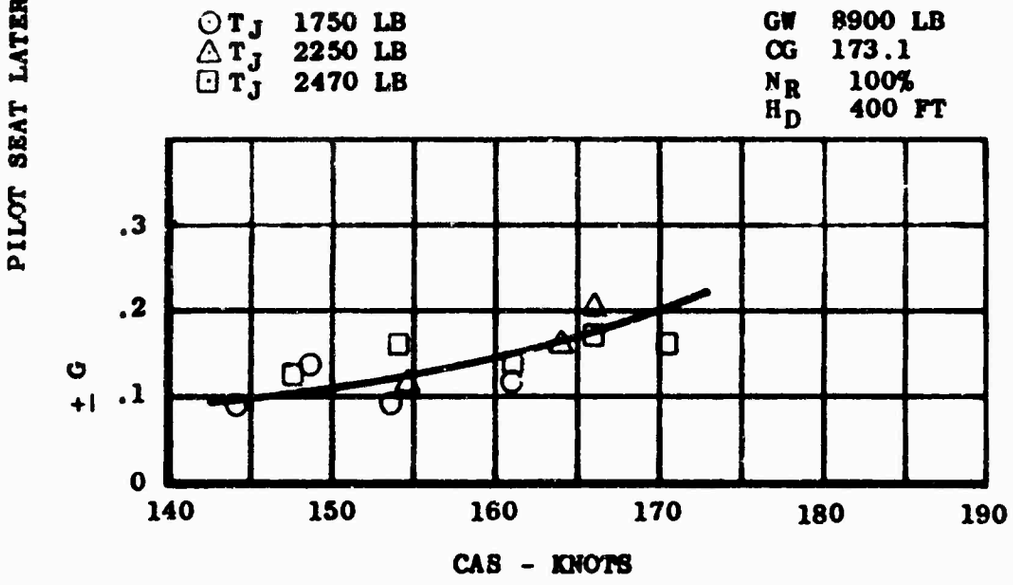

Figure I-20. (Continued)

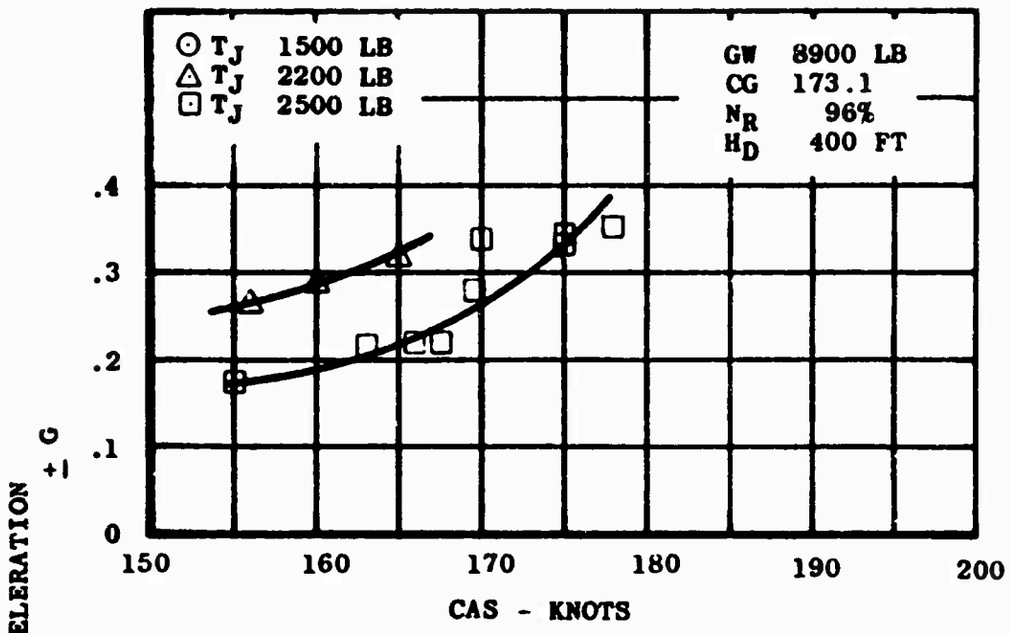

Figure I-21. C.G. VERTICAL VIBRATORY ACCELERATION

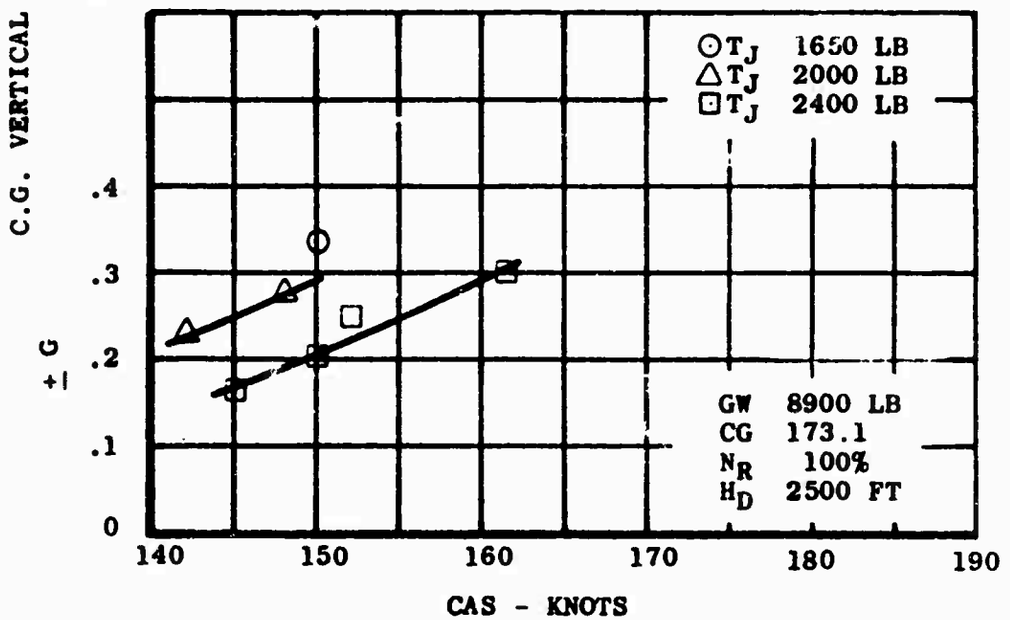

Figure I-21. (Continued)

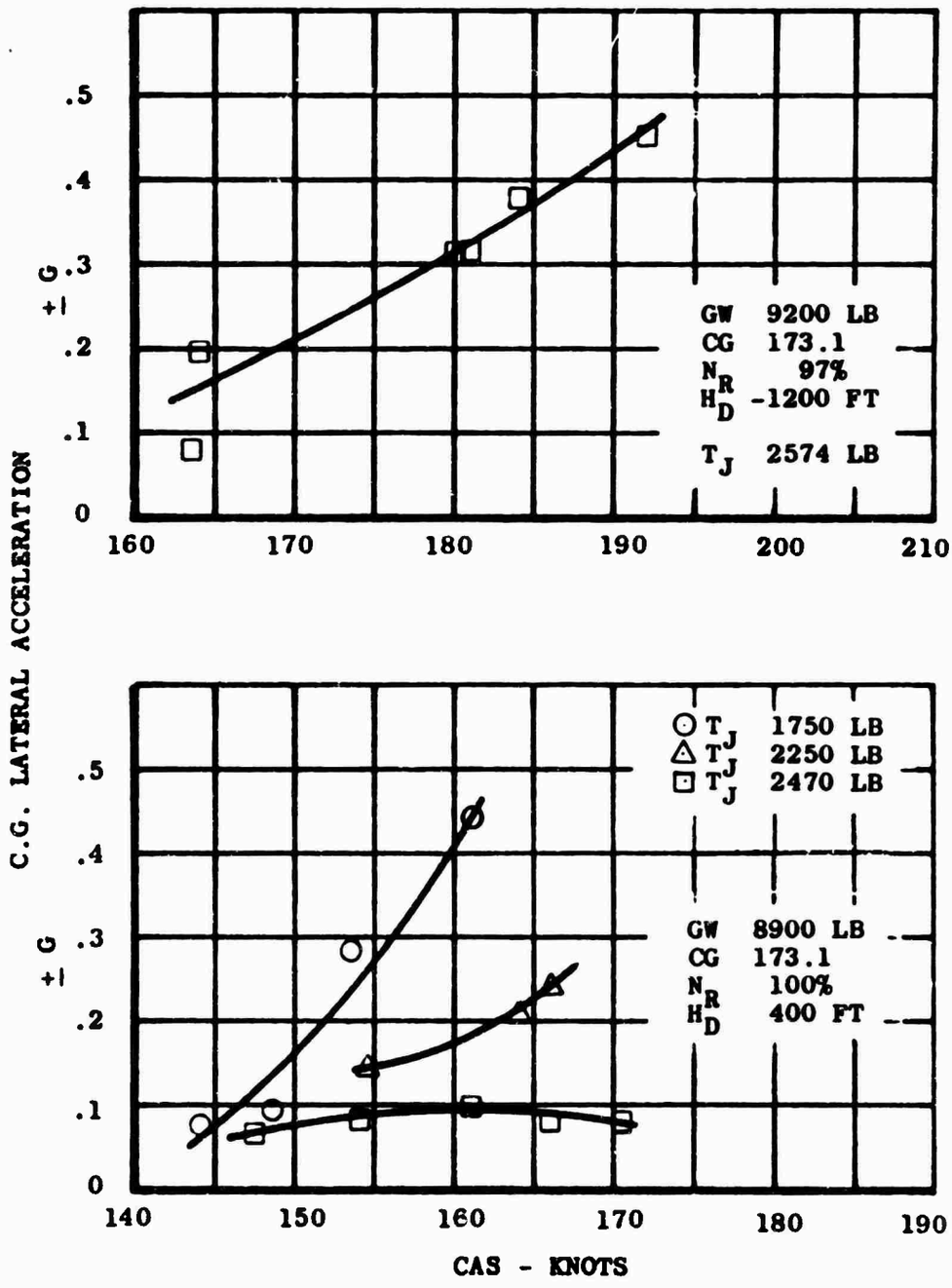

Figure I-22. C.G. LATERAL VIBRATORY ACCELERATION

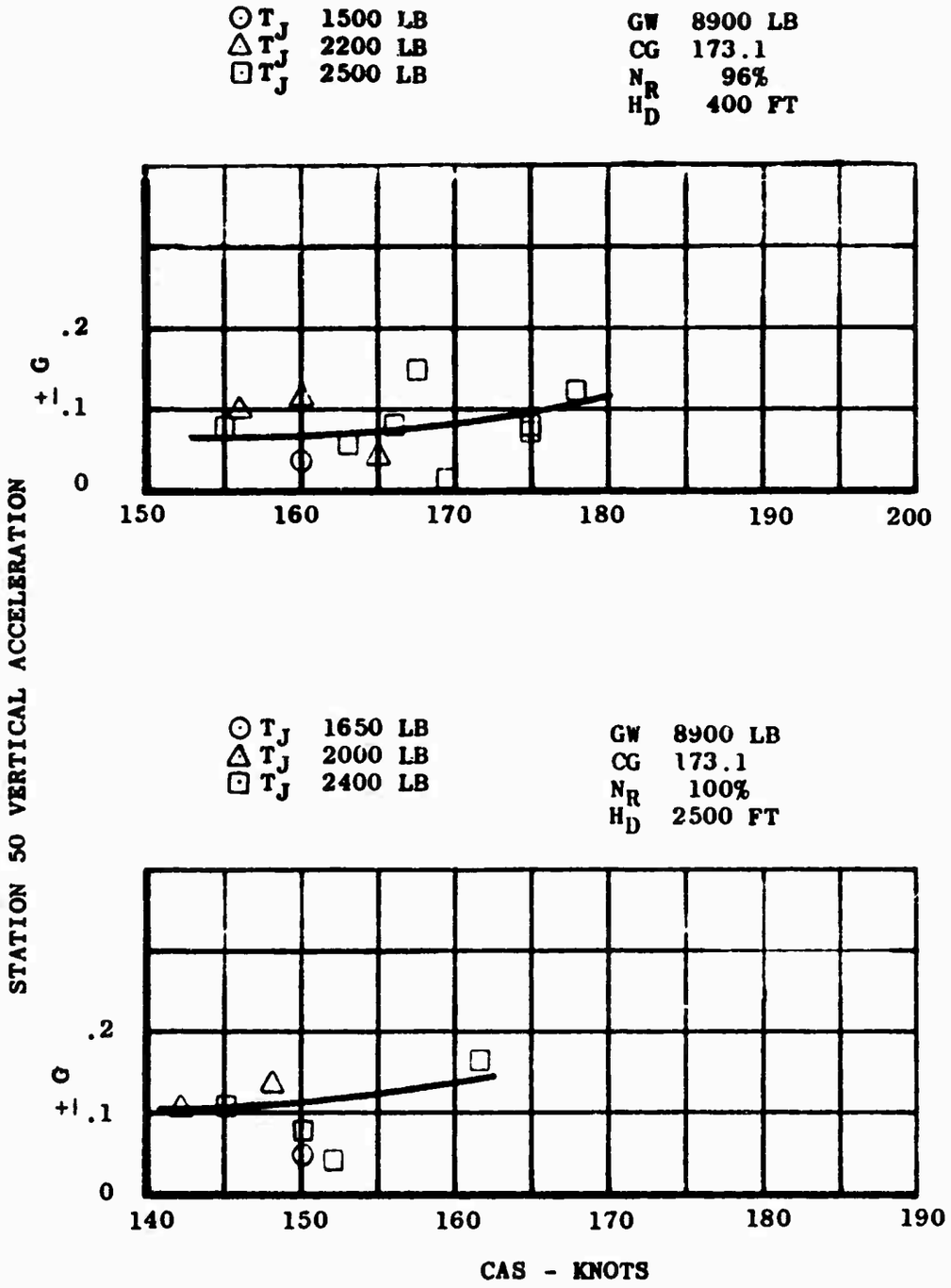

Figure I-23. STATION 50 VERTICAL VIBRATORY ACCELERATION.

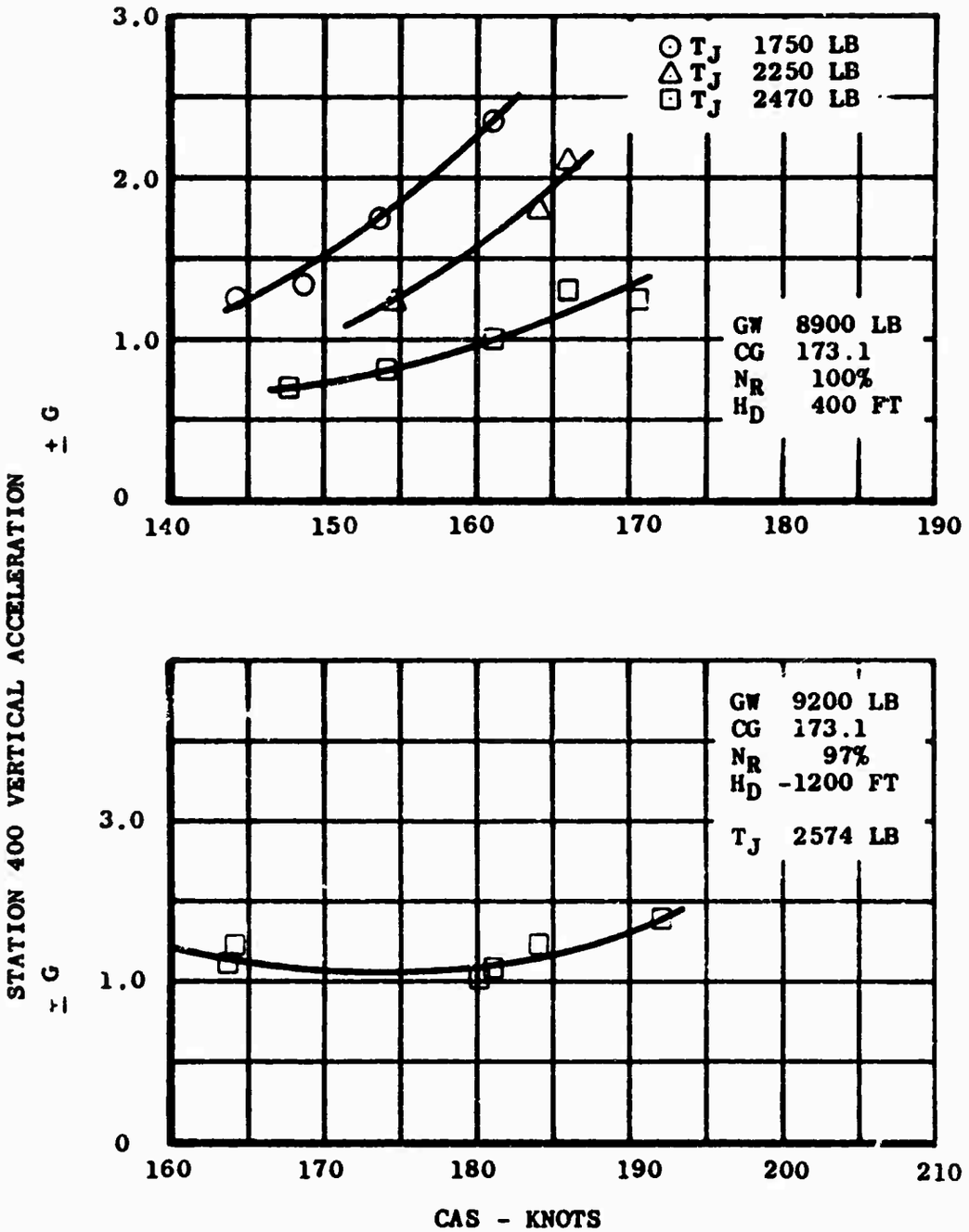

Figure I-24. STATION 400 VERTICAL VIBRATORY ACCELERATION

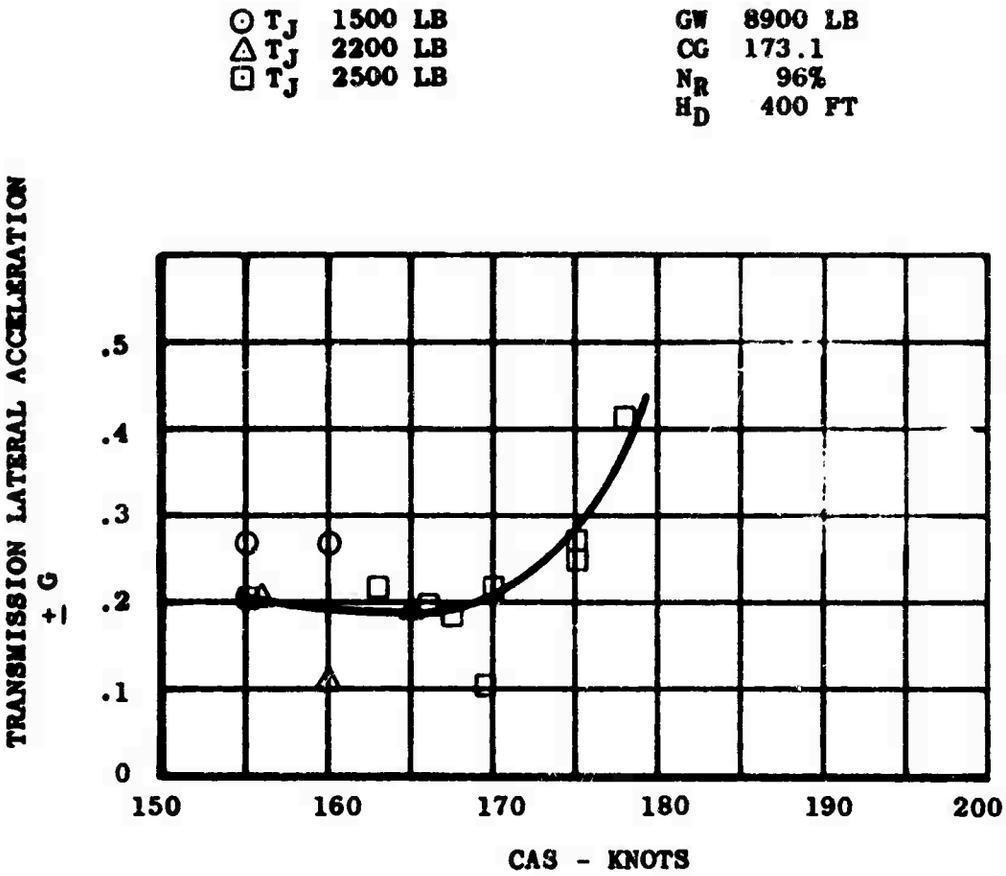

Figure I-25. TRANSMISSION LATERAL VIBRATORY ACCELERATION

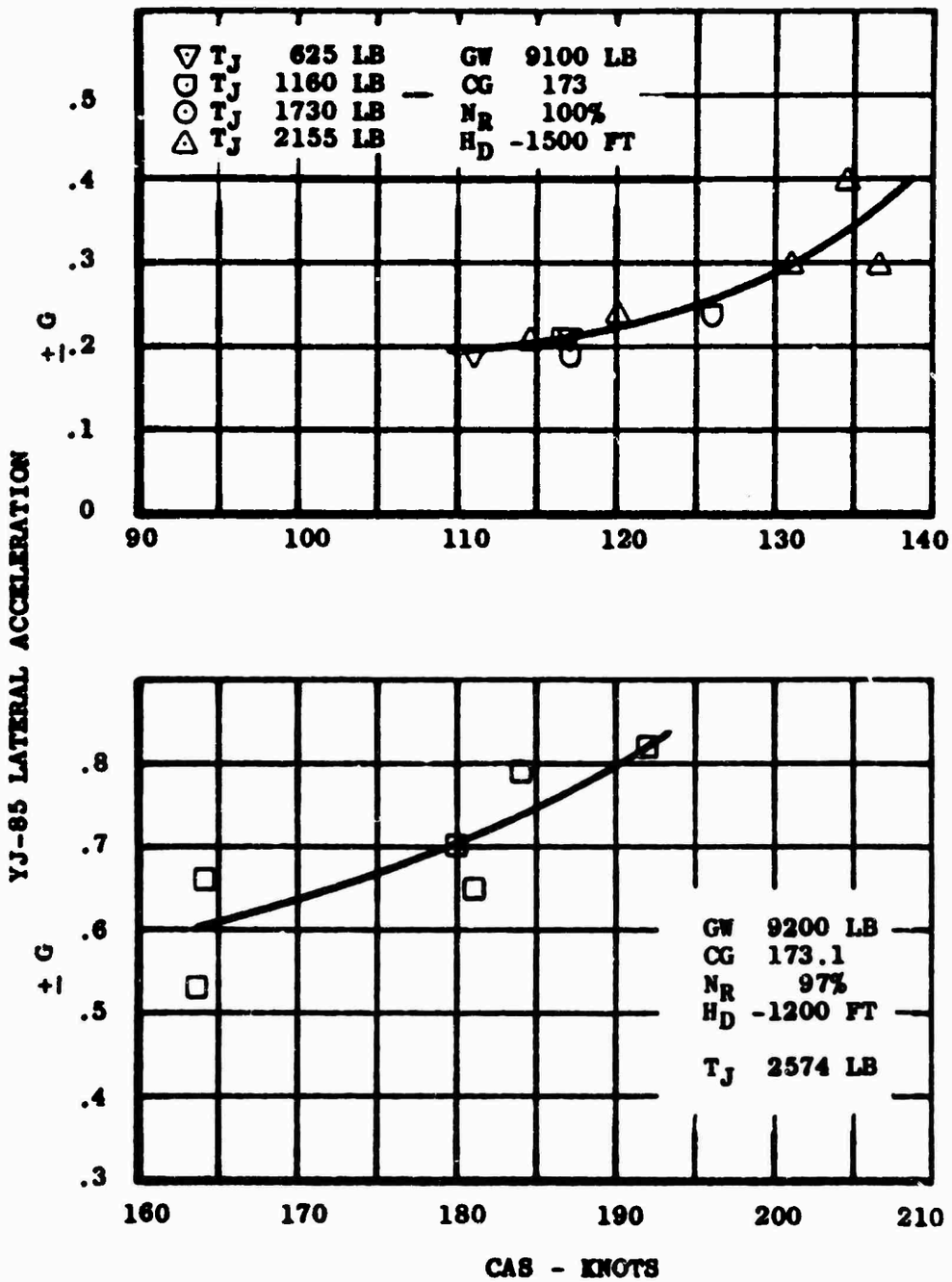

Figure I-26. YJ-85 LATERAL VIBRATORY ACCELERATION

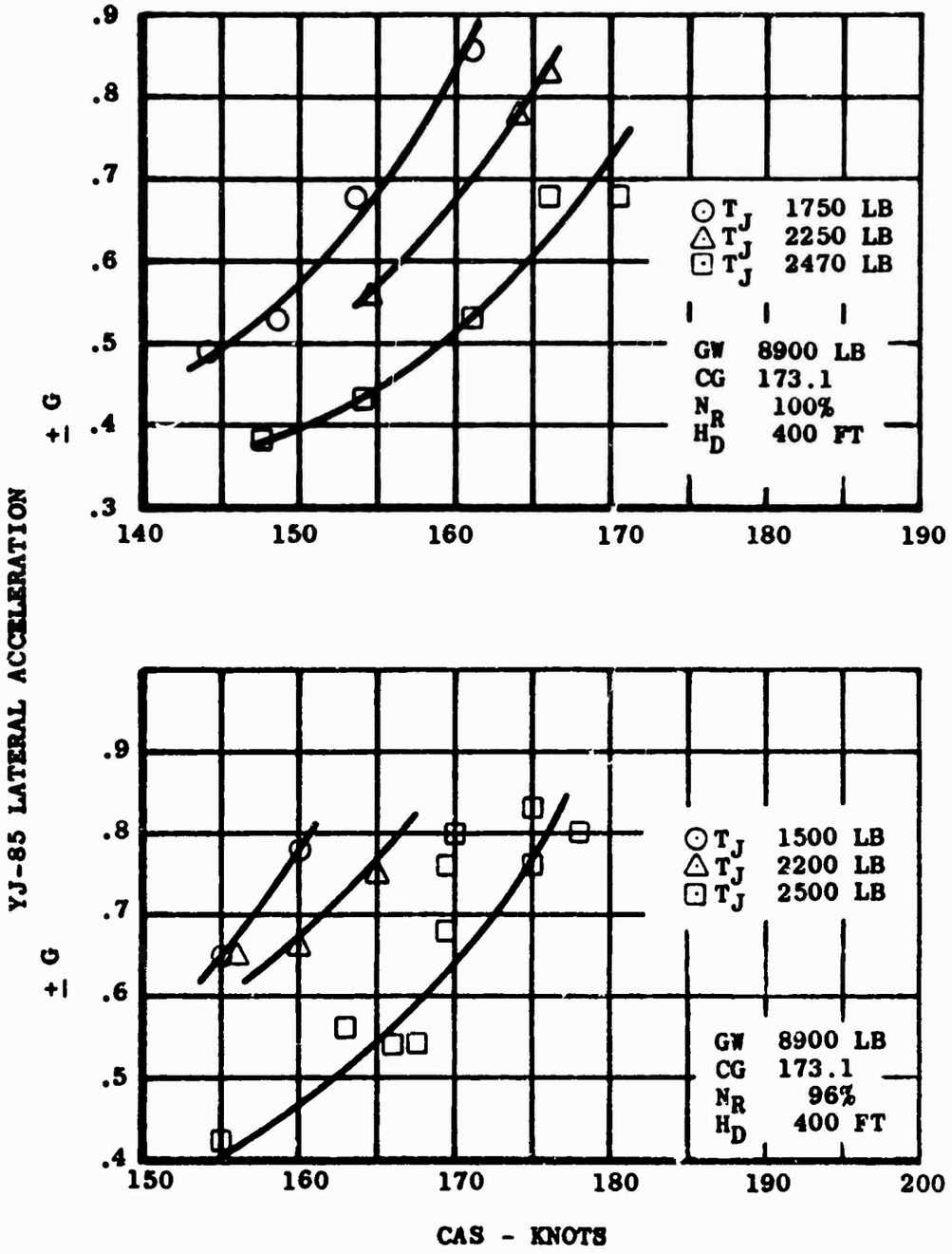

Figure I-26. (Continued)

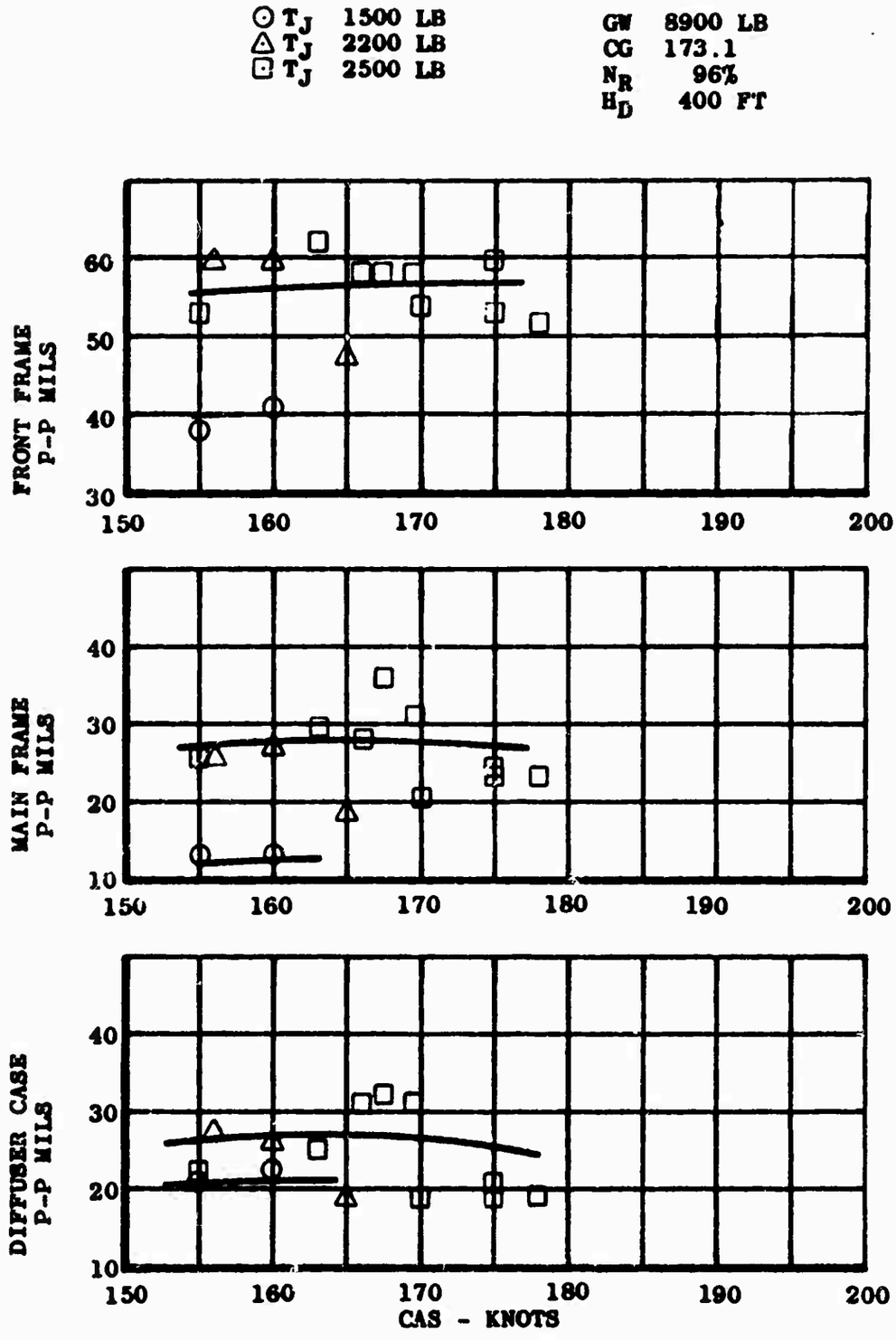

Figure I-27. YJ-85 VERTICAL VIBRATORY DISPLACEMENT (4/REV)

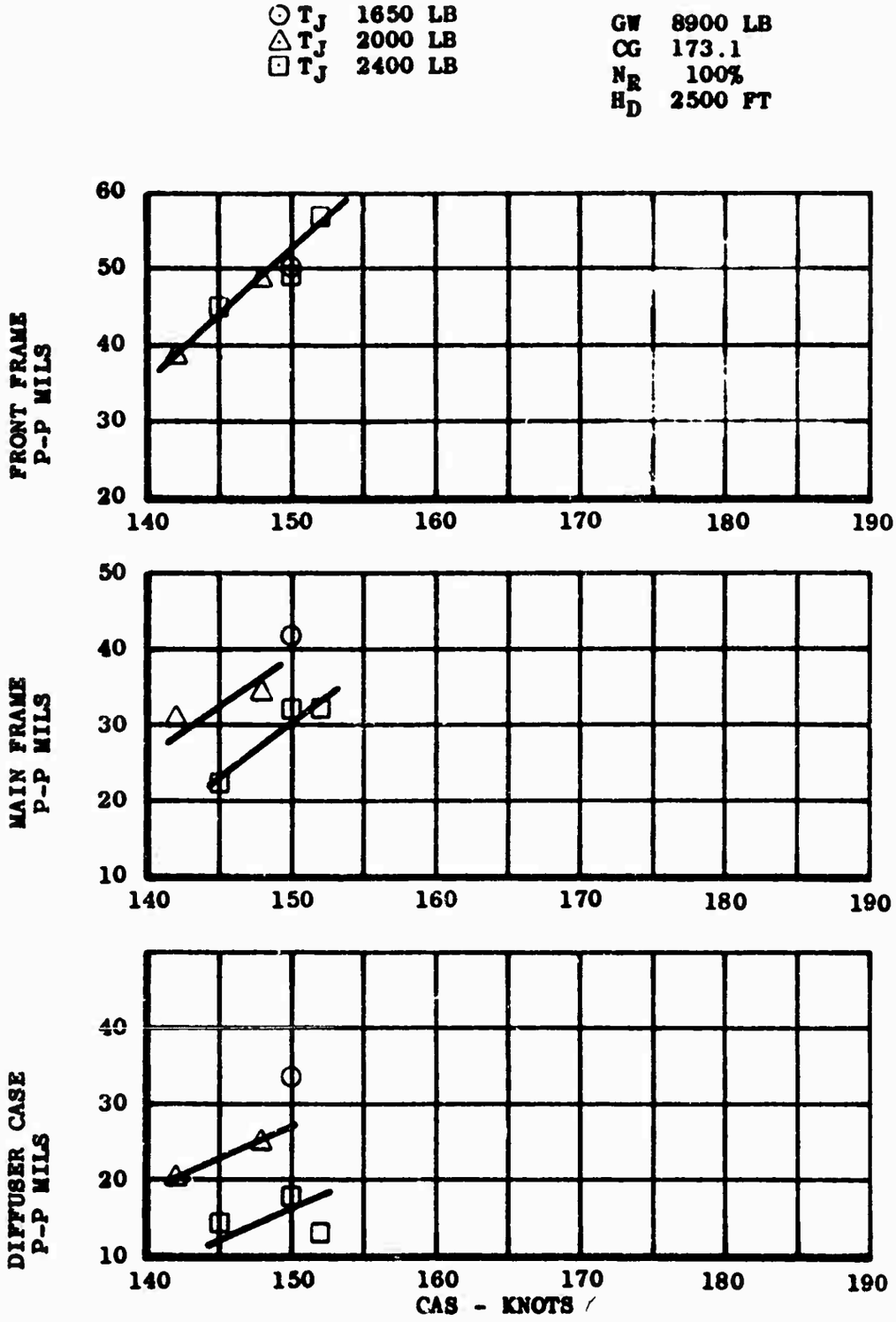

Figure I-27. (Continued)

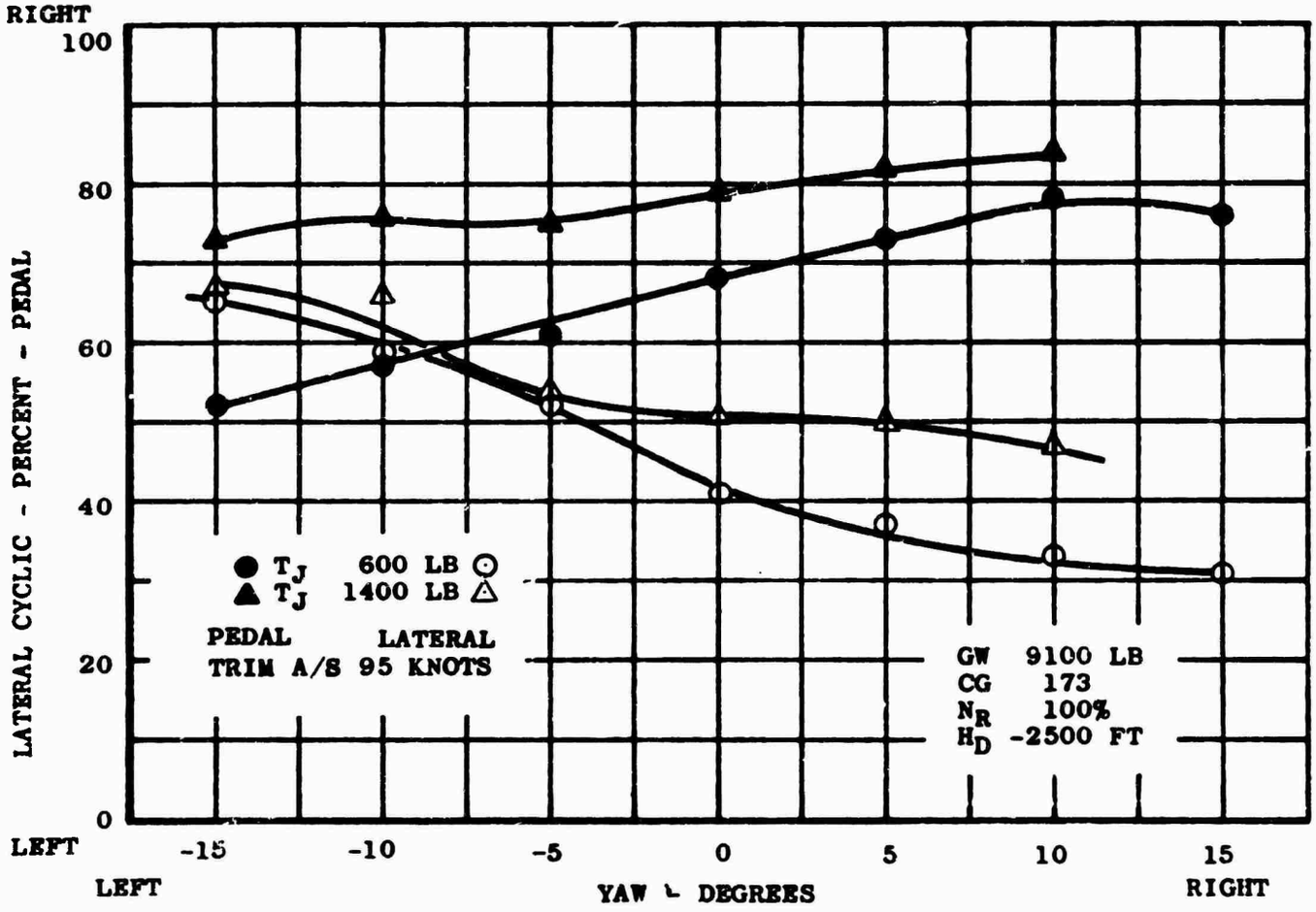

Figure I-28. STATIC LATERAL/DIRECTIONAL STABILITY AS AFFECTED BY THRUST AUGMENTATION.

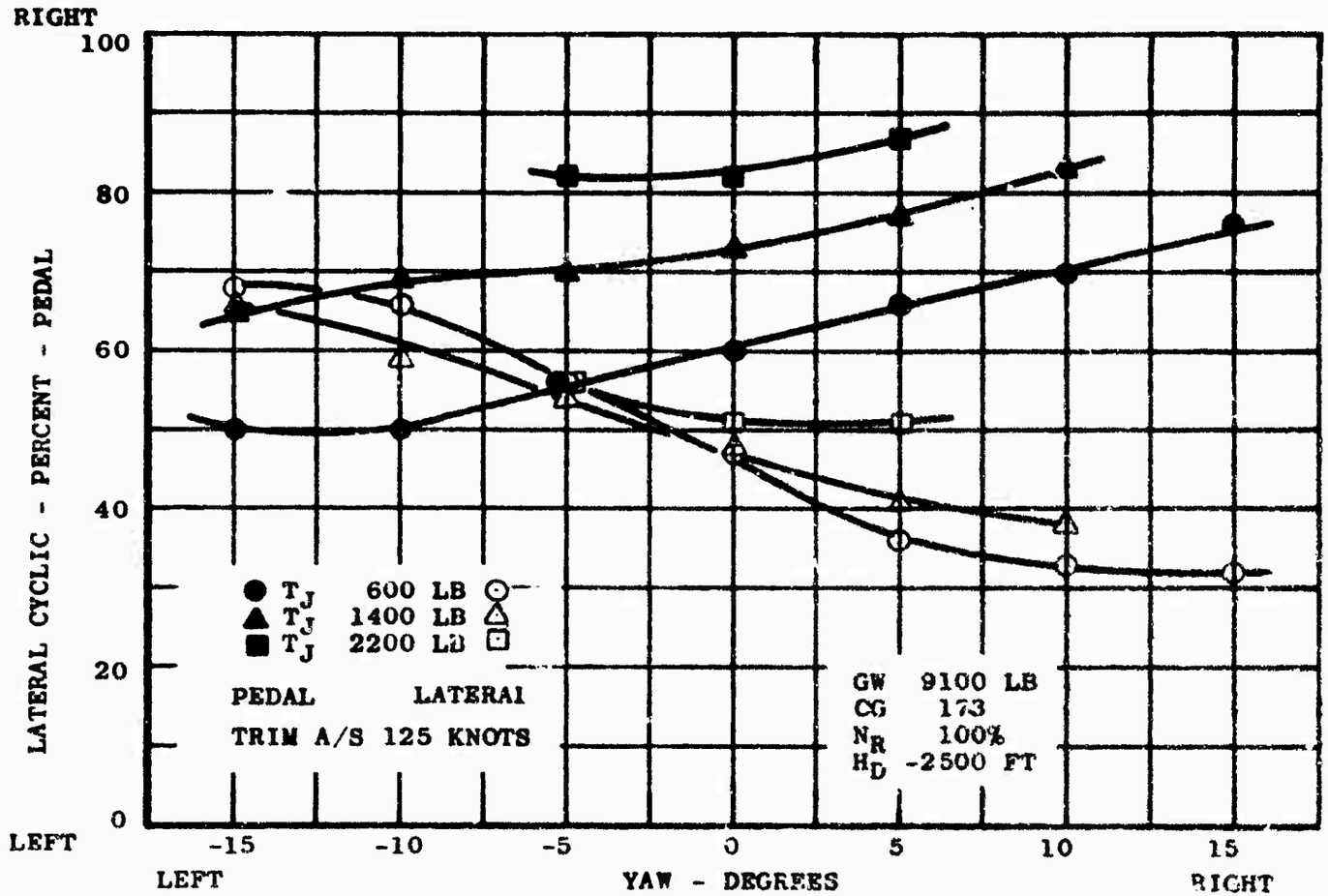

Figure I-28. (Continued).

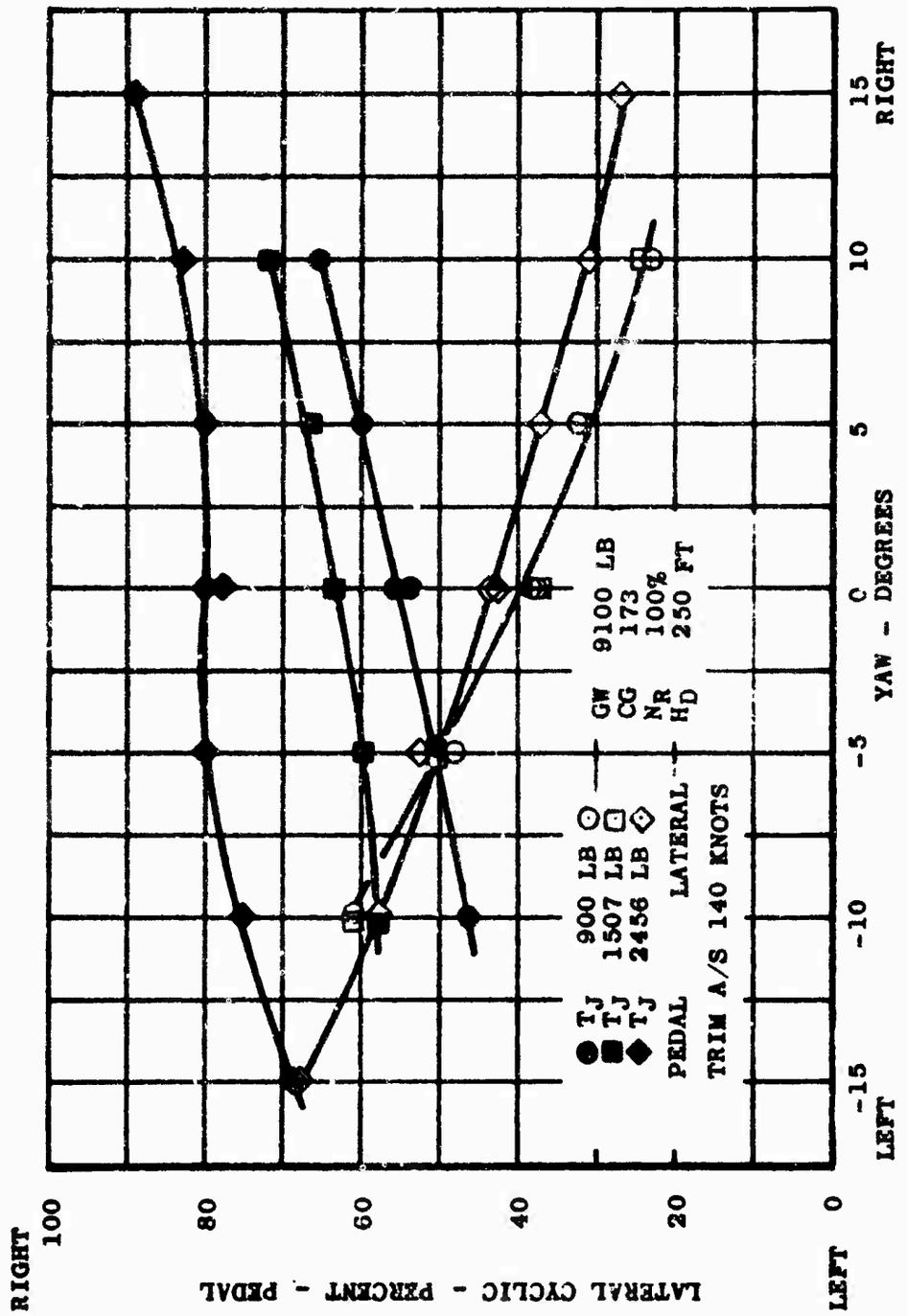

Figure I-28. (Continued).

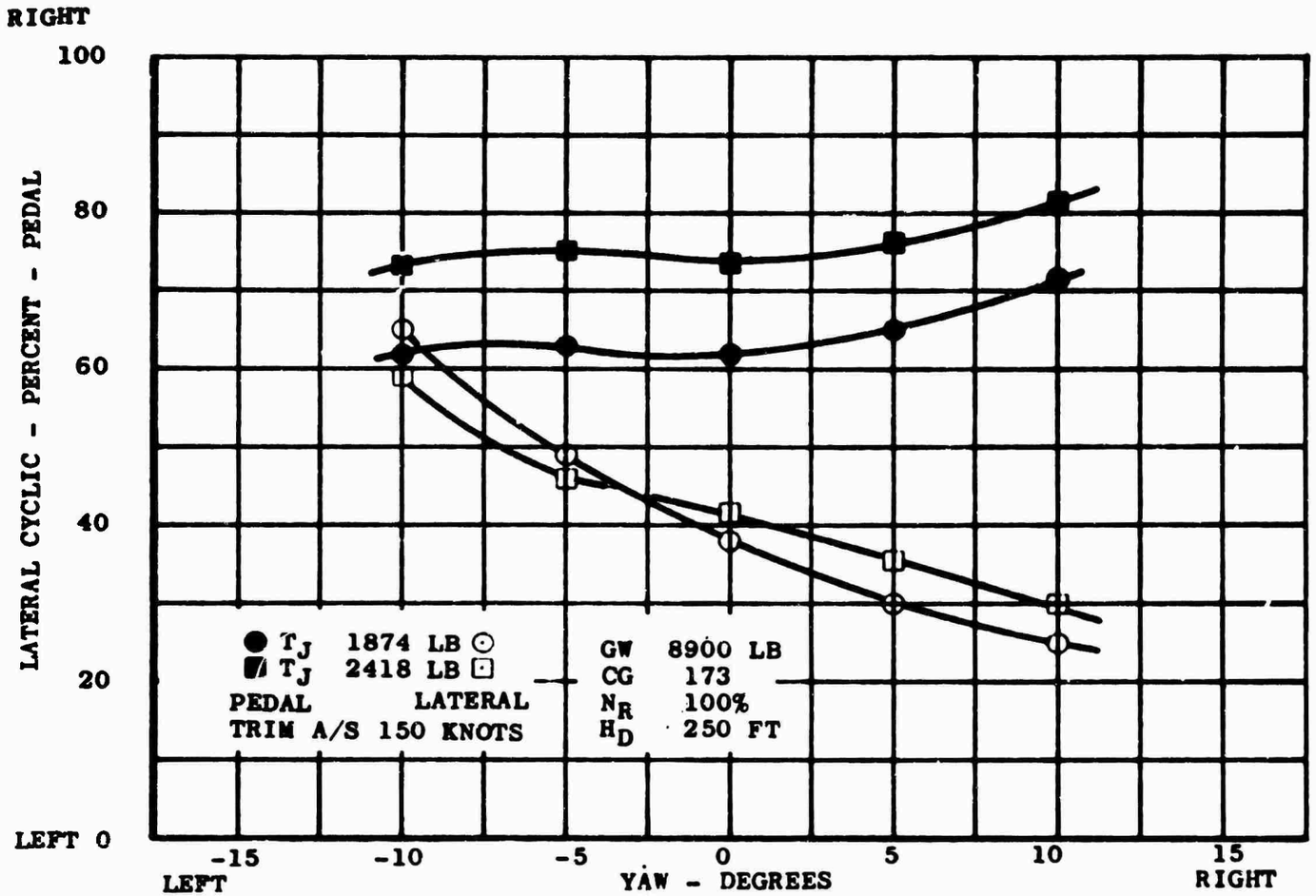

Figure I-28. (Continued).

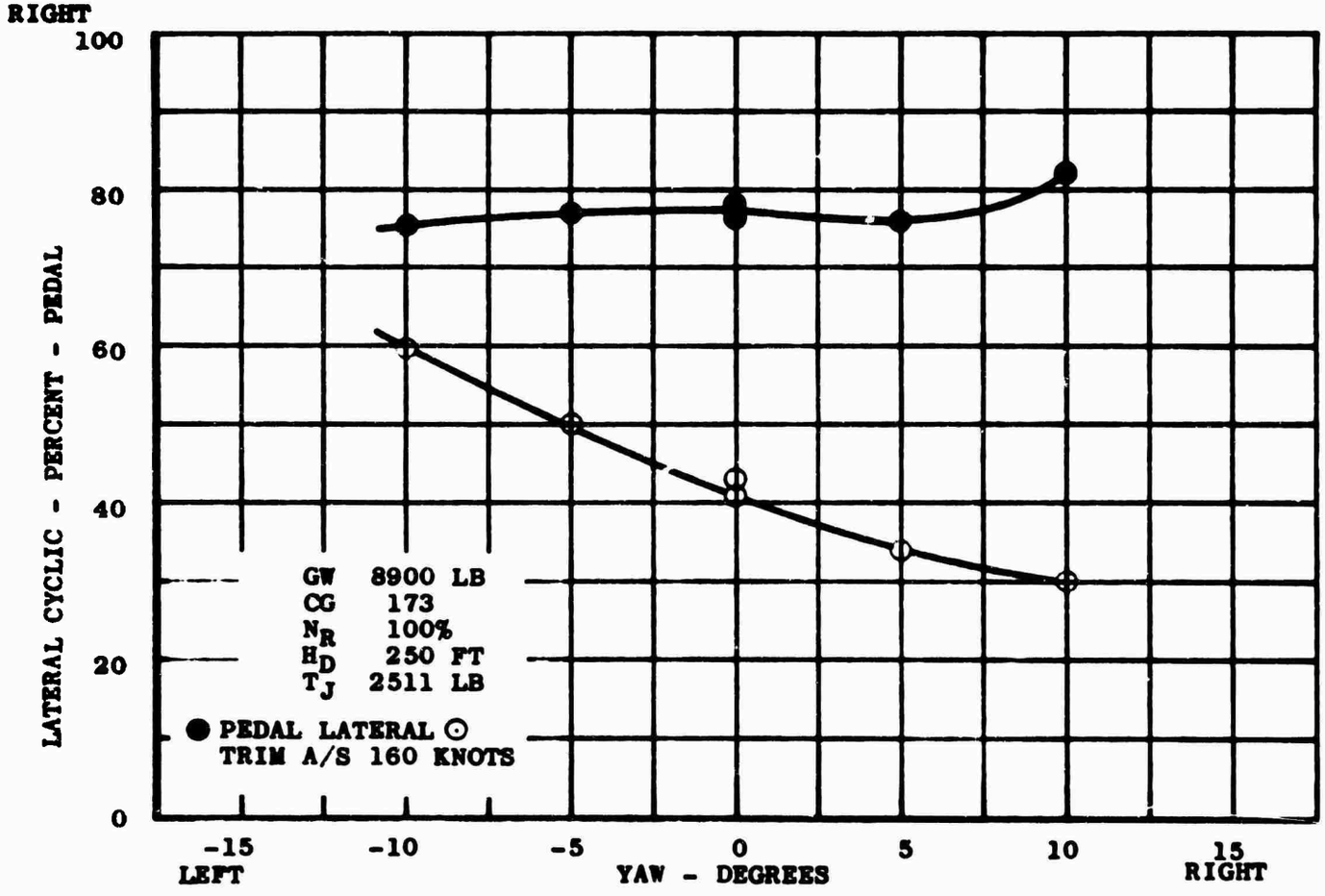

Figure I-28. (Continued).

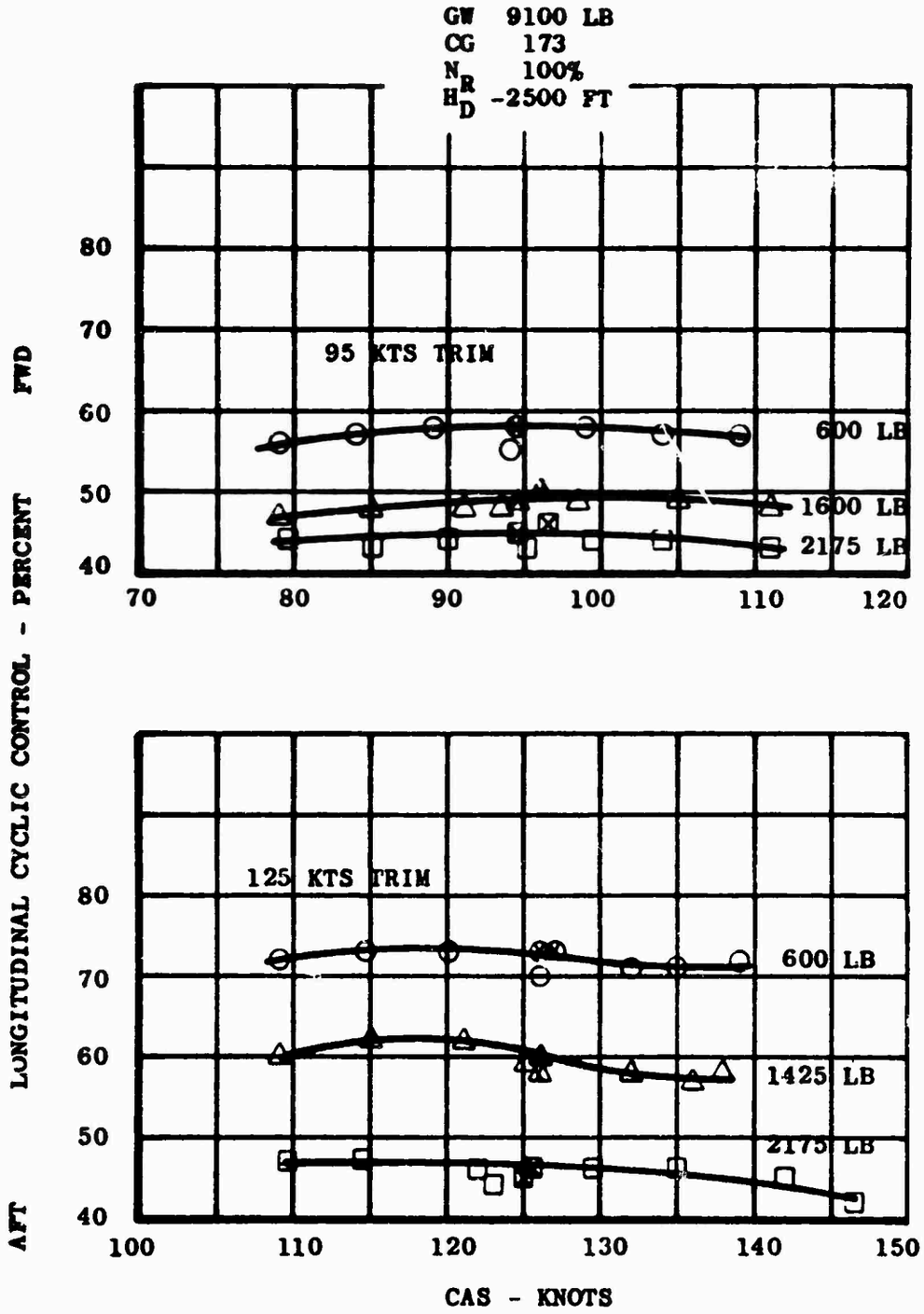

Figure I-29. EFFECT OF THRUST AUGMENTATION ON LONGITUDINAL STATIC STABILITY WITH RESPECT TO SPEED.

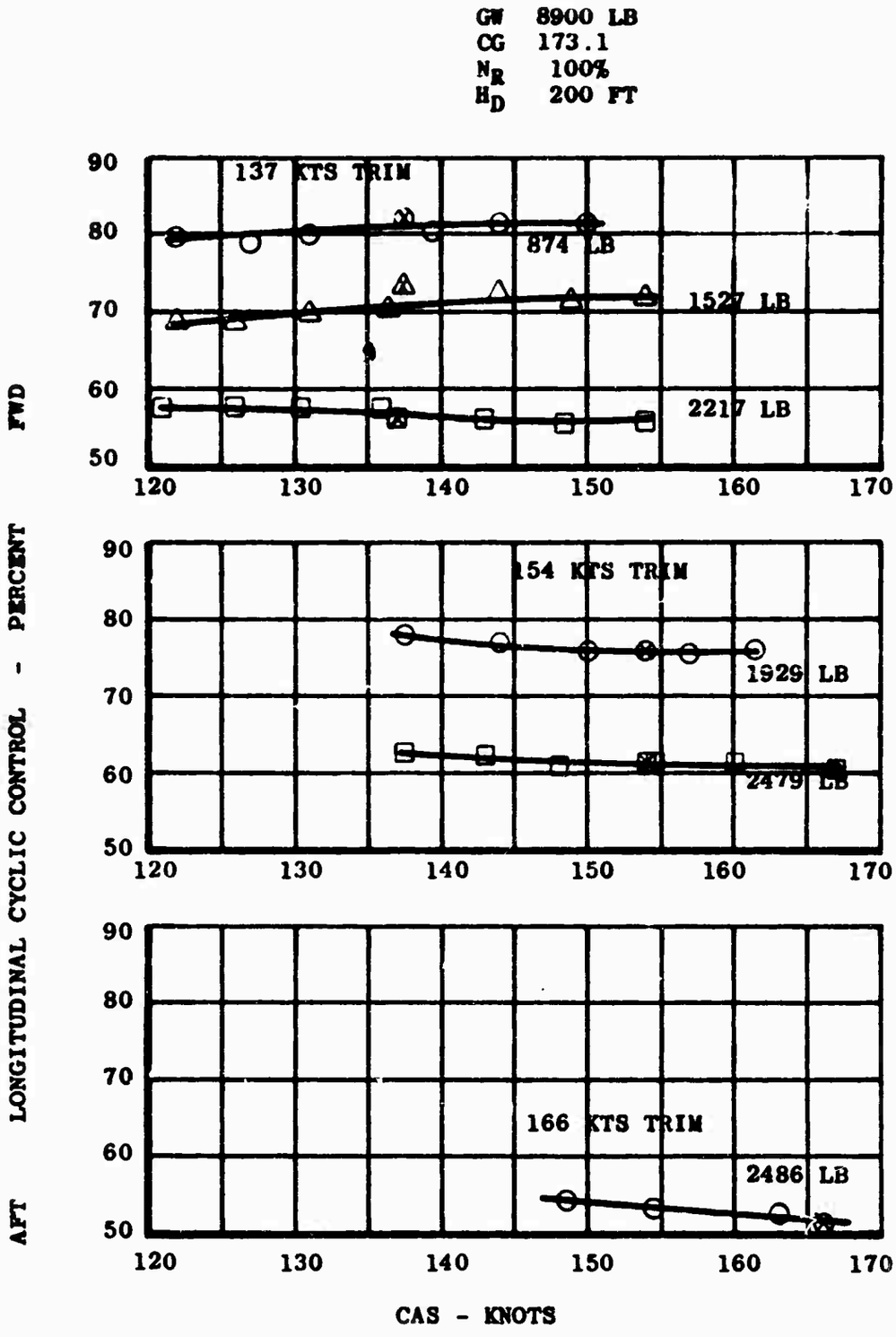

Figure I-29. (Continued)

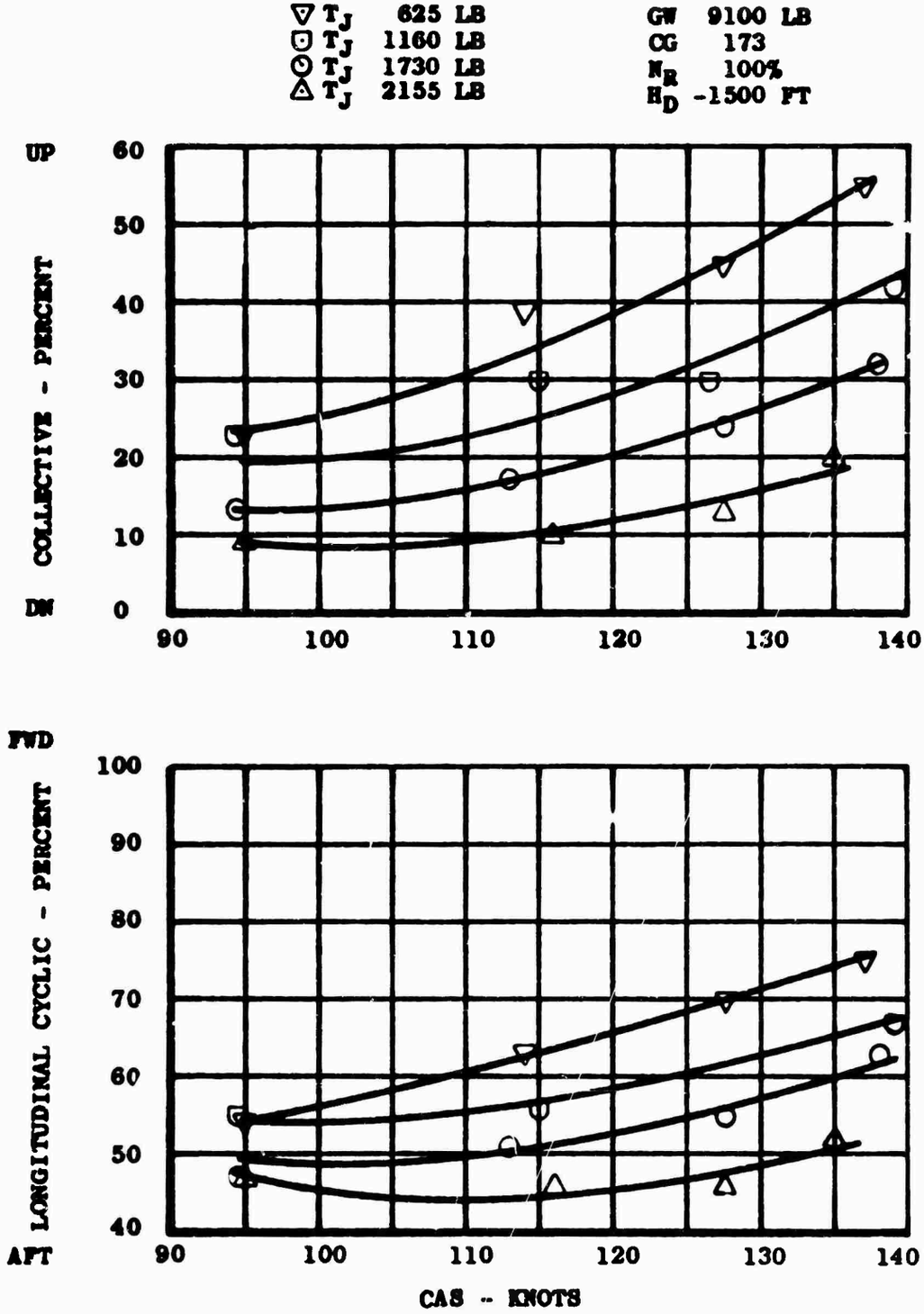

Figure I-30. EFFECT OF THRUST AUGMENTATION ON CONTROLLABILITY.

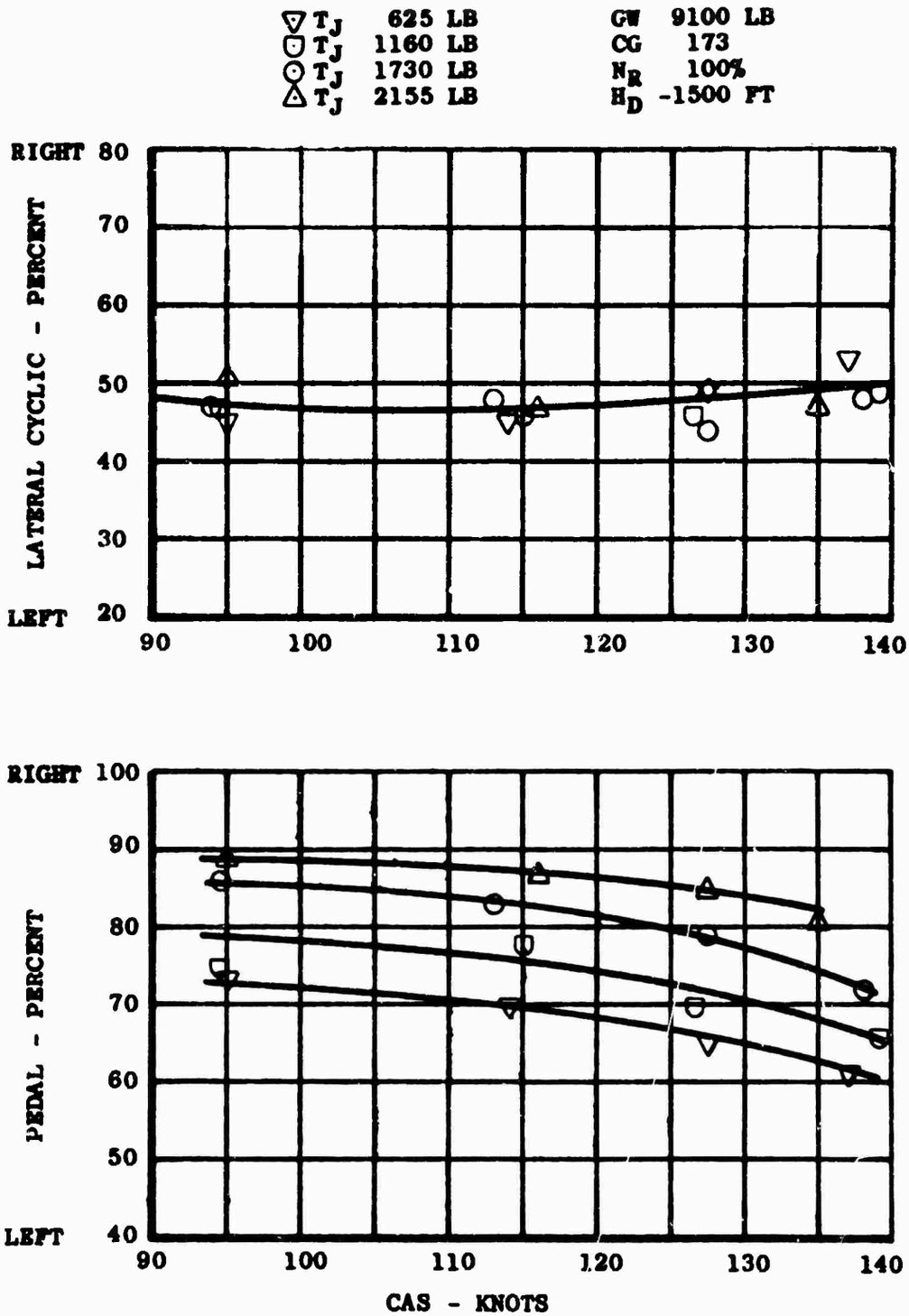

Figure I-30. (Continued)

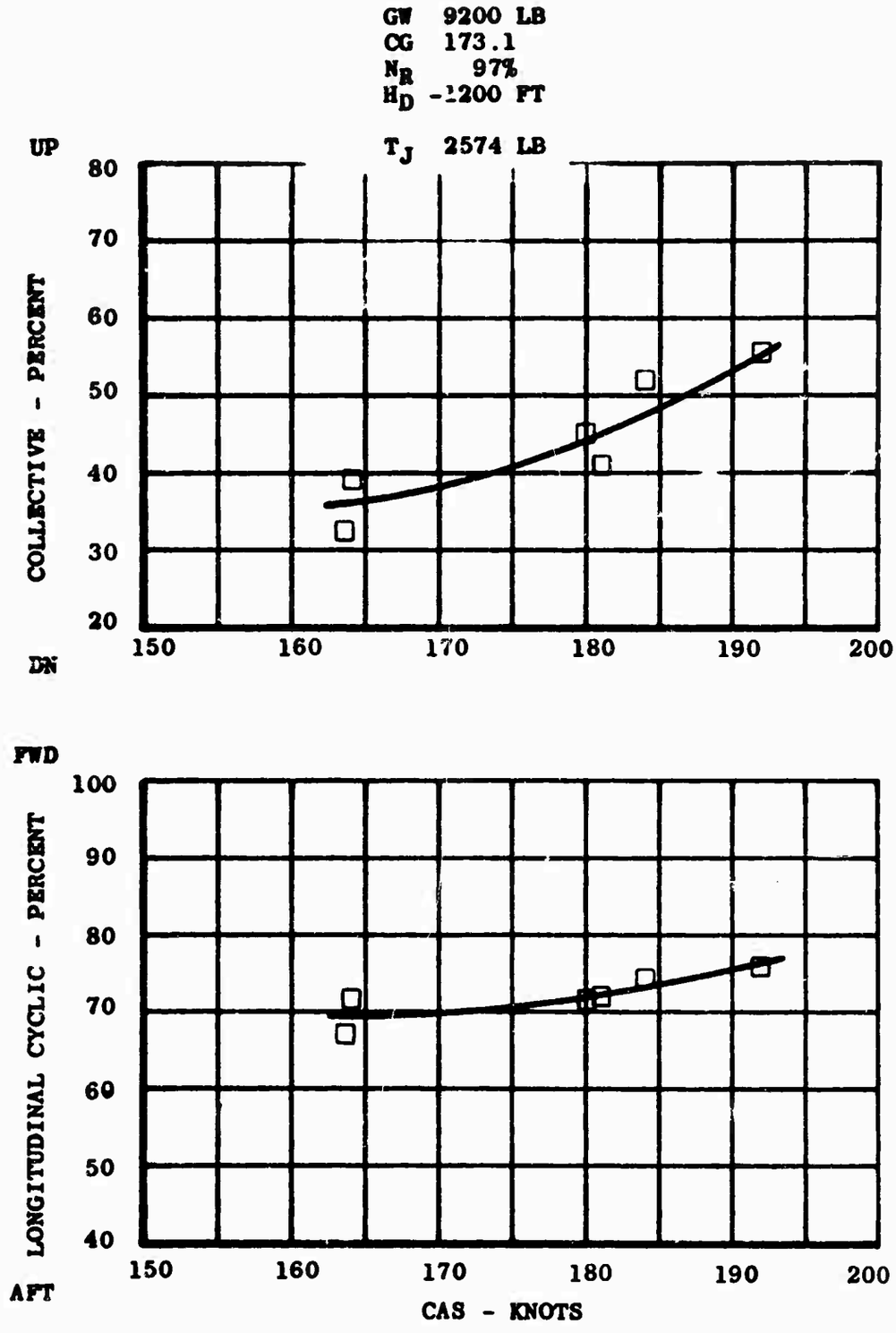

Figure I-30. (Continued)

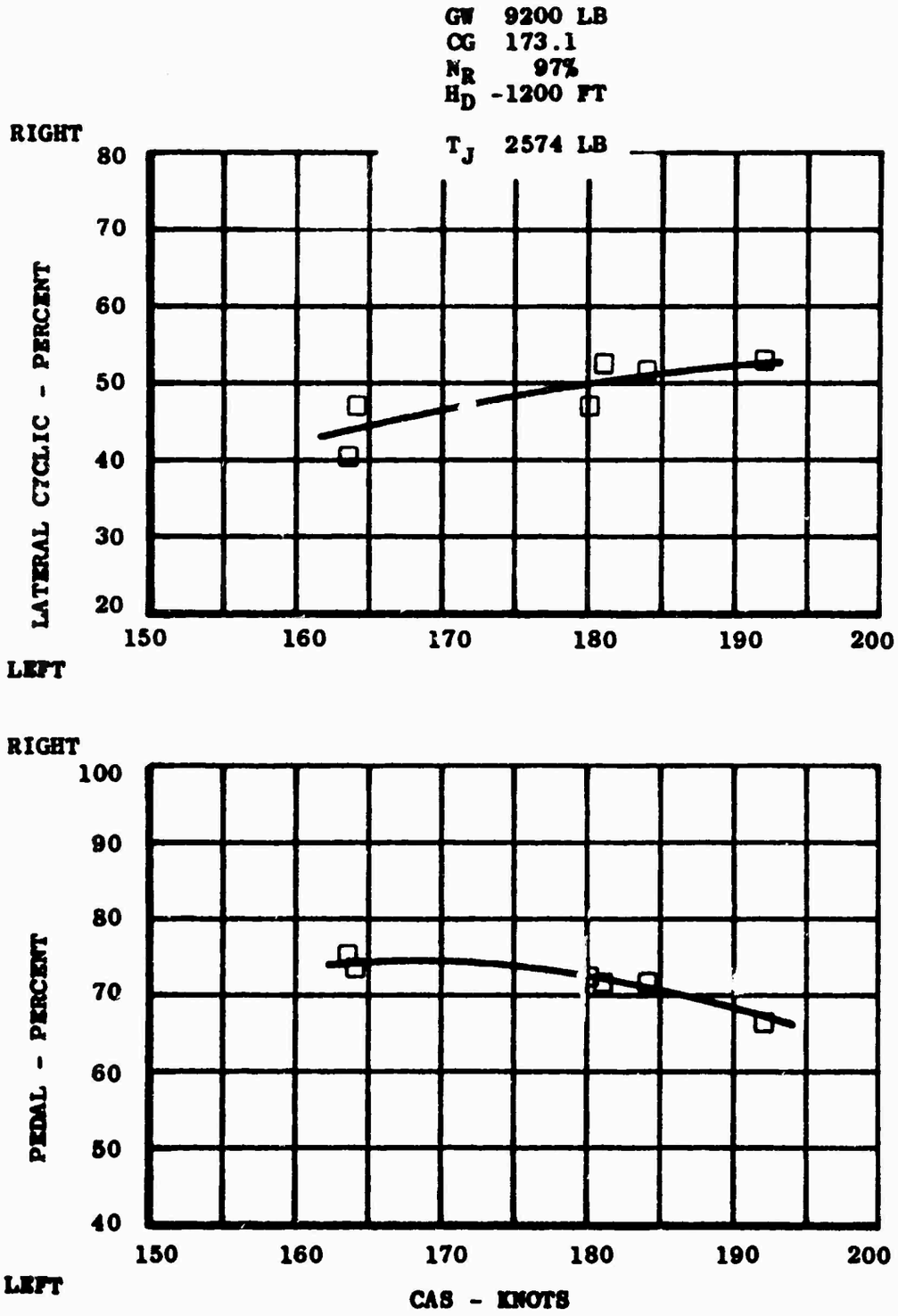

Figure I-30. (Continued)

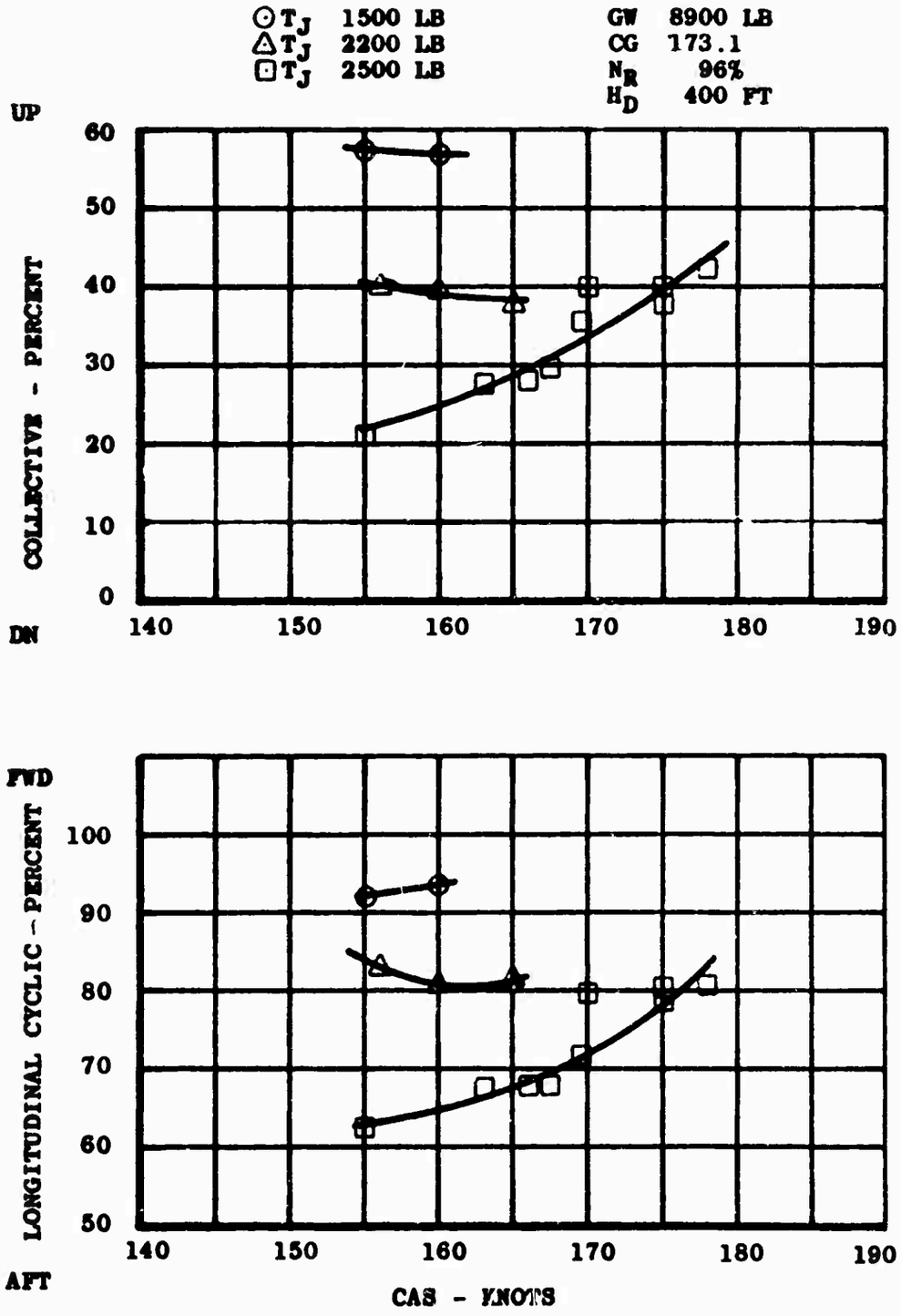

Figure I-30. (Continued)

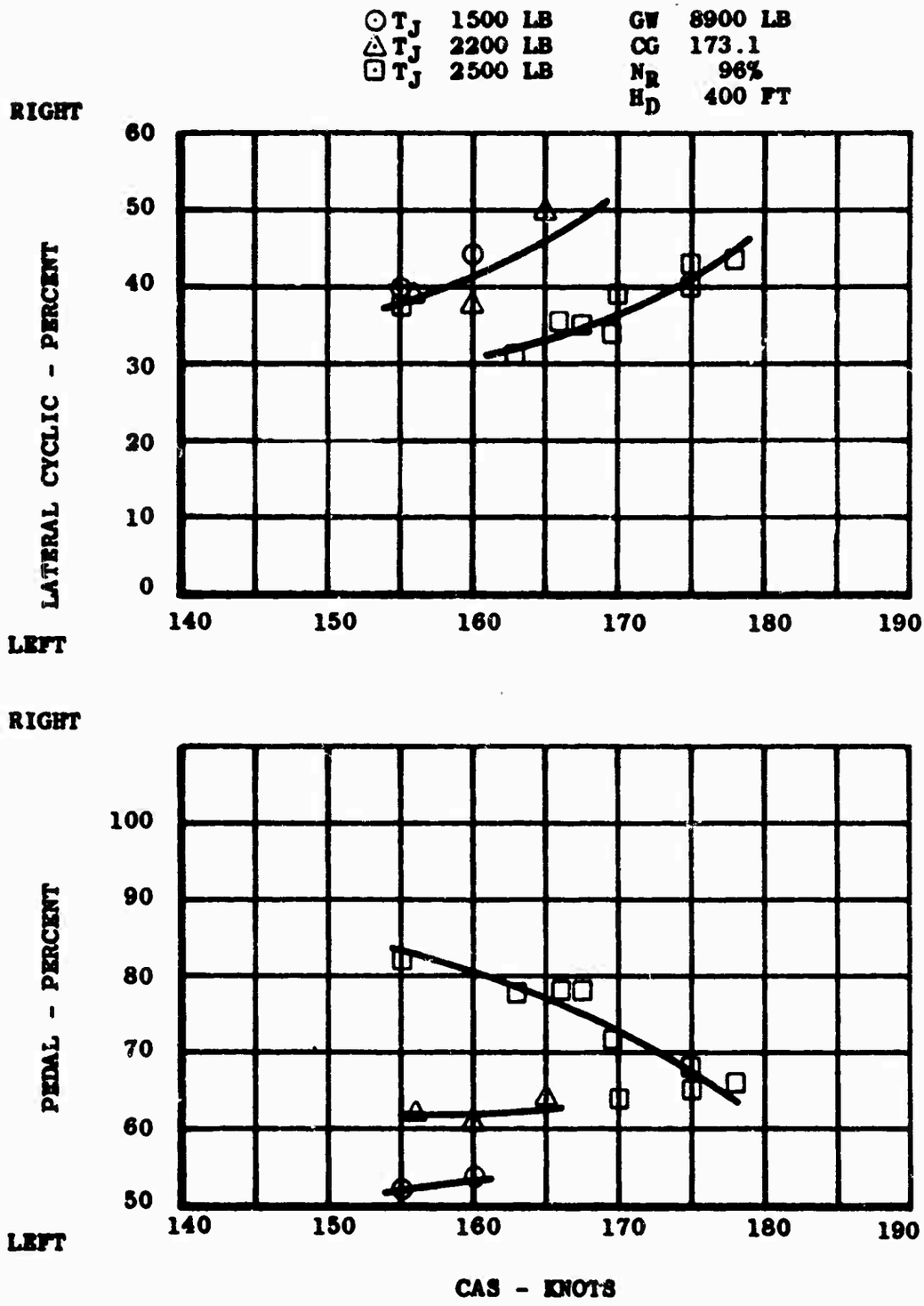

Figure I-30. (Continued)

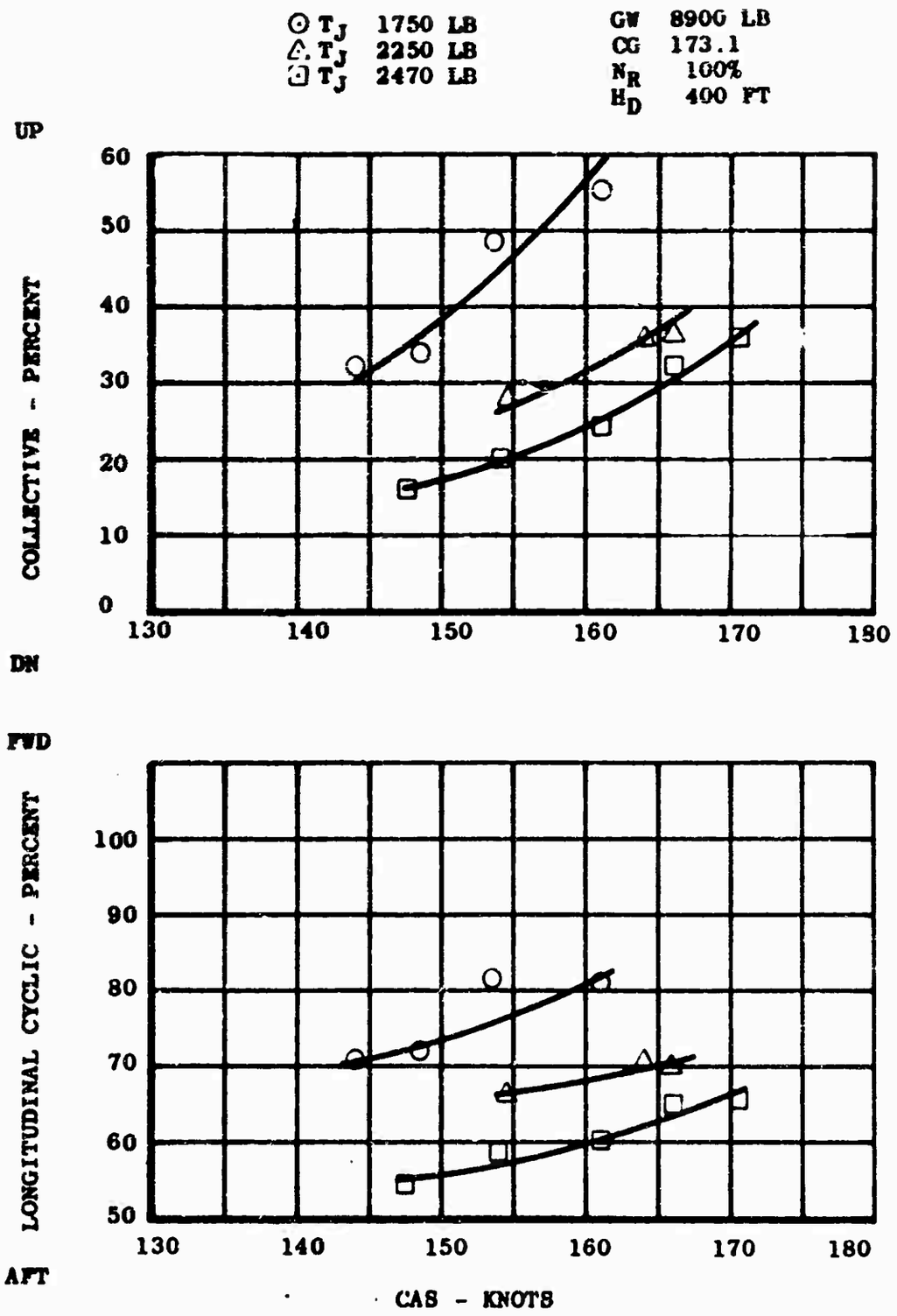

Figure I-30. (Continued)

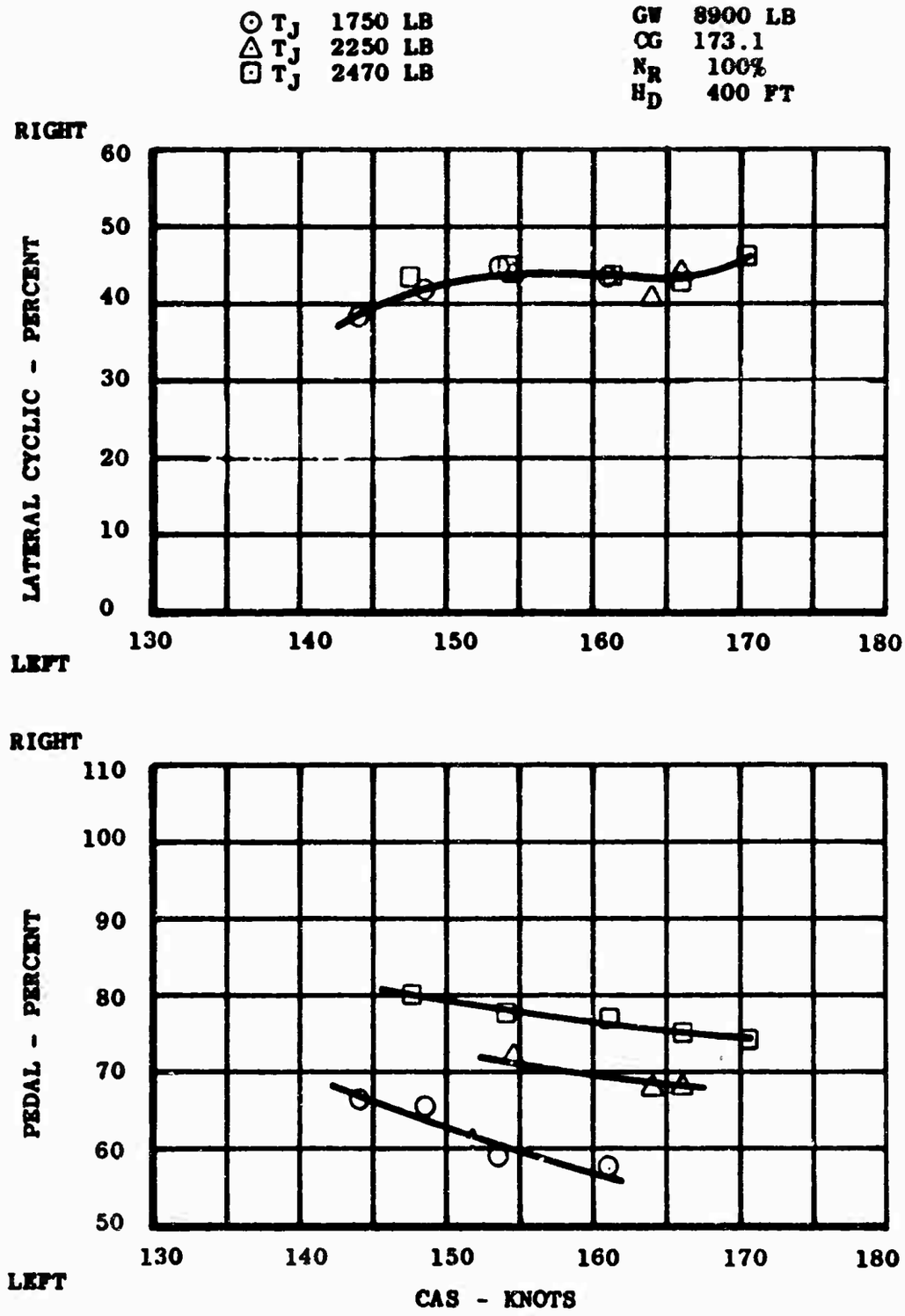

Figure I-30. (Continued)

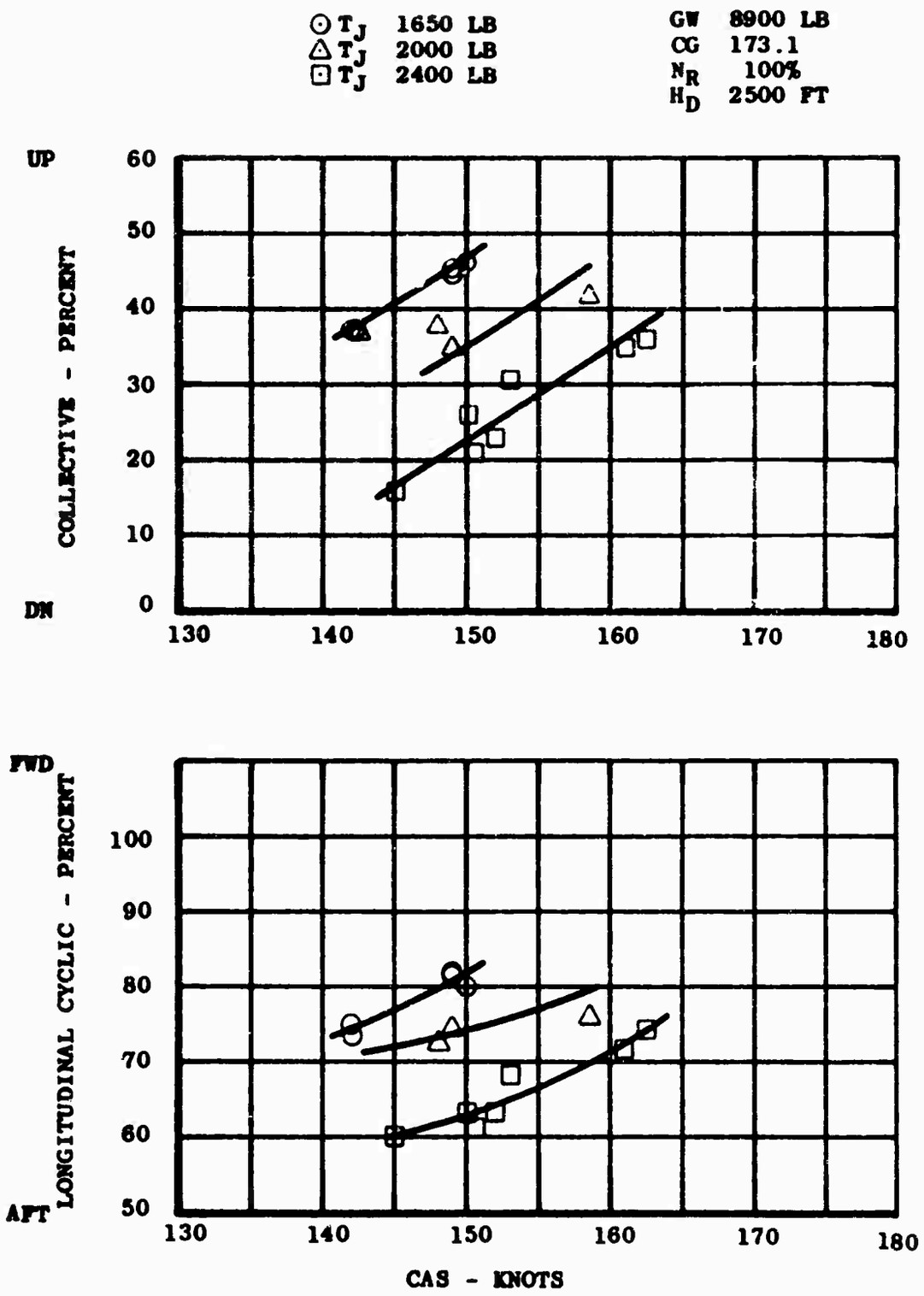

Figure I-30. (Continued)

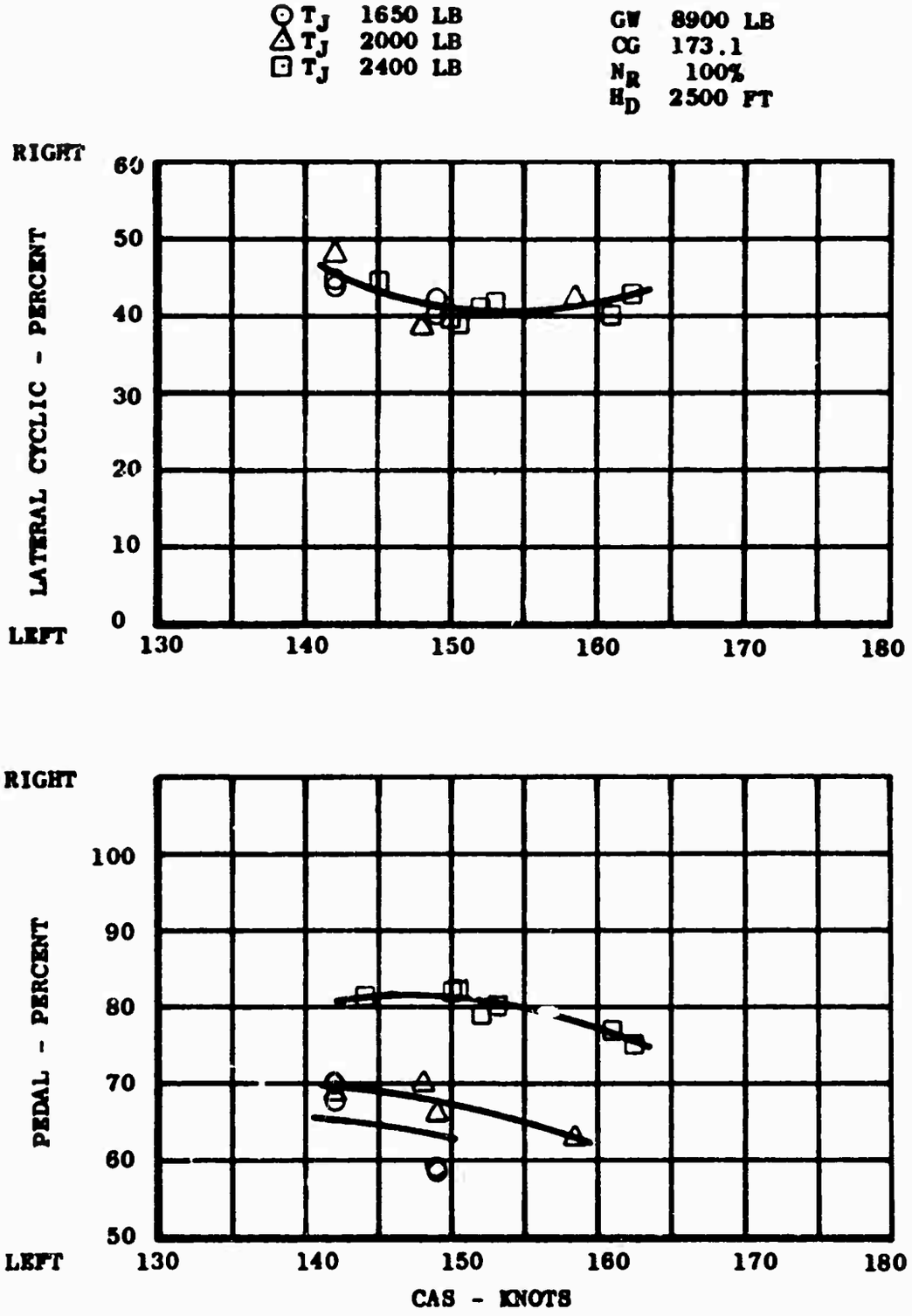

Figure I-30. (Continued)

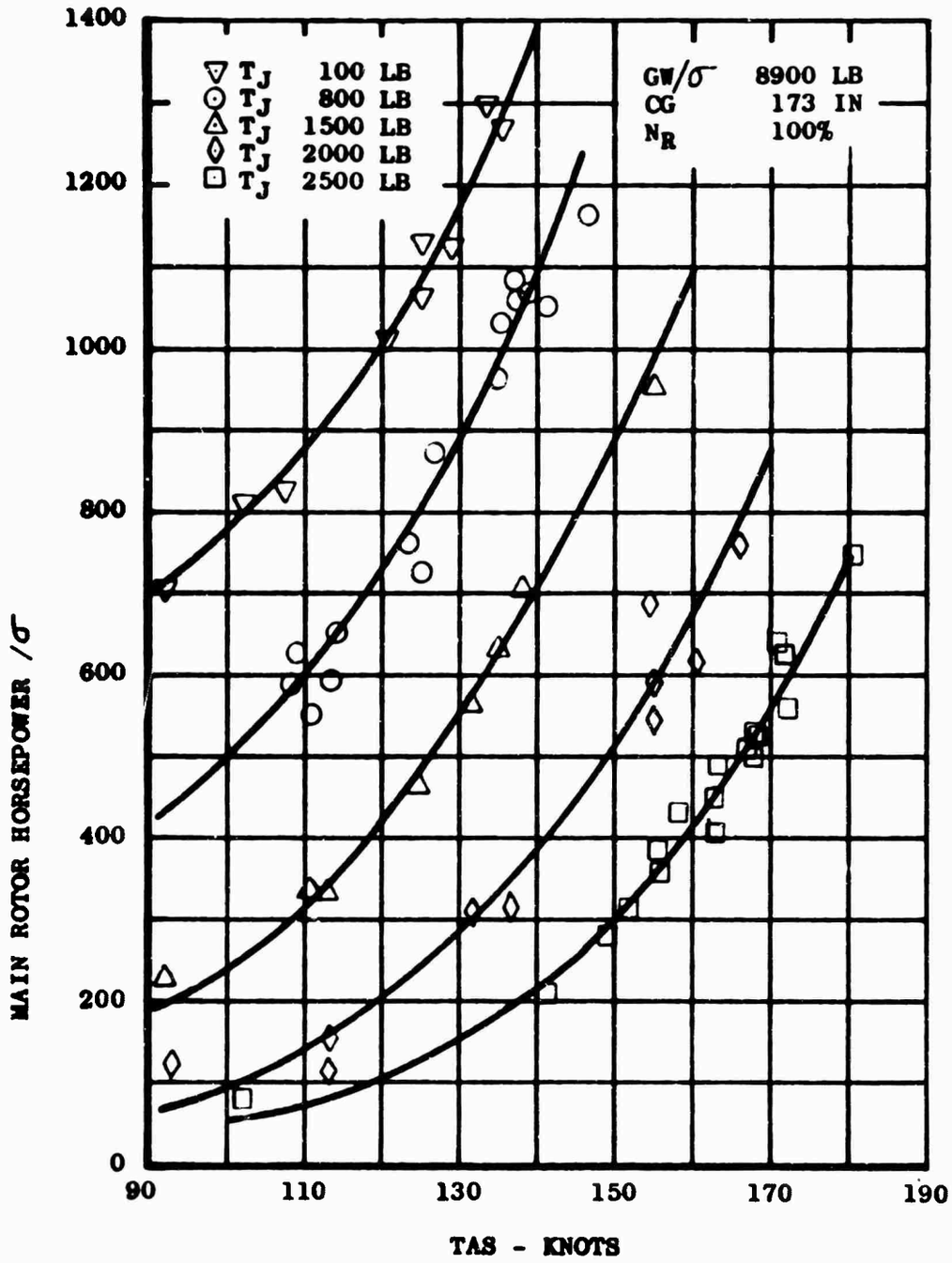

Figure I-31. EFFECT OF THRUST AUGMENTATION ON FORWARD FLIGHT PERFORMANCE.

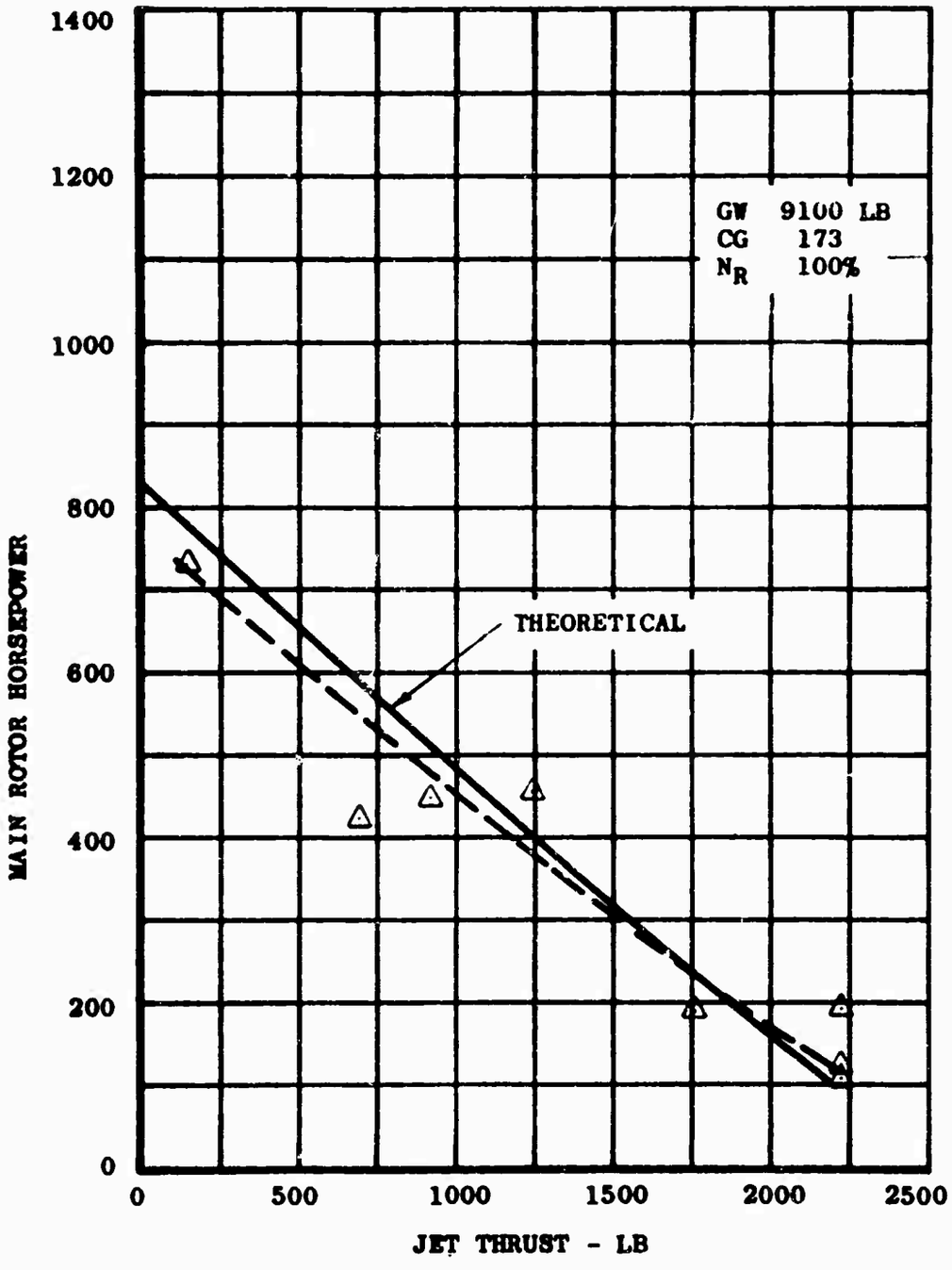

Figure I-32. EFFECT OF THRUST AUGMENTATION ON MAIN ROTOR POWER, CAS - 100 KT.

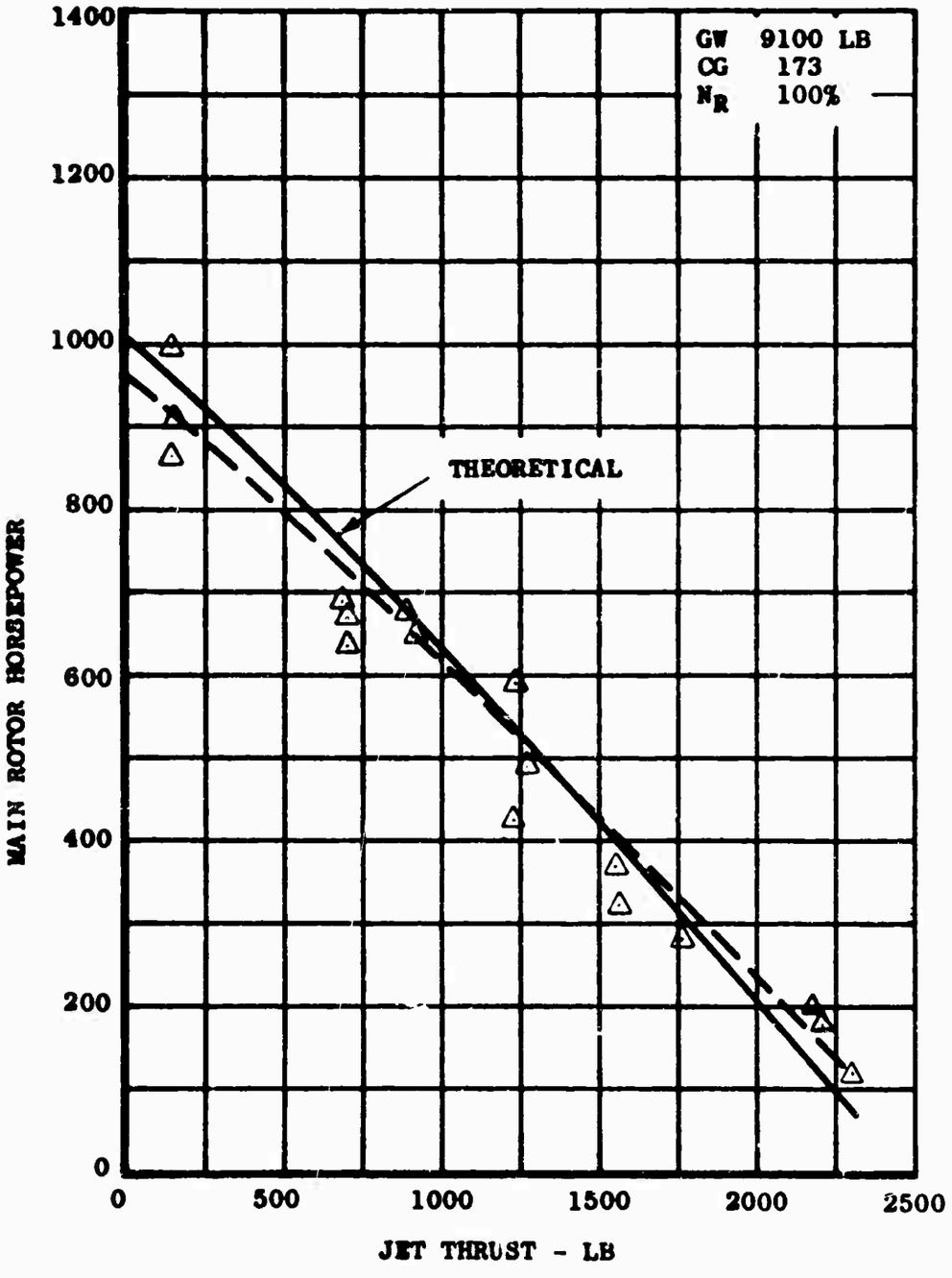

Figure I-32. (Continued), CAS = 120 KT.

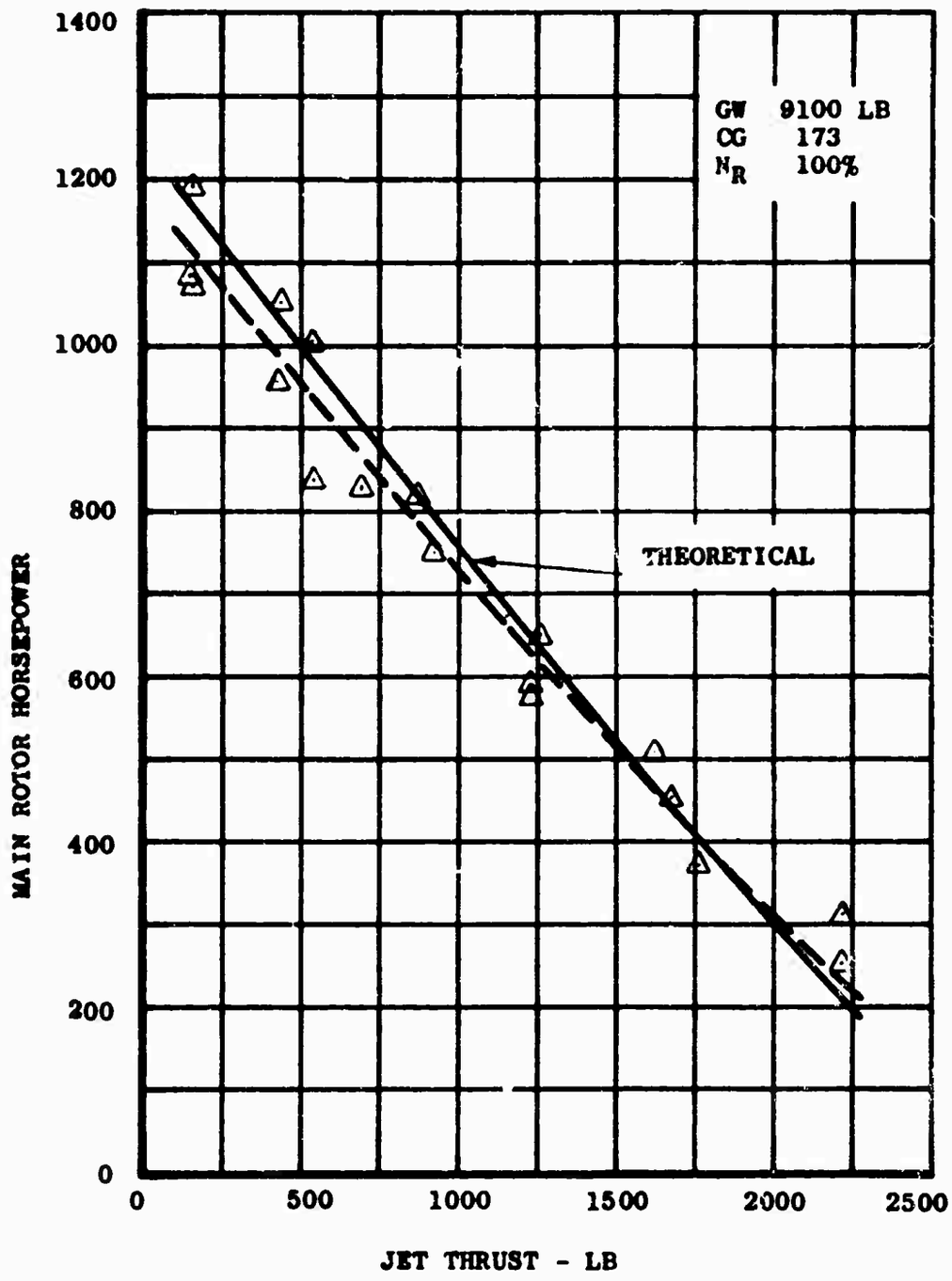

Figure I-32. (Continued), CAS = 130 KT.

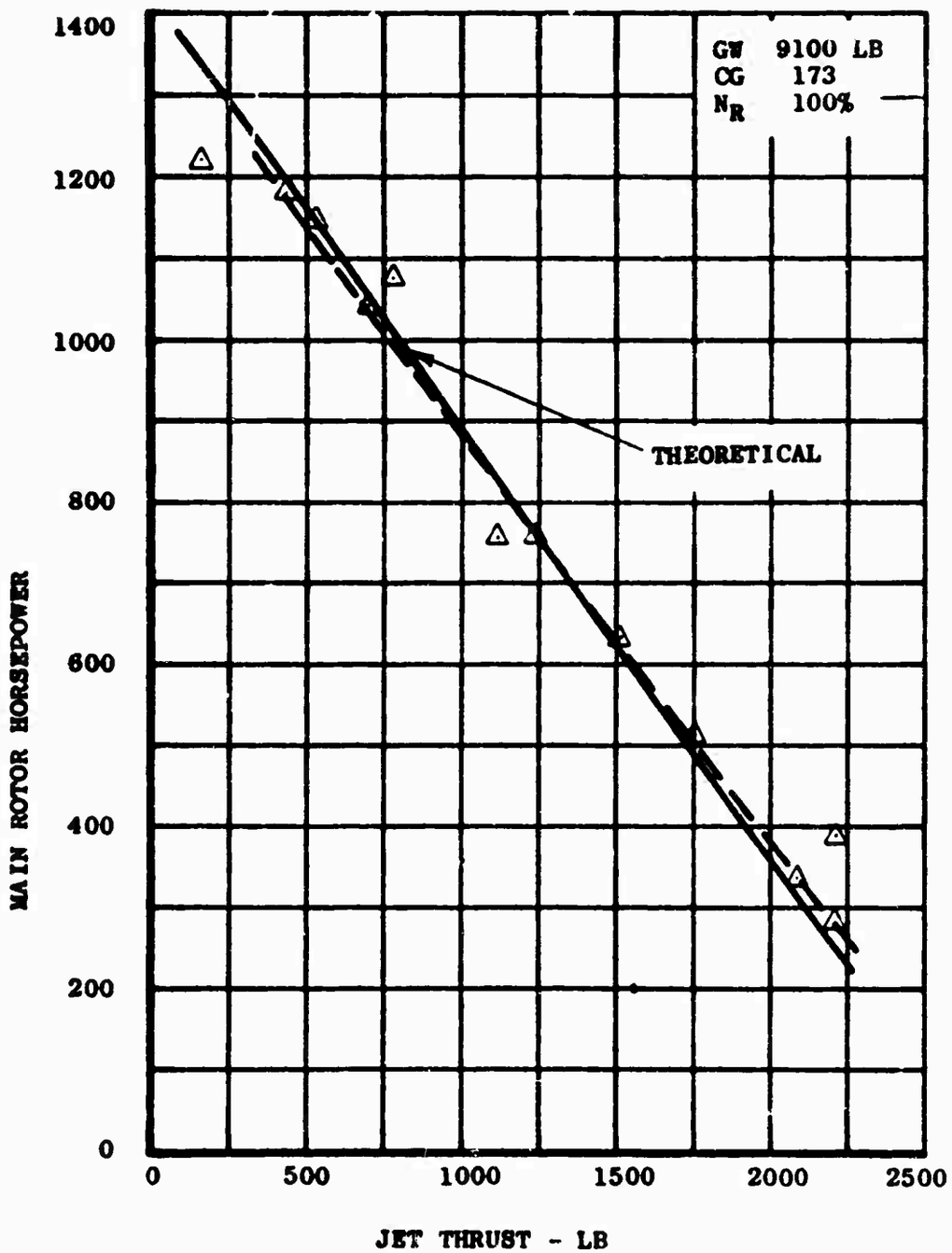

Figure I-32. (Continued), CAS = 140 KT.

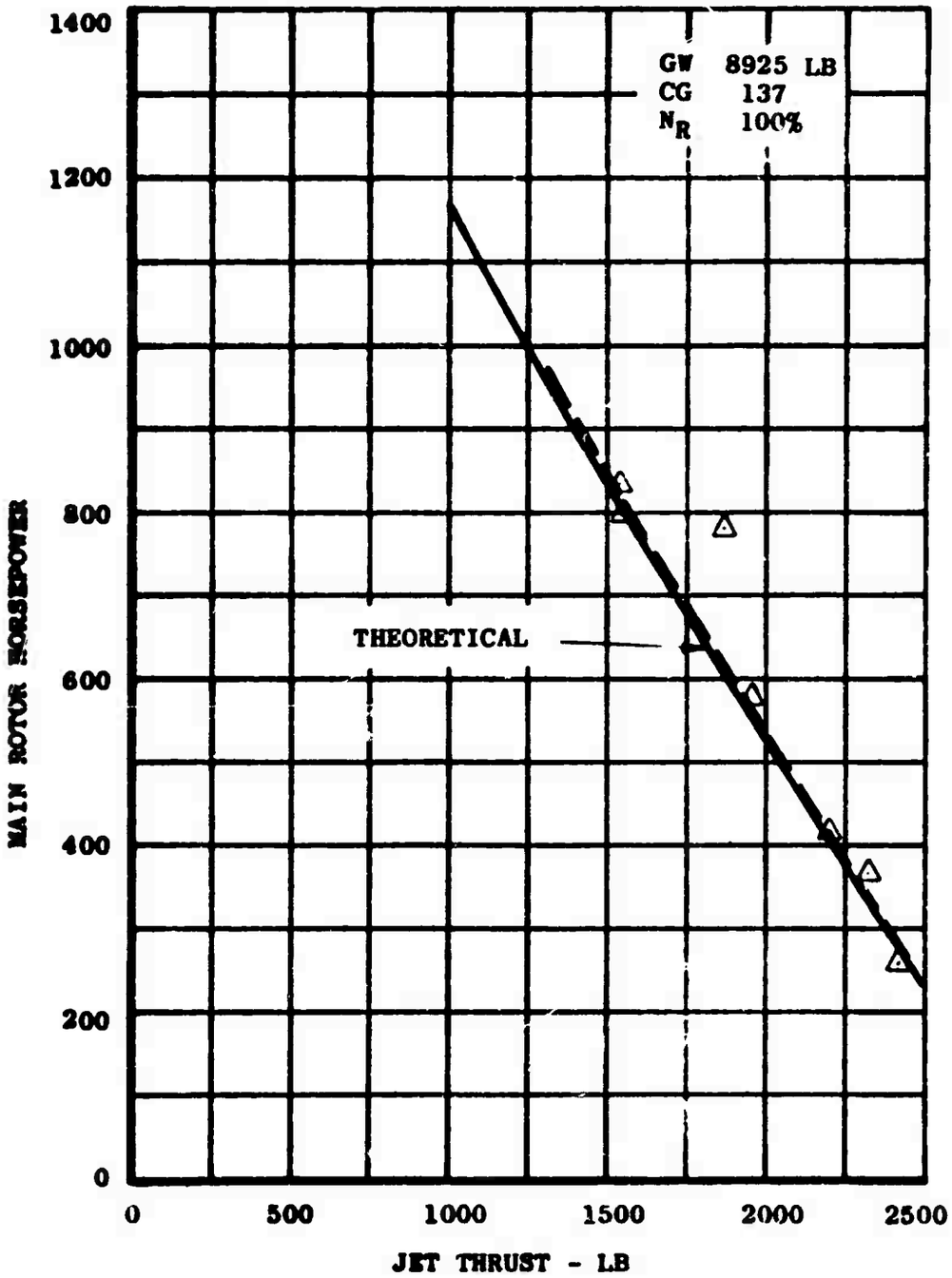

Figure I-32. (Continued), CAS = 150 KT.

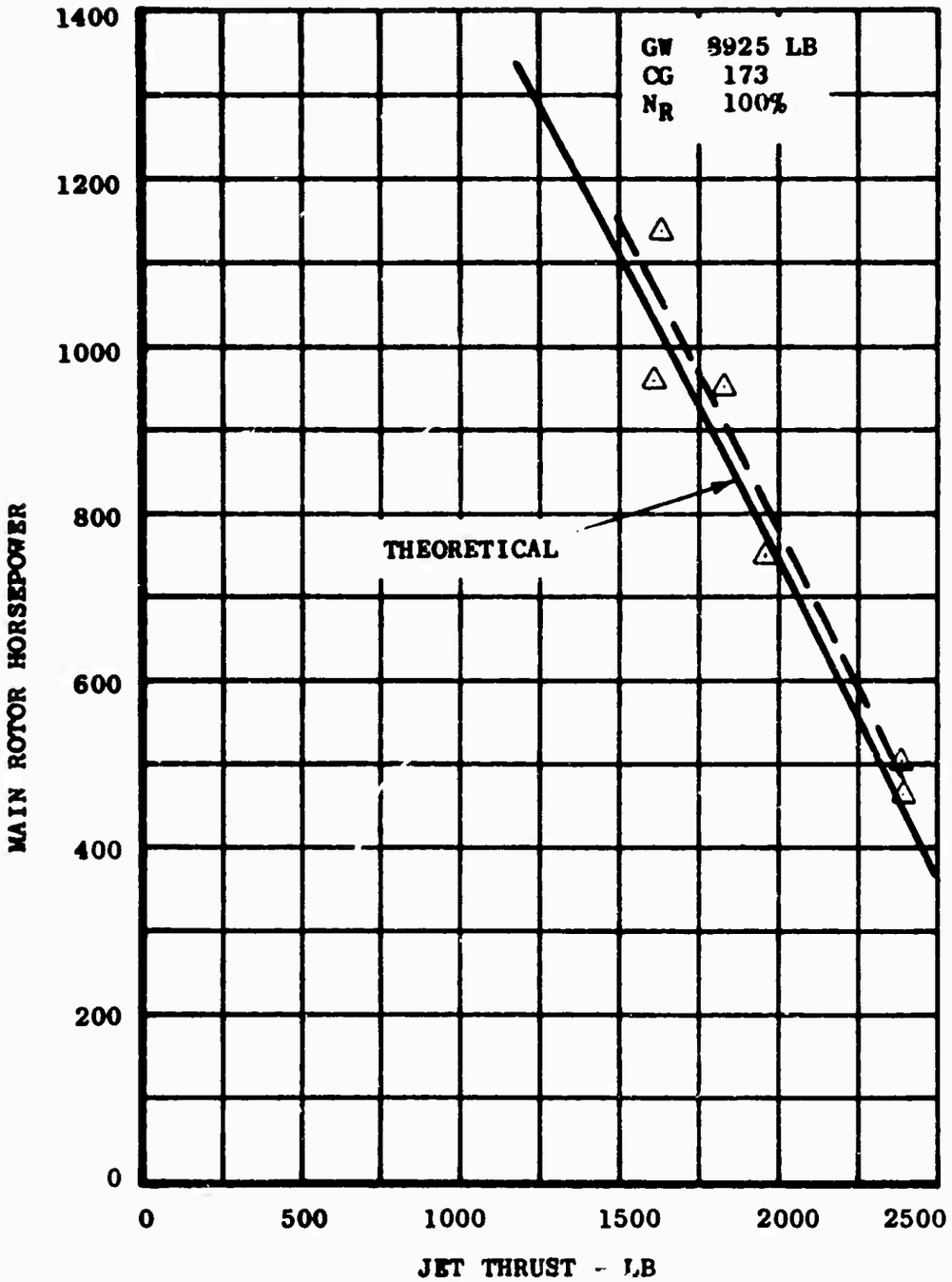

Figure I-32. (Continued), CAS = 160 KT.

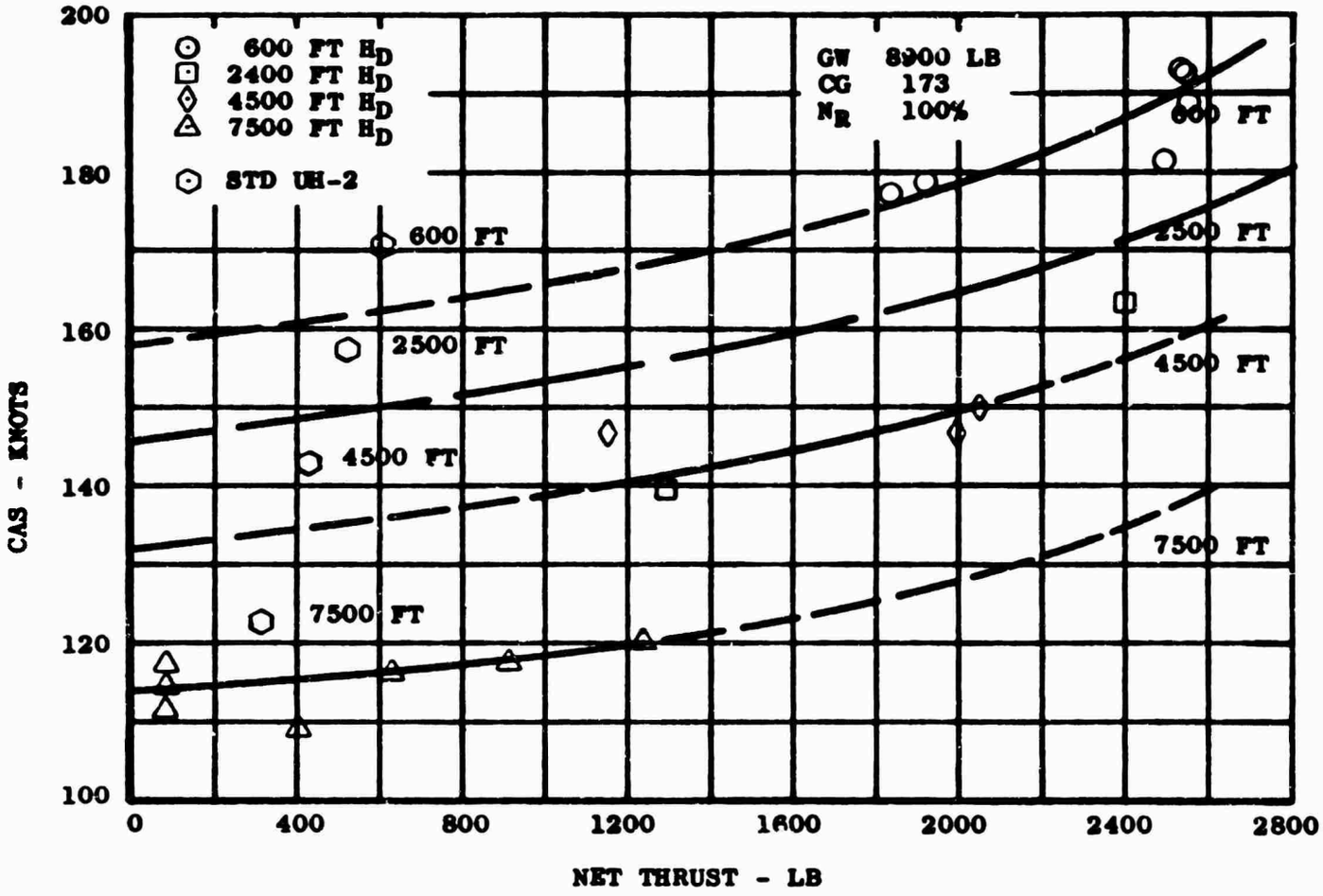

Figure I-33. EFFECT OF THRUST AUGMENTATION ON STALL-LIMITED AIRSPEED.

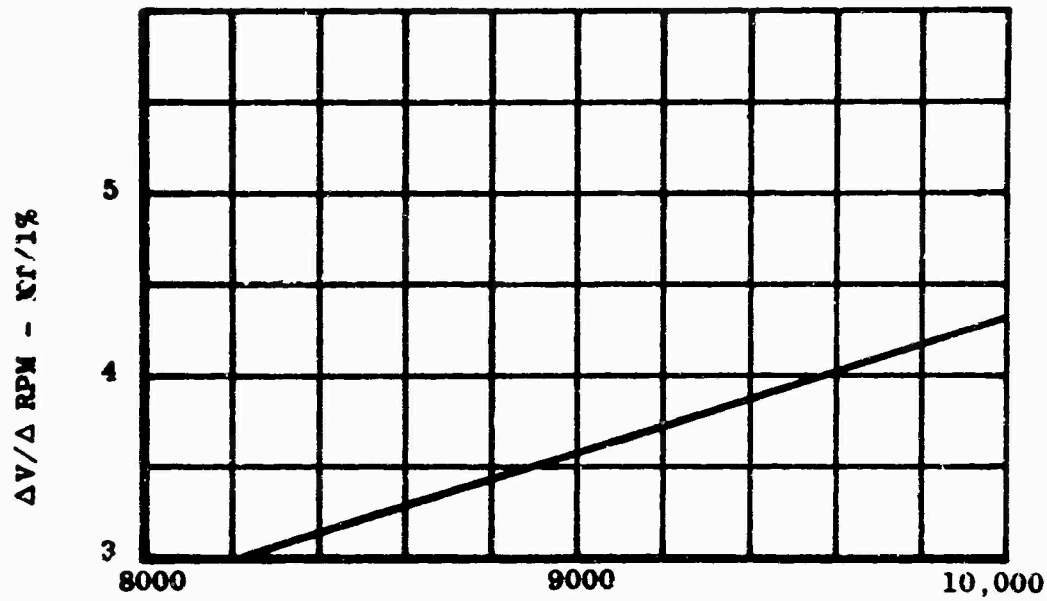

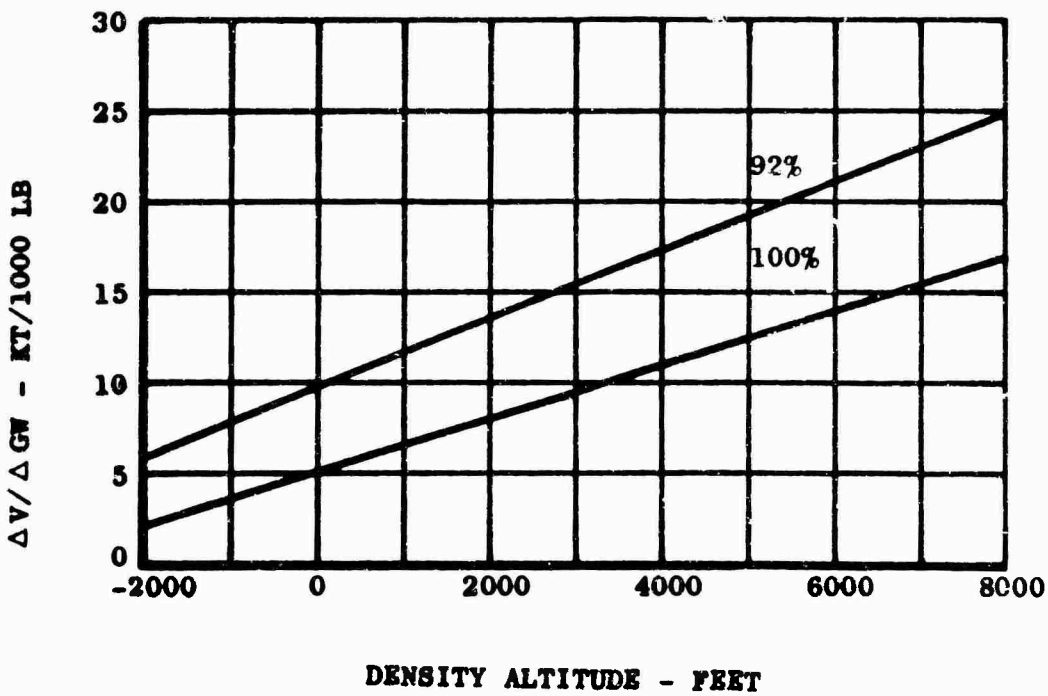

Figure I-34. CORRECTION FACTORS FOR STALL-LIMIT AIRSPEED.